THE INTERACTION OF METAL IONS AT THE HYDROUS MANGANESE DIOXIDE-SOLUTION INTERFACE

by

JAMES W. MURRAY

B.A., University of California
(1968)

SUBMITTED IN PARTIAL FULFILLMENT OF THE
REQUIREMENTS FOR THE DEGREE OF
DOCTOR OF PHILOSOPHY

at the

MASSACHUSETTS INSTITUTE OF TECHNOLOGY

and the

WOODS HOLE OCEANOGRAPHIC INSTITUTION

June, 1973

Signature of Author ..... James W. Murray .....
Joint Program in Oceanography, Massachusetts Institute of Technology - Woods Hole Oceanographic Institution, and Department of Earth and Planetary Sciences, Massachusetts Institute of Technology, April, 1973.

Certified by ..... Thesis Supervisor

Accepted by .....
Chairman, Joint Oceanography Committee on Earth Sciences, Massachusetts Institute of Technology - Woods Hole Oceanographic Institution

THE INTERACTION OF METAL IONS AT THE HYDROUS MANGANESE DIOXIDE-SOLUTION INTERFACE

by

JAMES W. MURRAY

Submitted to the Joint Oceanography Committee of the Department of Earth and Planetary Sciences, Massachusetts Institute of Technology, and the Woods Hole Oceanographic Institution on April 27, 1973 in partial fulfillment of the requirements for the degree of Doctor of Philosophy.

ABSTRACT

An experimental study of the interaction of metal ions with the surface of hydrous manganese dioxide has been completed. The results of these experiments have greatly improved our qualitative understanding of the adsorption mechanism and have also provided a means of testing quantitatively the proposal that the concentration of cobalt in manganese rich marine samples is due to adsorption of cobalt from sea water by hydrous manganese dioxide.

This study has shown that there are two reasons why manganese dioxide is an efficient scavenger of metal ions from sea water. These are coulombic attraction and specific adsorption. The coulombic attraction is in response to the surface charge that originates because of acid-base reactions at the surface. The surface charge is pH dependent, and the pH of zero point of charge for the hydrous manganese dioxide used in this study was 2.25. The surface charge increases rapidly for pH values greater than the pH of zero point of charge and reaches values of -100 $\mu coul/cm^2$ by pH 8.0. However, the high surface charge cannot explain all the adsorption. This is because some metal ions exhibit a strong specific adsorption on the surface. This specific adsorption is a direct reaction of the metal ions with the surface, releasing one proton from the surface for each metal ion adsorbed. The energy of this specific interaction is frequently greater than the energy of electrostatic attraction. Adsorption on hydrous manganese dioxide and the magnitude of the specific adsorption both increased in the order:

$$Na = K < Mn < Ca < Sr < Ba < Ni < Zn < Mn \leq Co$$

This suggests that the specific adsorption potential controls the adsorption selectivity of δMnO_2.

An adsorption isotherm was constructed for cobalt, and these data were used to test the hypothesis that the enrichment of cobalt in the suspended matter of the Black Sea and in ferromanganoan sediments from the East Pacific Rise is due to adsorption of cobalt from sea water by manganese dioxide. The calculations indicate that adsorption is a feasible explanation for these examples.

Thesis Supervisor: Derek W. Spencer
Senior Scientist, Department of Chemistry
Woods Hole Oceanographic Institution

ACKNOWLEDGEMENTS

This research has been completed with the advice and encouragement of many individuals. I wish to give special thanks to four: Dr. Werner Stumm, Dr. Derek W. Spencer, Dr. Peter G. Brewer and Dr. Geoffrey Thompson. Dr. Stumm provided many extensive discussions concerning the chemical mechanisms that operate in the natural environment. The education obtained from these discussions provided me with the necessary chemical foundation for selecting this topic of research. Dr. Spencer encouraged my independence and provided the stimuli necessary to keep me on a steady schedule toward completion. Dr. Brewer gave constant encouragement, and several parts of this thesis have benefitted from his criticism and ideas. Dr. Thompson critically reviewed the chapters of this thesis, and his patience in this regard is especially appreciated.

At various times during the course of this research, laboratory space was generously provided by Drs. Stumm, Spencer and Brewer.

Several other individuals were instrumental in the completion of this project and also deserve acknowledgement. Discussions with Dr. George Parks were extremely stimulating and provided a fresh, critical perspective on several aspects of my experimental results. Dr. James Morgan and Dr. Roger Burns read some of the chapters and made many valuable suggestions. Dr. Fred Sayles, Dr. Nelson Frew and Dr. Paul Mangelsdorf also critically discussed different aspects of the thesis with me.

Finally, I would like to acknowledge Miss Joanna Denman whose love and constant encouragement made life very enjoyable during the final stages of this project.

I gratefully acknowledge the efforts of Nancy Green who typed the final manuscript.

This research has been supported for various periods by funds granted by the National Science Foundation (GA-13574) and U. S. Atomic Energy Commission Contract AT-(30-1)3566 and Graduate Fellowships provided by the Pan American Petroleum Foundation and by the Woods Hole Oceanographic Institution.

BIOGRAPHICAL NOTE

The author was born on March 15, 1946 in Memphis, Tennessee. He grew up in Laguna Beach California, and graduated from Laguna Beach High School in June, 1964. In September, 1964, he entered the University of California from which he received a B.A. Degree in Geology in March, 1968. In September, 1968, he entered the M.I.T.-W.H.O.I. Joint Program in Oceanography as a candidate for the degree of Doctor of Philosophy.

While a candidate, the author prepared the following publications and lectures.

(1) "The Clay Mineralogy of Marine Sediments in the North Atlantic at 20 N Latitude," J.W. Murray, Earth and Planetary Science Letters, v. 10, p. 39, 1970.

(2) "Hydrographic Observations on the Red Sea Brines Indicate a Marked Increase in Temperature," P.G. Brewer, T.R.S. Wilson, J.W. Murray, R.G. Munns and C.D. Densmore, Nature, v. 231, p. 37, 1971).

(3) "The surface Chemistry of Hydrous Manganese Dioxide," J.W. Murray, submitted to the Journal of Colloid and Interface Science, 1972.

(4) "The Interaction of Metal Ions at the Manganese Dioxide-Solution Interface," presented at the American Chemical Society, New York, 1972.

(5) "Mechanisms of Removal of Manganese and Iron from Seawater," in preparation for Marine Manganese Deposits, edited by G.P. Glasby, Elsevier, 1973.

(6) "Carbon, Nitrogen and Phosphorus in the Black Sea," P.G. Brewer and J. W. Murray, submitted to Deep Sea Research, 1973.

(7) "The Interaction of Cobalt with MnO_2," J. W. Murray, presented at National AGU meeting, Washington, 1973.

TABLE OF CONTENTS

LIST OF FIGURES

CHAPTER 3
(continued)

CHAPTER 4

CHAPTER 4
(continued)

CHAPTER 5

LIST OF TABLES

CHAPTER 1

INTRODUCTION

I. INTRODUCTION

Most trace metals are known to pass relatively quickly through the oceans to the sediments. Barth (1952) originated a concept of residence time, later redefined by Goldberg and Arrhenius (1958) as:

$$\tau = \frac{A}{dA/dt}$$

where A is the total amount of the element in suspension and solution in the oceans and dA/dt is the amount introduced into the oceans each year. If it is assumed that (1) the present chemical composition of the oceans represents a steady state system in which the amount of material introduced per year is compensated by an equal amount deposited in the sediments, and (2) there is complete mixing of materials introduced into the oceans in times that are short with respect to the residence times, then the residence time calculated using the input rate and that calculated from removal date should agree. These values were calculated using the fluxes tabulated in Table 1 and are given in Table 2. Despite the difficulties involved in quantitatively assessing these fluxes, there is surprisingly good agreement between estimates of τ made by the two methods. It is reasonable to assume that each metal has long been at steady state with respect to a balance between the processes adding it to sea water and processes removing it from sea water.

If no other removal mechanism were operating, the concentration of a metal in sea water would be regulated by the solubility of its least soluble compound. Goldschmidt (1937), however, noted that several trace metals are soluble in sea water. This is not a problem of supply since he calculated that the amount of metal weathered from the continents

during geologic time far exceeds the quantity present in sea water (see also Rankama and Sahama (1952), 294-296; and Krauskopf (1956)). To explain this discrepancy, he suggested that the metal concentrations in sea water were removed by adsorption, particularly on iron oxide precipitates.

The comparatively short residence times of the transition elements (Table 2) suggest that their removal mechanism from sea water is extremely efficient. Krauskopf (1956) found that Pb, Ni, Co, Cu, Zn and Cd were all undersaturated with respect to their least soluble solid phase in sea water by factors ranging from 10^2 to 10^7, indicating that the processes of removal are more efficient for some metals than for others. A comparison of the metal concentration in sea water with the solubility of the least soluble solids is shown in Table 3 for Co, Ni, Cu and Zn.

II. MASS BALANCE FOR METALS

When the metal input fluxes are compared with the removal fluxes, it appears that steady state has been achieved. A summary of these fluxes is shown in Table 1. The predominant input flux is the dissolved and particulate load of streams. The inputs from low temperature weathering of basalts, hydrothermal emanations associated with spreading ridges (Appendix I-A), glacial weathering, and airborne dust can be shown to be negligible on a global scale (Garrels and MacKenzie 1971). The major removal pathways are through sedimentation and manganese nodules. Considering the uncertainties in the metal concentration of rivers and the possibility of recycling metals in the sediments, the agreement is quite good. If the system is at steady state and metals in sea water are undersaturated with respect to their least soluble solid phase, then some other mechanism must be operating to control the trace metal concentration in sea water.

TABLE 1

MASS BALANCE OF METALS IN SEA WATER(1)

METAL	DISSOLVED RIVER	SUSPENDED RIVER	AIRBORNE DUST	TOTAL INPUT	MANGANESE NODULES	DEEP SEA SEDIMENTS	ADJACENT SEA SEDIMENTS	TOTAL REMOVAL
Mn(2)	1.45×10^{11}	1.74×10^{13}	5.45×10^{10}	1.76×10^{13}	2.7×10^{11}	5.3×10^{12}	1.43×10^{13}	1.96×10^{13}
Co	5.79×10^{9}	4.57×10^{11}	1.50×10^{9}	4.64×10^{11}	4.1×10^{9}	4.9×10^{10}	2.18×10^{11}	2.71×10^{11}
Ni	8.69×10^{9}	1.37×10^{12}	4.50×10^{9}	1.38×10^{12}	7.0×10^{9}	1.55×10^{11}	9.24×10^{11}	1.09×10^{12}
Cu	1.45×10^{11}	1.02×10^{12}	3.30×10^{9}	1.17×10^{12}	4.0×10^{9}	1.69×10^{11}	8.06×10^{11}	0.98×10^{12}

(1) All fluxes in grams/year

(2) Not included is an estimate of the input rate of Mn associated with hydrothermal activity at mid-ocean ridges. An estimate for Mn may be as high as 1.2×10^{12} g/yr (Appendix I-A).

TABLE 2

ESTIMATED RESIDENCE TIMES OF METALS IN THE OCEAN

ELEMENT	AMOUNT IN OCEAN[1]		INPUT[2] (yrs)	REMOVAL[3] (yrs)
Fe	10	µg/kg	140	702
Mn	2	"	1.89×10^4	3.52×10^2
Co	0.03	"	7.10×10^3	5.70×10^2
Ni	2	"	3.15×10^5	1.19×10^4
Cu	2	"	1.89×10^4	1.10×10^4
Zn	5	"	2.36×10^4	1.90×10^4
Mg	1.326	g/kg	2.2×10^7	4.50×10^7
Ca	0.422	"	1.0×10^6	8.0×10^6
Sr	8.5	mg/kg	1.0×10^7	1.9×10^7
Ba	30	µg/kg	1.89×10^5	2.45×10^4

(1) Spencer and Brewer (1970)

(2) and (3) Appendix I-A

TABLE 3

A COMPARISON OF THE METAL CONCENTRATION OF SEA WATER WITH THE SOLUBILITY OF LEAST SOLUBLE SOLIDS.

METAL	CONCENTRATION IN SEA WATER	SOLUBILITY CONCENTRATION (1)	SOLID
Co	0.03×10^{-6} g/l	0.5×10^{-3} g/l	$CoCO_3$
Ni	2×10^{-6} g/l	658×10^{-3} g/l	$Ni(OH)_2$
Cu	2×10^{-6} g/l	21.6×10^{-6} g/l	CuO
Zn	5×10^{-6} g/l	28.8×10^{-6} g/l	$ZnCO_3$

(1) Solubility calculations made using solubility and stability constants from Sillen and Martell (1964).

$pK_{so}(CoCO_3) = +9.63$, $pK_{so}(Ni(OH)_2) = +15.21$, $pK_{so}(ZnCO_3) = +10.84$

pH8, $CO_3^{=} = 2 \times 10^{-5}$ m/l

$\gamma Me^{+2} = 0.12$ Latimer (1952)

$\gamma OH^{-} = 0.68$ Burns (1965)

$\gamma CO_3^{=} = 0.20$ Garrels & Thompson (1962)

III. EVIDENCE FOR ADSORPTION

Adsorption is one of the mechanisms most frequently proposed to account for the removal of metals from sea water in order to maintain the observed steady state. Riley and Chester (1972, p. 404) concluded that as the variations in the lattice-held trace elements of continental and submarine volcanic rocks are too small to account for the observed variations in deep sea sediments, adsorption of trace elements from sea water by river-borne iron and manganese oxides may be a major pathway by which they are removed.

Many workers have observed correlations among certain elements in manganese nodules, in sediments, and in suspended matter. These correlations have been established using statistical techniques, such as simple linear correlation coefficients (e.g. Cronan and Tooms 1969, Willis and Ahrens 1962, Carvajal and Landergren 1969), by more sophisticated multivariant analysis such as factor analysis (e.g. Turekian and Imbrie 1966, Cronan 1967, Spencer et al. 1972), and by studying in situ relationships using the electron-probe X-ray microanalyzer (e.g. Burns and Fuerstenau 1966. Cronan and Tooms 1968, Aumento et al. 1968, Friedrich et al. 1969). These correlations are summarized in Table 4.

The correlations most frequently observed are those of various elements with manganese or iron. This supports the suggestion that the enrichment mechanism is adsorption onto the oxides of iron and manganese.

Goldberg (1954) was the first to point out inter-element relationships in nodules. Using bulk chemical analyses and scatter plots, he found correlations of nickel and copper with manganese, and of titanium, zirconium and cobalt with iron. Riley and Sinhaseni (1958) suggested that

TABLE 4

A SUMMARY OF METAL CORRELATIONS IN MARINE SAMPLES*

REFERENCE	CORRELATIONS
NODULES	
1. Goldberg (1954)	Fe - Co - Ti - Zr; Mn - Ni - Cu
2. Willis and Ahrens (1962)	Ni - Cu; Fe - Co
	Mn - Fe (negative)
3. Burns and Fuerstenau (1966)	Fe - Co - Ti - Ca
	Mn - Ni - Cu - Zn - Mg - K - Ba - Al
4. Sevast'yanov and Volkov (1966)	Mn - Ni - Co - Cu - Mo
5. Barnes (1967)	Pb - Co; Co - δMnO_2
6. Aumento et al. (1968)	Mn - Co - Ni
7. Cronan (1967)	Fe - Ti - H_2O; Cr - Detrital.
8. Cronan and Tooms (1968)	Mn - Cu - Ni - Ca - K
9. Cronan (1969)	Mn - Ni - Cu - Mo; Co - Pb
10. Calvert and Price (1970)	Mn - Ba - Co - Ni - Si - Mo
	Fe - As - Pb - Y - Zn - P
11. Brown (1971)	Pb - Co; Mn - Cu - Ni - Co
SEDIMENTS	
1. Turekian and Imbrie (1966)	Mn - Co - Ni
	Cu - $CaCO_3$
2. Carvajal and Landergren (1968)	Mn - Co - Ni
3. Cronan (1969)	Mn - Co
4. Watson and Angino (1969)	Fe - Ni; Fe - Co; Co - Ni
5. Bostrom (1970)	Mn - Cu - Co - $CaCO_3$
6. Calvert and Price (1970)	Cu - Ni - Pb - Zn - organic matter

*Positive correlations unless otherwise stated.

his correlations of iron with zirconium, or of manganese with copper, were not statistically significant. However, later workers (Table 4) substantiated the correlation of manganese with copper.

Goldberg proposed that adsorption onto particulate Fe and Mn species accounted for the covariances. He suggested that the sorption depends on the relationship between the charge density of the adsorbed ion and that of the adsorbing surface. Adsorption will only take place in response to electrostatic forces (i.e. only ions with a charge opposite to the charge of the surface will be adsorbed); those ions with the largest charge densities will be most effectively scavenged. If MnO_2 were negatively charged and iron oxide positively charged, the distribution of adsorbed ions between these two phases should indicate which elements are present in sea water as cations and which as anions.

Adsorption onto iron and manganese oxides was also invoked by Dasch et al. (1971) and Sayles and Bischoff (1973) to explain the enrichment of metals in sediments from the East Pacific Rise, and by Aumento et al. (1968) to explain the enrichment of Co and Ni in manganese pavement from the San Pablo seamount. Sevast'yanov and Volkov (1966) used similar arguments to explain the correlation of Ni, Co, Cu and Mo with Mn in Black Sea nodules. They further hypothesized that the large adsorption capacity of solid manganese hydroxide ($MnO(OH)_2$) is due to the acid properties of the solid which will tend to form salts with divalent metals.

A strong correlation of Co and Sb with Mn was observed in particulate matter of the Black Sea (Spencer et al. 1972). Adsorption or co-precipitation of Co and Sb on solid MnO_2 was invoked to explain the associations.

Riley and Sinhaseni (1958) observed that if the majority of the minor elements in nodules are adsorbed directly from sea water, concentration

factors relative to sea water may prove useful in elucidating this mechanism. Their calculated concentration factors ranged from over 3×10^7 for manganese and iron to values less than 40 for elements that occur as major elements in sea water. They suggested that those elements with low enrichment factors are not strongly adsorbed from sea water because they tend to form hydroxides with ionic bonds, whereas those elements that have the highest enrichment factors (Co, Ni, Cu, Zn, and Pb) have high ionic potentials (i.e. charge/radius) that lead to their enhanced adsorption. If adsorption from sea water is the controlling mechanism, then the adsorption selectivity sequence found in the laboratory experiments should compare well with concentration factors observed in natural materials. Concentration factors, using recent values for the metal concentrations in sea water (Spencer and Brewer 1970), have been calculated and are shown in Table 5. Values for Atlantic and Pacific manganese nodules were taken from Arrhenius (1963), and the values for Pacific seamount nodules were taken from Goldberg (1954), Cronan and Tooms (1967, 1969), Mero (1964), and Menard et al. (1964). These results suggest that the selectivity sequence may be Co > Ni > Cu > Zn > Ba > Sr > Ca > Mg.

Carvajal and Landergren (1969) studied the interrelationships of manganese, cobalt and nickel in marine sediments and found that there is a strong correlation between these three metals. Their results further indicated that Co was relatively more enriched than nickel. If the removal of these elements from sea water is by adsorption on manganese phases, this implies that Co is more readily adsorbed than nickel. This implication is amenable to testing in laboratory experiments.

TABLE 5

ENRICHMENT FACTORS

ELEMENT	AVERAGE SEA WATER CONCENTRATION	PACIFIC DEEP SEA NODULES	ATLANTIC DEEP SEA NODULES	PACIFIC SEA MOUNT NODULES
Mg	1.294 g/kg	13.0	13.0	11.9
Ca	0.413 g/kg	46.0	65.5	69.0
Sr	0.008 g/kg	1.01×10^2	1.12×10^2	1.60×10^2
Ba	40 µg/kg	4.5×10^4	4.25×10^4	7.22×10^4
Mn	2 µg/kg	1.21×10^8	0.85×10^8	0.85×10^8
Fe	10 µg/kg	1.40×10^7	1.75×10^7	1.53×10^7
Co	.03 µg/kg	1.17×10^8	1.03×10^8	1.42×10^8
Ni	2 µg/kg	4.95×10^6	2.10×10^6	1.68×10^6
Cu	2 µg/kg	2.65×10^6	1.00×10^6	0.42×10^6
Zn	5 µg/kg	9.4×10^4	-	-

Average sea water values from Spencer and Brewer (1970).

Atlantic and Pacific nodule values from Mero, quoted in Arrhenius (1963).

Sea mount nodule values from Goldberg (1954), Mero (1965)

Cronan (1967, 1969), and Menard et al. (1964).

IV. SCOPE AND ORGANIZATION OF THIS THESIS

The preceding discussion has indicated the importance of metal adsorption onto iron and manganese oxides in marine geochemical cycles. Unfortunately, little quantitative research has been done to elucidate the chemical properties of the adsorption mechanism. The purpose of this thesis is to provide experimental evidence to help understand the adsorption process of metals onto manganese dioxide. Only with this knowledge can we evaluate this mechanism in the oceans.

In colloid and interfacial chemistry, manganese dioxide could be an important phase in the general understanding of the surface chemistry of metal oxides. Work on the surface chemistry of metal oxides has progressed rapidly in the last few years, and several models have been proposed to explain the interaction of metal ions with these surfaces (e.g. Stumm et al. 1970, James and Healy 1972). Surface chemistry is an important field for oceanographers. It is clear that many of the reactions that take place in the sea occur at the air-water or water-sediment interface.

A feasible approach is to integrate these two fields of study and apply our knowledge of surface chemistry to chemical oceanographic problems. The interaction of metal ions with the hydrous manganese dioxide-solution interface was selected as an aspect of the general problem of adsorption that could be looked at in detail in the laboratory. This study should provide a test of some of the hypotheses regarding the controls on trace metal concentrations in the oceans, and a test of previously proposed models for the interaction of metal ions with metal oxides. Clearly,

extrapolation of the laboratory experiments to explain all aspects of the metal distribution in marine samples will not be possible. Many factors such as mineralogy and the source of the metals (i.e. submarine volcanism, low temperature weathering of basalts and sedimentary diagenesis) can influence the metal content of manganese-rich deposits. The question I hope to examine most closely is how effective is adsorption as an enrichment mechanism.

Experiments have been done using a carefully and specially prepared manganese dioxide, first to understand the origin of the surface charge (chapter 2) and second to investigate the interaction of various metal ions with the surface (chapters 3 and 4). I have also made a reasonable attempt, bearing in mind the problem in extrapolation, to use the experimental results to test and invoke explanations for various metal distributions in marine deposits (chapter 5).

Each chapter is presented as an independent unit for ease of reference and to facilitate publication (for example, chapter 2 has been submitted for publication in J. Colloid.Interface Chemistry). However, to develop the thesis cogently and logically, cross referencing between chapters has been necessary and redundancy has thus been kept to a minimum. Necessary experimental details have been assembled in special appendices so as not to detract from the discussion of the experimental results.

REFERENCES

Aumento, F., Lawrence, D.E. and Plant, A.G. (1968) The ferro-manganese pavement on San Pablo Seamount. Geol. Surv. Can. Pap. 68-32, 1-30.

Arrhenius, G. (1963) Pelagic sediments. In The Sea,Vol. 3 (editor M.N. Hill). pp.665-727, Interscience

Barnes, S.S. (1967) Minor element composition of ferromanganese nodules. Science 157, 63-66.

Barth, T.W. (1952) Theoretical Petrology. pp. 367-379. Wiley

Bostrom, K. (1970) Deposition of manganese rich sediments during glacial periods. Nature 226, 629-630.

Brown, B.A. (1971) A geochemical investigation of inter-element relations in deep sea ferromanganese nodules. Ph.D. Thesis, Oxford University.

Burns, R.G. (1965) Formation of cobalt(III) in the amorphous $FeOOH \cdot nH_2O$ phase of manganese nodules. Nature 205, p. 999.

Burns, R.G. and Fuerstenau, D.W. (1966) Electron-probe determinations of inter-element relationships in manganese nodules. Am. Miner. 51, 895-902.

Calvert, S.E. and Price, N.B. (1970) Composition of manganese nodules and manganese carbonates from Loch Fyne, Scotland. Contr. Miner. Petrol. 29, 215-233.

Carvajal, M.C. and Landergren, S. (1969) Marine sedimentation processes. The inter-relationships of manganese, cobalt, and nickel. Stockh. Contr. Geol. 18, 99-122.

Cronan, D.S. (1967) The geochemistry of some manganese nodules and associated pelagic sediments. Ph.D. Thesis, Univ. of London.

Cronan, D.S. (1969) Inter-element associations in some pelagic deposits. Chem. Geol. 5, 99-106.

Cronan, D.S. and Tooms, J.S. (1967) Geochemistry of manganese nodules from the N.W. Indian Ocean. Deep-Sea Res. 14, 239-249.

Cronan, D.S. and Tooms, J.S. (1968) A microscopic and electron probe investigation of manganese nodules from the Northwest Indian Ocean. Deep-Sea Res. 15, 215-223.

Cronan, D.S. and Tooms, J.S. (1969) The geochemistry of manganese nodules and associated pelagic deposits from the Pacific and Indian Oceans. Deep-Sea Res., 16, 335-359.

Dasch, E.J., Dymond, J.R. and Heath, G.R. (1971) Isotopic analysis of metalliferous sediment from the East Pacific Rise. Earth Planet. Sci. Lett. 13, 175-180.

Friedrich, G., Rosner, B. and Demirsog, S. (1969) Erzmikroskopische und mikro-analytische Untersuchungen an Manganerzkonkretionen aus dem Pazifischen Ozean. Mineral. Deposita 4, 298-307.

Garrels, R.M. and Thompson, M.E. (1962) A chemical model for sea water. Amer. J. Sci. 260, 57-66.

Goldberg, E.D. (1954) Marine Geochemistry, 1. Chemical scavengers of the sea. J. Geol. 62, 249-265.

Goldberg, E.D. and Arrhenius, G.O.S. (1958) Chemistry of Pacific pelagic sediments. Geochim. Cosmochim. Acta 13, 153-212.

Goldschmidt, V.M. (1937) The principles of distribution of chemical elements in minerals and rocks. J. Chem. Soc., p. 655-674

James, R.O. and Healy, T.W. (1972) Adsorption of hydrolyzable metal ions at the oxide-water interface, III. A thermodynamic model of adsorption. J. Colloid.Interface Sci. 40, 65-81.

Krauskopf, K.B. (1956) Factors controlling the concentrations of thirteen rare metals in sea-water. Geochim. Cosmochim. Acta 9, 1-32B.

Latimer, W.M. (1952) Oxidation Potentials. 352 pp. Prentice-Hall.

Menard, H.W., Goldberg, E.D. and Hawkes, H.E. (1964) Composition of Pacific sea-floor manganese nodules. Scripps Inst. of Oceanography, Unpublished Report.

Mero, J. L. (1965) The mineral resources of the sea, 312 pp. Elsevier, Amsterdam.

Rankama, K. and Sahama, Th.G. (1950) Geochemistry., 911 pp. Univ. of Chicago Press.

Riley, J.P. and Chester, R. (1972) Introduction to marine chemistry. 465 pp. Academic Press, New York.

Riley, J.P. and Sinhaseni, P. (1958) Chemical composition of three manganese nodules from the Pacific Ocean. J. Mar. Res. 17, 466-482.

Sayles, F.L. and Bischoff, J.L. (1973) Ferromanganoan sediments in the Equatorial East Pacific. Earth Planet. Sci. Lett. In press.

Sevast'yanov, V.F. and Valkov, I.I. (1966) Chemical composition of iron-manganese concretions of the Black Sea. Dokl. Akad. Nauk. SSR 166, 701-704. (In Russian).

Sillen, L. G. and Martell, A.E. (1964) Stability Constants. London: The Chemical Society Burlington House

Spencer, D. W. and Brewer, P. G. (1970) Analytical methods in oceanography, 1. Inorganic methods. CRC Critical Reviews in Solid State Sciences, 409-478.

Spencer, D.W., Brewer, P.G. and Sachs, P.L. (1972) Aspects of the distribution and trace element composition of suspended matter in the Black Sea. Geochim. Cosmochim. Acta 36, 71-86.

Stumm, W., Huang, C.P. and Jenkins, S.R. (1970) Specific chemical interaction affecting the stability of dispersed systems. Croatica Chemica Acta 42, 223-245.

Turekian, K.K. and Imbrie, J. (1966) The distribution of trace elements in deep sea sediments of the Atlantic Ocean. Earth Planet. Sci. Lett. 1, 161-168.

Watson, J.A. and Angino, E.E. (1969) Iron rich layers in sediments from the Gulf of Mexico. J. Sed. Pet. 39, 1412-1419.

Willis, J.P. and Ahrens, L.H. (1962) Some investigations on the composition of manganese nodules, with particular reference to certain trace elements. Geochim. Cosmochim. Acta 26, 751-764.

CHAPTER 2

THE SURFACE CHEMISTRY OF HYDROUS MANGANESE DIOXIDE

Abstract

An experimental investigation has shown that H^+ and OH^- are potential-determining ions for the δMnO_2 surface. The pH(ZPC) was determined using electrophoretic mobilities and Na^+ and K^+ adsorption and found to be 2.25. Alkalimetric titration curves failed to provide a direct determination of the pH(ZPC); however, when combined with the Na^+ adsorption data, they provide a means for estimating the surface charge. Surface charge values of approximately -100 $\mu coul/cm^2$ were found at pH 8, considerably higher than the charge on SiO_2 which has a a similar pH(ZPC).

Below pH 3.5 manganese was released to solution, and the experimental data suggest that this is due to the reduction of MnO_2. δMnO_2 is thermodynamically unstable with respect to H_2O below that pH.

I. INTRODUCTION

Manganese dioxide is an import phase in marine geochemistry. Together with hydrous iron oxide, it is a major component of manganese nodules, ranging from 11 to 63% by weight (Mero 1965). It has also been found to be an important component in the sediments of the East Pacific Rise where Bostrom and Peterson (1969) have suggested that it is the result of precipitation following the injection of volcanic emanations into the seawater near the crest of the rise. In another context, Spencer and Brewer (1972) have found relatively high concentrations of suspended manganese just above the oxic-anoxic interface in the Black Sea.

In sedimentary materials, positive correlations between manganese and other elements are common (Riley and Sinhaseni 1958, Cronan 1969), and adsorption onto the manganese dioxide surface is one of the mechanisms frequently proposed to explain these relationships (Goldberg 1954, Krauskopf 1956, Jenne 1968). Unfortunately, relatively little is known about the electrochemistry of the manganese dioxide surface that can be used to evaluate this explanation. In fact, several different factors, such as the source of the elements and the structures of the minerals present, could also explain some of these correlations.

The nature of the electrochemical double layer separating metal oxides from aqueous solution has been studied for a number of metal oxides. DeBruyn and Stumm and their co-workers have been especially successful in looking at the oxide-solution interface in the same way that an electrochemist views the interface at a polarized electrode (Grahame 1947). Construction of reversible metal oxide electrodes is not always feasible

(Covington et al. 1963), and when direct measurement of the double layer parameters is not possible, the reversible interface model can be used (Stumm et al. 1970). The distinction between the reversible interface (metal oxides) and the polarizable interface (Hg) is a function of the mechanism by which the separation of charge originates. For a polarizable interface, the potential difference across the double layer is applied externally using a potentiometer. The change in electrostatic potential across the reversible interface results from the transfer of potential-determining ions across the solid-solution interface.

For the reversible metal oxide interface, it has been observed that hydrogen and hydroxyl ions play a unique role in determining the sign and magnitude of the surface charge and are, thus, the potential-determining ions for the surface (Berube and deBruyn 1968). As a consequence, metal oxides can be characterized by a solution pH for which the charge on the surface is zero. This pH, the pH(ZPC) (at the zero point of charge), is a convenient reference point that characterizes the amphoteric nature of the metal oxide. For a pH below the pH(ZPC), the surface charge is positive, and for a pH above the pH(ZPC), the surface charge is negative. Furthermore, the pH(ZPC) is useful in predicting the nature of the surface reactions (Stumm et al. 1970) since it is a function of the acidity of the central metal ion and the electrostatic field strength of the solid (Healy et al. 1966).

Healy et al.(1966) determined the pH(ZPC) for a number of different crystal modifications of manganese dioxides using electrophoresis and coagulation techniques and found that it ranged from 1.5 for Mn(II)-Manganite to 5.0 for βMnO_2. Several adsorption experiments have been performed using

a variety of inorganic electrolytes (Gabano et al. 1965, Murray et al. 1968, Possejt et al. 1968, Kozawa 1959). In particular, Morgan and Stumm (1964) have reported measuring directly the adsorption of H^+ and OH^- ions using the alkalimetric titration method initially used by Parks and deBruyn (1962) to study the ferric oxide-solution interface. However, Morgan and Stumm's results were incomplete in that the net OH^- bound to the solid as a function of pH was obtained at only one ionic strength. The values that have been reported for pH(ZPC) of hydrous manganese dioxides (δMnO_2-Mn(II)-Manganite) range from 1.5 to 4.5. Some of this variation could be due to the effect of crystal structure on the polarization of the surface as noted by Healy and Fuerstenau (1965). However, an equally important source of variation may be the sample preparation and subsequent aging effects, and neither has been well documented in the literature.

In order to evaluate the sign and magnitude of the charge on the hydrous manganese dioxide (δMnO_2) surface and to evaluate possible roles adsorption and/or reaction play in metal ion enrichments and correlations, a detailed study of the δMnO_2- solution interface has been undertaken. In this paper, the direct measurement of the adsorption density of H^+ (OH^-) ions on a preparation of δMnO_2 and the use of these measurements to construct a model for the electrochemical double layer at the surface are described and discussed.

II. MATERIALS AND METHODS

A. Preparation of MnO_2

In any surface chemistry experiment, it is important that the history of the sample be described thoroughly, because the dehydration of the

surface with drying or aging while in solution can have a pronounced effect on the location of the pH(ZPC) of the solid (Parks 1965).

The manganese dioxide used in these experiments was prepared by the oxidation of manganous ion by permanganate.

$$3\,Mn^{+2} + 2\,MnO_4^- + 10\,H_2O = 5\,MnO_2 + 4\,H^+ \qquad (1)$$

A known amount of $NaMnO_4$ (Mallinkrodt, reagent grade) was added to a 4-liter Erlenmeyer flask. An equivalent amount of base (NaOH) was added initially to neutralize the acid that is evolved by the above reaction and to keep the pH of the solution basic throughout the preparation. This tends to create a situation kinetically favoring the oxidation of Mn(II) (Morgan and Stumm 1964). Distilled water was added to bring the volume up to approximately 3 liters, and then the required stoichiometric amount of standardized $MnCl_2$ (B & A, reagent grade) was added dropwise while the entire solution was well mixed with a magnetic stirrer. The $NaMnO_4$ was standardized using sodium oxalate (Skoog and West 1963 , p.437) and the $MnCl_2$ was standardized using the method of Lingane and Karplus (1946). Several suspensions of MnO_2 were prepared at a concentration level of 5×10^{-3}M. The colloidal MnO_2 was allowed to settle, and the supernatant was removed and replaced with distilled H_2O. This washing procedure was repeated until the ionic strength was approximately 1×10^{-4}M. After the final removal of the supernatant, the MnO_2 was transferred to a 4-liter Erlenmeyer flask. This preparation and transfer procedure was repeated until the final 4-liter stock suspension contained 4.8×10^{-2}M MnO_2. The stock suspension was well mixed before each experiment, and then a suitable

aliquot was withdrawn. Twenty-five ml aliquots (containing 0.106 gms of MnO_2) of the stock suspension were used for the majority of the experiments described in this paper. To prevent possible dehydration of the surface due to drying, the MnO_2 was kept in suspension at all times.

B. Characterization of the MnO_2

The stoichiometry of the hydrous manganese dioxide was determined by using the O-tolidine method (Morgan and Stumm 1965)(Appendix II-A). The X-ray powder and oriented diffraction patterns were obtained using Cu radiation with a curved crystal monochromator to reduce secondary X-ray fluorescence (Appendix II-B).

The surface area was obtained by using the B.E.T. (Brunaeur et al. 1938) and t-plot (deBoer et al. 1966) methods (Appendix II-C). To obtain a suitable sample for these measurements, a suspension of MnO_2 was centrifuged, and the separated MnO_2 colloid was freeze-dried. The sample was resuspended in acetone and dried again under vacuum. The gas adsorption data were obtained using N_2 gas with a He carrier.

C. Location of the pH(ZPC)

In order to determine the amounts of Na^+ and K^+ adsorbed as a function of pH, suspensions of MnO_2 were spiked with NaCl and KCl. The pH of the suspensions was adjusted by dropwise addition of 3N NH_4OH. After equilibration, suitable aliquots of the suspensions were withdrawn, filtered and analyzed by atomic absorption spectrometry.

The electrophoretic mobilities were measured using a Briggs microelectrophoresis cell. The electrochemical cell can be represented by

(Pt), Hg, $Hg(NO_3)_2$, KNO_3 / suspension / KNO_3, $Hg(NO_3)_2$, Hg (Pt)

and the mobility was calculated as

$$U = \frac{d\,X}{i\,R_s\,T} \qquad (2)$$

where U = mobility (micrometer sec^{-1})/(volt cm^{-1})

i = applied d.c. current (amps)

R_s = specific resistance (ohm-cm)

$\bar{T}$ = average time for a particle to travel 69 micrometers (sec)
d = distance across grid (69 micrometers)
X = cross sectional area of cell (cm^2)

The alkalimetric titrations were performed using 25 ml of the MnO_2 stock suspension. After adjustment of the ionic strength using NaCl, the total volume was brought to 200 ml. The acid and base portions of the titration curves were done in different experiments. Small aliquots (0.03 - 0.15 ml) of standardized 0.1M HCl or 0.1M NaOH were added to the titration cell and the pH read after 2 minutes. The blank titrations were prepared in an identical manner. The MnO_2 was removed by centrifugation and the titration was performed on the supernatant solution. To calculate the adsorption density, the pH values were corrected to concentrations using the Debye-Huckel equation.

III. RESULTS

A. Characterization of the MnO_2

The stoichiometry of the hydrous manganese dioxide was found to be $MnO_{1.92}$. X-ray diffraction patterns of the air-dried (25^o) oxide showed a low degree of crystallinity with reflections at approximately 7.4 Å, 4.04 Å, 2.43 Å and 1.63 Å. The stoichiometry and X-ray analyses indicate that this synthetic manganese dioxide is similar structurally to the naturally occurring mineral birnesite (Jones and Milne 1956) and the synthetic products studied by Giovanoli et al. (1969,1970) called manganate-IV, by Morgan (1964) called δMnO_2, and by Healy et al. (1966) called Mn(II)-Manganite. For ease of reference, the manganese dioxide used in these experiments will be referred to as δMnO_2.

Transmission electron microscope pictures (Figure 1) show that the particles of δMnO_2 range from 0.2 to 1.0μ and appear to be aggregates of much smaller, spherically shaped, particles. Triplicate measurements of the surface area gave a value of 263 ± 5 m^2/gm by the B.E.T. method. A t-plot calculated from the N_2 adsorption data gave a surface area of 270 m^2/g .

B. Electrophoretic Mobilities

The electrophoresis measurements were made at low ionic strength (1×10^{-4}M) except below pH 4 where the ionic strength was controlled by the strong acid added to adjust the pH. The surface area of δMnO_2 used was 1.15m^2/l. Measurements were not possible for pH values less than about 2.5, because the combined effects of the reduction in surface charge and increase in ionic strength made the δMnO_2 suspension unstable causing the colloidal particles to settle out of the plane of focus. The calculated electrophoretic mobilities are plotted against pH in Figure 2. A positive mobility was never observed. The mobilities were strongly negative over most of the pH range and decreased rapidly below about pH 4. Extrapolation of the electrophoretic mobilities to zero gives a maximum value for the pH(ZPC) of 2.40. The strong dependence of the mobility on pH supports the model that H^+ and OH^- are potential-determining ions for the δMnO_2 surface.

C. Na^+ and K^+ Adsorption

The adsorption of Na^+ and K^+ was also used as an independent check on the location of the pH(ZPC). Assuming that the interaction of Na^+ and K^+ with the δMnO_2 surface is completely electrostatic, these cations should be completely desorbed at the pH(ZPC). The amounts of Na^+ and K^+ adsorbed as a function of pH are shown in Figure 2. Na^+ and K^+ were completely

desorbed from the surface at pH 2.25 and 2.15 respectively. The kinetics of adsorption and desorption were rapid and completely reversible.

D. Alkalimetric Titration Curves

1) Kinetics

Before undertaking the alkalimetric titration experiments on the δMnO_2 surface, it was necessary to evaluate the rate of response of the surface to the addition of various amounts of acid or base. Berube et al. (1967) have found that the reaction of protons with the metal oxide surface appears to be a two-step process. For pH values greater than the pH(ZPC), an aliquot of base produced a rapid rise in pH (although not as large a rise as would take place in an unbuffered solution), followed by a slow downward drift. The slow drift was found to last about 80 hours for Fe_2O_3 and 800 hours for TiO_2. A similarly rapid drop in pH occurred after the addition of acid for pH values less than the pH(ZPC). However, the occurrence of the slow step was only found for Fe_2O_3. Figure 3 shows the long term drift after the pH has been adjusted from 3.25 to 8.4. Equilibrium, in this example, appears to have been reached after 200 hours. In Figure 4, the H^+ ion activity is plotted against the square root of time ($t^{\frac{1}{2}}$). After rapid equilibration of the solution with the surface following the addition of base, protons are released to the bulk solution (or OH^- is consumed by the surface) giving a linear response against $t^{\frac{1}{2}}$ for approximately 10 minutes, whereupon the drift assumes an exponential character. Similar time plots have been used by others (Gallagher and Phillips 1968, Wyttenback 1961, Luce et al. 1972, Berube et al. 1967) to demonstrate diffusion controlled processes.

Berube and de Bruyn (1968) and Onoda et al. (1967) showed that if the titration is performed fast enough, the slow, diffusion controlled step may be suppressed. They concluded that under these conditions the experimental results should reflect only changes characteristic of a surface process. In this study, the short-term response of the δMnO_2 surface after the addition of small aliquots of base was found to be rapid, and as a result of adding small aliquots, the pH drift was minimized. When the titrations were performed with the aliquots (.05 - .15 ml) of base and acid added at regular two-minute intervals, they were found to be reversible to within 0.1 pH units.

2) Titration Curves

Recording the pH during the course of a titration of a suspension of δMnO_2 provides data that can be interpreted in terms of adsorption of hydrogen or hydroxyl ions. The adsorption density ($\Gamma_{H^+}^* - \Gamma_{OH^-}^*$) is obtained from a mass balance between the titration curve of the suspension and that of the supernatant of the suspension.

$$\frac{C_B - C_A + [H^+] - [OH^-]}{s} = \Gamma_{OH^-}^* - \Gamma_{H^+}^* = \frac{\sigma_o}{F} \qquad (3)$$

C_B = concentration of strong base

C_A = concentration of strong acid

S = surface area (cm^2)

Γ^* = specific adsorption density ($\frac{\text{equivalents}}{cm^2}$)

$[H^+]$, $[OH^-]$ = concentration of H^+ and OH^-

σo = surface charge ($coul/cm^2$)

F = Faraday constant (9.65×10^4 coul/eq.).

The quantity of acid or base that cannot be balanced in the solution phase and is present in the system is ascribed to the surface. Figure 5 shows the alkalimetric titration curves, and Figure 6 the net adsorption curves for the δMnO_2 surface at several different ionic strengths. The net adsorption curves result from subtracting the blank titration curves (Figure 5b) from the suspension titration curves (Figure 5a). Such a procedure takes into account any strong acid or strong base present in the system. The error in subtracting these curves increases at low pH values because of the decrease in slope.

3) Extrapolation of Titration Curves

The surface charge is conventionally calculated relative to the intersection of the titration curves determined at different ionic strengths (Parks and de Bruyn 1962). This intersection generally agrees well (except in the presence of specifically adsorbable cations or anions) with the pH(ZPC) located by other methods such as electrophoresis. For δMnO_2, the pH(ZPC) located by electrophoresis and Na^+ and K^+ adsorption cannot be reached by the alkalimetric titration method used. Thus, the surface charge calculated directly from the data gives only a minimum value as the correct value must be calculated from the pH(ZPC). In order to obtain a quantitative value for the surface charge, an alternate method must be used for extending the net titration curves to the pH(ZPC).

In this instance, the adsorption of Na^+ has been found to be a suitable means of extrapolating the titration curves. For a charged solid-solution interface, the surface charge on the solution side is equal but opposite in sign to the charge on the solid (Stumm and Morgan 1970, p. 459). When the surface is negatively charged, the charge on the solution side

is given by the sum of σ^+ (charge due to a surplus of cations) and σ^- (charge due to a deficiency of anions) in the absence of specific adsorption.

$$\sigma_{solution} = (\sigma^+ + \sigma^-) \qquad (4)$$

Assuming that both Cl^- and Na^+ react non-specifically with the surface and that the number of equivalents of Na^+ adsorbed on the surface equals the number of equivalents of Cl^- desorbed, the surface charge can be approximated at constant ionic strength and low surface potentials by:

$$\sigma_{surface} = F\,(2\,\Gamma_{Na^+}^{*}) \qquad (5)$$

Figure 7 shows the net titration curves for δMnO_2 extrapolated to pH 2.25 on the basis of measurements of Na^+ adsorption for $I = 10^{-3}$M and $I = 10^{-2}$M. The surface charge has been calculated relative to this intersection. The data in Figure 7 might also be described by the charge balance equation:

$$\Gamma_{OH^-}^{*} - \Gamma_{H^+}^{*} = \Gamma_{Cl^-}^{*} - \Gamma_{Na^+}^{*}$$

however, electrophoresis experiments showed that the mobility was controlled by the pH and that variations in the NaCl concentration had little effect. Thus, it appears that the interaction of Na^+ and Cl^- with MnO_2 is in response to the charged surface that is produced by the dissociation of surface protons.

4) Aging

The alkalimetric titration experiments were repeated after one month, and it was found that the volume of base that must be added to reach a given pH had decreased by approximately 10 - 15%. Parks (1965) has noted that treatment likely to lead to bulk or surface dehydration often results in more acid pH(ZPC). It is likely that the decrease observed above is due to the aging of the freshly precipitated "active" form of δMnO_2.

IV. DISCUSSION

The thermodynamics and coordination chemistry of the metal oxide-electrolyte interface have been described in detail (Parks and de Bruyn 1962, de Bruyn and Agar 1962, Berube and de Bruyn 1968, Atkinson et al. 1967, Stumm et al. 1970).

The origin of the charge at the metal oxide-solution interface is viewed as a two-step process. The surface hydrates by pulling H^+ ions, OH^- ions or water molecules from solution as the surface atoms attempt to complete their coordination. The metal hydroxide groups formed in this manner participate in acid-base reactions to produce a positively or negatively charged surface. The surface metal hydroxide groups can either dissociate or accept H^+ or OH^- ions.

$$-Me\text{-}OH^0 + H_2O = -Me\text{-}O^- + H_3O^+ \quad \text{or}$$

$$-Me\text{-}OH^0 + OH^- = -Me\text{-}(OH)_2^- \qquad (6)$$

$$-Me\text{-}OH^0 + H_3O^+ = -Me\text{-}OH_2^+ + H_2O \quad \text{or}$$

$$-Me\text{-}OH^0 = -Me^{+} + OH^- \qquad (7)$$

It is impossible to determine experimentally whether the reaction is due to the adsorption of H^+ and OH^- ions or to the dissociation of surface sites. The exact location of the pH(ZPC) will depend on the relative acidity of the surface groups,

$$Me\text{-}OH_2^+ \underset{K_1}{=} Me\text{-}OH^\circ + H^+ \underset{K_2}{=} Me\text{-}O^- + 2H^+ \qquad (8)$$

and the pH(ZPC) will lie at the pH value for which an equal number of

$Me\text{-}OH_2^+$ and $Me\text{-}O^-$ groups are present, i.e. when the surface is uncharged. Using reaction (8), the pH(ZPC) will be characterized by:

$$[Me\text{-}OH_2^+] = [Me\text{-}O^-]$$

and $$H^+_{ZPC} = K_1K_2^{1/2} \quad \text{or} \quad pH(ZPC) = 1/2(pK_1 + pK_2) \qquad (9)$$

where K_1 and K_2 define the acidity constants of the surface sites (Stumm et al. 1970). The location of the pH(ZPC) will thus depend on such factors as the acidity of the metal ion and the electrostatic field strength of the solid (Healy et al. 1966, Healy and Fuerstenau 1965). Table 1 compares the pH(ZPC) of several metal oxides. In general, the pH(ZPC) is inversely proportional to the charge of the metal (Parks 1965) and the size of the unit cell of the solid (Healy et al. 1966).

As shown in reactions (6) and (7), only H^+ and OH^- are potential-determining. This is a simplification of the more general model proposed by Parks and de Bruyn (1962) in which the establishment of the surface charge can also be explained by the adsorption from solution of dissolved metal hydrolysis species. If the affinity of all the dissolved metal hydrolysis species in equilibrium with a metal oxide for the surface of that metal oxide were equal, then one would expect good agreement between the pH(ZPC) and the isoelectric point of the complex solution.

The results of this study indicate that H^+ and OH^- are potential-determining ions for the δMnO_2 surface and that the pH(ZPC) is located at approximately pH 2.25. As δMnO_2 is highly insoluble ($K_{so} = 10^{-56}$) (Charlot and Bezier 1957), the adsorption from solution of dissolved Mn(IV) hydrolysis species can be neglected. The hydrolysis of Mn^{+2} can also be neglected as ${}^*K_1 = 10^{-10.6}$ (Perrin 1962). This low pH(ZPC) implies that, compared with most other metal oxides, δMnO_2

is a relatively strong acid. Combining reactions (6) and (7) gives an overall reaction for the surface of:

$$-Mn\text{-}OH_2^+ \text{ (surface)} = -Mn\text{-}O^- \text{(surface)} + 2H^+$$

which has an equilibrium constant of:

$$K_{12} = \frac{[-Mn\text{-}O^- \text{(surface)}]}{[-Mn\text{-}OH_2^+ \text{(surface)}]} \times \left(\frac{\gamma^-}{\gamma^+}\right) \alpha_{H^+}^{\ 2} \qquad (10)$$

where γ_-, γ_+ are the activity coefficients of the two surface sites, and α_{H^+} is the activity of hydrogen ions. Assuming that at the pH(ZPC) the positive and negative sites are equal and the activity coefficients for the sites are equal, $K_{12} = 10^{-4.5}$ for δMnO_2. This value compares with a K_{12} of 10^{-17} calculated in a similar manner for Fe_2O_3 (Parks and de Bruyn 1962) and shows that δMnO_2 attracts protons much less strongly than Fe_2O_3.

A more rigorous theoretical treatment of the δMnO_2 surface is not feasible because of the uncertainties in the extrapolation of the titration curves. An additional uncertainty is related to the assumption that H^+ and OH^- are the sole potential-determining ions. As discussed previously, the solubility of δMnO_2 is extremely low, and thus Mn(IV) solution species can be neglected. However, at low pH values, Mn is released to solution. Morgan (1964) reported that Mn(II) is released from δMnO_2 in acid solution, and he attributed this to H^+/Mn^{+2} exchange and to reduction of MnO_2 by H_2O. Figure 8 shows the release of Mn to solution versus time for suspensions adjusted to different initial pH values. With time, Mn was released to solution in increasing quantities suggesting that the release of Mn from the solid is not due to H^+/Mn^{+2} exchange. The release of Mn versus time

would decrease as the gradients decreased if it was diffusion controlled. That the release of Mn was not observed for any samples above pH 3.5 suggests an alternative mechanism for the release. Figure 9 shows a pE - pH diagram for manganese constructed with calculations using thermodynamic data available in Sillen and Martell (1964). From the relative positions of the $\delta MnO_2 - Mn^{+2}$ and O_2 - H_2O lines, it is apparent that MnO_2 becomes unstable with respect to the oxidation of water at pH values below 3.5. This suggests that the reduction of δMnO_2 by H_2O takes place liberating Mn^{+2},

$$\delta MnO_2(s) + 2H^+ = \tfrac{1}{2}O_2 + H_2O + Mn^{+2} \qquad (11)$$

This instability may be enhanced by Cl^-. For example, the reaction

$$\tfrac{1}{2}\,\delta MnO_2 + Cl^- + 2H^+ = \tfrac{1}{2}Mn^{+2} + \tfrac{1}{2}Cl_2 + H_2O;\ \log K = -2.6. \qquad (12)$$

might occur at low pH (W. Stumm, personal communication). Though there is a considerable time lag before any Mn can be detected in solution for pH values between 2 and 3, it is possible that small amounts of Mn^{+2} are released during the course of an alkalimetric titration and re-adsorbed specifically by the negative surface, thus acting as another potential-determining ion. As a consequence, the alkalimetric titration results cannot be used below pH 3.5 unless the assumption is made that the reduction is slow compared with the duration of the titrations. Participation of Mn^{+2} as a potential determining ion below pH 3.5 would mean that the location of the pH(ZPC) at 2.25 is not entirely due to reversible H^+ (OH^-) adsorption, thus indicating that δMnO_2 has even less affinity for protons than was previously calculated. The pH(ZPC) has been located for βMnO_2

using the alkalimetric titration method (Jenkins 1970), so it is reasonable to expect that H^+ and OH^- should be considered the potential-determining ions for δMnO_2 for pH values greater than 3.5.

Table 1 indicates that the material with a pH(ZPC) closely similar to that of δMnO_2 is SiO_2. Figure 10 compares the charge-versus-pH values for amorphous SiO_2 (pH(ZPC) = 3.0) obtained by Tadros and Lyklema (1968) with the charge-versus-pH data for δMnO_2 obtained in this paper. The calculated surface charge increases much more rapidly for δMnO_2, reaching approximately -100 μcoul/cm^2 by pH 8.0, demonstrating the much greater surface activity for δMnO_2 compared with SiO_2 even though they have similar pH(ZPC). A possible explanation for this difference is the fact that Mn^{+2} may be acting as a potential determining ion below pH 3.5.

It is also possible that although the pH(ZPC) of δMnO_2 is similar to that of SiO_2, its second intrinsic acidity constant K_2 for reaction (8) may be markedly different. Stumm and Morgan (1970) report that SiO_2 has an intrinsic acidity constant (pK_2) of about 6.8. Thus, this surface loses significant H^+ only above that pH. If pK_2 for δMnO_2 were markedly lower, (for example pK_2 = 3), then H^+ would be lost much earlier from δMnO_2 than from SiO_2.

This surface charge (-100 μcoul/m^2) is equivalent to 1 x 10^{-5} eq/m^2 or 260 meq/100g . The upper limit of the ion exchange capacities for kaolinite and smectite are 15 meq/100g and 150 meq/100g respectively (Grim 1968, p. 189). Thus at pH 8, δMnO_2 is almost twice as surface active as the most surface active clay mineral.

V. SUMMARY AND CONCLUSIONS

An experimental investigation of the pH(ZPC) and surface charge was made for a sample of hydrous manganese dioxide (δMnO_2). As for other metal

oxides, H^+ and OH^- were found to be potential-determining ions; however, below pH 3.5, Mn^{+2} may be acting as a potential-determining ion as well.

The alkalimetric titration curves failed to provide a unique location for the pH(ZPC). In order to locate the pH(ZPC), electrophoretic mobilities and Na^+ and K^+ adsorption measurements were used. These methods agreed well and gave a pH(ZPC) of approximately 2.25 for the sample studied. Once the pH(ZPC) was located, the net alkalimetric titration curves were extrapolated to that point using the adsorption of Na^+. The charge values calculated by this procedure give values of approximately -100 μcoul/cm^2 at pH 8, considerably higher than the charge on SiO_2, which has a similar pH(ZPC). The difference in surface charge for these two substances gives a possible explanation of why manganese rich sediments and manganese nodules have much larger concentrations of rare metals than silica rich sediments (Krauskopf 1956).

TABLE 1

COMPARISON OF THE pH OF ZPC FOR VARIOUS METAL OXIDES

OXIDE	pH(ZPC)	REFERENCE
WO_3	0.5	El Wakkad and Rizk (1957)
δMnO_2	2.25	This work
SiO_2 (qtz.)	2.0	Li (1958)
(amorphous)	3.5	Bolt (1957)
"	3.0	Tadros and Lyklema (1968)
TiO_2	6.0	Berube and de Bruyn (1968)
γ-Al_2O_3	7.6	Stumm, Huang and Jenkins (1970)
α-Fe_2O_3	8.5	Parks and de Bruyn (1962)
ZnO	8.9	Blok and de Bruyn (1970)
Ag_2O	11.2	Parks and de Bruyn (1962)

Figure 1

Transmission electron microscope photograph of δMnO_2

Magnification: 15,000 x

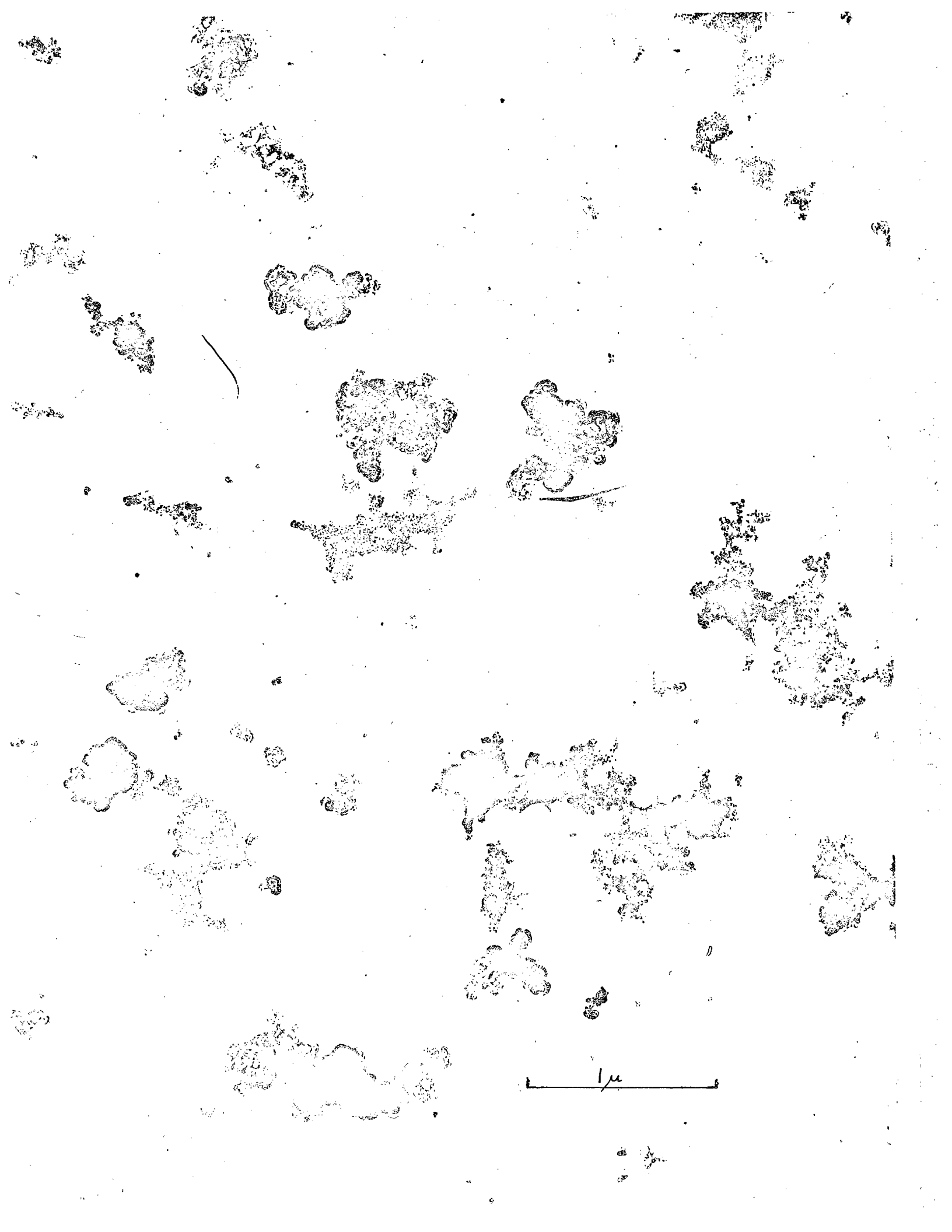
1μ

Figure 2

Electrophoretic mobilities and Na^+ and K^+ adsorption measurements for δMnO_2.

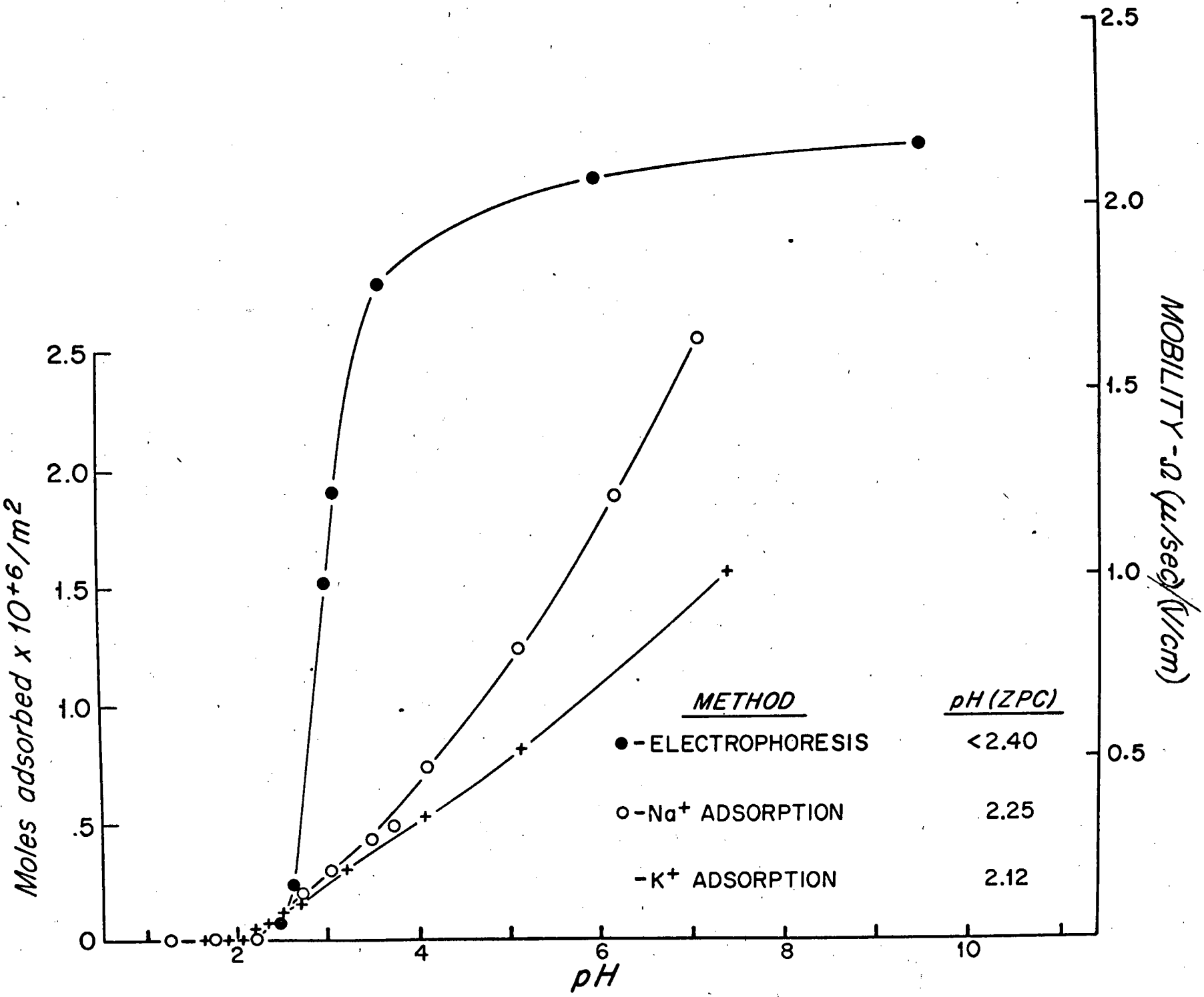
Moles adsorbed x 10+6/m2
MOBILITY-ζ (μ/sec)/(V/cm)
pH
2.5
2.0
1.5
1.0
.5
0
2
4
6
8
10
METHOD
pH (ZPC)
●-ELECTROPHORESIS
<2.40
o-Na+ ADSORPTION
2.25
-K+ ADSORPTION
2.12

Figure 3

Long-term pH Drift

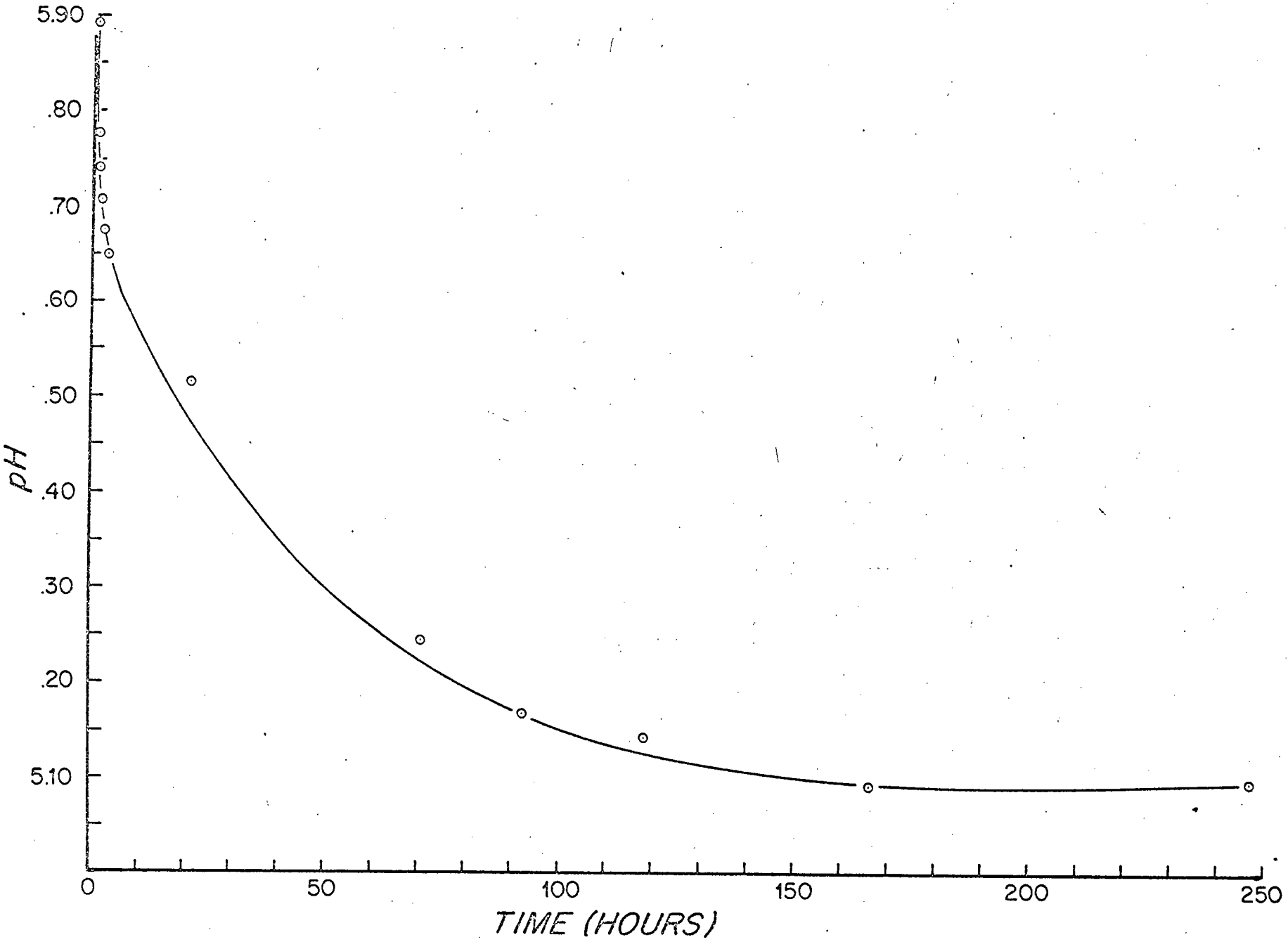
5.90
.80
.70
.60
.50
.40
.30
.20
5.10
pH
0
50
100
150
200
250
TIME (HOURS)

Figure 4

Change in H^+ concentration with $time^{\frac{1}{2}}$

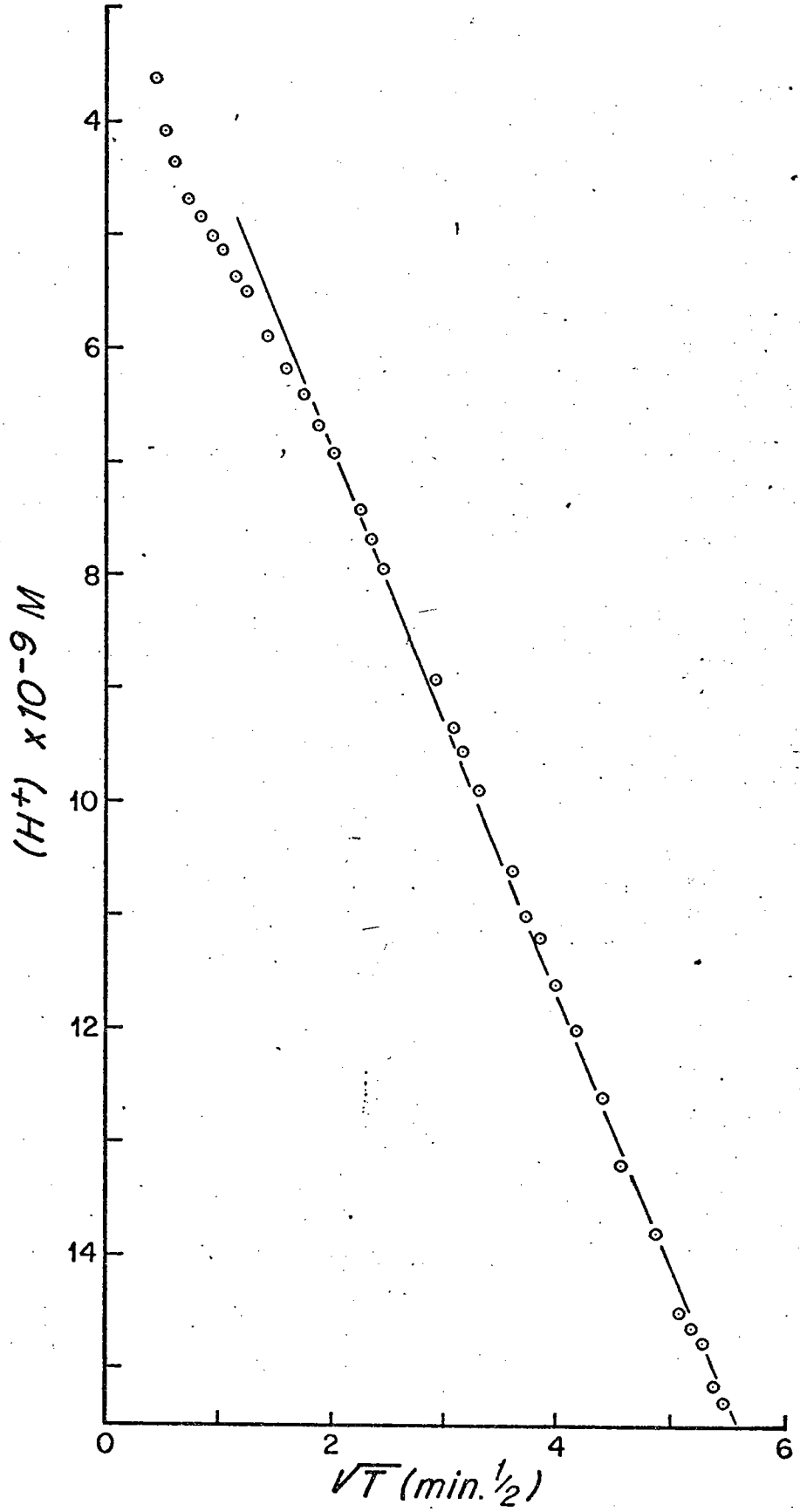
4
6
8
10
12
14
(H+) x10-9 M
0
2
4
6
√T (min.½)

Figure 5a

Alkalimetric titration curves for δMnO_2 at several ionic strengths. The titrations were performed using 0.1 g ($26m^2$) of δMnO_2, and the ionic strength was adjusted using NaCl. Total volume of the titration cell was 200 ml. The acid and base portions of the titration curves were done in different experiments.

Figure 5b

Blank titration curves performed on the supernatent solutions after the removal of the δMnO_2.

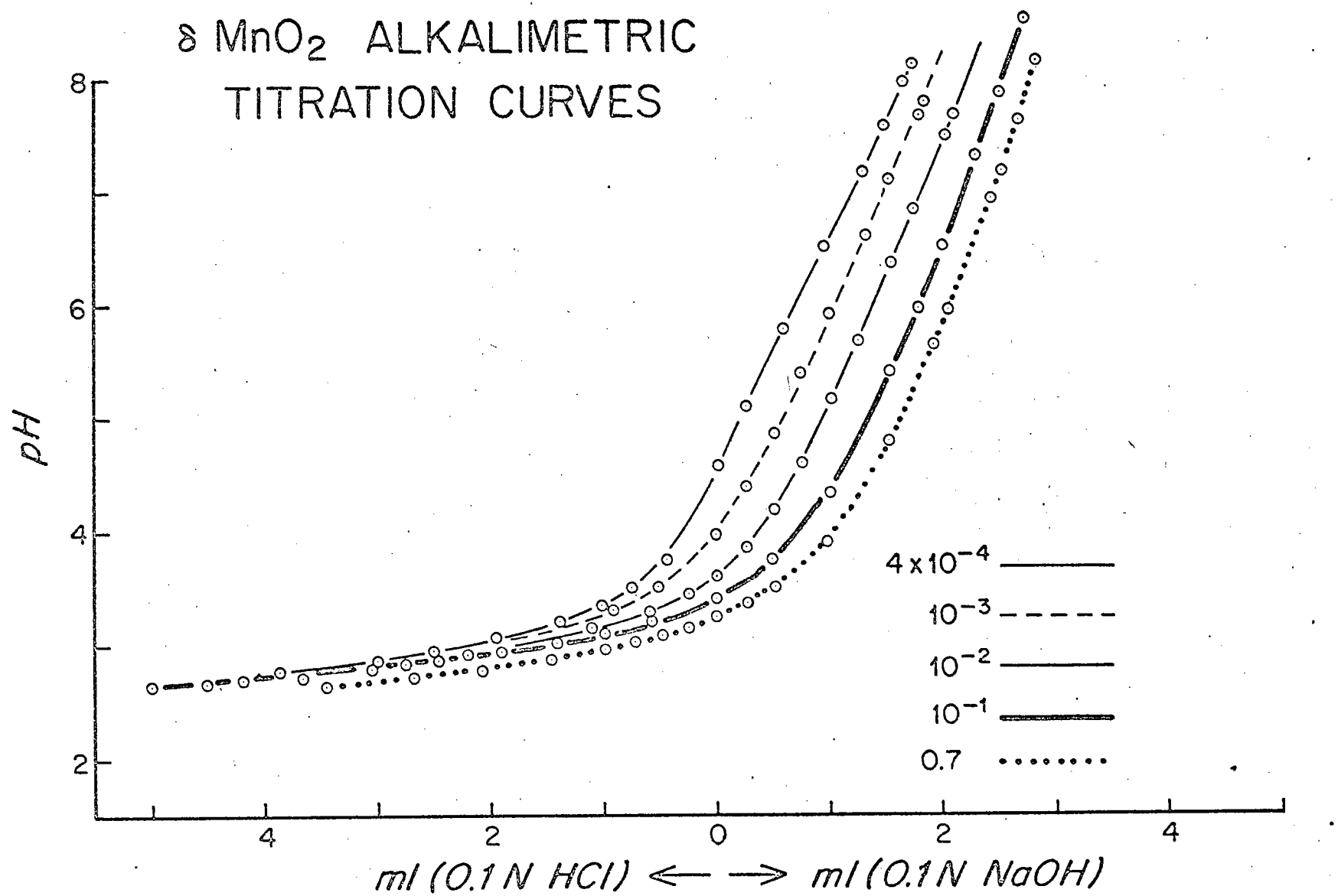
δ MnO2 ALKALIMETRIC
TITRATION CURVES
pH
8
6
4
2
4
2
0
2
4
ml (0.1 N HCl) ← → ml (0.1 N NaOH)
4 x 10⁻⁴
10⁻³
10⁻²
10⁻¹
0.7

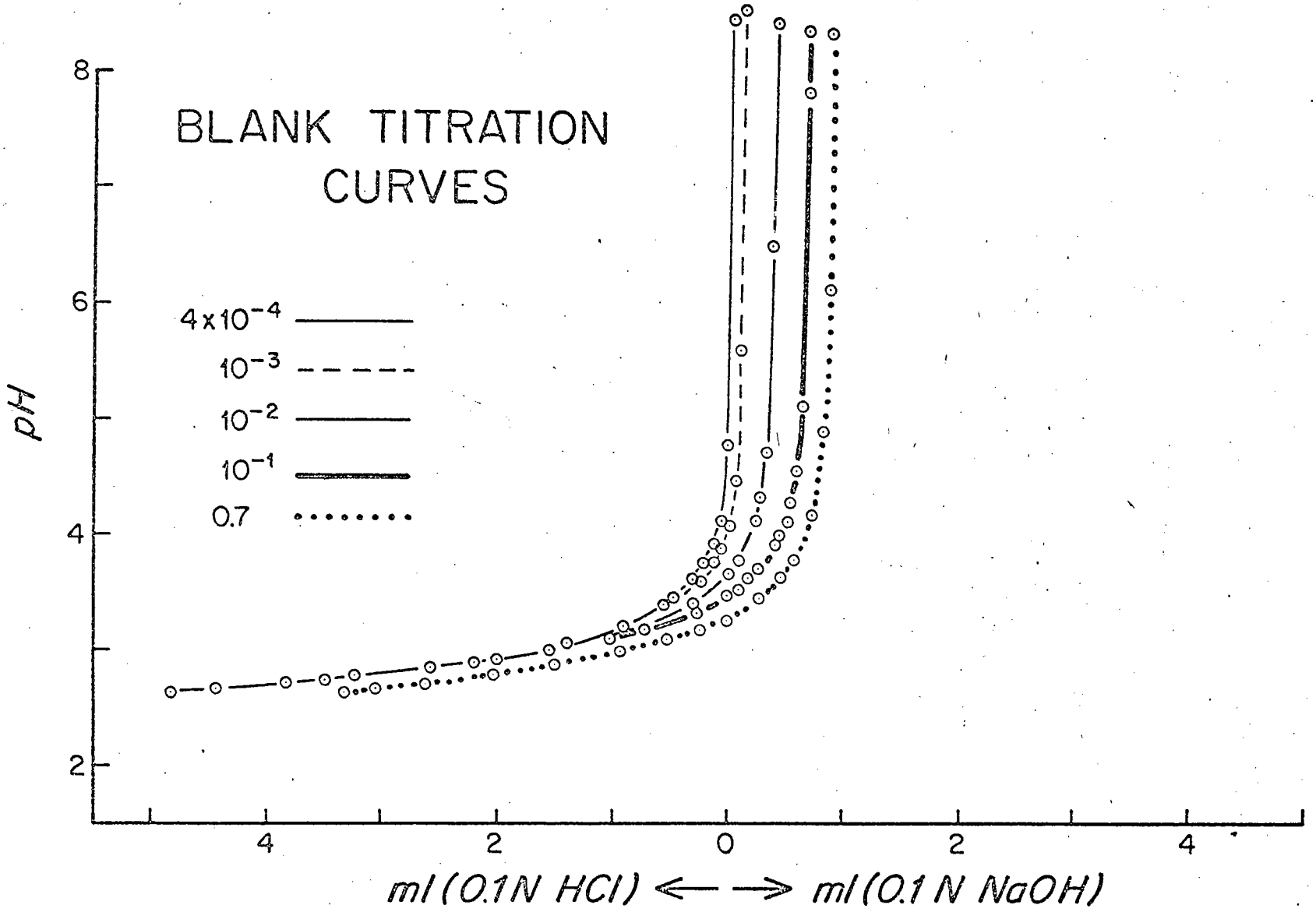
BLANK TITRATION CURVES
4x10⁻⁴
10⁻³
10⁻²
10⁻¹
0.7
pH
8
6
4
2
4
2
0
2
4
ml (0.1N HCl) ⟵ ⟶ ml (0.1 N NaOH)

Figure 6

Net alkalimetric titration curves for δMnO_2

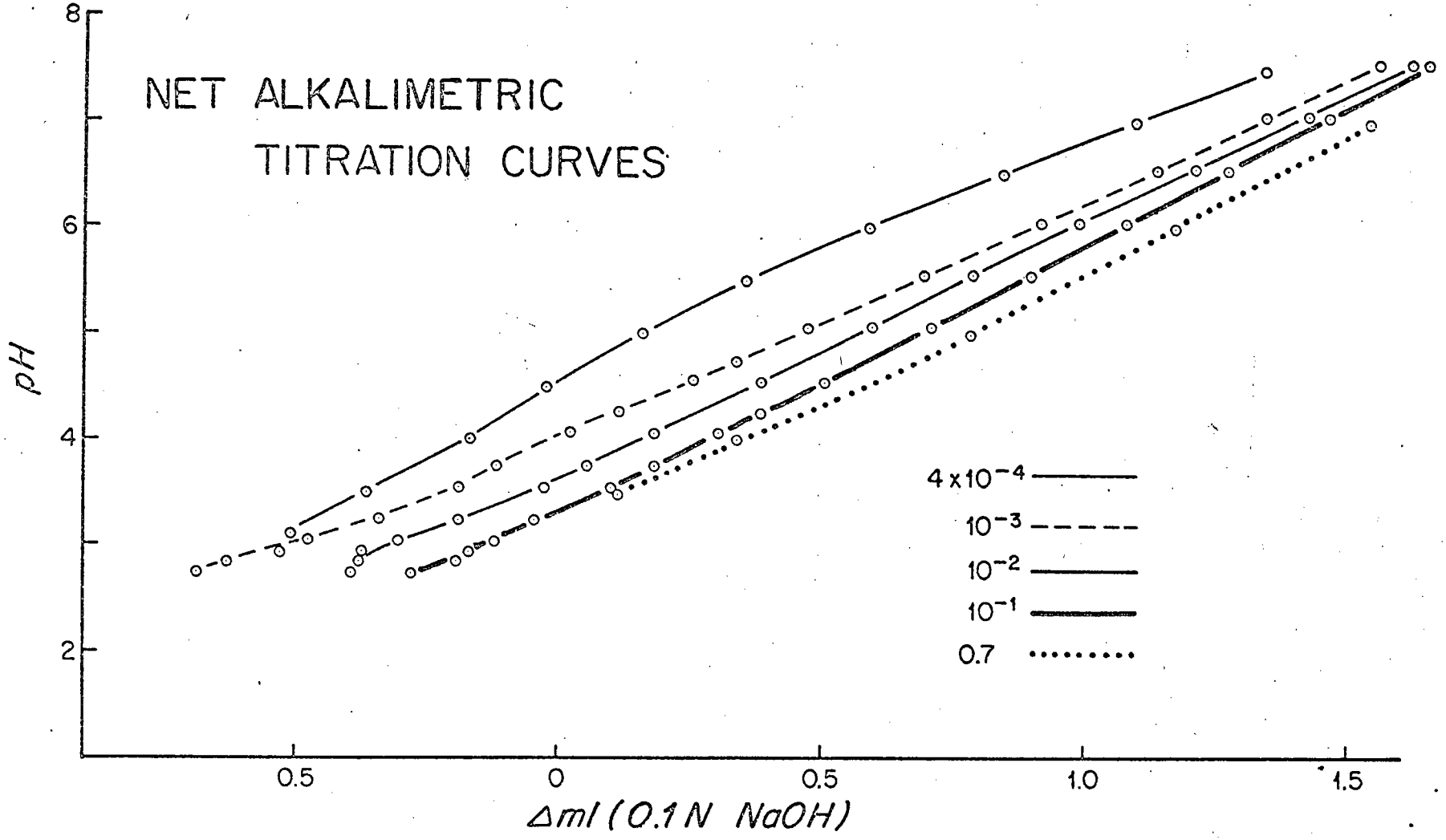
NET ALKALIMETRIC
TITRATION CURVES
pH
8
6
4
2
0.5
0
0.5
1.0
1.5
Δml (0.1 N NaOH)
4 x 10⁻⁴
10⁻³
10⁻²
10⁻¹
0.7

Figure 7

Surface charge calculations for the alkalimetric titration curves extrapolated to the pH(ZPC) using Na^+ adsorption data. Charge values in $\mu coul/cm^2$ were calculated relative to the intersection of the titration curves using equation 3.

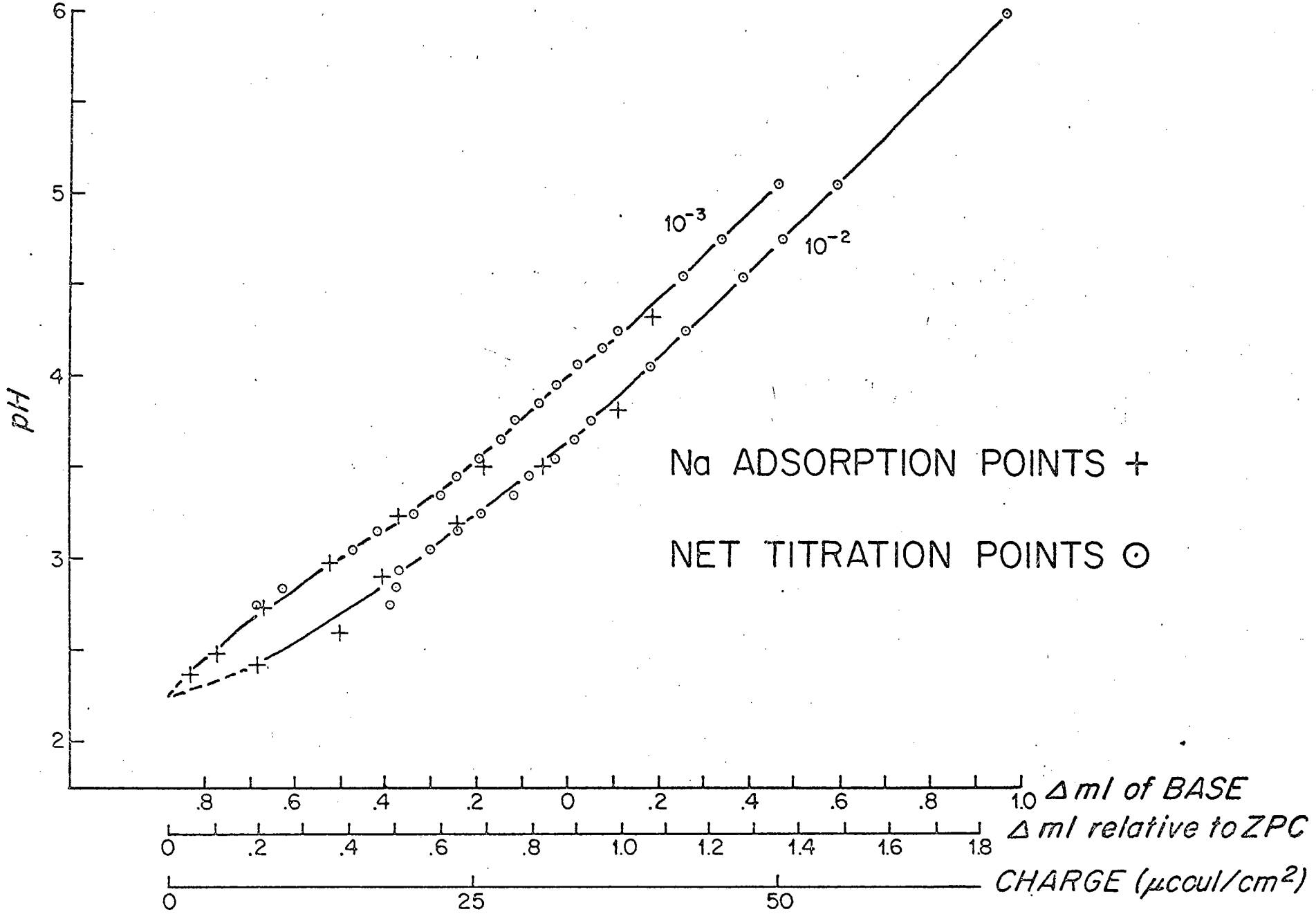
6
5
4
3
2
pH
10^{-3}
10^{-2}
Na ADSORPTION POINTS +
NET TITRATION POINTS ⊙
.8 .6 .4 .2 0 .2 .4 .6 .8 1.0
Δ ml of BASE
0 .2 .4 .6 .8 1.0 1.2 1.4 1.6 1.8
Δ ml relative to ZPC
0 25 50
CHARGE (μcoul/cm²)

Figure 8

The release of manganese to solution from suspensions of δMnO_2 adjusted to different initial pH values.

Curve	pH
I	1.50
II	2.30
III	2.45

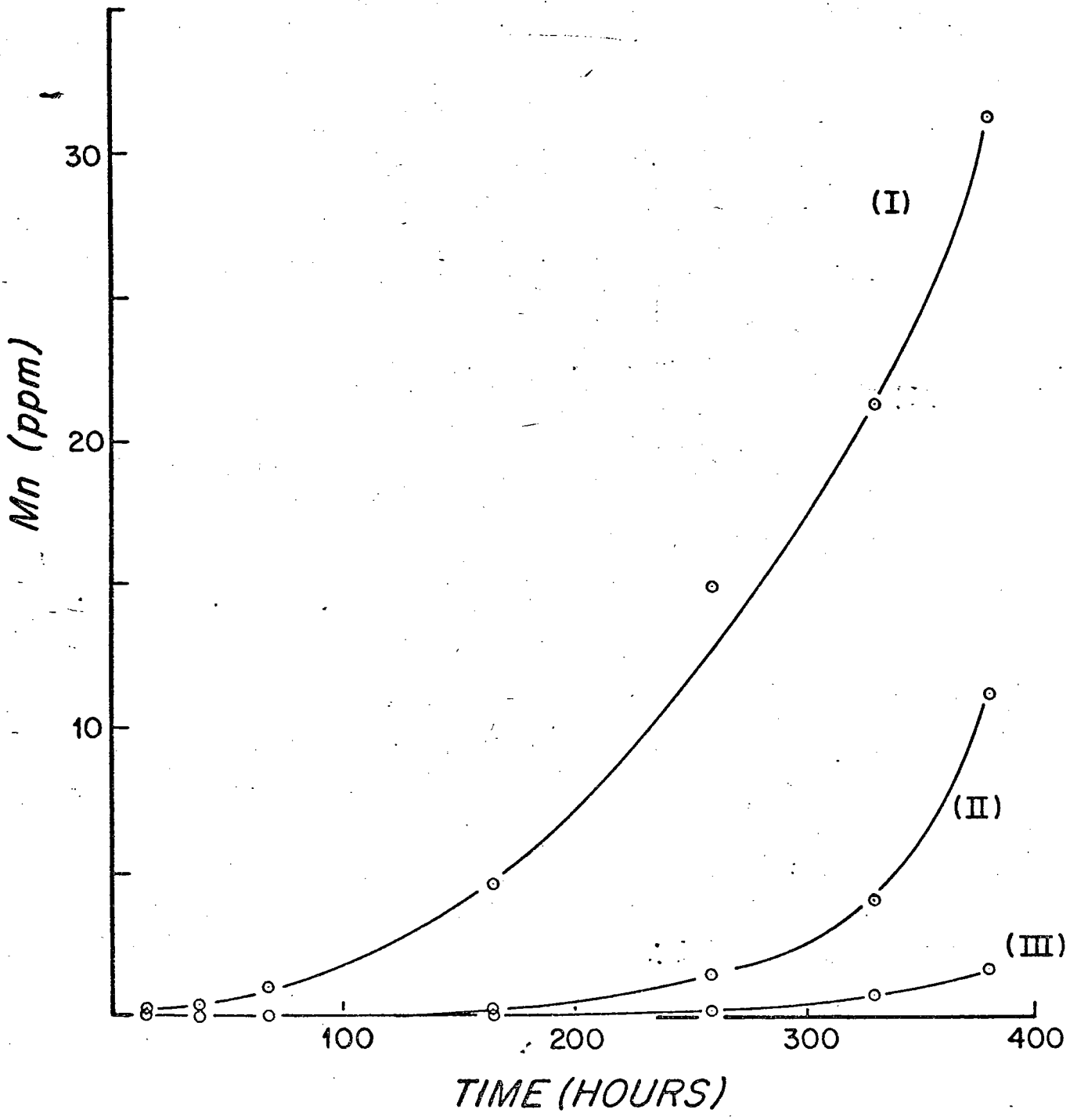
30
20
10
Mn (ppm)
(I)
(II)
(III)
100
200
300
400
TIME (HOURS)

Figure 9

pE - pH diagram for manganese

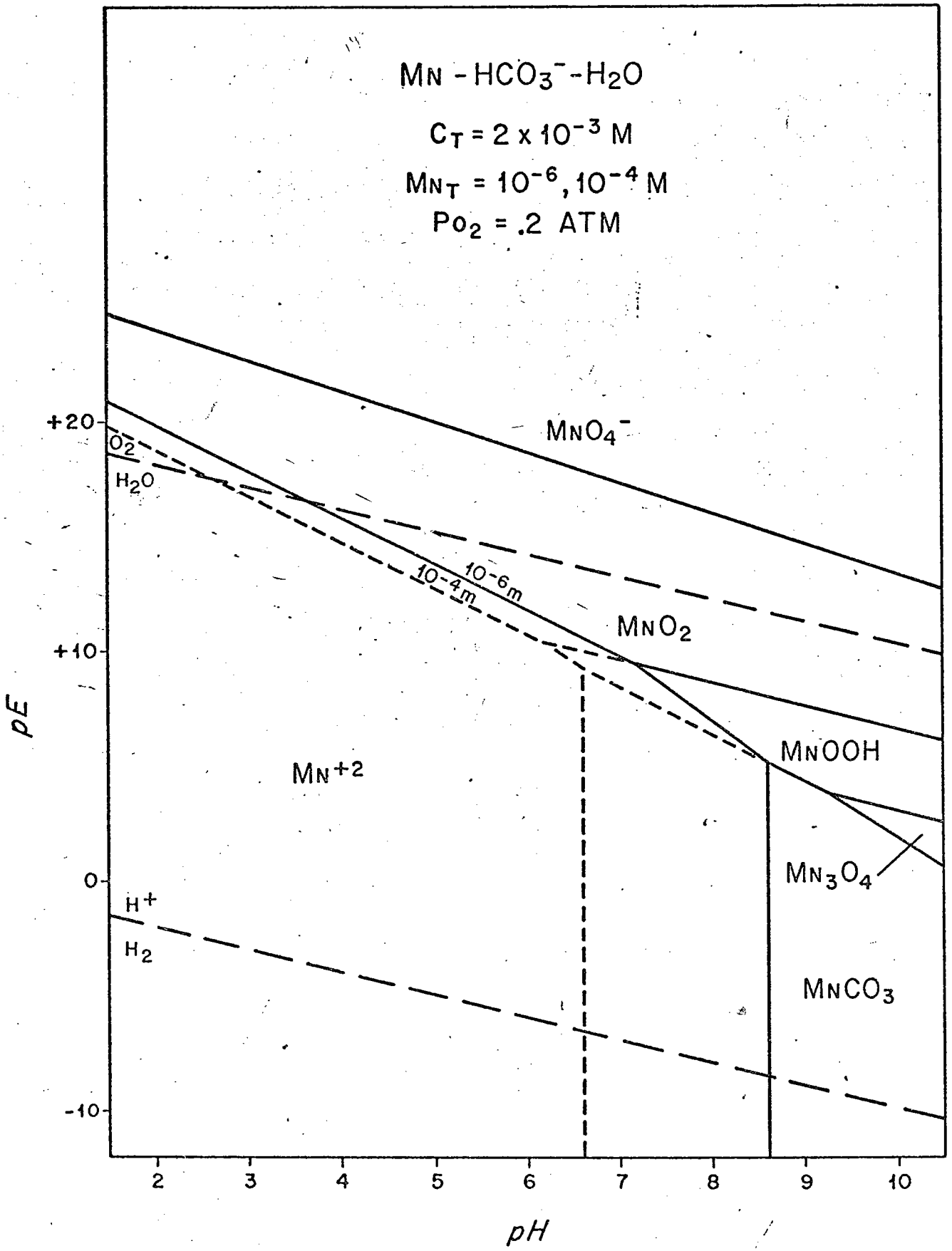
MN - HCO3- - H2O
CT = 2 x 10-3 M
MNT = 10-6, 10-4 M
PO2 = .2 ATM
MNO4-
O2
H2O
10-6m
10-4m
MNO2
MNOOH
MN+2
MN3O4
MNCO3
H+
H2
+20
+10
0
-10
pE
2
3
4
5
6
7
8
9
10
pH

Figure 10

A comparison of the charge-versus-pH values for δMnO_2 and SiO_2. The charge values for δMnO_2 were calculated using alkalimetric titration curves extrapolated to the pH(ZPC) using Na^+ adsorption. The charge values for SiO_2 were taken from Tadros and Lyklema (1968).

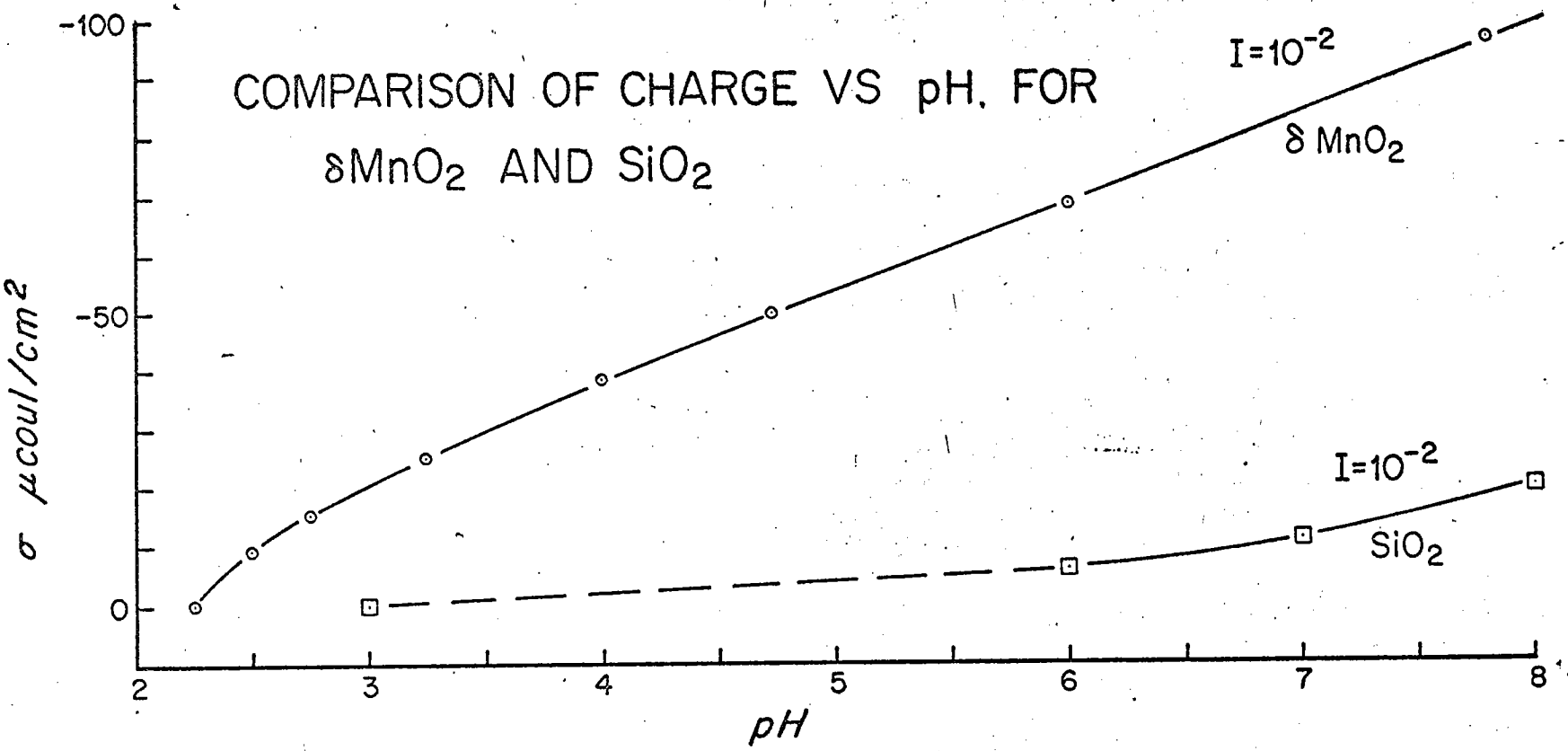
COMPARISON OF CHARGE VS pH. FOR
δMnO2 AND SiO2
-100
-50
0
σ μcoul/cm2
2
3
4
5
6
7
8
pH
I=10-2
δ MnO2
I=10-2
SiO2

BIBLIOGRAPHY

Atkinson R.J., Posner A.M. and Quirk J.P. (1967) Adsorption of potential-determining ions at the ferric oxide - aqueous electrolyte interface. J. Phys. Chem. 71, 550-558.

Berube Y.G., Onoda G.Y. and de Bruyn P.L. (1967) Proton adsorption at the ferric oxide-aqueous solution interface. II Analysis of kinetic data. Surface Science 8, 448-461.

Berube Y.G. and de Bruyn P.L. (1968) Adsorption at the rutile-solution interface. 1. Thermodynamic and experimental study. J. of Colloid. and Interface Sci. 27, 305-318.

Block L. and de Bruyn P.L. (1970) The ionic double layer at the ZnO/solution interface. I) The experimental point of zero charge. J. of Colloid. and Interface Sci. 32 , 518-526.

Bolt G.H. (1957) Determination of the charge density of silica soils. J. Phys. Chem. 61, 1166-1169.

Bostrom K. and Peterson M.N. (1969) The origin of aluminium poor ferro-manganoan sediments in areas of high heat flow on the East Pacific Rise. Marine Geol. 7, 427-477.

Brunauer S., Emmett P.H. and Teller E. (1938) Adsorption of gases in multimolecular layers. J. Am. Chem. Soc. 60, 309-361.

Charlot G. and Bezier D. (1957) Quantitative inorganic analysis. Wiley-Interscience.

Covington A.K., Cressey T., Lever B.G. and Thirsk H.R. (1963) Trans. Faraday Soc. 58, 1975-1988

Cronan D.S. (1969) Inter-element associations in some pelagic deposits. Chem. Geol. 5, 99-106.

de Boer J.H., Tippens B.C., Tinsen B.G., Broekhoff J.C.P., van den Heuval A. and Osinga Th. J. (1966) The t-curve of multimolecular N_2-adsorption. J. of Colloid. & Interface Science 21, 405-414.

de Bruyn P.L. and Agar G.E. (1962) Surface chemistry of flotation. In Froth Flotation (editor D.W. Fuerstenau). Am. Inst. of Mining, Metallurgical and Petroleum Engrs. Inc.

El Wakkad S.E.S. and Rizk H.A. (1957) The polytungstates and the colloidal nature and the amphoteric character of tungstic acid. J. Phys. Chem. 61, 494-497.

Gabano J.P., Etienne P. and Laurent J.F. (1965) Etude des proprietes de surface du bioxide de manganese γ. Electrochimica Acta 10, 947-963.

Gallagher K.J. and Phillips D.N. (1968) Proton transfer studies in the ferric oxyhydroxides. Part 1 - Hydrogen exchange between γFeOOH and water. Trans. Faraday Society 64, 785-795.

Giovanoli R., Stahli E. and Feitknecht W. (1970) Über Oxidhydroxide des vierwertigen Mangans mit Schichtengitter . Helvetica Chimica Acta 53, 453-456.

Giovanoli R., Stahli E. and Feitknecht W. (1969) Über Struktur und Reaktivität von Mangan(IV) oxiden. Chimia 23, 264-266.

Goldberg E.D. (1954) Marine Geochemistry. 1. Chemical scavengers of the sea. J. Geol. 62, 249-265.

Grahame D.C. (1947) The electrical double layer and the theory of electrocapillarity. Chem. Rev. 41, 441-501.

Grim R.E. (1968) Clay mineralogy. 596 pp. McGraw-Hill Book Co.

Healy T.W. and Fuerstenau D.W. (1965) The oxide-water interface-interrelation of the zero point of charge and the heat of immersion. J. Colloid. Sci. 20, 376-386.

Healy T.W., Herring A.P. and Fuerstenau D.W. (1966) The effect of crystal structure on the surface properties of a series of manganese dioxides. J. Colloid. and Interface Science 21, 435-444.

Jenkins S.R. (1970) The colloid chemistry of hydrous MnO_2 as related to manganese removal. Ph.D. Thesis. Harvard University.

Jenne E.A. (1968) Controls on Mn, Fe, Co, Ni, Cu and Zn concentrations in soils and water: the significant role of hydrous Mn and Fe oxides. Adv. Chem. Ser. 73, 337-387.

Jones L.H.P. and Milne A.A. (1956) Birnenite, a new manganese mineral from Aberdeenshire, Scotland. Mineral. Mag 31, 283-288.

Kozawa A. (1959) On an ion-exchange property of manganese dioxide. J. of the Electrochemical Society 106, 552-556.

Krauskopf K.B. (1956) Factors controlling the concentrations of thirteen rare metals in sea water. Geochim. Cosmochim. Acta 9, p. 1-32B

Li H.C. (1958) Adsorption of inorganic ions on quartz. Sc.D. Thesis. M.I.T.

Lingane J.J. and Karplus R. (1946) New method for determination of manganese. Anal. Chem. 18, 191-194.

Luce R.W., Bartlett R.W. and Parks G.A. (1972) Dissolution kinetics of magnesium silicates. Geochim. Cosmochim. Acta 36, 35-50.

Mero, J.L. (1965) The mineral resources of the sea. Elsevier Publishing Co., Amsterdam. 312 pp.

Morgan J.J. (1964) Chemistry of aqueous manganese(II) and (IV). Ph.D. Thesis. Harvard University.

Morgan J.J. and Stumm W. (1965) Analytical chemistry of aqueous manganese. J. Amer. Water Wks. Assn. 57, 107-119.

Morgan J.J. and Stumm W. (1964) Colloid-chemical properties of manganese dioxide. J. of Colloid. Science 19, 347-359.

Murray D.J., Healy T.W. and Fuerstenau D.W. (1970) The adsorption of aqueous metal on colloidal hydrous manganese oxide. Adv. in Chemistry 79, 74-81.

Onoda G.Y., Berube Y.G. and de Bruyn P.L. (1967) Proton adsorption at the ferric oxide / aqueous solution interface. Surface Science 8, 448-461.

Parks G.A. (1965) The isoelectric points of solid oxides, solid hydroxides and aqueous hydroxo complex systems. Chem. Rev. 65, 177-198.

Parks G.A. and de Bruyn P.L. (1962) The zero point of charge of oxides. J. Phys. Chem.66, 967-973.

Perrin D.D. (1962) The hydrolysis of manganese (II) ion. J. Chem. Soc. 2197-2200.

Posselt H.S., Anderson F.J. and Weber W.J.Jr. (1968) Cation sorption on colloidal hydrous manganese dioxide. Env. Sci. and Tech. 2, 1087-1093.

Riley J.P. and Sinhaseni P. (1958) Chemical composition of three manganese nodules from the Pacific Ocean. J. Marine Res. 17, 466-482.

Sillen L.G. and Martell A.E. (1964) Stability constants of metal-ion complexes. Spec. Publ. No. 17. Chem. Soc. London.

Skoog D.A. and West D.M. (1963) Fundamentals of analytical chemistry. Holt, Rinehart and Winston, New York. 786 pp.

Spencer D.W., Brewer P.G. and Sachs P.L.

trace element composition of suspended matter in the Black Sea. Geochim. Cosmochim. Acta 36, 71-86.

Stumm W. and Morgan J.J. (1970) Aquatic chemistry. 583 pp. Wiley-Interscience.

Stumm W., Huang C.P. and Jenkins S.R. (1970) Specific chemical interaction affecting the stability of dispersed systems.Croatica Chemica Acta 42, 223-245.

Tadros Th.F. and Lyklema (1968) Adsorption of potential-determining ions at the silica-aqueous electrolyte interface and the role of some cations. J. Electroanal. Chem. 17, 267-275.

Wyttenback A. (1961) Diffusionsmessungen durch heterogenen Isotopenaustausch an $Ni(OH)_2$ und γ-FeOOH. Helvetica Chimica Acta 64, 418-429.

ACKNOWLEDGEMENTS

The author expresses his indebtedness to Dr. W. Stumm for his many helpful discussions on the surface chemistry of metal oxides and to Dr. G. Thompson, Dr. P. Brewer and Dr. D. Spencer for their reviews and constructive criticisms of this manuscript.

This research was supported by A.E.C. contract number 80 (30/1) 3566 and N.S.F. grant number GA 13574.

CHAPTER 3

THE INTERACTION OF METAL IONS AT THE MANGANESE DIOXIDE-SOLUTION INTERFACE

ABSTRACT

The adsorption of metal ions was measured and alkalimetric titrations were performed on a synthetic sample of hydrous manganese dioxide. The principal characteristics of this phase, its stoichiometry, X-ray diffraction pattern and surface area, resemble closely the mineral birnessite.

Both sets of experiments indicate that the affinity of the metals for the surface followed the order:

$$Mg < Ca < Sr < Ba < Ni < Zn < Mn \leq Co$$

Linear Kurbatov plots indicate that the interaction can be characterized by its pH dependence. A comparison of the amount of metal adsorbed with the amount of acid released by the surface showed that the interaction of metals with the hydrous manganese dioxide surface involves (1) the separation of a proton from the covalent bond at the surface, and (2) the association of a solute cation with this site.

$$-\overset{|}{\underset{|}{Mn}}\text{-}OH^{o} + Co^{+2} = -\overset{|}{\underset{|}{Mn}}\text{-}O\text{-}Co^{+} + H^{+}$$

The relative degree of the bond strength is reflected by the specific adsorption potentials, which are determined from the amount of metal that is adsorbed by the surface, in the absence of any electrostatic attraction, at the pH of zero point of charge.

I. INTRODUCTION

Manganese dioxide is a well known scavenger in marine and fresh water environments (Goldberg 1954, Krauskopf 1956, Morgan and Stumm 1965, Jenne 1968). Field observations show that MnO_2 is very sensitive to changes in pE, and it is only found in oxidizing environments; thermodynamic calculations show (Stumm and Morgan 1970, p. 533) that at pH 8, it can become reduced at values of pE less than 8. The combination of the two characteristics of MnO_2, its scavenging ability and its limited stability field with respect to pE, make it both an important source and sink for trace elements. Under oxidizing conditions, MnO_2 will immobilize those metals that are attracted to its surface. If the environment is made reducing, the MnO_2 will be reduced releasing its adsorbed metal ions.

Several authors have investigated the interaction of metals with MnO_2. In an attempt to understand the catalytic effect that MnO_2 has on the oxidation of Mn(II) and to understand the colloidal stability of MnO_2, Morgan and Stumm (1964b) studied the adsorption of Mn(II) and other cations on δMnO_2. D.J. Murray et al. (1968) investigated the adsorption of Co, Cu, Ni, Ca, Ba, K, Na, and Li on 10 Å manganite in the vicinity of the pH of zero point of charge pH(ZPC) in order to obtain quantitative data on the specific adsorption potentials of these ions. Studies of the coagulation and flocculation of hydrous manganese dioxide indicate they are strongly dependent on the presence of slightly hydrolyzed metal ions (Morgan and Stumm 1965, Jenkins 1970, Posselt et al. 1968). Previous research on the surface charge characteristics of δMnO_2 has shown that

H^+ and OH^- are potential-determining ions and that the pH(ZPC) ranges from 1.5 to 2.7 (D.J. Murray et al. 1968, Morgan and Stumm 1965, see also chapter 2), however, a simple model of reversible H^+ and OH^- adsorption is complicated below pH 3.5 because of the reduction of MnO_2 by H_2O. Results of the surface charge determinations indicate that δMnO_2 has a much higher surface charge than SiO_2 in the pH range of natural waters (Chapter 2). In addition to the electrostatic attraction of cations by the high surface charge, the positive adsorption of some metal ions at the pH(ZPC) indicates that some form of specific adsorption can enhance their adsorption (D.J. Murray et al. 1968). Loganathan and Burau (1973) suggested that this is substitution of the adsorbing divalent metal ions for Mn(II) and Mn(III) included in the structure of the δMnO_2.

In this paper, I report on the interaction of several metal ions with the surface of δMnO_2. These interactions were studied directly by measuring metal ion adsorption by atomic absorption spectrophotometry and indirectly by using alkalimetric titrations. From these experiments, I will describe the reactions that take place at the δMnO_2-solution interface and suggest the chemical factors that must be considered in order to explain them.

II. MATERIALS AND METHODS

A. Materials

The δMnO_2 used in these experiments was prepared as described in Chapter 2 by the reaction:

$$3\ Mn^{+2} + 2\ MnO_4^- + 2\ H_2O = 5\ MnO_2 + 4\ H^+ \qquad (1)$$

The δMnO_2 from several preparations was combined to produce a stock suspension that was used for all the experiments presented in this paper. The δMnO_2 was kept in suspension at all times since the results cited in Parks (1965) indicate that drying the materials used in surface chemistry experiments will affect the response of the surface.

Surface area determinations by the B.E.T. and t-plot methods both gave a surface area of 260 m^2/g (Appendix II-C), and X-ray diffraction gave weak reflections at 7.4 Å, 4.04 Å, 2.43 Å, and 1.63 Å (Appendix II-B) which are characteristic of hydrous manganese dioxide. The stoichiometry of $MnO_{1.93}$ was determined by using O-tolidine to measure the oxidized equivalents (Morgan and Stumm 1965) and atomic absorption spectrophotometry to measure the total manganese (Appendix II-A).

The pH(ZPC) for this preparation was determined by electrophoresis and Na^+ and K^+ adsorption (Figure 1) and was found to be approximately 2.25. Alkalimetric titrations of the surface with NaCl as a background electrolyte showed that the surface charge increased rapidly for pH values greater than the pH(ZPC) and reached over -100 $\mu coul/m^2$ by pH 8.0.

B. Adsorption Experiments

The adsorption-desorption and alkalimetric titration experiments were prepared by adding appropriate amounts of $Co(NO_3)_2$, $Ni(NO_3)_2$, $MnCl_2$, $ZnSO_4$, $CaCl_2$, $MgSO_4$, $SrCl_2$ or $BaCl_2$ stock solutions to a suspension of δMnO_2. If the initial pH was adjusted, it was done before the addition of metal ions. Each experiment contained 0.10 g of MnO_2, and the total volume was 200 ml. The ionic strength was adjusted using NaCl.

In the adsorption experiments, 5 ml aliquots were drawn from the suspension, the δMnO_2 was removed by centrifugation (30 min. 15,000 rpm),

and the supernatant was analyzed by atomic absorption spectrophotometry (Appendix III-A). After each sample was drawn, the pH was adjusted using 0.1 N NaOH or 0.1 N HCl, and after equilibration, another sample was taken.

Each adsorption experiment was begun at about the pH(ZPC). The pH was increased in increments, and samples were taken up to approximately pH 7. Then the pH was lowered in increments, and samples were taken to measure the amount desorbed. The supernatant solutions were analyzed for Mn as well as the metal being studied.

C. Alkalimetric Titration Experiments

The suspensions for the alkalimetric titration experiments were prepared in the same way as those for the adsorption experiments. The experiments were performed using standardized 0.1 N NaOH. The addition of aliquots of titrant were made at regular three minute intervals, and pH measurements were made using a combination glass electrode(Fisher Scientific Co.). Blank titration curves were performed on the supernatant solutions after removal of the δMnO_2 from the suspension by centrifugation.

III. RESULTS

A. Adsorption-Desorption

1) Kinetics

The adsorption of alkaline earth and transition metal ions on δMnO_2 has been well documented, but widespread disagreement exists concerning the kinetics of the process. Morgan and Stumm (1964a) observed that the rate of adsorption at constant pH was rapid (< 5 min.). However, they found a decrease in the rate with increasing ionic strength, which was attributed to increased flocculation of the δMnO_2 caused by the increased Na^+ concen-

tration. Posselt et al. (1968) found similar rapid kinetics, equilibrium was reached in less than five to ten minutes in their experiments. On the other hand, D. J. Murray et al. (1968) and Loganathan and Burau (1973) found that final attainment of equilibrium was often very slow, in some cases lasting from several hours to a few days.

The kinetics of adsorption of alkaline earth and transition metal ions on the δMnO_2 used in the experiments in the present study was reasonably rapid. Thus, adsorption equilibrium was reached within an hour after the addition of metal ions to a suspension of δMnO_2 at an ionic strength of 0.1N. When the pH in the adsorption experiments was increased in small increments, equilibrium was reached very rapidly; however, the time to reach equilibrium was a function of the amount of the pH change. Figure 2a shows the adsorption kinetics of cobalt on δMnO_2 following an increase in pH from 3.88 to 4.72. In this example, adsorption equilibrium was reached after approximately 15 minutes.

The adsorption of metal ions onto δMnO_2 results in a release of protons. A general reaction involving the exchange of metal ions in solution with H^+ bound to the oxide surface has been used to explain the adsorption of metal ions on metal oxides (Kurbatov et al. 1951). This results in a pH drift that can also be used to monitor the kinetics of metal ion adsorption. The termination of the pH drift and adsorption kinetics were found to coincide.

In order to evaluate the reversibility of the metal ion adsorption, desorption kinetics were studied. Figure 2b shows the amount of cobalt released after the pH was lowered from 6.49 to 3.24. The rate of desorption of metal from the surface was slower than the adsorption rate. For

cobalt and the other transition and alkaline earth metal ions studied, between 6 and 12 hours were necessary to reach equilibrium.

2) Adsorption of Alkaline Earth and Transition Metal Ions

Figure 3 shows the adsorption of the alkaline earth metal ions on δMnO_2 as a function of pH. The data are plotted as adsorption density (moles/m^2) to facilitate comparison with the alkalimetric titration experiments. The concentration of total metal was 1×10^{-3} M, and the ionic strength was 10^{-1} N. The amount of metal adsorbed increased with pH, and the observed selectivity sequence was Ba > Sr > Ca > Mg. The ease of desorption reflected the adsorption selectivity; Mg adsorbed more reversibly than Ba. The desorption of the alkaline earths by lowering the pH was not complete. The adsorption-desorption results for calcium are shown in Figure 4. The initial pH of the experiment was approximately 2.0. The pH was adjusted upward to approximately 7.0 and then lowered again to pH 2.5. The arrows in the figure indicate which parts of the curves are adsorption and which are desorption. The adsorption-desorption results for cobalt, manganese and nickel are also given in Figure 4. A comparison of the adsorption results for Co, Mn, Cu, Ni and Zn at 1×10^{-3} M is given in Figure 5.

The adsorption results for cobalt at concentrations ranging from 2.5×10^{-4}M to 1×10^{-3}M are shown in Figure 6. The amount of cobalt adsorbed at low pH values was very high compared with the alkaline earths. For 1×10^{-3}M, at pH 3, over 50% of the cobalt was adsorbed. Only 30% of the barium and less than 10% of the magnesium were adsorbed under the same conditions. Increasing amounts of cobalt were adsorbed with increasing pH, and by pH 7.0 essentially 100% of the cobalt had been adsorbed. Some manganese was released to solution with the adsorption of cobalt. The amounts released for 1×10^{-3}M cobalt are also shown in Figure 6. Approximately

10% of the cobalt adsorbed at pH 3 can be accounted for by the Mn released, and this percentage decreased with increasing pH.

The adsorption of cobalt was highly irreversible as shown by the amounts of cobalt released to solution with a decrease in pH (Figure 6). The inability to desorb the cobalt is apparently not due to the short term kinetics of desorption; as Figure 2 indicates, for all practical purposes desorption equilibrium was reached within a few hours. This hysteresis was a very pronounced feature for all of the transition metal ions studied (see Figure 4).

B. Alkalimetric Titration Experiments

The alkalimetric titration curves and the blank titration curves are shown for the alkaline earth metal ions at 1×10^{-3}M in Figure 7, for cobalt at concentrations ranging from 1×10^{-3}M to 2.5×10^{-4}M in Figure 8, and for Co, Cu, Ni, Zn and Mn at 1×10^{-3}M in Figure 9. All of these titration curves were done in an ionic medium of 10^{-1}N NaCl. Included for comparison in each figure is a titration curve of the δMnO_2 surface in 10^{-1}N NaCl in the absence of any metal ions. The results for Cu, Ni, Zn and Mn at different concentrations were similar to the cobalt results and can be described by using the cobalt data alone.

Net titration curves, obtained by subtracting the blank titration curves from the titration curves of the surface, are shown in Figures 10, 11, and 12. These curves show the amount of strong base that has reacted with the surface in the absence or presence of the different metal ions. The presence of metal ions shifts the titration curves to the right of the titration curve of the surface in the absence of any metal ions (Figures 7, 8, 9). At 1×10^{-3}M the titration curves were shifted to the right in increasing amounts following a sequence of:

Cu > Co > Mn > Zn > Ni and Ba > Sr > Ca > Mg.

When the net titration curve for the surface in the absence of metal ions is subtracted from the net titration curve of the surface in the presence of metal ions, the resulting curve shows the excess amount of base consumed by the surface and must be due to the presence of the metal ions. This excess base for cobalt, at four concentrations, is shown in Figure 13.

IV. DISCUSSION

A. Alkaline Earth Metal Ions

The adsorption results (Figure 3) indicate that the affinity of the alkaline earths for the δMnO_2 surface is in the order Ba > Sr > Ca > Mg, which is similar to the results of Posselt et al.(1968). The amount of H^+ released is found by adding the amount of H^+ released by the initial adsorption of alkaline earth metal ion to the equivalent amount of acid obtained from the shift in the alkalimetric titration curves (Figure 7). These calculated values for the amounts of H^+ released can be compared with the amounts of metal adsorbed, giving the resulting H^+ released/metal adsorbed ratios plotted in Figure 14. The ratios of H^+ released to metal adsorbed are less than or equal to 0.5 for all the alkaline earth metal ions.

Stumm et al. (1970) found that alkalimetric titration curves of a δMnO_2 suspension were affected by the presence of Ca^{+2}, and they proposed that the interaction of Ca^{+2} with the δMnO_2 surface involves (1) the separation of a proton from the covalent bond at the surface, and (2) the association of a solute cation with this site.

$$-\overset{|}{\underset{|}{Mn}}-OH^0 + Ca^{+2} = -\overset{|}{\underset{|}{Mn}}O-Ca^+ + H^+ \qquad (2)$$

Their observations that Ca^{+2} is able to reverse the electrophoretic mobility of a δMnO_2 suspension at pH = 7 indicates that the ratio of the concentration of protons released from the surface to Ca^{+2} adsorbed is less than 2. This proposal is supported by the results shown in Figure 14. If an ionic species was adsorbed in response to the coulombic attraction of the surface alone, it would not be possible to reverse the surface charge. However, by replacing a monovalent proton by a divalent cation, such a charge reversal can occur. The fact that the proton to metal ratio is considerably less than 1 indicates that a significant amount of the alkaline earths adsorb without penetrating close to the surface to react with specific sites and release protons.

Kurbatov et al. (1951) applied the law of mass action to explain the type of reaction shown above (eqn. 2). They found that in the region of adsorption isotherms where Henry's law applies, i.e. where the activity of the sorbent is unchanged by the sorption reaction, equation 3 can be used to characterize the pH dependence of the sorption reaction.

$$j(HX) + M^{+z} = MX_j^{z-j} + j\,H^{+} \qquad (3)$$

HX = unassociated neutral hydrous oxide site with one dissociable proton, H, and solid matrix, X.

M^{+z} = metal ion with +Z valence

MX_j^{z-j} = surface complex

Equation 2 can be rewritten as:

$$b_j = \frac{(H^{+})^j\ (MX_j)^{z-j}}{(HX)^j\ (M^{+z})} \qquad (4)$$

where b_j = equilibrium constant.

Taking the log of both sides gives:

$$\log \frac{(MX_j)^{z-j}}{(M^{+z})} = \log b_j + j \log \frac{(HX)}{(H^+)} \qquad (5)$$

Under ideal conditions, a plot of $\log \frac{(MX_j)^{z-j}}{(M^{+z})}$ against $\log \frac{(HX)}{(H^+)}$ can be used to obtain the value of the H^+ released/metal adsorbed ratio . Such a plot was successfully used by Huang (1971) for studying the interaction of metal ions with γAl_2O_3 because he was able to predict the concentration of protonated surface sites from his alkalimetric titration data, thus enabling him to calculate b_j for reaction 4 directly. Unfortunately, the experimental determination of the concentration of protonated (undissociated) surface sites is difficult, thus most authors use a plot of $\log \frac{(\text{metal (solution)})}{(\text{metal (adsorbed)})}$ as a function of pH. This adaption of the mass law equation has been found to give linear plots for many hydrous oxide systems: e.g. Sr^{+2} on Fe_2O_3 (Kolarik 1961), Sr^{+2} on Al_2O_3 (Bonner et al. 1966), Mn^{+2} on MnO_2 (Morgan and Stumm 1964b), Co^{+2} on Fe_2O_3 (Kurbatov et al. 1951), and UO_2^+ on silica gel (Stanton and Maatman 1963).

In my experiments, (HX), the total exchange capacity, could not be estimated. Thus, $\log b_j$ and (HX) are combined, and equation 5 becomes:

$$\log \frac{(\text{metal) solution}}{(\text{metal) adsorbed}} = Z + n \log H^+ \qquad (6)$$

where Z is a constant dependent upon the total mass of sorbent and upon the equilibrium constant for reaction 3.

Figure 15 shows the Kurbatov plots (log ((metal) solution/(metal) adsorbed) versus pH) for the alkaline earth metal ions. A linear relationship exists from pH 2 to 8, indicating that the type of mass action described by reaction 6 probably describes the interaction of alkaline earths with the δMnO_2 surface. Reaction 6 indicates that the slope of the Kurbatov plots should indicate the amount of H^+ released per mole of metal adsorbed. The value of n in equation 6 (obtained from Figure 15) is approximately 0.30 for all of the alkaline earths. This agrees reasonably well with the H^+ released/metal adsorbed ratios (Figure 14) calculated from the alkalimetric titration data (Figure 7). This independent agreement suggests that the assumption in the theoretical model that the activity of the sorbent is constant is obeyed for the alkaline earths.

The selectivity sequence observed for δMnO_2 in these experiments (Ba > Sr > Ca > Mg) is the reverse of the sequence found for γAl_2O_3 (Huang 1971). This suggests that there is no easy way to predict the relative adsorption from solution without some knowledge of the solid phases involved. This difference in selectivity is due to basic structural differences between these two solids and can be described by the semiquantitative electrostatic model proposed by Stumm et al. (1970). This model is similar to the one proposed by Eisenman (1965) to explain the selectivity of glasses.

In this model, the free energy change of an ion exchange reaction is the sum of the coulombic work done and the energy involved with the partial change in hydration that accompanies the exchange process depicted in Figure 16. The free energy for the process:

$$BaX + Mg^{+}_{(aq)} = MgX + Ba^{+2}_{(aq)} \; ; \; K_{Mg/Ba} \qquad (7)$$

where X is an anionic surface site, is given by:

$$\Delta G + -RT \ln K_{Mg/Ba} = \left(\frac{e^2}{R_X + R_{Ba}} - \frac{e^2}{R_X + R_{Mg}} \right)$$

$$-(\Delta G_{HYD_{Ba}} - \Delta G_{HYD_{Mg}}) \qquad (8)$$

R_X is the "hypothetical" radius of the fixed anionic site on the solid. This fixed anionic site is dependent on the equivalent field strength which, in turn, is related to the size of the unit cell per central ion (Healy et al. 1966). Two extreme cases can be described by this model which explain the difference in selectivity exhibited by γAl_2O_3 and δMnO_2.

1) Strong Field Strength

When the fixed anionic site has a small radius, the first term of equation 8 dominates the exchange reaction, and this equation predicts that the smaller ion (non-hydrated) is preferred by the fixed anion over the ion with the larger radius. Because of the high ratio of charge to radius, H^+ has a strong association with the fixed anion; thus, HX is a weak acid. This model should apply, therefore, to metal oxides with relatively high pH(ZPC) such as γAl_2O_3 and βMnO_2. In fact, both of these solids exhibit the selectivity of Mg > Ba (Jenkins 1970, Huang 1971).

2) Weak Field Strength

When the radius of the fixed anionic site is large and the field strength, and thus the polarity of the solid, is low, the ΔG of equation 8 is controlled by the free energy of hydration. Under such conditions the fixed anion associates preferentially with the less hydrated cations (Ba > Mg). The decreased polarity of the solid decreases the acid strength

of the protonated surface sites. Such weak field strengths are represented by strong acid, cation exchangers such as δMnO_2, SiO_2 and most clay minerals.

B. Transition Metal Ions

Morgan and Stumm (1964b) found that the addition of Mn^{+2} to δMnO_2 suspensions led to a shift in the alkalimetric titration curves similar to the shifts shown in Figures 8 and 9 and that adsorption increased with pH. Experiments they ran at constant pH, with the aid of an automatic titrator, revealed that as Mn^{+2} was adsorbed, protons were released to solution in approximately equal amounts. Their calculated ratios of H^+ released to Mn^{+2} adsorbed were approximately 1, except for pH values greater than 8.0 where they increased slightly. They suggested that this increase may be due to the oxidation of Mn(II).

Loganathan and Burau (1973) suggested that when all the cations (i.e. Na^+, K^+, and Mn^{+2}) in the system are taken into account, and when allowance is made for replacement of structural Mn(II) and Mn(III), the ratio of equivalents of charge released to equivalents of charge adsorbed is very close to 1. Stumm et al. (1970), however, observed that at pH 7, Ca^{+2} is able to reverse the electrophoretic mobility of δMnO_2. This observation indicates that the charge on the surface is not conserved during the adsorption of metal ions and that the ratio of charge equivalents released to charge equivalents adsorbed is less than 1. Huang (1971) has also demonstrated that for γ-Al_2O_3 the molar ratio of H^+ released to divalent metal adsorbed is close to 1 for Zn(II), Co(II), Ni(II) and Cu(II), and that these ions penetrate the compact part of the double layer and react specifically with the surface. He found specific adsorption potentials

up to 10 kcal/mole.

My experiments indicate that adsorption increased with pH and that there is a selectivity sequence for the metal ions investigated of Cu > Co > Mn > Zn > Ni over the pH range 2 to 8 (Figure 6). This sequence agrees with the results of D.J. Murray et al. (1968), who also found Co > Cu > Ni at 5×10^{-4}M; however, although my studies indicated the adsorption of Cu at 1×10^{-3}M was greater than Co, under these conditions Cu forms various hydrolysis and polymeric species that can greatly enhance metal ion adsorption (Stumm and O'Melia 1968, James and Healy 1972). Similar species are not formed by the other transition metal ions under these conditions. Thus, the results of the Cu experiments should not be considered in this sequence.

The adsorption isotherms (Figure 6) in moles per unit area as a function of pH at constant equilibrium concentration can be compared with calculated monolayer values. James and Healy (1972) found that for SiO_2 and TiO_2 the isotherms converged toward the precipitation region. They compared their isotherms with monolayer coverages calculated as:

a. the bare ion plus an inner coordination sphere of water i.e. $(r_{ion} + 2r_{H_2O})$,and,

b. the bare ion plus inner and outer coordination spheres of water $(r_{ion} + 4r_{H_2O})$

For both oxides, the maximum adsorption coverages corresponded to the monolayer coverages that would be predicted for bare ions being separated by two to four water molecules. They interpreted this as implying that a single layer of water molecules on the surface limits the distance of closest approach and that loss of the inner coordination sphere is apparently energetically prohibited.

Table 1 shows the calculated monolayer coverages predicted for cobalt under three different conditions. The value used for the radius of water was 1.38 Å.

TABLE 1

CALCULATED MONOLAYER COVERAGES FOR COBALT

Condition	Radius	Monolayer Coverage
Υ ion	0.70×10^{-10} m	1.08×10^{-4} moles/m^2
Υ ion + 1 Υ H_2O	2.08×10^{-10} m	1.22×10^{-5} moles/m^2
Υ ion + 2 Υ H_2O	3.46×10^{-10} m	4.40×10^{-6} moles/m^2

The maximum adsorption densities of the metal ions shown in Figure 6 are greater than those predicted assuming the ions retain their inner hydration sphere, i.e. (Υ ion + 2 Υ H_2O) and appear to be converging on a value between coverages predicted assuming Υ ion + Υ H_2O and Υ ion + 2 Υ H_2O.

Adsorption and alkalimetric titration data for the transition elements (Figures 4,6,8, and 9) can be used to calculate the H^+ released/metal adsorbed ratios as discussed earlier for the alkaline earth data (Figure 14). The resulting ratios are shown in Figure 17 for Cu, Ni, Co, Mn and Zn at 1×10^{-3}M, and in Figure 18 for cobalt at three different concentrations.

In the adsorption experiments, Mn was monitored as well as the metals of interest, because of the possibility of some exchange of metal for Mn(II) in the δMnO_2 structure. For cobalt, the amounts of Mn(II) released amounted to about 10% of the adsorbed metal at 1×10^{-3}M (Figure 5). However, this percentage decreased with increasing pH, possibly because the Mn(II) that was released was being readsorbed by the δMnO_2 surface, which becomes increasingly negatively charged with increasing pH. For the other transition metals studied, the release of Mn to solutions during the adsorption

experiments amounted to less than 2% of the metal adsorbed. It is not possible from these results to determine if the cobalt and other transition metals are penetrating into the layered structure of the δMnO_2 to replace Mn(II) or are exchanging for Mn(II) in sites on the surface. Regardless, the release of Mn(II) appears to be less important than estimated by Loganathan and Burau (1973). The fact that the (H^+) released/(metal) adsorbed ratio is also approximately 1 for Mn^{+2} clearly indicates that the exchange of metal ions for structural Mn(II) will not drastically affect the results.

The (H^+) released/(metal) adsorbed ratios can also be determined by using the drop in pH that occurs after the addition of metal ions to a δMnO_2 suspension. The moles of H^+ released, the moles of metal adsorbed and the calculated ratios for various metals at different concentrations are given in Table 2. When manganese was found to be released during the adsorption, it was subtracted from the moles adsorbed of the metal of interest on an equal molar basis on the assumption that the release of Mn was due to the exchange of one metal ion for one manganese ion. The ratios calculated in this manner are also close to one and the the release of Mn has little effect on the calculation.

All of these experiments were run at a constant ionic strength (I= 0.1N, NaCl); thus it was not possible to determine directly if Na^+ was released during the adsorption process. The results in Figure 18 show that a decrease in the cobalt concentration by a factor of 2, while maintaining I constant at 0.1N NaCl, increased the (H^+) released/(Co^{+2}) adsorbed ratio slightly. One would expect that if exchange with Na^+ were

TABLE 2

THE RATIO OF PROTONS RELEASED TO METAL ADSORBED

METAL	CONCENTRATION	$\frac{\text{MOLES } H^+ \text{ RELEASED}}{m^2}$	$\frac{\text{MOLES Co ADSORBED}}{m^2}$	RATIO
Co	1×10^{-3}M	3.84×10^{-6}	3.75×10^{-6}	1.02
	7.5×10^{-4}M	3.84×10^{-6}	3.52×10^{-6}	1.09
	5.0×10^{-4}M	3.18×10^{-6}	3.22×10^{-6}	0.99
Mn	1.0×10^{-3}M	3.76×10^{-6}	4.31×10^{-6}	0.87
	5.0×10^{-4}M	3.18×10^{-6}	3.38×10^{-6}	0.94
Ni	1.0×10^{-3}M	2.46×10^{-6}	2.08×10^{-6}	1.18
Zn	1.0×10^{-3}M	2.22×10^{-6}	3.02×10^{-6}	0.74

important, the H^+/Co^{+2} ratio would decrease as cobalt exchanged for proportionally more Na^+, relative to H^+, as the Na^+/Co^{+2} ratio was increased.

C. Specific Adsorption

Adsorption onto δMnO_2, as for other metal oxides, is in part a response to a pH dependent charged surface. My previous experiments indicated that the pH of zero point of charge for the MnO used in these experiments is 2.25 (Chapter 2) and that Na^+ and K^+ are completely desorbed from the surface at that pH. The experiments described here indicate that there may be some adsorption of the alkaline earths at the pH(ZPC) (Figure 3) and that very large amounts of transition metals are adsorbed at the pH(ZPC) (Figure 6). Experiments designed to measure this specific adsorption must approach the pH(ZPC) from lower pH values because the amount of metal adsorbed is much larger when the pH(ZPC) is approached from higher pH values. The total free energy of adsorption, ΔG^o_{ads}, is the sum of the electrostatic work, ΔG^o_{coul}, the total specific adsorption energy, ΔG^o_{chem}, and the change in secondary solvation energy, ΔG_{solv} (James and Healy 1972).

$$\Delta G^o_{ads} = \Delta G^o_{chem} + \Delta G^o_{coulombic} + \Delta G^o_{solv} \qquad (9)$$

$$= ZF\phi + ZF\Delta\psi_x + \Delta G^o_{solv} \qquad (10)$$

If the potential difference across the double layer is 100mv, the coulombic contribution ($ZF\Delta\psi$) is 2.3 kcal/mole. For a positive ion to adsorb on a positive surface with $\Delta\psi_x$ = 100 MV, it must have a specific adsorption energy of attraction greater than 2.3 kcal/mole. This is a minimum value since it neglects the change in secondary solvation energy that would also act to inhibit adsorption. The ΔG^o_{chem} portion of the free energy of adsorption can be estimated by combining equation 10 with Graham's (1947) equation

for the adsorption density (equation 11).

As shown by Graham (1947), we can express the adsorption of cations as

$$\Gamma^{+} = 2\, r[c] \exp \frac{-ze\,(\psi_{\delta} + \phi)}{kt} \qquad (11)$$

where Γ^{+} is the adsorption density at the pH(ZPC) , r is the radius of the adsorbed ion, [c] is the equilibrium concentration, ψ_{δ} is the double layer potential given by,

$$\psi_{\delta} = \frac{RT}{F} \ln \frac{a_{H^+}}{a^{o}_{H^+}} \qquad (12)$$

where $a^{o}_{H^+}$ represents the activity of hydrogen at the pH(ZPC) and ϕ is the specific adsorption potential of the ion. At the pH(ZPC), ψ_{δ} is zero, so equation 11 simplifies to:

$$\Gamma^{+} = 2\, r[c] \exp \frac{-ze\,\phi}{kt} \qquad (13)$$

Table 3 shows the calculated values of Φ from these experiments using the specific adsorption densities at the pH(ZPC) in Figure 6.

These ϕ values were calculated using for r the sum of the ionic radius plus the radius of two water molecules (each 1.38 Å). The selectivity of transition metal ions for δMnO_2 (Mn ≥ Co > Cu > Zn > Ni), as demonstrated by the specific adsorption potentials, does not follow the Irving-Williams order (Zn < Cu > Ni > Co > Fe > Mn) as found by Huang (1971) on γ-Al_2O_3. The Irving-Williams order is a reasonably well established rule for the sequence of complex stability that is explained using crystal field theory. Thus, it appears that the factors controlling the selectivity involve more than than crystal field stabilization energies as proposed by Loganathan and Burau (1973).

TABLE 3

Specific Adsorption Potentials on δMnO_2

Metal	Concentration	ϕ(kcal/mole)
Cobalt	1.0×10^{-3} M	-5.27
	7.5×10^{-4} M	-5.50
	5.0×10^{-4} M	-5.52
Manganese	1.0×10^{-3} M	-5.44
	5.0×10^{-4} M	-5.48
Nickel	1.0×10^{-3} M	-4.25
Zinc	1.0×10^{-3} M	-4.85
Copper	1.0×10^{-3} M	-5.17

D. Comparison with SiO_2 and TiO_2

James and Healy (1972) have recently proposed a model for the adsorption of metal ions at solid-solution interfaces that describes the adsorption of hydrolyzable metal ions at the solid-solution interface in terms of changes in the coulombic, solvation and specific chemical energy interactions (equation 10). In their model, there are basically two types of metal oxides: those with a high dielectric constant and those with a low dielectric constant. For solids with a low dielectric constant such as SiO_2 (ε solid = 4.3), ion-solvent interactions present a barrier for close approach of highly charged ions to the solid-solution interface. According to this model, the characteristics of the interaction of metal ions with metal oxides can be described using the dielectric constant of the solid. For solids with a low dielectric constant, work must be done to remove part of the secondary hydrated layer of the cation and replace it with interfacial water of very low dielectric constant. This involves a large positive, and therefore unfavorable, change in solvation energy which opposes the coulombic and specific interactions favoring adsorption. Specific adsorption of metal ions does not appear to occur on low dielectric solids. When the ionic charge is lowered by hydrolysis or complex formation, this ion-solvent interaction is decreased, thus lowering the energy barrier. For high dielectric solids such as TiO_2 (ε solid = 78), the change in solvation energy for the adsorption of an ion is small compared with the adsorption onto silica. The coulombic and specific chemical interactions dominate the free energy of adsorption, and thus, significant amounts of specific adsorption can occur on TiO_2. The comparison of the data for the interaction of metals with δMnO_2 presented in this paper with the data of James and Healy (1972) on the metal interactions with SiO_2 and TiO_2 is useful in understanding the δMnO_2 surface.

In Table 4, several properties of SiO_2 and δMnO_2 are compared. Using purely a classical approach, one might expect that because SiO_2 and δMnO_2 have a similar pH(ZPC), they would have basically the same surface chemistry. However, they differ markedly in several important aspects: the surface charge increases much faster as pH increases for δMnO_2 than it does for SiO_2; transition metal ions and alkaline earth metal ions exhibit large specific adsorption potentials on δMnO_2 (Table 3) which are absent on SiO_2; the adsorption densities on δMnO_2 are not limited by monolayer coverage corresponding to the bare ion plus an inner coordination sphere of water (Γ ion + $2\Gamma H_2O$) as they are for SiO_2. The adsorption isotherms for δMnO_2 appear to plateau somewhere between monolayer coverages predicted using Γion + $2\Gamma H_2O$ and Γion + $1\Gamma H_2O$. The failure of the isotherms to be limited by the expected monolayer coverage corresponding to the metal ion plus its first hydration sphere (Γion + $2\Gamma H_2O$) may be due to an error in the surface area by a factor of 2. However, it appears equally feasible that because of the large specific adsorption potentials exhibited by these metals, the distance of closest approach of the metal ions to the surface is not limited by a single layer of water molecules as it appears to be for SiO_2.

From the results reported here, δMnO_2 appears to have adsorption characteristics resembling TiO_2 rather than SiO_2. This is concluded from the fact that specific adsorption of transition and alkali earth metal ions takes place on δMnO_2 and TiO_2 and does not take place on SiO_2. Values of ε for δMnO_2 are not available. βMnO_2 has been used in the construction of electrodes; thus following the reasoning of James and Healy, it should have a large dielectric because it is a conducting material. Measurements done in this laboratory (Appendix III-B) indicate that the dielectric

constant of δMnO_2 is close to 32. This is not as high as the value of the dielectric for TiO_2 (78.5); however, it is higher than the value for most metal oxides.

Because the dielectric for δMnO_2 is high, this suggests that δMnO_2 should behave more like TiO_2 than SiO_2. The evidence from the surface chemistry experiments confirms that the δMnO_2 surface behaves more like TiO_2 than SiO_2, even though δMnO_2 and SiO_2 have similar pH(ZPC). Thus, it appears that it would be misleading to try to predict the interaction of metal ions with metal oxides simply on the basis of the pH(ZPC) alone.

V. CONCLUSIONS

The results of the experiments presented in this paper have improved greatly our understanding of the mechanism of adsorption on δMnO_2. These results can be used to construct a model for the adsorption mechanism that can help explain why δMnO_2 is such a strong adsorbent in the marine environment.

Transition metal ions were found to adsorb much more strongly on δMnO_2 than alkaline earth metal ions when compared at equal concentrations. The selectivity order observed was:

$$Co \geq Mn > Zn > Ni > Ba > Sr > Ca > Mg$$

This sequence provides a possible explanation for the observation that the Ni/Co ratio in sea water is approximately 100, while in manganese nodules it is 1. The degree of adsorption was also related to the reversibility of adsorption. Na^+ and K^+ adsorb the least on δMnO_2, and their adsorption isotherms are completely reversible against pH. The alkaline earth metal ions

adsorb to a greater extent than the alkali metals and also exhibit a slight degree of irreversibility, which is reflected in the fact that they also show some specific adsorption at the pH(ZPC). This specific adsorption increases from Mg to Ba. The transition metals show the greatest attraction for δMnO_2. They also show the greatest amount of irreversible adsorption and the largest specific adsorption potentials. Some Mn is released concurrently with the adsorption of Co on δMnO_2, however, the amount released is insufficient to explain the specific adsorption potential in terms of replacement of structural Mn(II) or Mn(III) by Co(II).

The calculated ratios of (H^+) released/(metal) adsorbed indicate that this ratio correlates with the degree of specific adsorption and the irreversibility of adsorption. Among the alkaline earths, the amount of H^+ released increases from Mg to Ba, and among the transition metals, the amount of H^+ released increases from Zn to Ni to Mn to Co. This indicates that the metal ions from Mg to Co can penetrate in increasing amounts into the compact part of the double layer to react with protonated sites on the δMnO_2 surface. This type of reaction involves the replacement of a proton on the surface by a divalent metal ion, thus explaining the reversal of charge of δMnO_2 by Ca^+ observed by Jenkins (1970). The available data can be explained by invoking a model with only one type of site for which the various metal ions have different affinities. There is no definitive evidence that suggests that these metals penetrate into the δMnO_2 structure to replace Mn(II) or Mn(III).

The model of James and Healy (1972) that describes the characteristics of the interactions of metal ions with metal oxides on the basis of their dielectric constants is supported by these experiments. The large specific adsorption of metals on δMnO_2 suggests that δMnO_2 is a high dielectric

solid like TiO_2. Although δMnO_2 and SiO_2 have similar pH(ZPC), their surface chemistry characteristics are very different.

TABLE 4

SiO_2	vs.	δMnO_2
1. pH(ZPC) = 2.0 to 3.0		pH(ZPC) = 2.25
2. $H^+(OH^-)$ are potential-determining ions		$H^+(OH^-)$ are potential-determining ions
3. large unit cell and low electrostatic field strength		large unit cell and low electrostatic field strength
4. low specific surface area		high specific surface area
5. ϵ low (4.5)		ϵ high (32)
6. Co does not specifically adsorb		Co and other metals exhibit specific adsorption. Specific adsorption potentials are comparable to values for TiO_2.
7. Adsorption coverage limited by the radii of the metal ion plus its inner hydration sphere ($r + 2r_{H_2O}$)		Adsorption coverage not limited by the condition ($r + 2r_{H_2O}$)

FIGURE 1

Electrophoretic mobility values and Na^+ and K^+ adsorption measurements as a function of pH for δMnO_2.

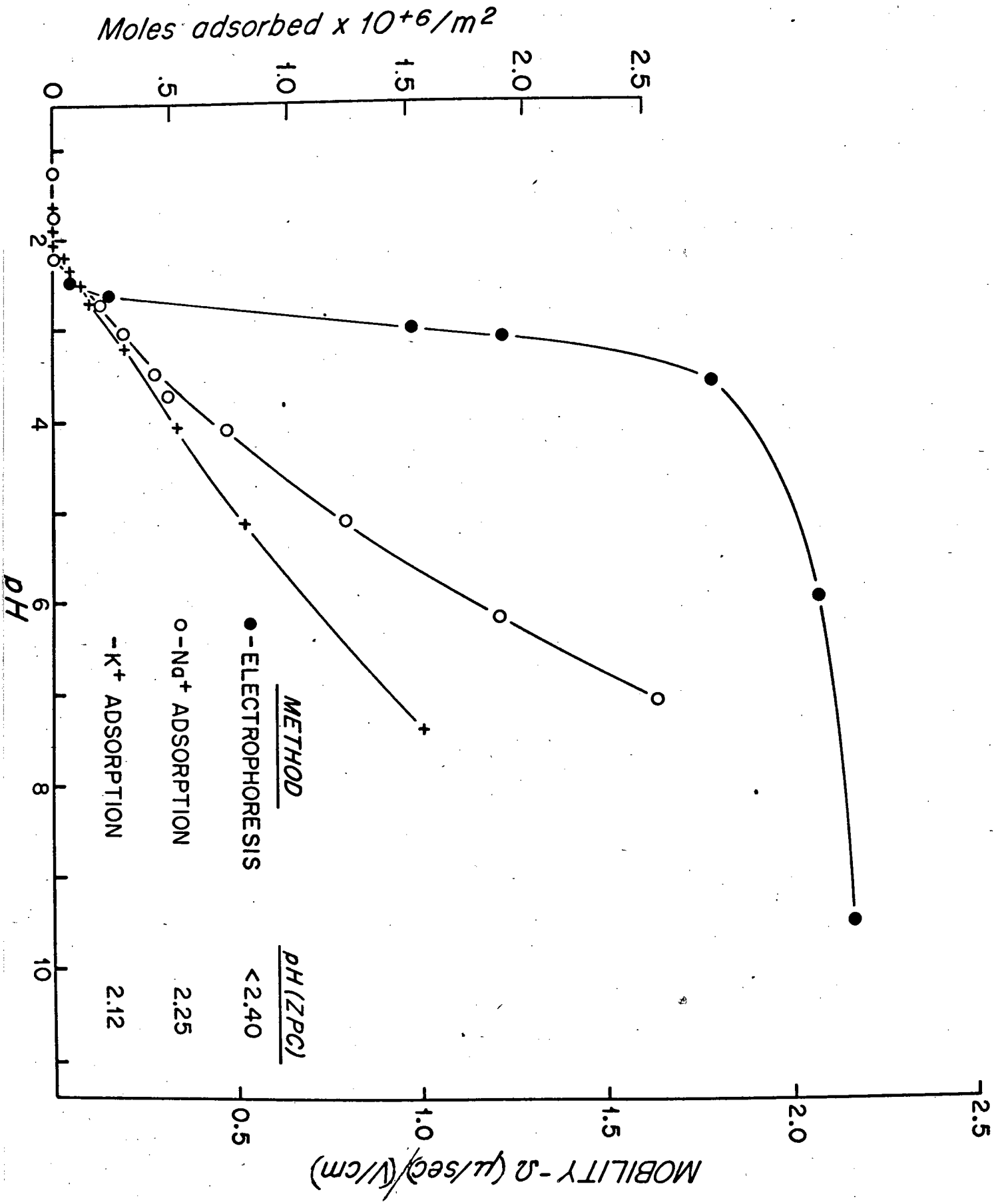
Moles adsorbed x 10+6/m2
0
.5
1.0
1.5
2.0
2.5
pH
2
4
6
8
10
MOBILITY -μ (μ/sec/(V/cm))
0.5
1.0
1.5
2.0
2.5
METHOD
pH (ZPC)
●-ELECTROPHORESIS
<2.40
o-Na+ ADSORPTION
2.25
+-K+ ADSORPTION
2.12

FIGURE 2a

Adsorption kinetics of Cobalt on δMnO_2 following an increase in pH from 3.88 to 4.72.

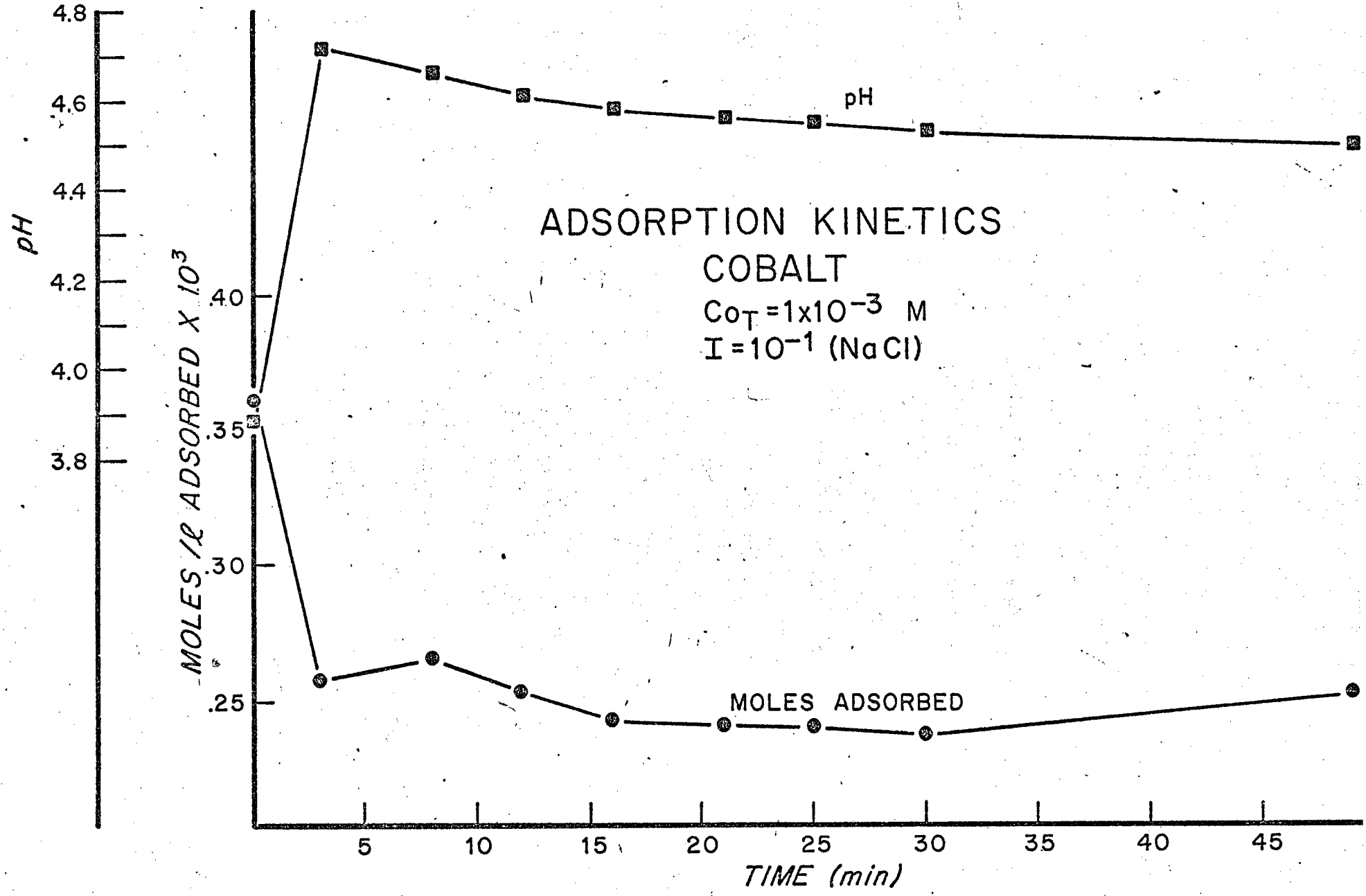
ADSORPTION KINETICS
COBALT
$Co_T = 1 \times 10^{-3}$ M
$I = 10^{-1}$ (NaCl)
pH
MOLES ADSORBED
pH
MOLES /ℓ ADSORBED X 10^3
TIME (min)
4.8
4.6
4.4
4.2
4.0
3.8
.40
.35
.30
.25
5
10
15
20
25
30
35
40
45

FIGURE 2b

Desorption kinetics of cobalt from δMnO_2 following a decrease in pH from 6.49 to 3.24.

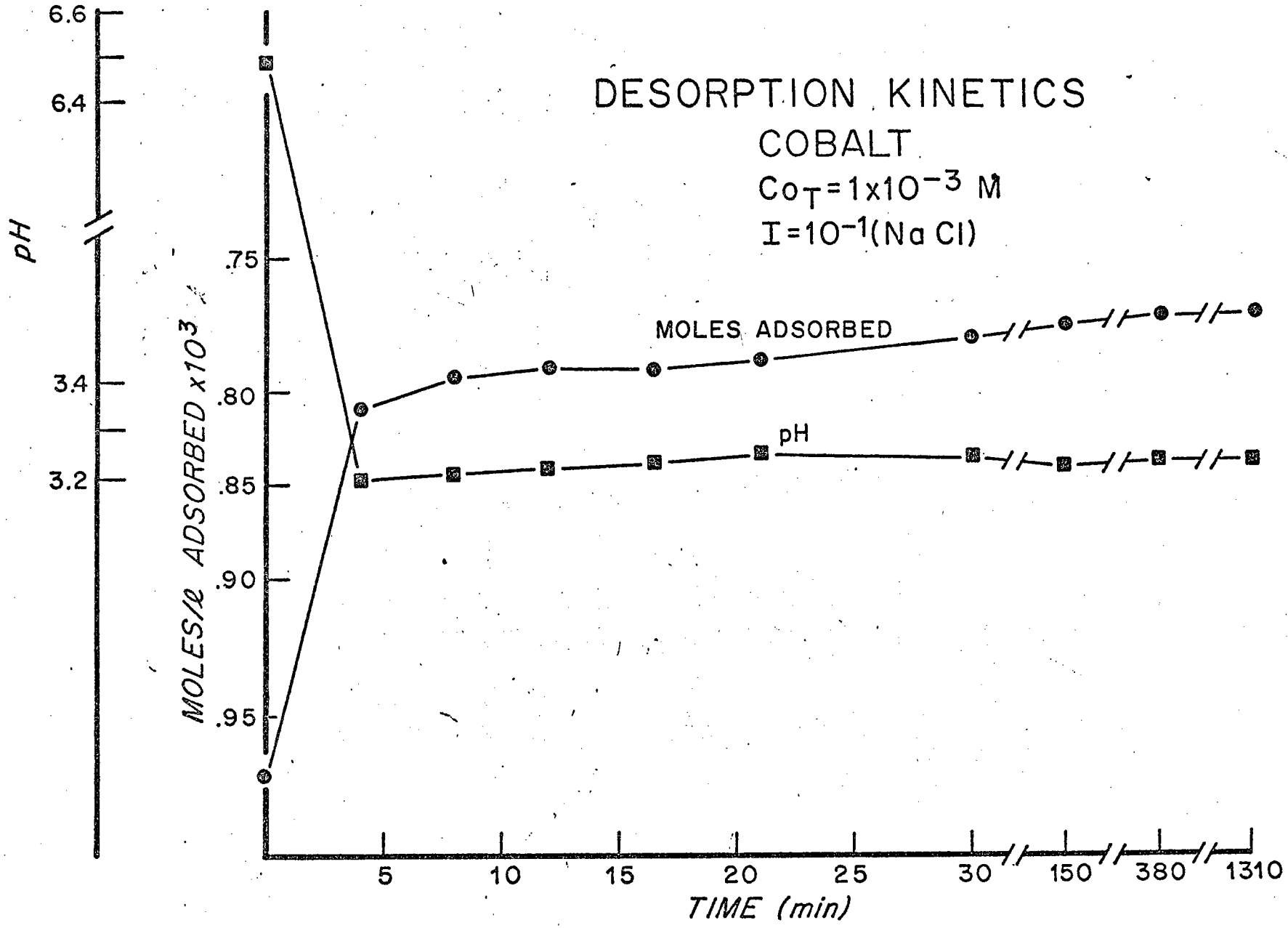
DESORPTION KINETICS
COBALT
$Co_T = 1 \times 10^{-3}$ M
$I = 10^{-1}$ (Na Cl)
MOLES ADSORBED
pH
MOLES/ℓ ADSORBED x10³
pH
TIME (min)
6.6
6.4
3.4
3.2
.75
.80
.85
.90
.95
5
10
15
20
25
30
150
380
1310

FIGURE 3

Adsorption of alkaline earth metal ions on δMnO_2 as a function of pH.

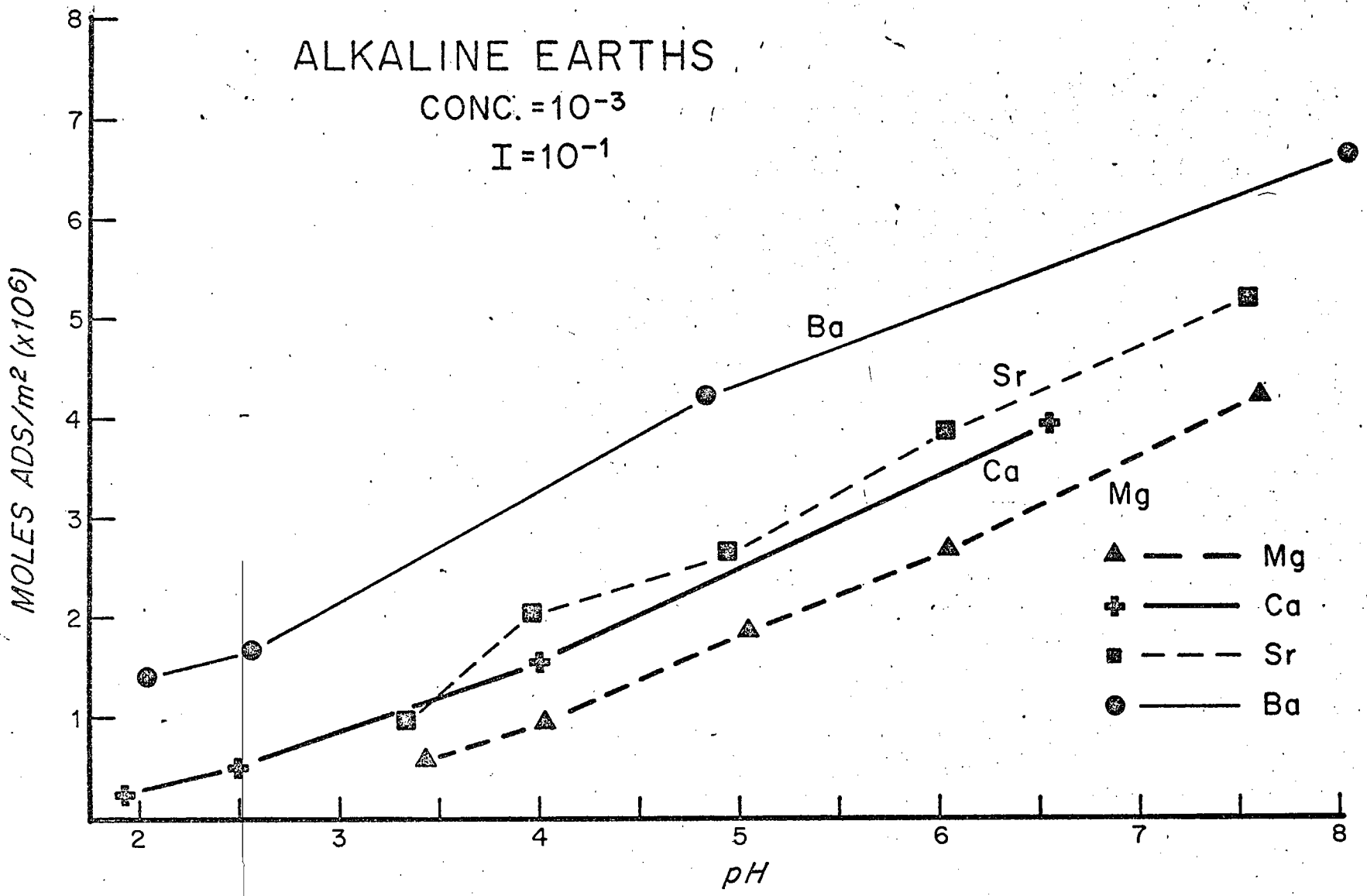
ALKALINE EARTHS
CONC. = 10⁻³
I = 10⁻¹
MOLES ADS/m² (x106)
pH
Ba
Sr
Ca
Mg
Mg
Ca
Sr
Ba
1
2
3
4
5
6
7
8
2
3
4
5
6
7
8

FIGURE 4

Adsorption-desorption results for cobalt, manganese, nickel, and calcium on δMnO_2 . The metal concentrations were 1×10^{-3} M, and the ionic strength was 0.1N (NaCl). The experiments were begun at approximately pH 2.25. The pH was first adjusted upward using 0.1 N NaOH, and then downward using 0.1 N HCl. The arrows indicate which portions of the curves are adsorption ($\rightarrow$) and which are desorption ($\leftarrow$) .

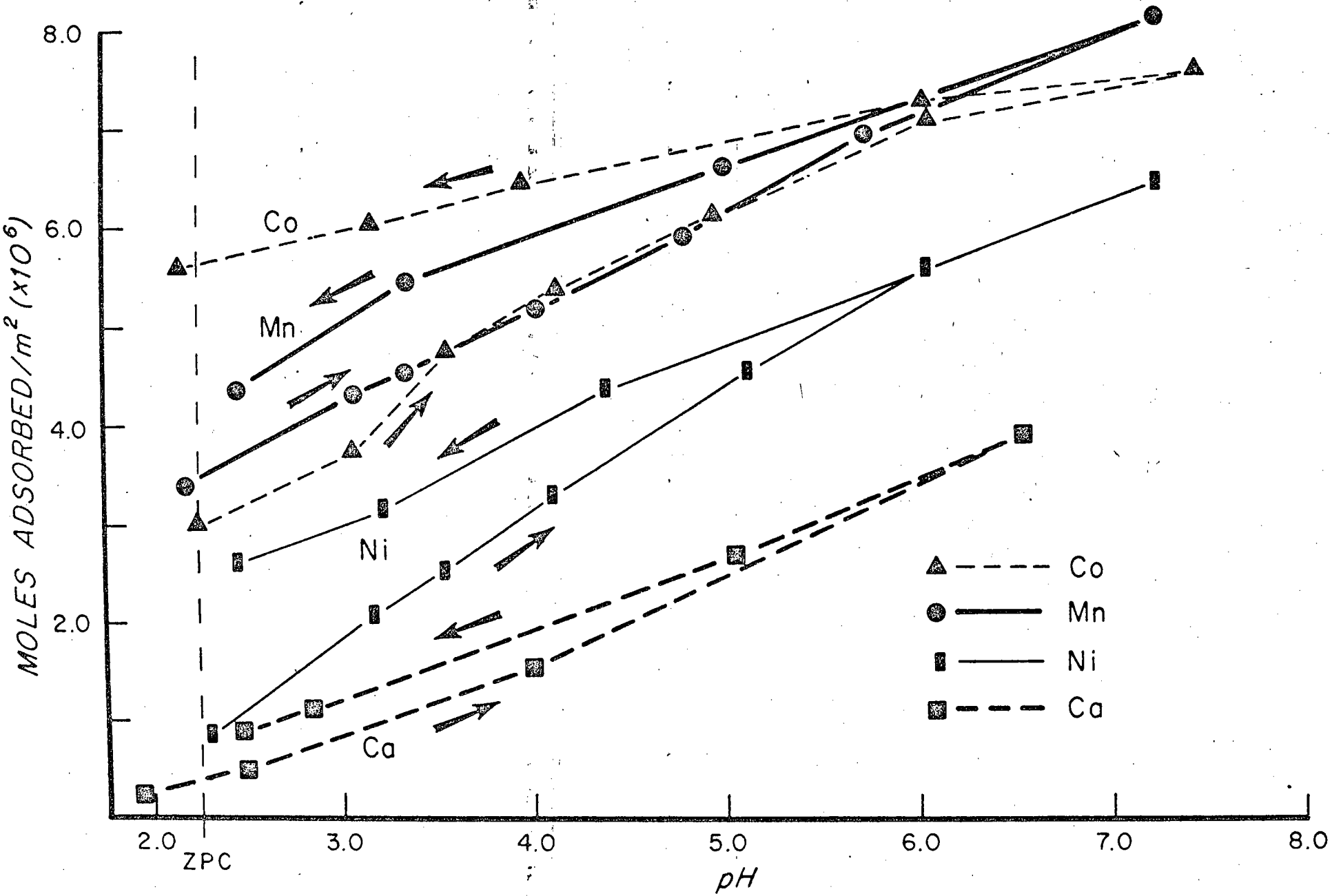
8.0
6.0
4.0
2.0
MOLES ADSORBED/m² (X10⁶)
Co
Mn
Ni
Ca
Co
Mn
Ni
Ca
2.0
ZPC
3.0
4.0
5.0
6.0
7.0
8.0
pH

FIGURE 5

Adsorption as a function of pH for cobalt, manganese, copper, zinc and nickel. The experiments were begun at pH 2.25 and the pH was adjusted upward using 0.1M NaOH.

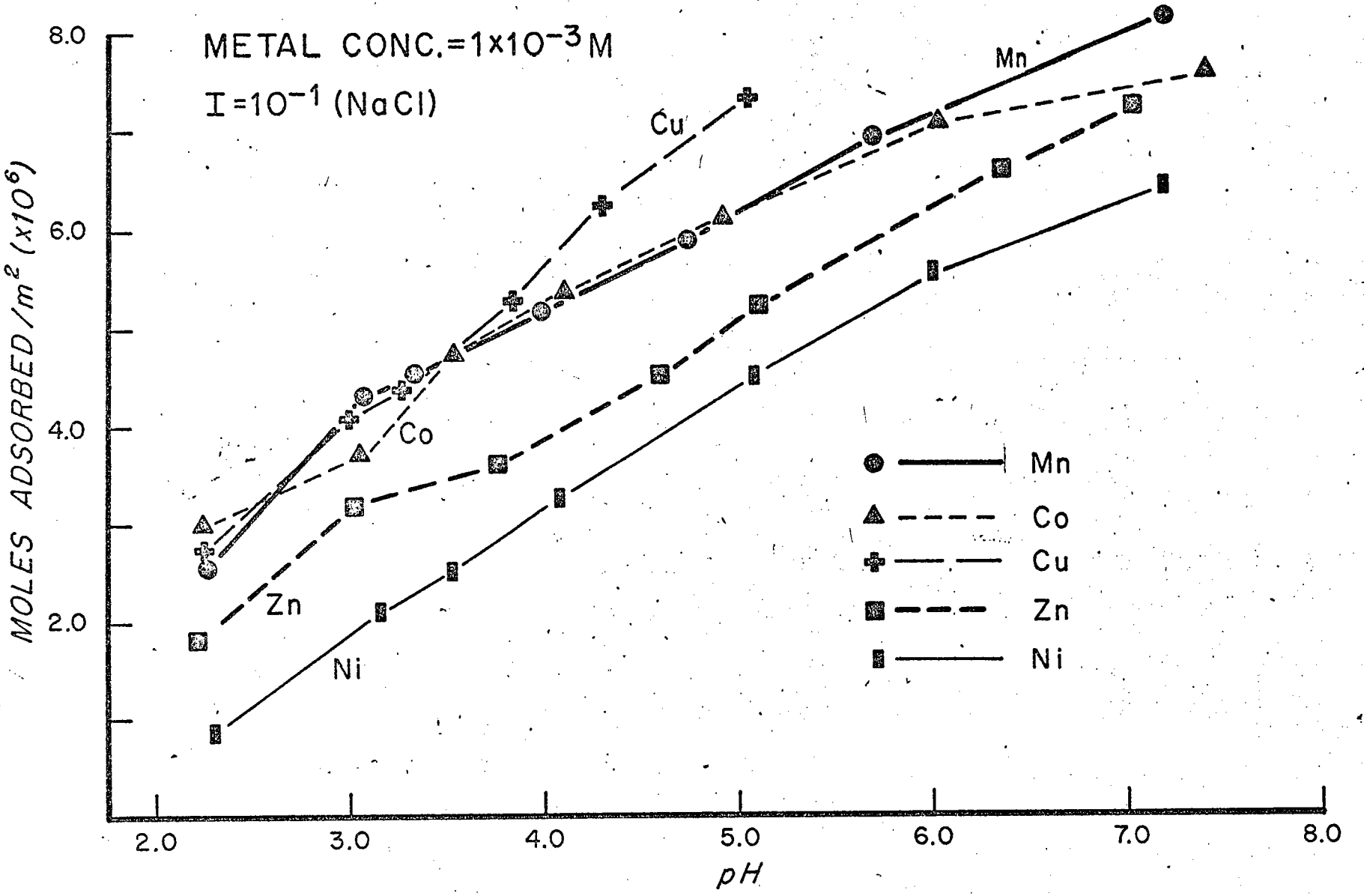
METAL CONC.=1x10⁻³M
I=10⁻¹ (NaCl)
MOLES ADSORBED/m² (x10⁶)
8.0
6.0
4.0
2.0
2.0
3.0
4.0
5.0
6.0
7.0
8.0
pH
Mn
Co
Cu
Zn
Ni
Mn
Co
Cu
Zn
Ni

FIGURE 6

Adsorption-desorption results for cobalt at concentrations from 2.5×10^{-4} M to 1.0×10^{-3} M. Adsorption was increased by upward adjustments of the pH from the initial value of approximately 2.25 using 0.1 N NaOH. After reaching approximately pH 7.0, the pH was decreased using 0.1 N HCl.
adsorption ($\rightarrow$), desorption ($\leftarrow$)

The amount of manganese released during the adsorption of 1×10^{-3} M cobalt is shown in the lower part of the figure.

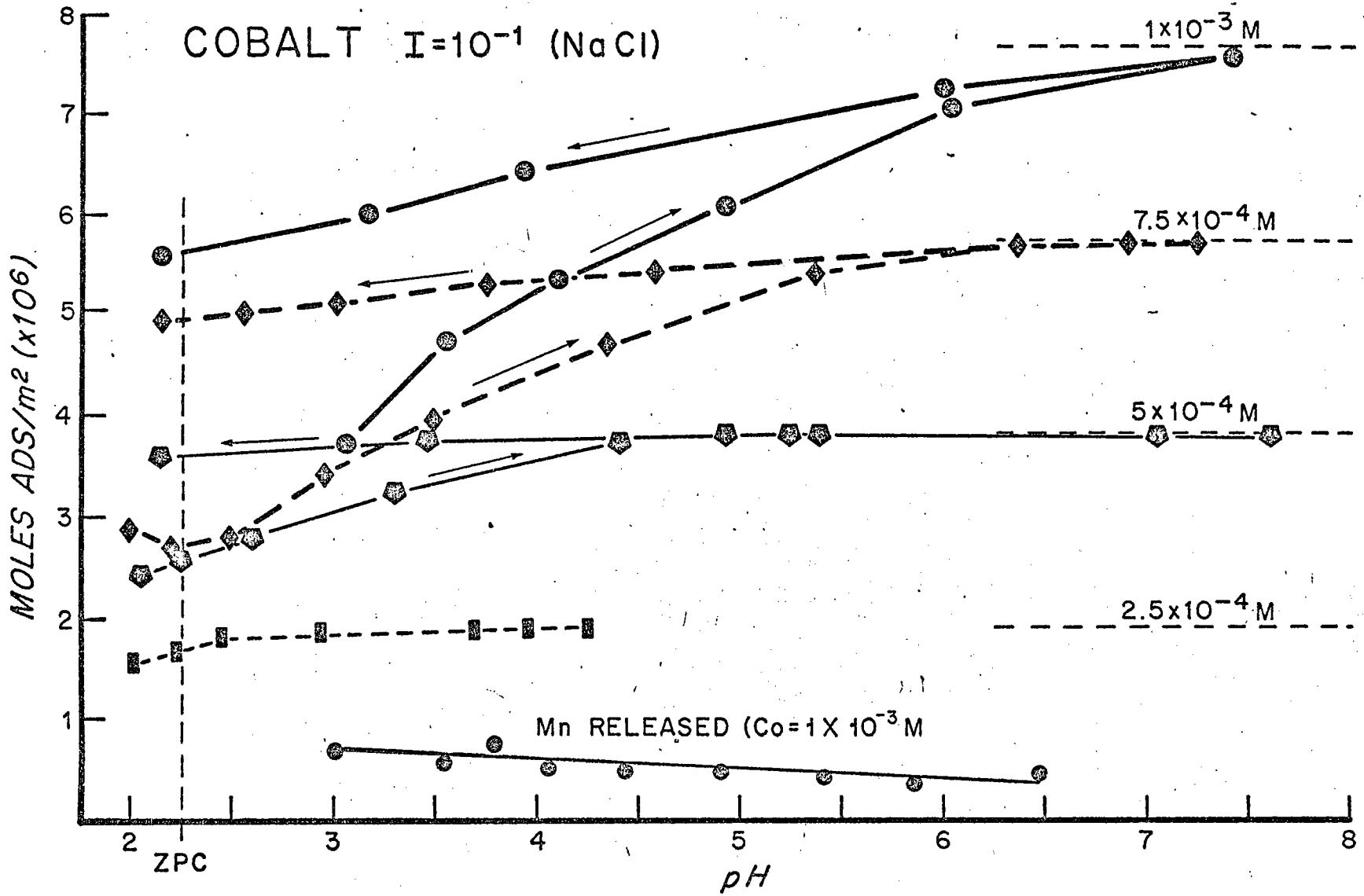
COBALT I=10⁻¹ (NaCl)
1x10⁻³ M
7.5x10⁻⁴ M
5x10⁻⁴ M
2.5x10⁻⁴ M
Mn RELEASED (Co=1X 10⁻³ M
MOLES ADS/m² (x106)
pH
ZPC
1
2
3
4
5
6
7
8

FIGURE 7

Alkalimetric titration curves and blank titration curves of δMnO_2 in the presence and absence of the alkaline earths. The metal ion concentration was 1×10^{-3}M. The titrant was 0.1N NaOH. Each experiment contained $26m^2$ of MnO_2. Total volume was 200 ml. The total ionic strength was 0.1 N (NaCl).

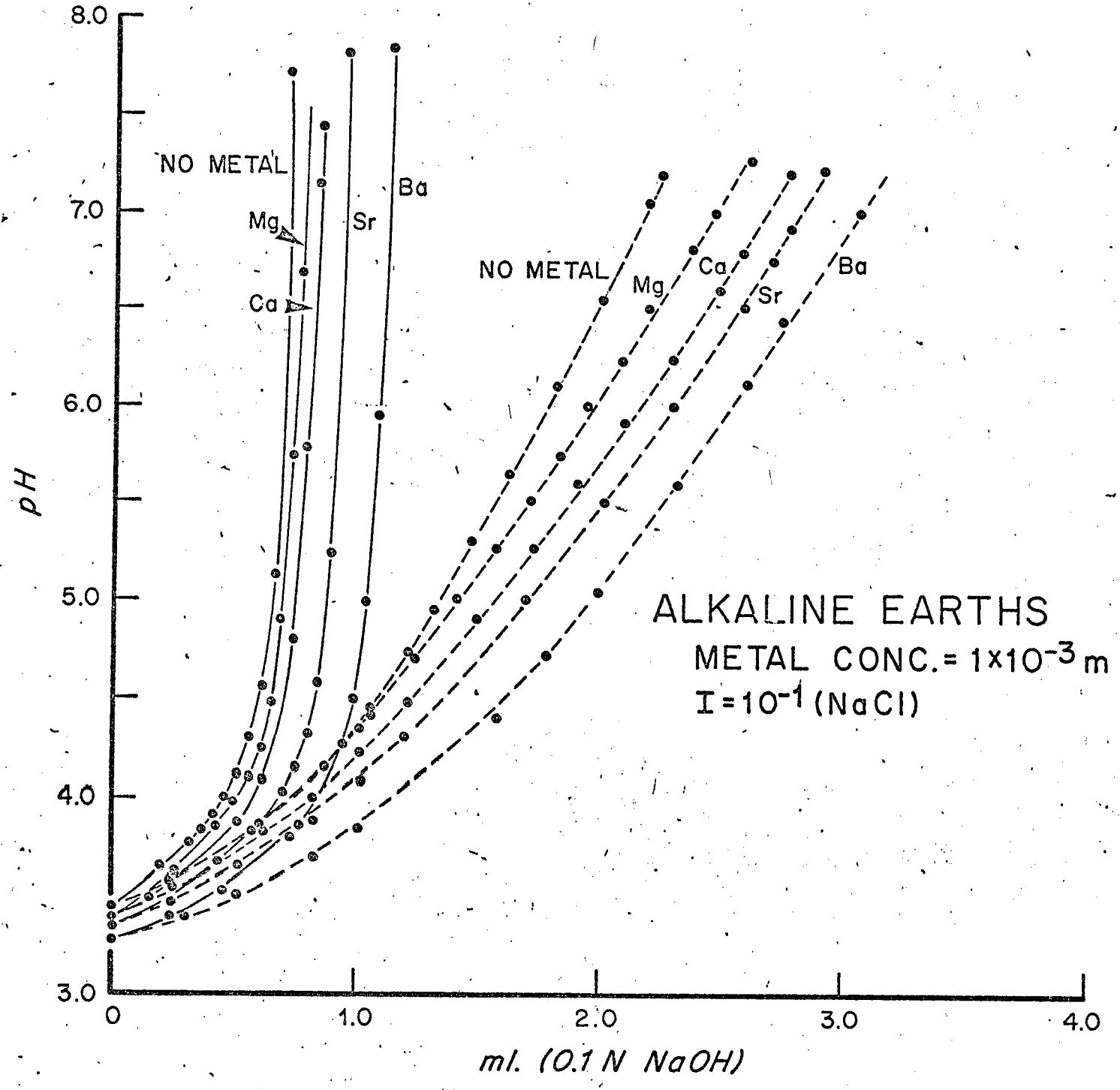
8.0
7.0
6.0
5.0
4.0
3.0
pH
NO METAL
Mg
Ca
Sr
Ba
NO METAL
Mg
Ca
Sr
Ba
ALKALINE EARTHS
METAL CONC. = 1x10⁻³ m
I = 10⁻¹ (NaCl)
0
1.0
2.0
3.0
4.0
ml. (0.1 N NaOH)

FIGURE 8

Alkalimetric titration curves and blank titration curves of δMnO_2 in the presence and absence of cobalt at concentrations from 2.5×10^{-4}M to 1.0×10^{-3}M. The experimental conditions were the same as for Figure 7.

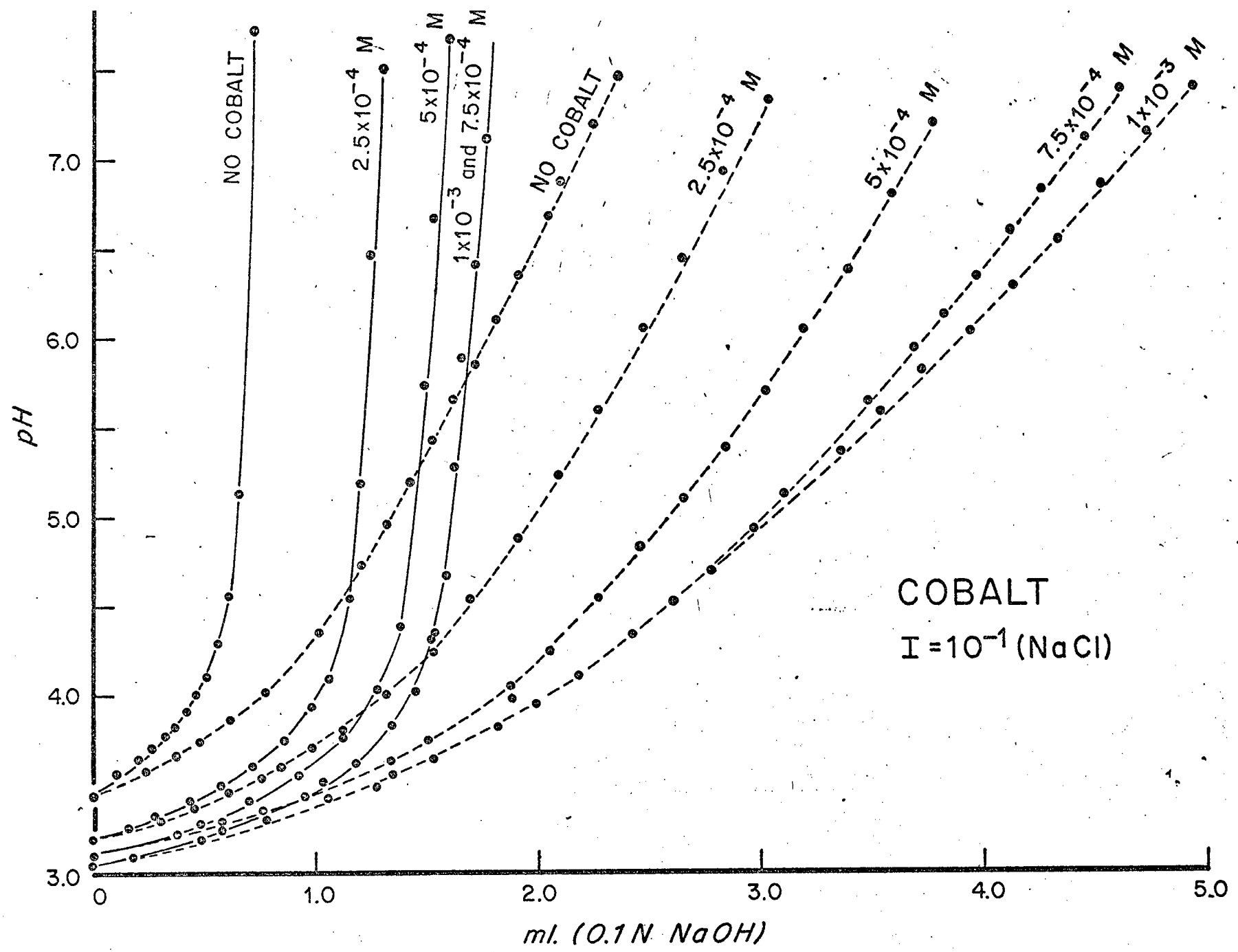
NO COBALT
2.5x10⁻⁴ M
5x10⁻⁴ M
1x10⁻³ and 7.5x10⁻⁴ M
NO COBALT
2.5x10⁻⁴ M
5x10⁻⁴ M
7.5x10⁻⁴ M
1x10⁻³ M
COBALT
I = 10⁻¹ (NaCl)
pH
7.0
6.0
5.0
4.0
3.0
0
1.0
2.0
3.0
4.0
5.0
ml. (0.1 N NaOH)

FIGURE 9

Alkalimetric titration curves and blank titration curves of δMnO_2 in the presence of 1×10^{-3}M cobalt, copper, nickel, zinc and manganese. The experimental conditions were the same as for Figure 7.

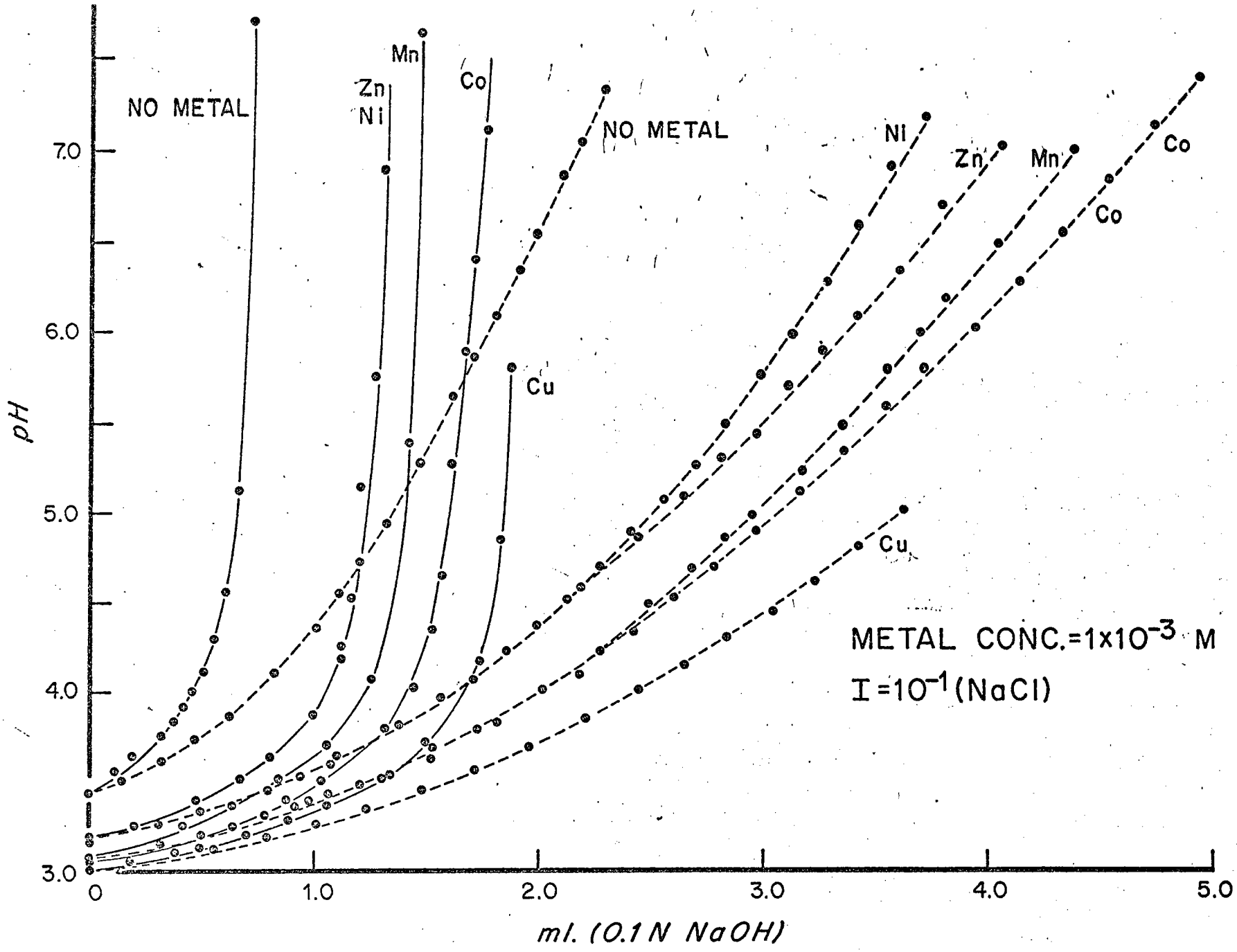
NO METAL
Zn
Ni
Mn
Co
NO METAL
Cu
Ni
Zn
Mn
Co
Co
Cu
METAL CONC.=1x10⁻³ M
I=10⁻¹(NaCl)
pH
7.0
6.0
5.0
4.0
3.0
0
1.0
2.0
3.0
4.0
5.0
ml. (0.1 N NaOH)

FIGURE 10

The net titration curves for the alkaline earths. These curves were obtained by subtracting the blank titration curves from the alkalimetric titration curves in Figure 7.

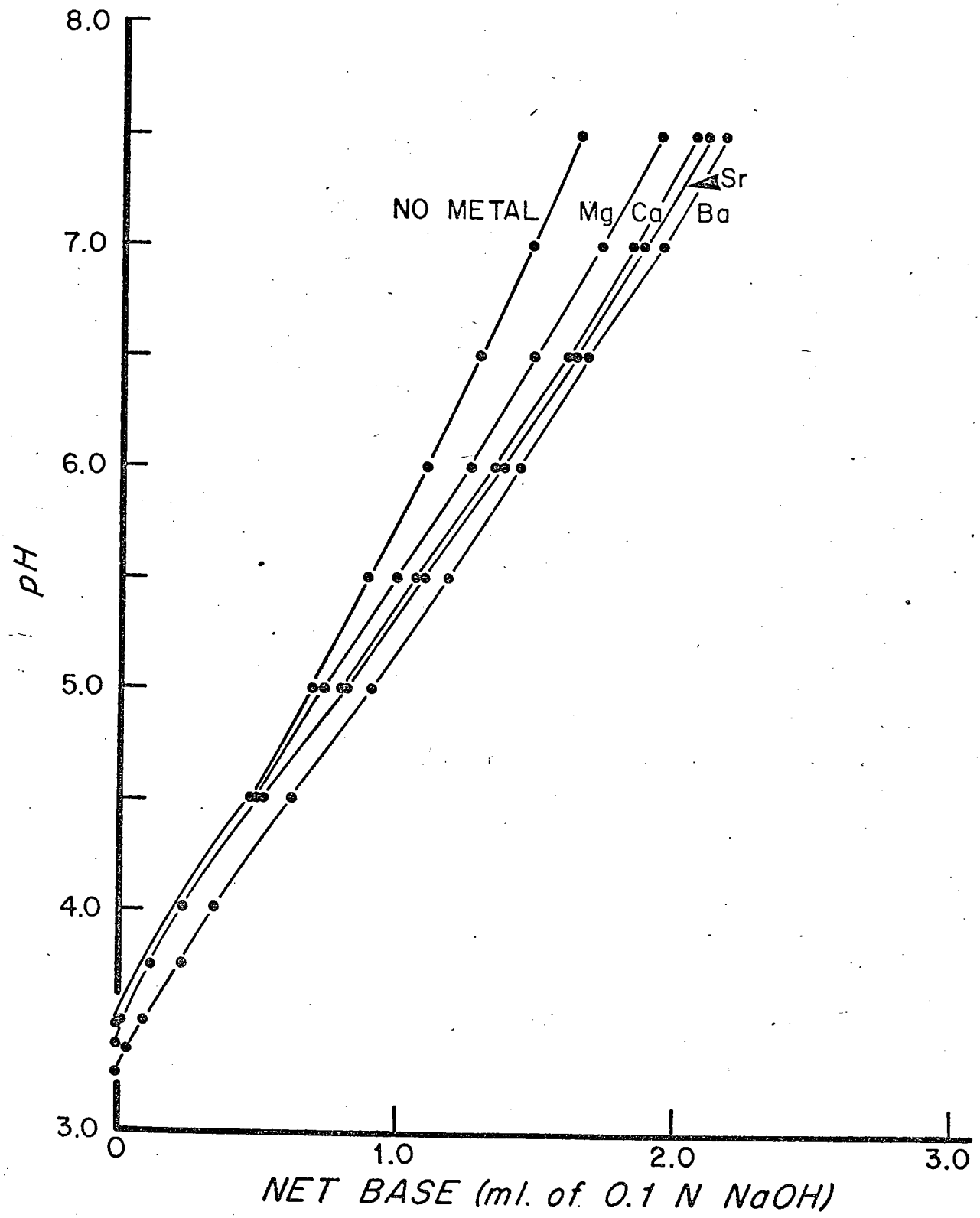
8.0
7.0
6.0
5.0
4.0
3.0
pH
NO METAL
Mg
Ca
Sr
Ba
0
1.0
2.0
3.0
NET BASE (ml. of 0.1 N NaOH)

FIGURE 11

The net titration curves for cobalt at different concentrations.

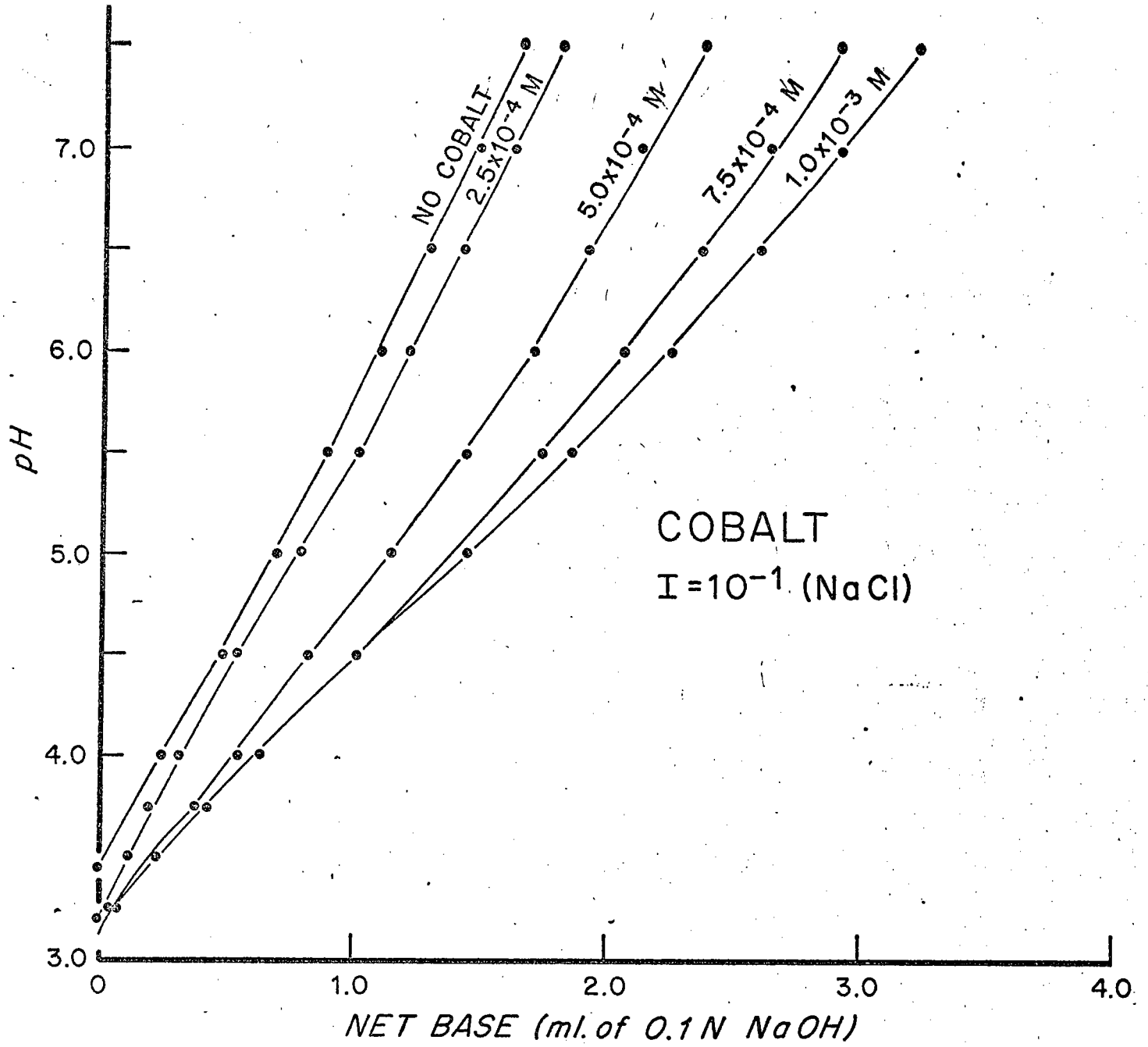
NO COBALT
2.5x10⁻⁴ M
5.0x10⁻⁴ M
7.5x10⁻⁴ M
1.0x10⁻³ M
COBALT
I=10⁻¹ (NaCl)
pH
7.0
6.0
5.0
4.0
3.0
0
1.0
2.0
3.0
4.0
NET BASE (ml. of 0.1 N NaOH)

FIGURE 12

The net titration curves for copper, cobalt, manganese, zinc and nickel.

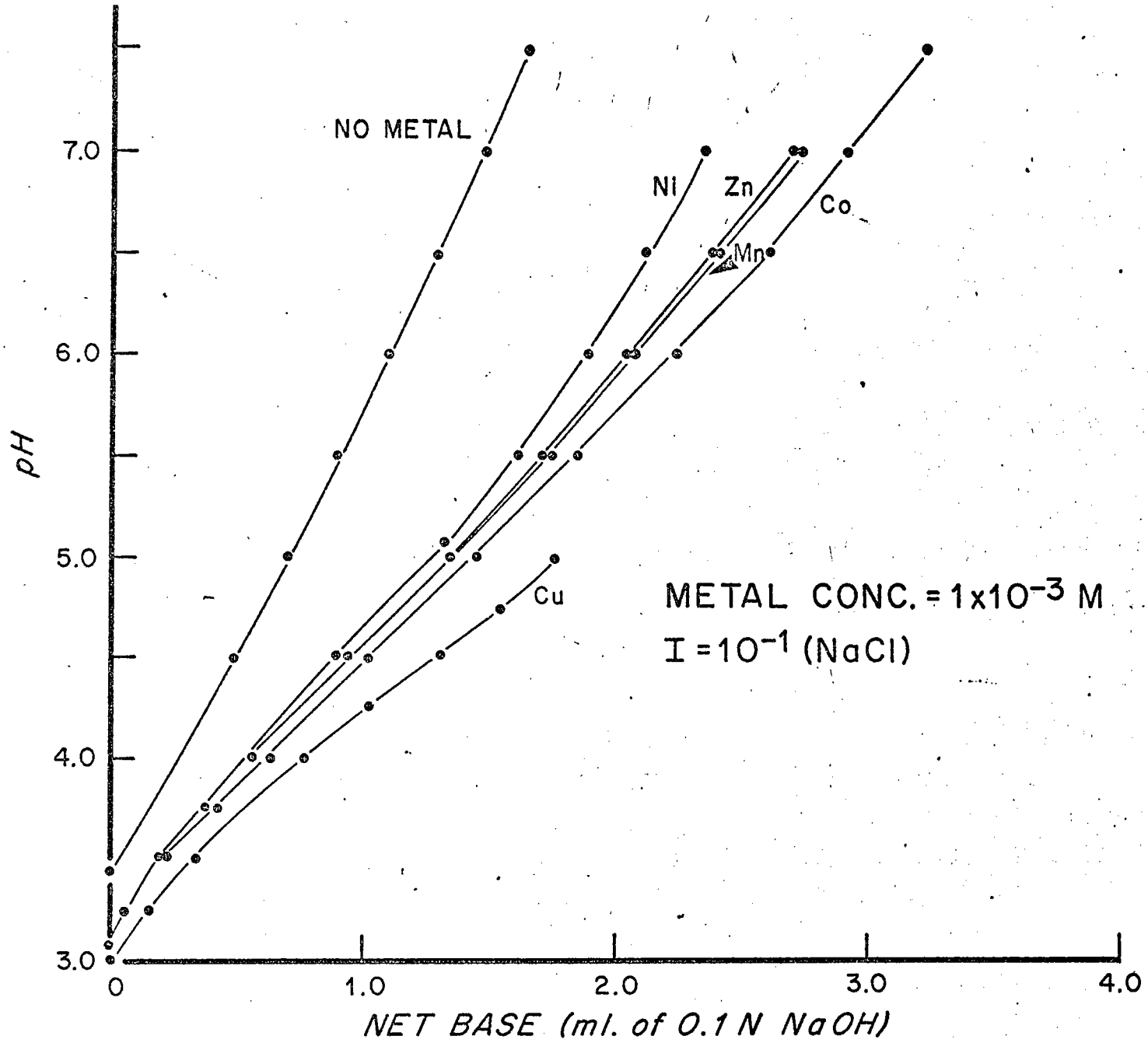
NO METAL
Ni
Zn
Co
Mn
Cu
7.0
6.0
5.0
4.0
3.0
pH
0
1.0
2.0
3.0
4.0
NET BASE (ml. of 0.1 N NaOH)
METAL CONC. = 1x10⁻³ M
I = 10⁻¹ (NaCl)

FIGURE 13

Excess base for cobalt at 2.5×10^{-4}M to 1×10^{-3}M. This represents the amount of base that is consumed by the surface that is due to the presence of cobalt.

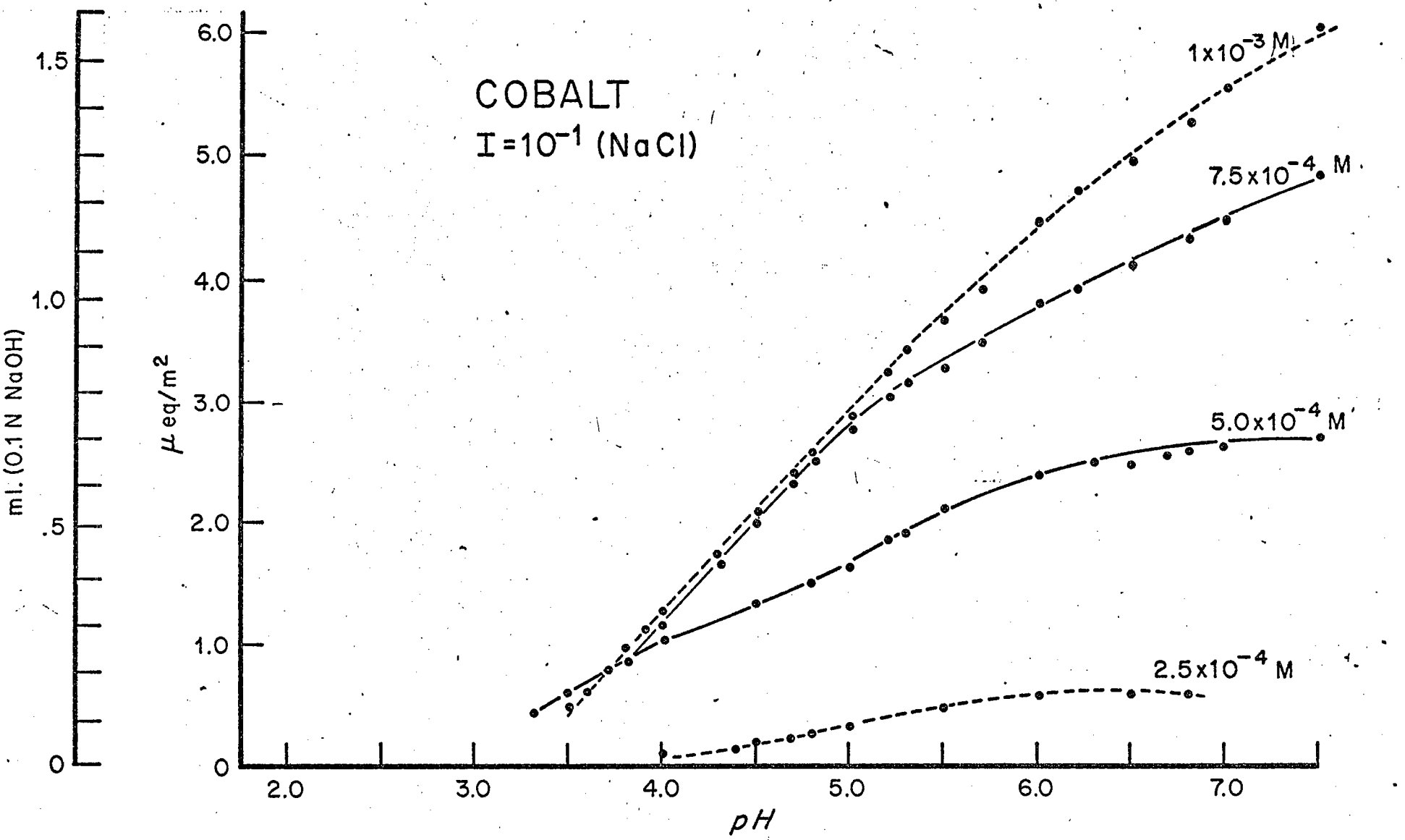
COBALT
I=10⁻¹ (NaCl)
1x10⁻³ M
7.5x10⁻⁴ M
5.0x10⁻⁴ M
2.5x10⁻⁴ M
ml. (0.1 N NaOH)
μ eq/m²
pH
0
.5
1.0
1.5
2.0
3.0
4.0
5.0
6.0
7.0

FIGURE 14

H^+ released/metal adsorbed ratios for the alkaline earths as a function pH. The metal concentrations are 1×10^{-3}M.

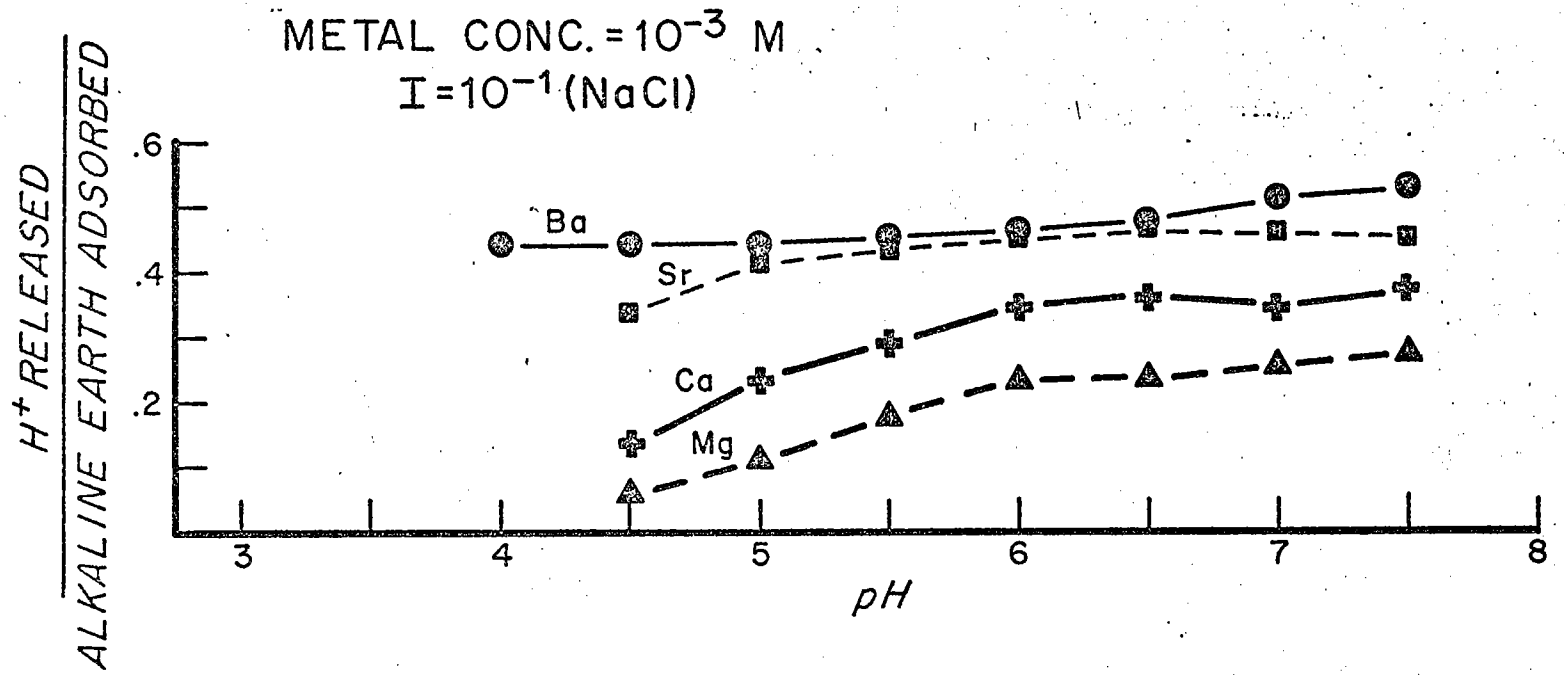
METAL CONC. = 10⁻³ M
I = 10⁻¹ (NaCl)
H⁺ RELEASED / ALKALINE EARTH ADSORBED
.6
.4
.2
Ba
Sr
Ca
Mg
3
4
5
6
7
8
pH

FIGURE 15

Kurbatov plots for the alkaline earth metal ions. Metal concentrations equal 1×10^{-3}M.

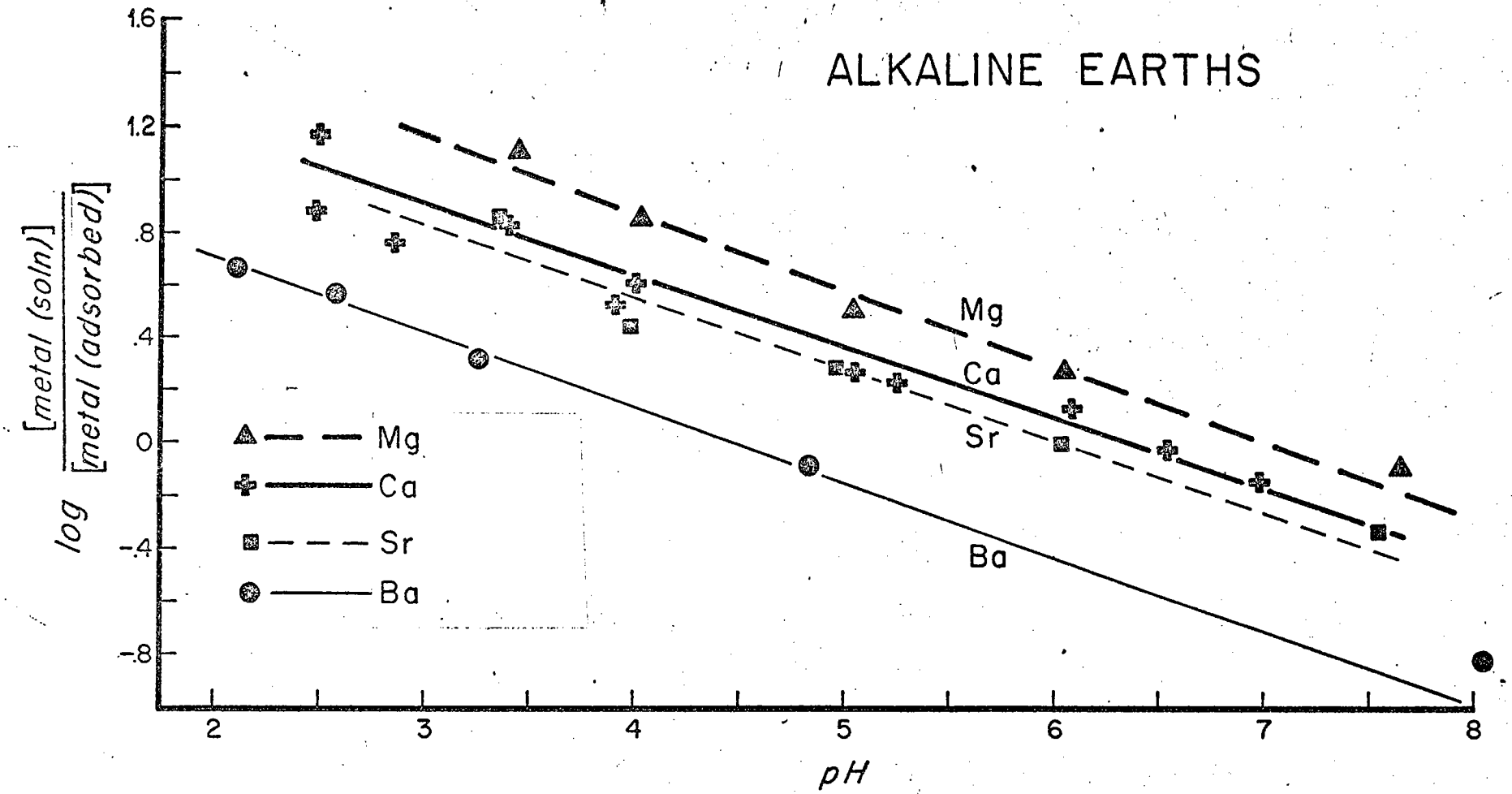
ALKALINE EARTHS
1.6
1.2
.8
.4
0
-.4
-.8
log [metal (soln)] / [metal (adsorbed)]
Mg
Ca
Sr
Ba
2
3
4
5
6
7
8
pH

FIGURE 16

Ion exchange at a fixed anionic site. The free energy change involved is a combination of the coulombic work and the energy involved in the change of the state of hydration.

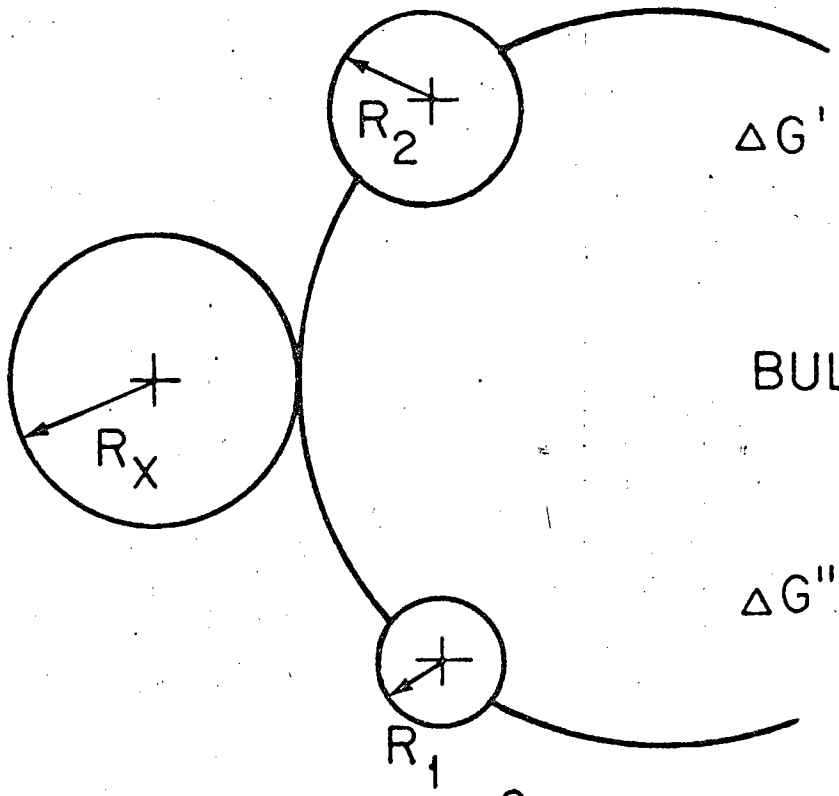

$$\Delta G' = \frac{e^2}{R_X + R_2} - \Delta G_{hydr(2)}$$

BULK SOLUTION

$$\Delta G'' = \frac{e^2}{R_X + R_1} - \Delta G_{hydr(1)}$$

$$\Delta G' = -RT \ln K_{1/2} = \frac{e^2}{R_X + R_2} - \frac{e^2}{R_X + R_1} - (\Delta G_{hydr(2)} - \Delta G_{hydr(1)}$$

EXCHANGE REACTION: $CsX + Na(aq) \rightleftharpoons NaX + Cs(aq)$; $K_{Na/Cs}$

FIGURE 17

H^+ released/metal adsorbed ratios for copper, nickel, cobalt, manganese and zinc.

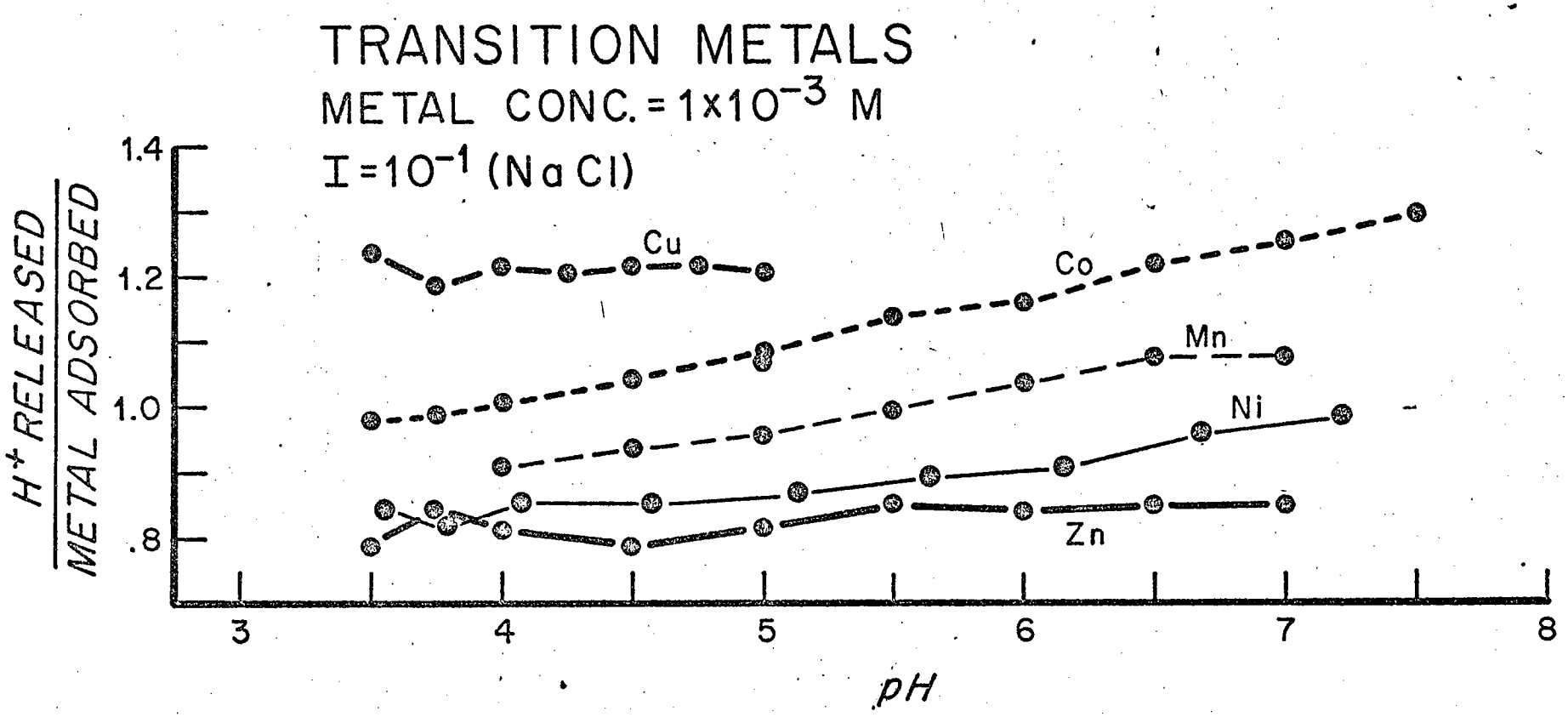
TRANSITION METALS
METAL CONC. = 1x10⁻³ M
I = 10⁻¹ (NaCl)
H⁺ RELEASED / METAL ADSORBED
1.4
1.2
1.0
.8
Cu
Co
Mn
Ni
Zn
3
4
5
6
7
8
pH

FIGURE 18

H^+ released/metal adsorbed ratios for cobalt at 5×10^{-4}M, 7.5×10^{-4}M and 1.0×10^{-3}M.

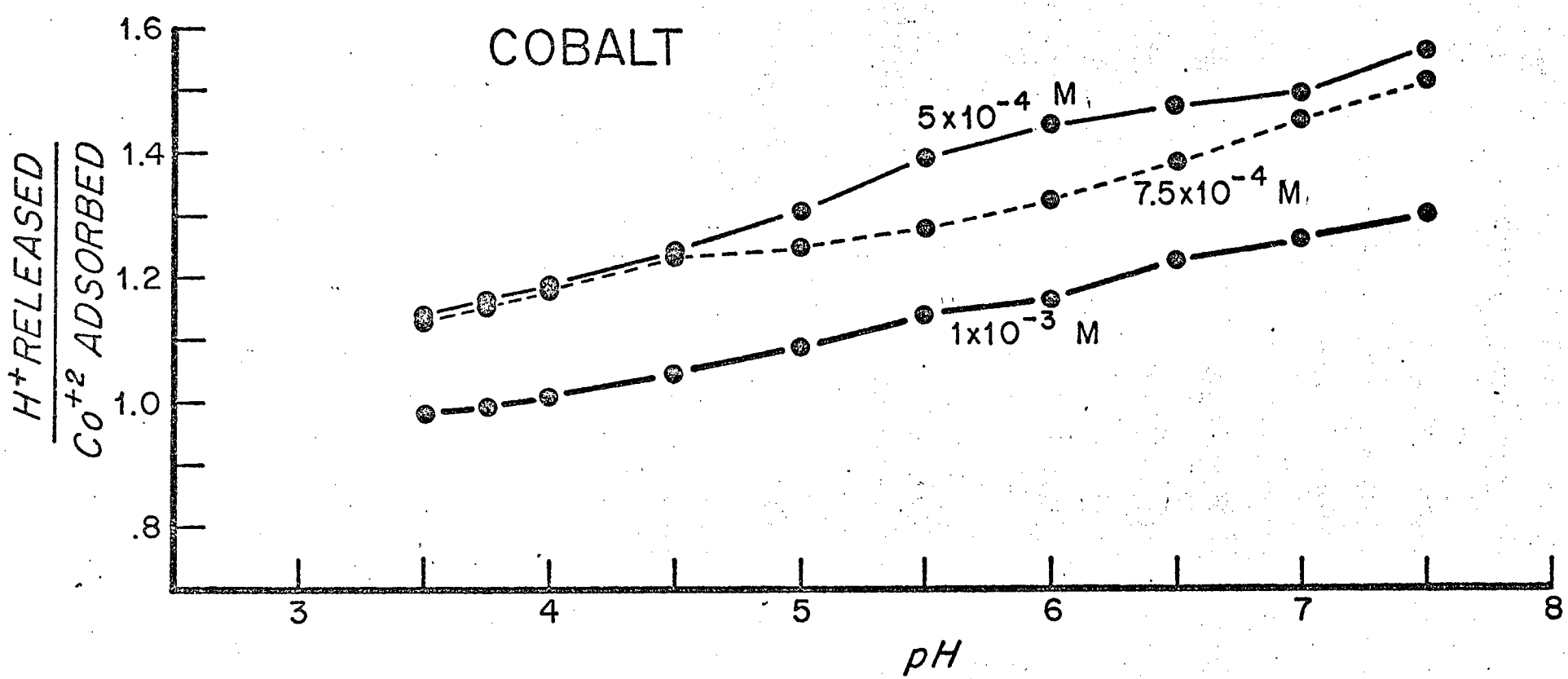
COBALT
$\frac{H^+ RELEASED}{Co^{+2} ADSORBED}$
1.6
1.4
1.2
1.0
.8
3
4
5
6
7
8
pH
5x10^{-4} M
7.5x10^{-4} M
1x10^{-3} M

REFERENCES

Bonner W.P., Bevis H.A. and Morgan J.J. (1966) Removal of strontium from water by activated alumina. Health Phys. 12, 1691-1700.

Eisenmann G. (1965) The electrochemistry of cation-sensitive glass electrodes. In Advances in Analytical Chemistry (editor C.N. Reilley),Vol 4, pp. 213-369, Wiley.

Goldberg E.D. (1954) Marine geochemistry, 1. Chemical scavengers of the sea. J. Geol. 62, 249-265.

Grahame D.C. (1947) The electrical double layer and the theory of electrocapillarity. Chem. Rev. 41, 441-501.

Healy T.W., Herring A.P. and Fuerstenau D.W. (1966) The effect of crystal structure on the surface properties of a series of manganese dioxides. J. of Colloid and Interface Science 21, 435-444.

Huang C.P. (1971) The chemistry of the aluminum oxide-electrolyte interface. Ph.D. Thesis, Harvard University.

James R.O. and Healy T.W. (1972) Adsorption of hydrolyzable metal ions at the oxide-water interface, I. Co(II) adsorption of SiO_2 and TiO_2 as model systems. J. of Colloid and Interface Science 40, 42-52.

Jenkins S.R. (1970) The colloid chemistry of hydrous MnO_2 as related to manganese removal. Ph.D. Thesis, Harvard University.

Jenne E.A. (1968) Controls on Mn, Fe, Co, Ni, Cu and Zn concentrations in solid and water; the significant role of hydrous Mn and Fe oxides. Adv. Chem. Ser. 73, 337-387.

Kolarik Z. (1961) Sorption radioaktiver Isotopen an Niederschlägen VI. System Eisen (III) - Hydroxyd-Strontiumnitratlösung und die allgemeinen Gesetzmässigkeiten der Sorption am Eisen (III)-Hydroxyd. Coll. Czech. Chem. Commu. 27, 938-949.

Krauskopf K.B. (1956) Factors controlling the concentrations of thirteen rare metals in sea water. Geochim. Cosmochim. Acta 9, 1-32B.

Kurbatov M.H., Wood G.B. and Kurbatov J.D. (1951) Application of the mass law to adsorption of divalent ions on hydrous ferric oxide. J. Phys. Chem. 55, 258-259

Kurbatov M.H., Wood G.B. and Kurbatov J.D. (1952) Isothermal adsorption of cobalt from dilute solutions. J. Phys. Chem. 56, 1170-1182.

Loganathan P. and Burau R.G. (1973) Sorption of heavy metal ions by a hydrous manganese oxide. Geochim. Cosmochim. Acta, in press.

Morgan J.J. and Stumm W. (1965) Analytical chemistry of aqueous manganese. J. Amer. Water Wks. Assn. 57, 107-119.

Morgan J.J. and Stumm W. (1964a) The role of multivalent metal oxides in limnological transformations, as exemplified by iron and manganese. Proceedings of the 2nd International Water Pollution Research Conference, Tokyo, 103-131.

Morgan J.J. and Stumm W. (1964b) Colloid-chemical properties of manganese dioxide. J. of Colloid Science 19, 347-359.

Murray D.J., Healy T.W. and Fuerstenau D.W. (1968) The adsorption of aqueous metal on colloidal hydrous manganese oxide. Adv. in Chemistry 79, 74-81.

Posselt H.S., Anderson F.J. and Weber W.J. (1968) Cation sorption on colloidal hydrous manganese dioxide. Environmental Science and Technology 2, 1097-1093.

Parks G.A. (1965) The isoelectric points of solid oxides, solid hydroxides, and aqueous hydroxo complex systems. Chem. Rev. 65, 177-198.

Spencer D.W. and Brewer P.G. (1971) Vertical advection diffusion and redox potentials as controls on the distribution of manganese and other trace metals dissolved in waters of the Black Sea. J. Geophys. Res. 76, 5877-5892.

Stanton J. and Maatman R.W. (1963) The reaction between aqueous uranyl ion and the surface of silica gel. J. Colloid Science, 18, 132-142

Stumm W., Huang C.P. and Jenkins S.R. (1970) Specific chemical interaction affecting the stability of dispersed systems. Croatica Chemica Acta 42, 223-245

Stumm W. and O'Melia C. (1968) Stoichiometry of coagulation. J. Amer. Water Wks. Assn. 60, 514-534.

Stumm W. and Morgan J.J. (1970) Aquatic Chemistry. Wiley-Interscience. 583 pp.

CHAPTER 4

THE INTERACTION OF COBALT WITH δMnO_2

ABSTRACT

Because geochemical correlations have been found between cobalt and manganese, experiments were performed to look in detail at the interaction of cobalt with the solid-solution interface of a synthetic sample of hydrous manganese dioxide.

Adsorption of cobalt on the hydrous manganese dioxide was studied as a function of pH and surface area in NaCl solutions and solutions containing sea water concentrations of Na, Ca and Mg. ^{58}Co was used, and the total cobalt concentration was varied from 1×10^{-3}M to 1×10^{-8}M. The amount of cobalt adsorbed increased sharply at pH 6, a significantly lower pH than that required for precipitation in bulk solution or significant hydrolysis of Co(II). Sea water concentrations of Na, Ca and Mg have little effect on adsorption until the cobalt concentration is less than 10^{-7}M.

Micro-electrophoresis experiments from 1×10^{-3}M to 1×10^{-5}M show three charge reversals. The first is the pH of zero point charge of δMnO_2. The second correlates well with the abrupt increase in adsorbtion at pH 6. The third agrees well with literature values for the pH of zero point of charge of $Co(OH)_2$. This suggests that the abrupt increase in adsorption and the second charge reversal are caused by the precipitation of $Co(OH)_2$ on the δMnO_2 surface. The fact that this precipitation occurs at a much lower pH than precipitation occurs in bulk solution suggests that the solubility product is reduced by the presence of the strong electric fields in the interfacial region.

This process is complicated, however, by the fact that unhydrolyzed Co^{+2} ions can reduce the charge of the surface. Thus, the second charge reversal probably reflects both specific adsorption of Co(II) and precipitation of $Co(OH)_2$ on the surface.

I. INTRODUCTION

Geochemical relationships have been found between cobalt and manganese in the marine environment. Spencer at al. (1972) found an enrichment of cobalt and manganese in the suspended matter of the Black Sea just above the anoxic interface. They suggested that it was due to the precipitation of MnO_2 followed by subsequent scavenging of cobalt from sea water. Cobalt is one of the elements most enriched relative to sea water in manganese nodules, and adsorption onto the surface of manganese and iron oxides has been suggested as the mechanism of enrichment (Goldberg 1954). Similarly, in deep sea sediments, a correlation has been found between manganese and cobalt (Turekian and Imbrie 1966, Carvajal and Landergren 1969). The efficacy of the adsorption mechanism has been shown by Fukai (1968), who used MnO_2 to pre-concentrate cobalt from sea water as part of an analytical procedure.

The interaction of cobalt with MnO_2 is also a useful system for evaluating models for the adsorption of metal ions by metal oxides. It has been suggested that the formation of metal hydrolysis species enhances the adsorption of metal ions (for example: Matijevic et al. (1960,1961); Hahn and Stumm 1968). Most results indicate that the hydrolysis products of multivalent ions are adsorbed more readily than nonhydrolyzed metal ions at solid-solution interfaces. James and Healy (1972c) recently proposed a model to explain this phenomenon based on experiments on the Co(II)-SiO_2 and Co(II)-TiO_2 systems. The comparison of the results presented in this paper with their model can provide a test of the generality of their model and increased understanding of the surface characteristics of δMnO_2.

The implied geochemical relationship and the need for a better understanding of the interaction of metal ions with metal oxides prompted a detailed study of the interaction of cobalt with the δMnO_2-solution interface, the results of which are reported in this chapter. The purpose of these experiments was 1) to examine the adsorptive characteristics of Co(II) with δMnO_2 over a wide range of concentrations and to establish whether or not adsorption and hydrolysis are related, 2) to compare the adsorption of cobalt in the presence and absence of sea water to see if adsorption can take place at trace concentration levels in the presence of sea water concentrations of Na^+, Ca^+ and Mg^{+2}, and 3) to test the hypothesis proposed in the previous chapter that the adsorbtion of Co^{+2} results in the release of H^+ on a one to one molar basis thus enabling unhydrolyzed Co(II) to reverse the charge of the δMnO_2 surface.

Cobalt is convenient to use because 1) it hydrolyzes, but the hydrolysis products are relatively simple and well characterized; 2) its hydrolysis products are not important below pH 8, and its solubility is not restricted until about pH 9 when $Co(OH)_2$ precipitates; 3) it does not appear to form polynuclear species that might greatly enhance the adsorptive process; and 4) it can be studied at low concentrations through the use of ^{58}Co.

II. MATERIALS AND METHODS

The δMnO_2 used in these experiments was prepared in the same manner as described in chapter 2. The characterization of this material is described in Appendices II-A, II-B and II-C .

A. Tracer Experiments

Cobalt-58 (Amersham Searle Corp.) was used for the tracer experiments because of its suitable half life (71d), its decay mode (γ, 0.810 MEV (99%)), and its availability as a carrier free isotope ($>2 \times 10^{-3}$ Ci/μg Co). The details of the tracer preparation, counting and experimental procedures are presented in Appendix IV-A.

B. Electrophoresis Experiments

The electrophoretic mobility measurements were made using a Briggs microelectrophoresis flat cell. A detailed discussion of the cell and the experimental procedure are discussed in Appendix IV-B.

III. RESULTS

A. Tracer Experiments

1) Kinetics

Kurbatov and Wood (1952) have studied the kinetics of the interaction of cobalt with hydrous ferric oxide under a variety of conditions. They found that the rate of adsorption was slower at low adsorbent concentrations, at high pH values, at high ionic strengths and low cobalt concentrations. In most of their experiments, adsorption equilibrium was reached within 24 hours. As discussed in chapter 3, there is a large difference in the equilibrium kinetics done on δMnO_2 by different workers due to the difference in preparation of the δMnO_2. Those workers who dried their δMnO_2 after preparation (Loganathan and Burau 1973 ; D.J. Murray et al. 1968) found slower kinetics than those who left the δMnO_2 in suspension (Morgan and Stumm 1964, Posselt et al. 1968 ; chapter 2). In order to properly simulate the natural aqueous environment, the δMnO_2 used in these experiments was kept in suspension at all times. In order to ensure that the adsorption curves represented equilibrium adsorption, the kinetics of adsorption were

tested for the experimental conditions used in these experiments.

Three types of kinetics were investigated: the initial equilibration after the experiment was set up, the equilibration after an increase in pH, and the equilibration after a decrease in pH. The initial adsorption was studied using 1×10^{-5}M and 1×10^{-7}M cobalt, and $0.208 m^2$ of MnO_2 ($9.6 \mu M\ MnO_2$) at an ionic strength of 0.1 M (NaCl) and pH of 2.50. Equilibrium for 1×10^{-5}M (Figure 1) was reached in less than 2 hours. The results for 1×10^{-7}M were approximately the same. Thus after being set up, all the experiments reported in this chapter were left more than 2 hours for equilibration. The kinetics after pH adjustment are shown in Figure 2. This experiment was performed on the same suspension used in the initial equilibration experiment. The pH was adjusted from pH 2.48 to 6.50. Equilibrium was reached after approximately one hour. Again similar results were found for 1×10^{-7}M cobalt. In all the ensuing adsorption experiments, more than one hour was allowed for equilibration. After the equilibration shown in Figure 2 at pH 6.50, the pH was adjusted back to pH 2.48, and the amount of cobalt adsorbed was monitored against time (Figure 3). The rate of desorption was approximately three times slower than that for adsorption. In addition, the desorption was incomplete; only 75% of the adsorbed cobalt was desorbed by the decrease in pH.

2) Effect of Surface Area

If the removal of cobalt is due to a surface reaction, the amount removed should double if the surface area is doubled. In addition, if the results are to be compared with results from the natural environment, it is necessary to approximate natural concentrations in the experiments. In order to study this effect, four experiments were set up with a cobalt

concentration of 5×10^{-6}M and varying amounts of δMnO_2. The ionic strength was 0.1N (NaCl). The amounts of δMnO_2 used were 96.0, 48.0, 24.0, and 12.0μM as MnO_2. It was impossible to work at lower concentrations of δMnO_2 as the colloid was lost to the walls of the container and to bubbles, thus affecting the results. For comparison, the maximum particulate manganese concentration above the anoxic interface in the Black Sea is approximately 1.0μM (Spencer et al. 1972).

In Figure 4, the amount of cobalt adsorbed is plotted as a function of pH for various amounts of solid. In figure 5, the same data are plotted as a function of the concentration of MnO_2 for various pH values. For comparison, two lines are drawn in Figure 5 to show the predicted amount adsorbed if doubling the amount of solid (i.e. surface area) doubles the amount adsorbed. These lines were calculated with reference to hypothetical starting points having 0.5μM and 0.75μM Co adsorbed by 12.0μM of δMnO_2. The agreement of the experimental lines with the predicted doubling lines is good. The deviation of the highest surface area is due to the fact that 100% adsorption is approached above pH = 4.5.

In Figure 6, the results of Figure 4 are plotted as adsorption density (moles/m^2) calculated using a surface area of 260m^2/g. Although there is a large difference in the percent adsorbed by the different amounts of MnO_2 when these amounts are normalized to surface area, the resulting coverage at any given pH is constant indicating that the amount adsorbed is proportional to the surface area.

3) Effect of Cobalt Concentration

The amount of cobalt adsorbed as a function of pH for various cobalt concentrations at a constant surface area (48.0μM MnO_2; 1.04m^2/l) is shown in Figure 7. The ionic strength was 0.1N. The results show that for a

given surface area the percent adsorbed increases as the cobalt concentration is decreased. This points out the necessity of scaling the amount of δMnO_2 to the cobalt concentration in each experiment. If too much δMnO_2 is used at low cobalt concentrations, all the cobalt is adsorbed, and the data are not very useful. Thus, separate experiments were done with the δMnO_2 concentration scaled to cobalt concentrations ranging from 1×10^{-3}M to 1×10^{-8}M, and the results were then normalized to surface area (Figure 8). Also shown in Figure 8 is a line corresponding to monolayer coverage predicted assuming that the cobalt retains its inner hydration sphere (i.e. $r_{Co^{+2}} + 2r_{H_2O}$).

4) The Effect of Na^+, Ca^{+2}, and Mg^{+2}

Tewari et al. (1972) studied the adsorption of cobalt on MnO_2 at 5×10^{-4}M. They found that the presence of 0.1M Ba^{+2} and Mg^{+2} had no significant effect on the amount of cobalt adsorbed between pH 6 and pH 8. Similar results were found in the experiments reported in chapter 3, which were done over a cobalt concentration range of 1×10^{-4} M to 1×10^{-3}M (Figure 10), and 5×10^{-8}M (Figure 11) cobalt in 0.1M and 0.6M NaCl and in sea water concentrations of Na^+, Ca^{+2}, and Mg^{+2} (Na^+ = 0.47M, Mg^{+2} = 0.055M, Ca^{+2} = 0.01M). At 5×10^{-6}M cobalt, 0.6M NaCl and the sea water mixture decrease the amount adsorbed slightly between pH 6.5 to 8.5. At 1×10^{-7}M, there is again little difference between 0.1M and 0.6M NaCl; however, the presence of sea water concentrations of Ca^{+2} and Mg^{+2} produces a significant suppression in adsorption over the entire pH range. At 5×10^{-8}M, both 0.6M NaCl and sea water concentrations of Ca^{+2} and Mg^{+2} suppress the adsorption.

B. Electrophoresis Experiments

The ability of hydrolyzable metal ions to reverse the charge of

anionic colloidal substrates has been of considerable theoretical interest in elucidating the mechanism of metal ion adsorption (Matijevic 1967). James and Healy (1972b) measured the electrophoretic mobility of SiO_2 and TiO_2 in the presence of various metal ions and concluded that the role of the free cations or first hydrolysis product in charge reversal could be dismissed. They concluded that there is no evidence that specific chemical interaction sufficient to lead to charge reversal occurs.

The results of the electrophoretic mobility experiments using δMnO_2 are shown in Figures 12 and 13. In Figure 12, the mobility values are shown as a function of pH for dissolved cobalt concentrations of 0, 1×10^{-5}M, 1×10^{-4}M, 5×10^{-4}M, and 1×10^{-3}M. The surface area used in these experiments was $1.13 m^2/l$, which corresponded to 0.004g/l. In order to compare electrophoretic mobilities, it is essential either to use a constant surface area or to vary the surface area in a systematic manner. The ionic strength was kept constant at 1×10^{-3}M (NaCl).

The surface area effects on the electrophoretic mobility were studied by varying the area of solid from $2.26 m^2/l$ (.0088g/l) to $0.56 m^2/l$ (.0022g/l) Figure 13). It is clear that the available surface area per unit volume must be controlled precisely if metal concentration and pH effects are to be interpreted correctly. This is due to the fact that the sign and magnitude of the mobility is determined by the adsorption density of the metal ions.

IV. DISCUSSION

A. The Interaction of Cobalt with δMnO_2 and SiO_2

There is a marked increase in cobalt adsorption on δMnO_2 over a narrow pH range as shown in Figure 7. This increased adsorption begins between pH 6

and 8. When compared with the solubility diagram for Co(II) (Figure 14), it is clear that this increase cannot be explained by an increase in the relative concentration of the first hydrolysis species, $CoOH^+$. This abrupt increase is also well below the pH at which $Co(OH)_2(s)$ will precipitate in free solution. A similar sharp increase in cobalt adsorption was found by Kurbatov et al. (1951) on hydrous ferric oxide, by Hodgson (1960) on montmorillonite, and by James and Healy (1972a)on TiO_2 and SiO_2.

Coincident with the sharp increase in adsorption is the negative to positive reversal of the surface charge of δMnO_2, which also occurs over the pH range of 6 to 8 (Figure 12). This charge reversal (C.R.2) is only the second of three charge reversals commonly found in systems involving the interaction of hydrolyzable metal ions with an anionic metal oxide surface. The first charge reversal (C.R.1) commonly is the pH(ZPC) of the metal oxide, and the third charge reversal (C.R.3) is the pH(ZPC) of the metal hydroxide that has precipitated and completely coated the surface. Incomplete coating due to lower concentrations of metal or higher concentrations of colloidal substrate will result in a dual surface of coated and uncoated areas. Thus, C.R.3 will occur at or below the pH(ZPC) of the metal hydroxide depending on the coverage achieved. Similar charge reversals were found by James and Healy (1972b)with the Co(II) - SiO_2 system.

The interaction of Co(II) with SiO_2 appears to lack any pronounced specific adsorption. In fact, there appears to be a large positive, and therefore unfavorable, change in solvation energy that tends to prevent metal ion adsorption (James and Healy 1972a). The available evidence for

metal interaction with SiO_2 indicates that adsorbed species are separated from the surface by at least one layer of water molecules precluding direct chemical bonding with the surface. The second charge reversal in the Co(II) - SiO_2 system appears to be caused by precipitation of $Co(OH)_2$ on the SiO_2 surface. This charge reversal occurs at a lower pH than that at which $Co(OH)_2$ would be expected to precipitate in bulk solution and can be explained by the effect of the high electric field at the solid-solution interface on the solubility product of $Co(OH)_2$. Under the influence of the high electric field at the surface, the dielectric constant of the interfacial medium is reduced well below the value for bulk aqueous solution. The solubility product of the metal hydroxide will be smaller and thus more insoluble in the presence of the surface. A more rigorous treatment of this effect is outlined in Appendix IV-C.

To check this conclusion, James and Healy (1927b) assumed that C.R.2 is caused by surface precipitation and determined C.R.2 as a function of surface area for constant cobalt concentration (10^{-4}m/l). The extrapolated value for C.R.2 at zero surface area gave a value of pH 7.8 which is well below the expected precipitation pH for the cobalt concentration used assuming a solubility product of $10^{-15.0}$ for $Co(OH)_2$ in bulk solution. If pH 7.8 can be assumed to indicate precipitation, a solubility product of $10^{-16.4}$ is indicated for the $Co(OH)_2(s)$ surface precipitate. As their other experiments failed to indicate any specific interaction of a covalent nature, it seems likely that the reduction of the solubility product at the SiO_2-solution interface is the best explanation for the sharp increase in adsorption and associated charge reversal observed between pH 7 to 8 for the Co(II) - SiO_2 system.

To test this hypothesis for the Co(II) - δMnO_2 system, C.R.2 was measured as a function of surface area at a constant cobalt concentration of 5×10^{-4}M (Figure 13). When the values of C.R.2 are plotted against the surface area and extrapolated to zero surface area, the extrapolated value, pH 6.18, is well below the expected pH of precipitation in bulk solution. In fact, if the extrapolated value of C.R.2 is assumed to indicate precipitation, and have no contribution due to specific adsorption, a value for K_{so} of $10^{-18.9}$ is calculated for the $Co(OH)_2$ surface precipitate. The argument that $Co(OH)_2$ (solid) is being precipitated at the surface is supported by the third charge reversal (C.R.3) shown in Figure 11. This charge reversal agrees very well with literature values (Parks 1965, James and Healy 1972b) for the pH(ZPC) for $Co(OH)_2$ (solid) of 11.0±.2. Nevertheless, the interpretation of the second charge reversal is complicated by the observation that Co(II) exhibits strong specific adsorption on δMnO_2. The value of C.R.2 for 1×10^{-3}M Co of 5.2 is less than the extrapolated pH of precipitation (6.18), and the electrophoretic mobility curves do not exhibit the sharp break in slope at C.R.2 that would be expected if precipitation were the only process occurring.

B. The Adsorption Model

Previous experiments using Mn(II), Co(II), Ni(II), and Zn(II) at concentrations between 1×10^{-4}M and 1×10^{-3}M have been used to propose a model for the adsorption process for δMnO_2 (chapter 3). The results of the experiments presented in this chapter using cobalt at concentrations down to 1×10^{-8}M support this model and indicate its validity for metal concentrations approaching sea water values. In addition, they also point

out important differences between the adsorption model presented here and the one presented by James and Healy (1972c) for SiO_2.

The principal points of my model are:

(1) The surface charge and the amount of cobalt adsorbed tend to increase with pH, indicating that as the surface becomes more negatively charged, more cobalt is electrostatically attracted to the surface. This pH dependence was shown by the linear nature of the Kurbatov plot in chapter 3 for metals at 1×10^{-3}M and can also be shown to exist at the lower concentrations used in these experiments. The derivation and assumptions of the Kurbatov plot were discussed in chapter 3. A Kurbatov plot is shown in Figure 15 for the 1×10^{-5}M cobalt data from Figure 7. The linearity of the data in Figure 15 is good up to approximately pH 7, and the deviations at higher pH values appears to be due to the onset of precipitation.

(2) Specific adsorption of transition metal ions (and to some extent alkali earth metal ions) takes place on δMnO_2 (chapter 3). Specific adsorption potentials of approximately -5.5 Kcal/mole were calculated for cobalt at concentrations between 1×10^{-4}M and 1×10^{-3}M. When specific adsorption occurs, it adds to the coulombic attraction to enhance adsorption. The adsorption experiments in this chapter do not quite extend to the pH(ZPC) (2.25); however, extrapolation of the results shown in Figures 7 and 8 suggests that significant amounts of specific adsorption can occur at lower concentrations. No specific adsorption was found to occur on SiO_2 by James and Healy (1972a). This is a significant point of difference between the model presented here and the model of James and Healy, and it suggests that the value of the second charge reversal (C.R.2) may not be entirely due to the inducement of precipitation by the charged surface.

(3) This specific adsorption, as measured by the amount of adsorption at the pH(ZPC), cannot be accounted for by the substitution of a divalent metal ion for structural Mn^{+2} or Na^{+} but must be due to a specific reaction with the surface resulting in the release of approximately one proton for each cobalt ion adsorbed. Thus, since this reaction does not maintain a constant charge on the surface, it should be possible for the unhydrolyzed metal ion. i.e. Co^{+2}, to react specifically with the surface. As unhydrolyzed Co^{+2} does not specifically adsorb on SiO_2, it should not have an effect on the charge of that surface. Comparison of the electrophoretic mobility curves of the Co(II) - δMnO_2 and Co(II) - SiO_2 systems indicates that this important difference in the adsorption models is substantiated. C.R.2 for the Co(II) - SiO_2 system is an abrupt transition, as it should be if due to precipitation; and at lower pH values, the presence of metal ions has little effect on the mobility values. For the Co(II) - δMnO_2 system, C.R.2 is not as sharply defined, and at pH values below C.R.2, increased amounts of cobalt significantly reduce the electrophoretic mobility (Figure 12). The two electrophoresis experiments using Mn(II) at 1×10^{-3}M and 1×10^{-4}M (Figure 12) prove that it is possible for an unhydrolyzed metal ion to reverse the charge at the surface. Manganese was chosen because it has a very low stability constant for the first hydrolysis species ($^{*}K_1(MnOH^{+}) = 10^{-10.6}$ (Perrin 1962)), and because it will oxidize to δMnO_2 before precipitating as $Mn(OH)_2$ (Morgan and Stumm 1964). Thus, any reversal of charge using Mn(II) must be due to specific adsorption of the unhydrolyzed metal ion. On oxidation to δMnO_2, the mobility should drop to the highly negative values expected for δMnO_2 rather than reverse the charge by the precipitation of the solid hydroxide as expected for other metal ions such as Co(II).

The mobility curves in Figure 12 show that increasing amounts of Mn(II) can reduce and reverse the potential at the surface below pH 8.0 where the Mn(II) begins to oxidize to δMnO_2. As there was little difference in the specific adsorption potentials for cobalt and manganese calculated in chapter 3, it appears reasonable to expect that unhydrolyzed Co(II) can also reverse the potential on the surface of δMnO_2.

(4) The results of both this chapter and chapter 3 show that the adsorption of δMnO_2 appears to plateau at a monolayer value that is greater than what would be calculated assuming that the cobalt ions retained their inner hydration sphere (Figure 8). This is consistent with (2) above, as it indicates that because specific adsorption occurs cobalt ions are not necessarily separated from the δMnO_2 surface by a layer of water molecules as found by James and Healy (1972a) for Co on SiO_2.

C. Oxidation of Co(II) to Co(III)

It has been suggested that δMnO_2 and FeOOH can catalyze the oxidation of Co(II) to Co(III) (Burns 1965, D.J. Murray et al. 1968). In chapter 3, it was observed that Co(II) adsorbes much more strongly than Ni(II) on δMnO_2. The solution chemistry of these two elements is practically identical, thus suggesting that the enhanced adsorption of Co(II) is due to its oxidation at the interface to Co(III).

Using thermodynamic calculations, Burns (1965) showed that reaction 1 is favorable in sea water at 2°C when the Co^{+2} ion concentration exceeds 3.0×10^{-8}M.

$$2Co^{+2}aq + 4OH^{-}aq + {}^{1}/_{2}O_2\ (g) + H_2O = 2Co(OH)_3\ (solid) \qquad (1)$$

Figure 16 shows the free energy of reaction 1 as a function of pH and

cobalt concentration for the condition of these experiments (25°C, pO_2 = .20 atm). This calculation indicates that $Co(OH)_3$ should precipitate from more concentrated solutions, and this has not been observed (Cotton and Wilkinson 1966 p.864). This discrepancy is due either to an error in the free energy values used to calculate ΔG^0 or to slow kinetics of the reaction in the absence of a suitable catalyst or to the fact that $Co(OH)_3$ is not the precipitated phase.

A possible indicator of the presence of $Co(OH)_3$ is the value for C.R.3. If Co(II) oxidizes on the surface of δMnO_2 and coats the surface, the value of C.R.3 should reflect the pH(ZPC) of $Co(OH)_3$. As $Co(OH)_3$ is not stable in free solution, its pH(ZPC) has not been measured. Parks (1965) observed that the pH(ZPC) of metal oxides of different oxidation states fall within different ranges. Those metal oxides with divalent metal ions have pH(ZPC) in the range of 8.5 to 12.5, and those with trivalent metal ions in the range 6.5 to 10.4. For example, $Fe(OH)_2$ has a pH(ZPC) of approximately 12, while the value for $Fe(OH)_3$ is 8.5. Thus, if Co(II) was oxidizing on the surface to form Co(III), the value for C.R.3 should be less than 11.0. However, the value of C.R.3 in Figure 12 is very close to the expected value for $Co(OH)_2$ (11.0), thus suggesting that under these conditions cobalt is primarily in the divalent oxidation state.

This cannot be taken as unequivocal proof that Co(III) does not or cannot form on the δMnO_2 surface, because the conditions under which the electrophoresis experiments were done are such that $Co(OH)_2$ may be precipitated at the surface at a critical pH, thus masking the influence or presence of any $Co(OH)_3$ that may be present.

D. The Effect of Ca^{+2} and Mg^{+2}

The competitive effect of sea water concentrations of Ca^{+2}, Mg^{+2} and Na^{+} is only effective at and below cobalt concentrations of 1×10^{-7} M. At 5×10^{-8}M, the lowest concentration for which 0.6M NaCl and artificial sea water (ASW) were compared, approximately 40% of the cobalt was adsorbed in the ASW mixture. This was approximately half of the amount adsorbed in 0.6M NaCl (Figure 10) showing that Ca and Mg do have some effect at these low concentrations.

The most important implications of these experiments are their extension to problems in the marine environment, and this will be the subject of the next chapter.

V. CONCLUSIONS

The amount of cobalt adsorbed by δMnO_2 shows a sharp increase between pH 6 and 8. Coincident with this sharp increase is a charge reversal (C.R.2) in the electrophoretic mobility of δMnO_2 in the same pH range. The value of the third charge reversal (11.0) indicates that the precipitation of $Co(OH)_2$ contributes to the increase in adsorption and the second charge reversal.

In addition, unhydrolyzed Co^{+2} ions can significantly reduce the charge of δMnO_2. The proposed reaction is an exchange of Co^{+2} ions in solution for protons bound on the surface on a one to one molar basis, thus reducing the negative charge of the surface. Thus, the value of the second charge reversal is a combination of two effects: the specific adsorption of the metal ion with the surface, and the precipitation on the surface of the metal hydroxide.

It has been found that Co(II) adsorbs much more strongly than Ni(II)

on δMnO_2, and although direct evidence is lacking, this relative enhancement is possibly due to the oxidation of Co(II) to Co(III). Thermodynamic calculations presented by Burns (1965) show that this is a feasible explanation under the conditions of these experiments.

The comparison of these experiments on the Co(II)-MnO_2 system with the Co(II)-SiO_2 system done by James and Healy (1972a) indicates that δMnO_2 can absorb Co(II) much more strongly than SiO_2 even though δMnO_2 and SiO_2 have a similar pH(PZC). This gives further support to the conclusions of chapter 3 that the pH(ZPC) can not be the sole indicator of the ability of a metal oxide to adsorb metal ions from solution.

Figure 1

Initial adsorption kinetics for 1×10^{-5}M cobalt and 1.0m^2/l of δMnO_2 in an ionic strength of 0.1N(NaCl) at pH 2.50. Total volume was 200 ml.

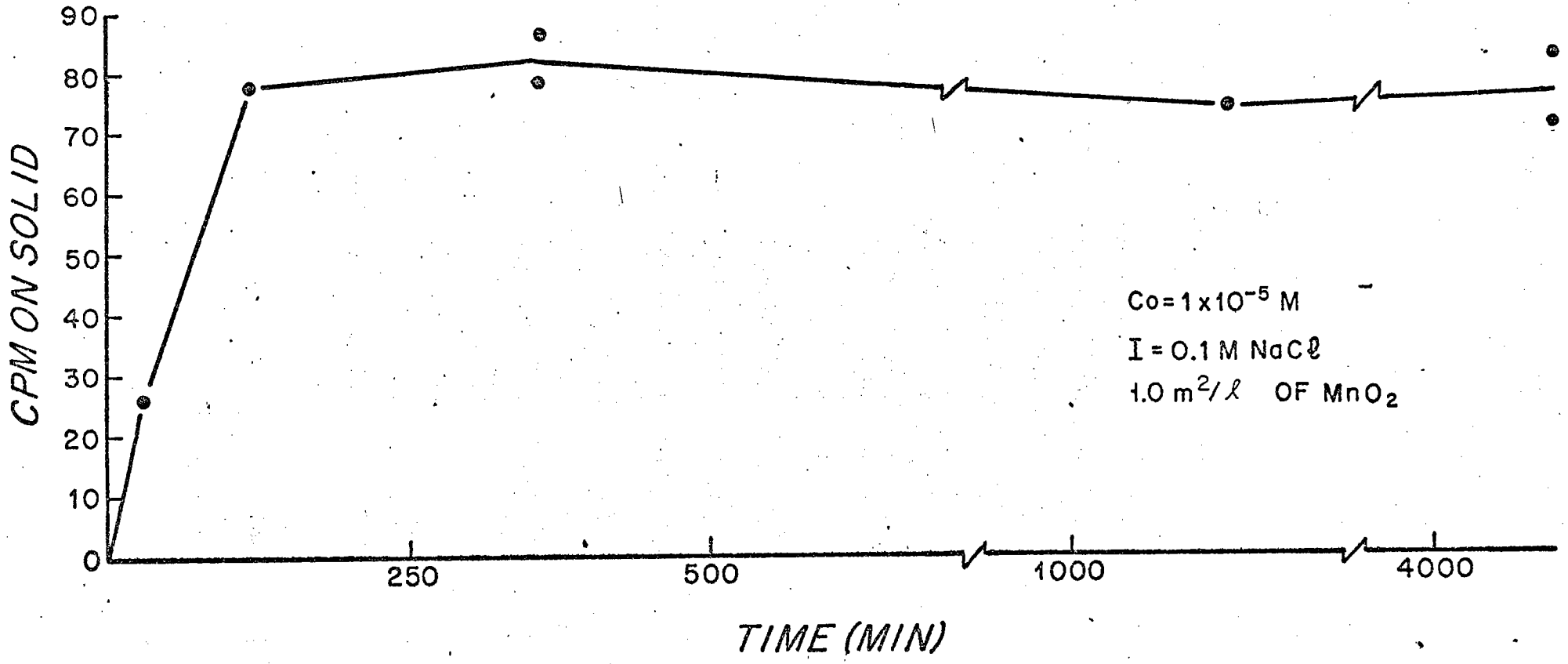
CPM ON SOLID
90
80
70
60
50
40
30
20
10
0
250
500
1000
4000
TIME (MIN)
Co = 1 x 10⁻⁵ M
I = 0.1 M NaCℓ
1.0 m²/ℓ OF MnO₂

Figure 2

The adsorption kinetics following an increase in pH from 2.48 to 6.50. This change in pH was made on the same experiment shown in Figure 1 after it had reached equilibrium.

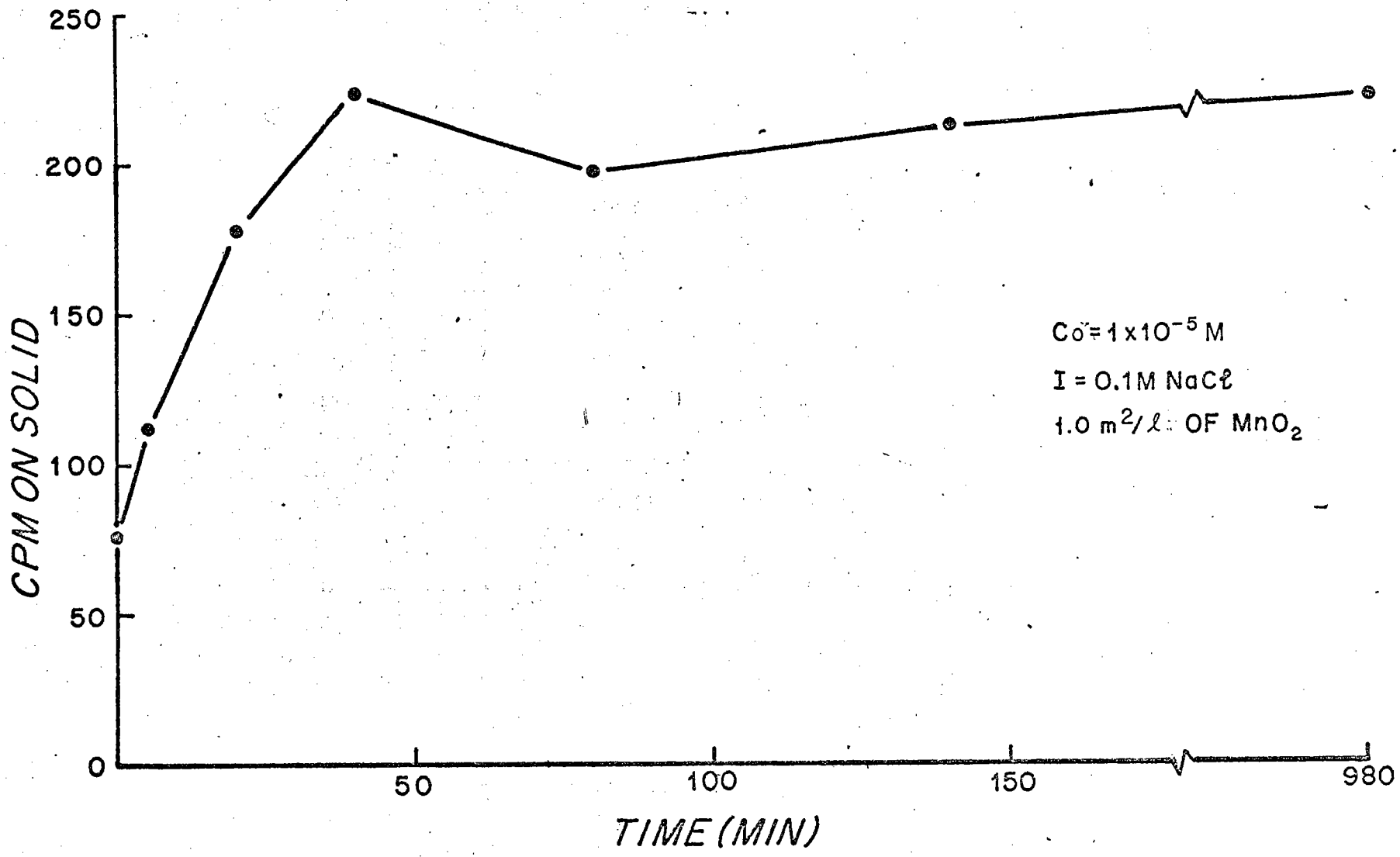
250
200
150
100
50
0
CPM ON SOLID
50
100
150
980
TIME (MIN)
Co = 1 x 10⁻⁵ M
I = 0.1M NaCℓ
1.0 m²/ℓ OF MnO₂

Figure 3

The desorption kinetics for the same experiment shown in Figures 1 and 2. After the adsorption had equilibrated in Figure 2 at pH 6.50, the pH was adjusted back to pH 2.48, the initial pH of the experiment.

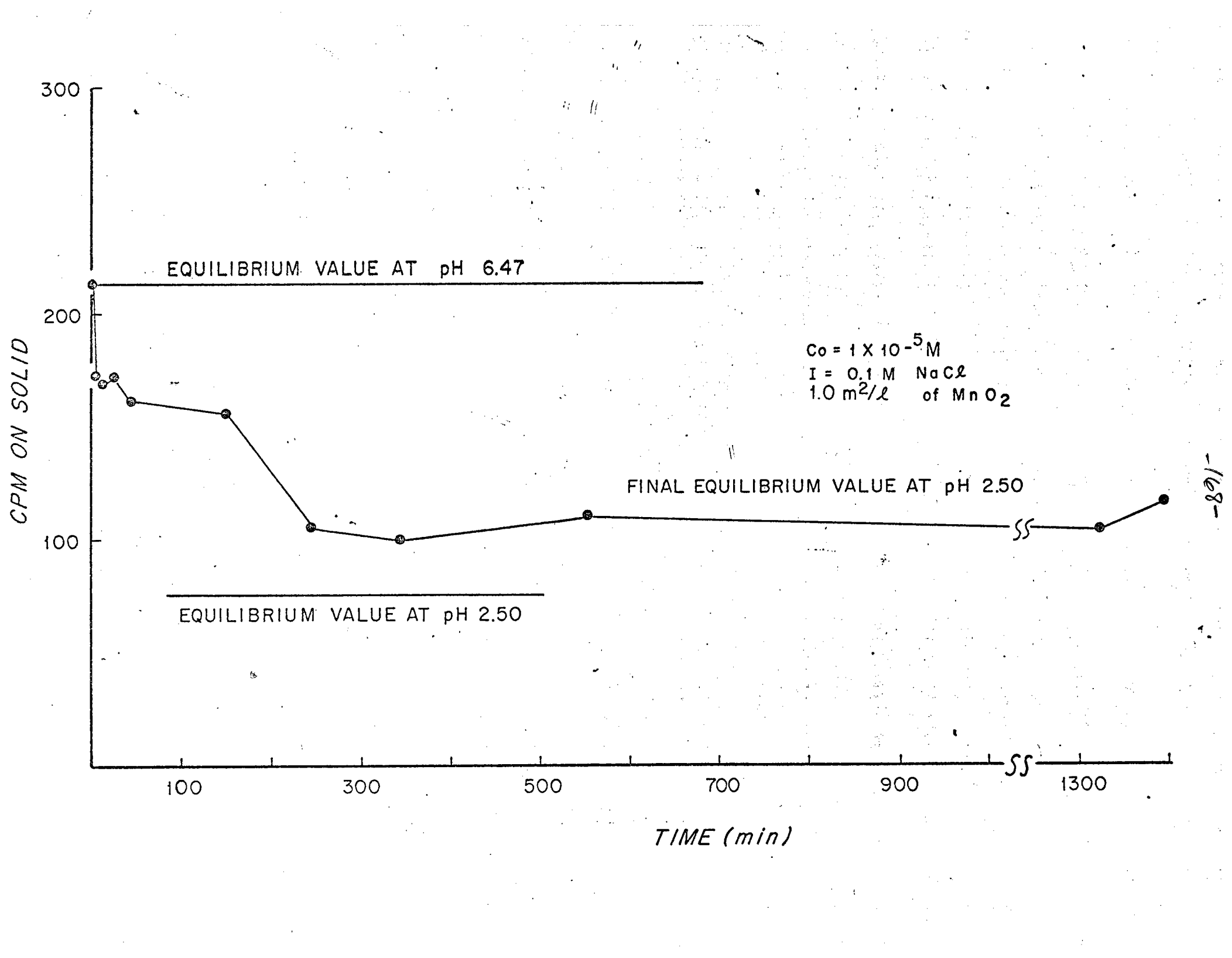
300
200
100
CPM ON SOLID
EQUILIBRIUM VALUE AT pH 6.47
Co = 1 X 10-5 M
I = 0.1 M NaCl
1.0 m2/l of MnO2
FINAL EQUILIBRIUM VALUE AT pH 2.50
EQUILIBRIUM VALUE AT pH 2.50
100
300
500
700
900
1300
TIME (min)

Figure 4

The percent and moles/l of cobalt adsorbed as a function of pH for surface areas ranging from 0.26 m^2/l to 2.08 m^2/l. The ionic strength was 0.1 M (NaCl) and the total volume was 200 ml.

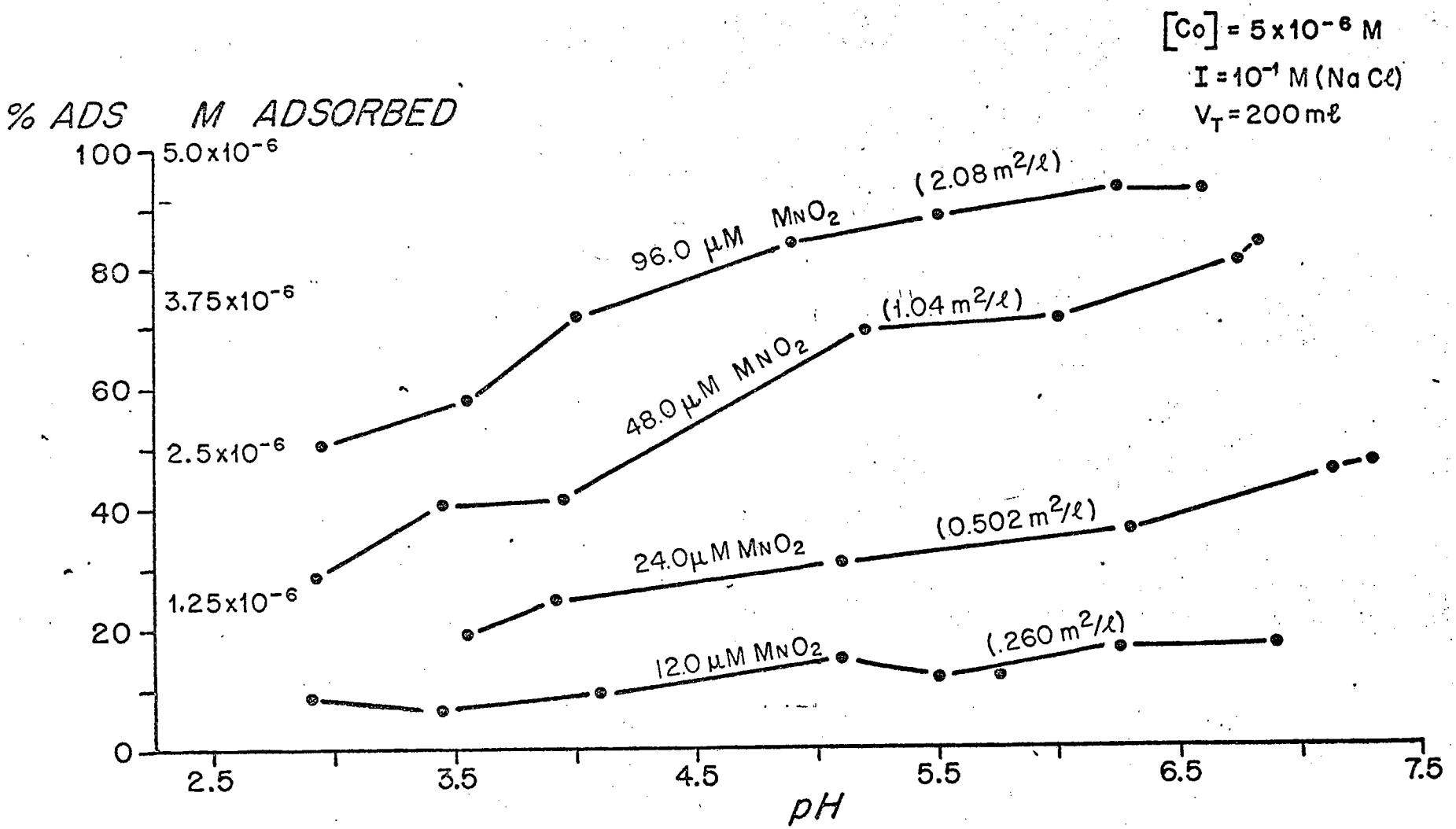
% ADS M ADSORBED
[Co] = 5x10⁻⁶ M
I = 10⁻¹ M (Na Cl)
V_T = 200 mℓ
100
80
60
40
20
0
5.0x10⁻⁶
3.75x10⁻⁶
2.5x10⁻⁶
1.25x10⁻⁶
96.0 μM MnO2
(2.08 m²/ℓ)
48.0 μM MnO2
(1.04 m²/ℓ)
24.0 μM MnO2
(0.502 m²/ℓ)
12.0 μM MnO2
(.260 m²/ℓ)
2.5
3.5
4.5
5.5
6.5
7.5
pH

Figure 5

The data from Figure 4 replotted as moles of cobalt adsorbed as a function of the amount of solid for different pH values. Doubling the surface area doubles the amount adsorbed except as 100% adsorption is approached. The dotted lines marked a and b represent the expected slope if doubling the surface area doubles the amount adsorbed. Lines a and b assume 0.15×10^{-6} moles and 0.10×10^{-6} moles adsorbed on 0.60 m^2 of MnO_2 as initial conditions.

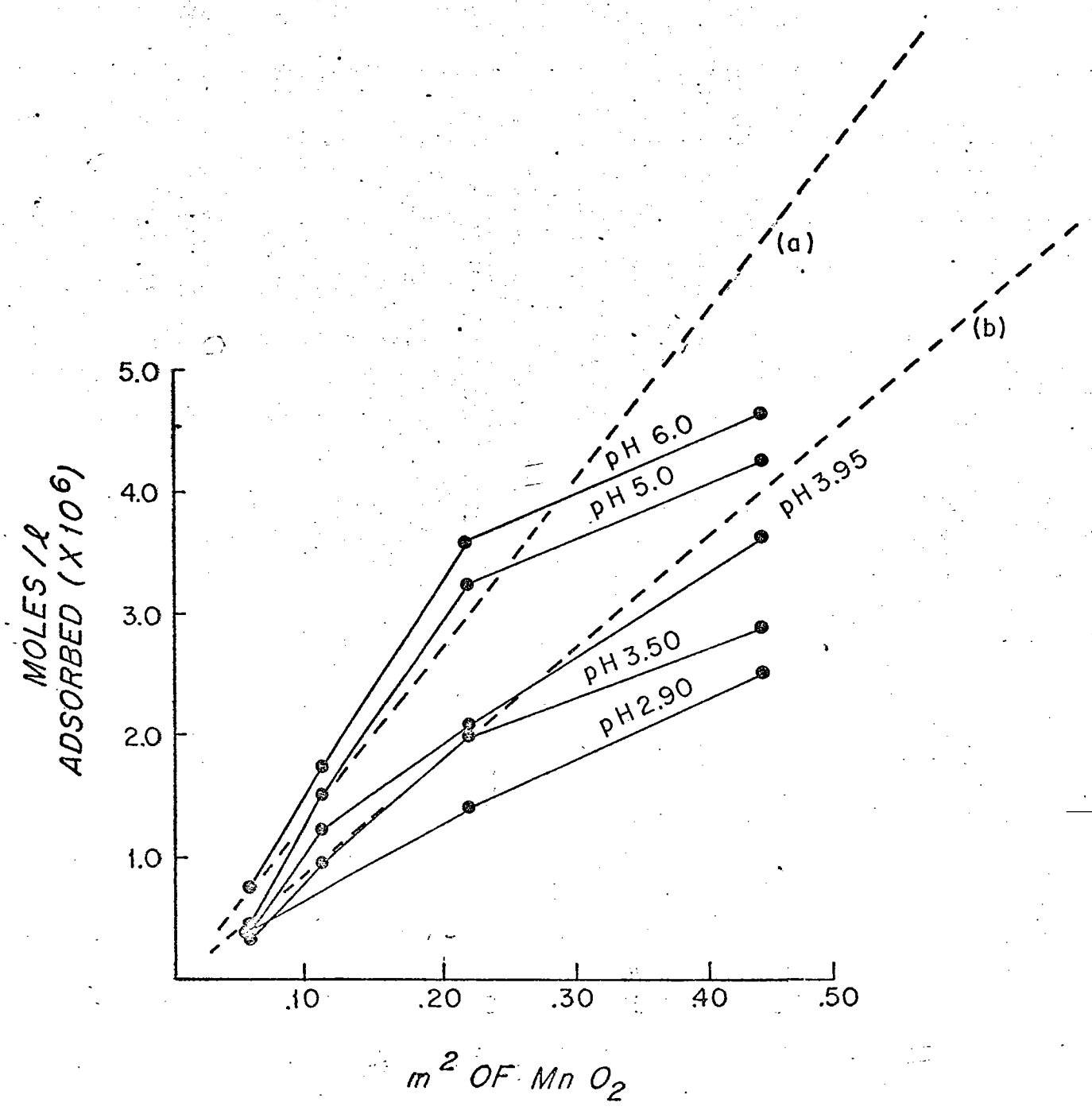
(a)
(b)
pH 6.0
pH 5.0
pH 3.95
pH 3.50
pH 2.90
5.0
4.0
3.0
2.0
1.0
.10
.20
.30
.40
.50
MOLES / ℓ ADSORBED (X 10 6)
m 2 OF Mn O2

Figure 6

The data from Figure 4 plotted as adsorption density as a function of pH. The surface area used in this calculation was $260 m^2/g$.

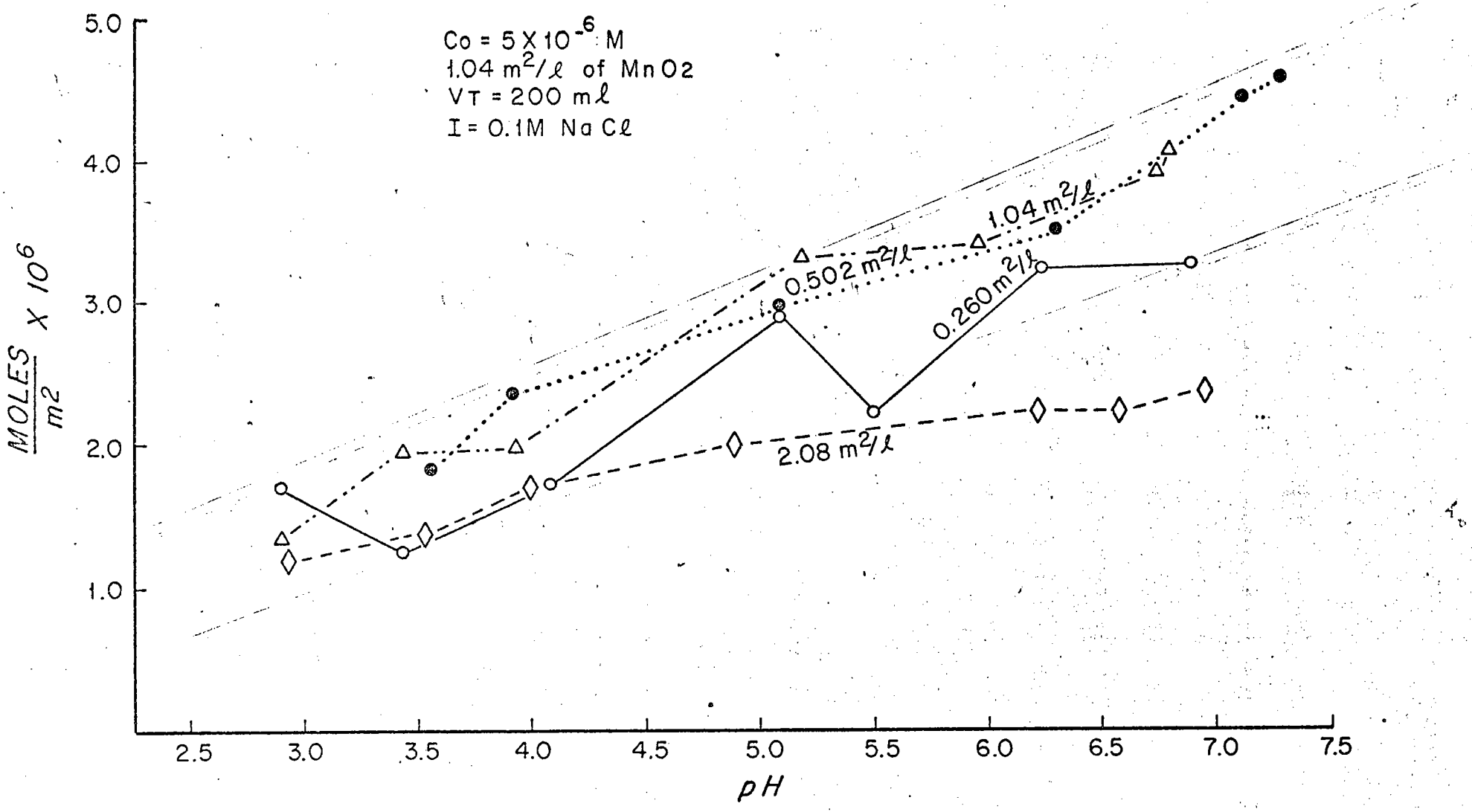
Co = 5 X 10⁻⁶ M
1.04 m²/ℓ of MnO2
VT = 200 mℓ
I = 0.1M NaCℓ
1.04 m²/ℓ
0.502 m²/ℓ
0.260 m²/ℓ
2.08 m²/ℓ
MOLES/m² X 10⁶
pH
5.0
4.0
3.0
2.0
1.0
2.5
3.0
3.5
4.0
4.5
5.0
5.5
6.0
6.5
7.0
7.5

Figure 7

The amount of cobalt adsorbed as a function of pH for a constant surface area (1.04 m^2/l). The cobalt concentrations were varied from 1.0×10^{-5}M to 1.0×10^{-6}M, and the ionic strength was 0.1 M (NaCl).

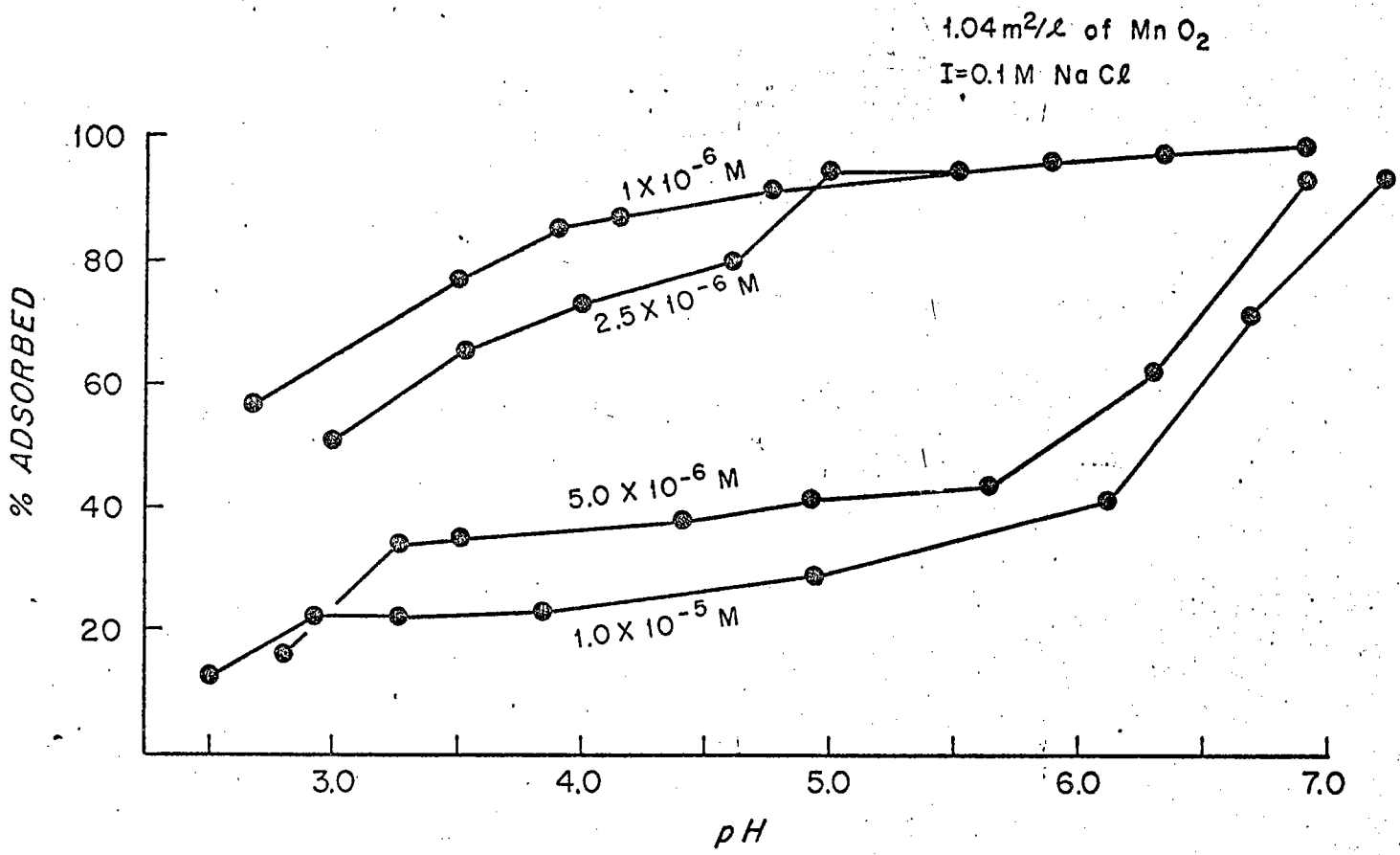
1.04 m²/ℓ of Mn O₂
I=0.1 M Na Cℓ
1X10⁻⁶ M
2.5X10⁻⁶ M
5.0 X 10⁻⁶ M
1.0X10⁻⁵ M
% ADSORBED
100
80
60
40
20
3.0
4.0
5.0
6.0
7.0
pH

Figure 8

The adsorption data for cobalt plotted as adsorption density (moles/m^2) as a function of pH and cobalt concentration. The surface areas used in each experiment are shown in parentheses. The ionic strength was 0.1 M (NaCl).

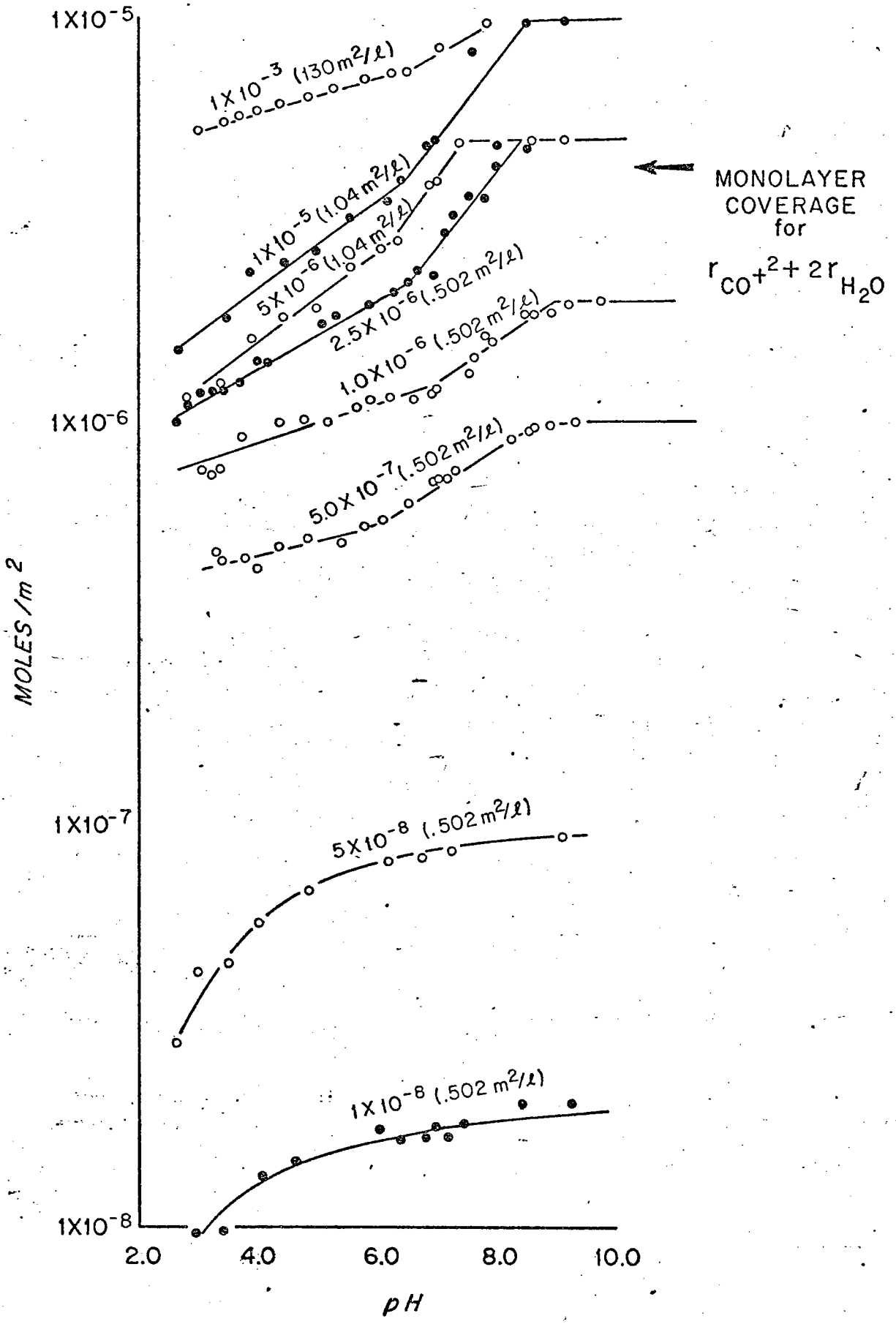
1X10⁻⁵
1X10⁻⁶
1X10⁻⁷
1X10⁻⁸
MOLES/m²
1X10⁻³ (130m²/ℓ)
1X10⁻⁵ (1.04 m²/ℓ)
5X10⁻⁶ (1.04 m²/ℓ)
2.5X10⁻⁶ (.502 m²/ℓ)
1.0X10⁻⁶ (.502 m²/ℓ)
5.0X10⁻⁷ (.502 m²/ℓ)
5X10⁻⁸ (.502 m²/ℓ)
1X10⁻⁸ (.502 m²/ℓ)
MONOLAYER COVERAGE for
r_CO+2 + 2r_H2O
2.0
4.0
6.0
8.0
10.0
pH

Figure 9

The adsorption of 5×10^{-6}M cobalt on 1.04 m^2/l of δMnO_2 in 0.1M NaCl, 0.6 M NaCl and sea water concentrations of NaCl (0.47M), $MgSO_4$ (0.055M) and $CaCl_2$ (0.01M).

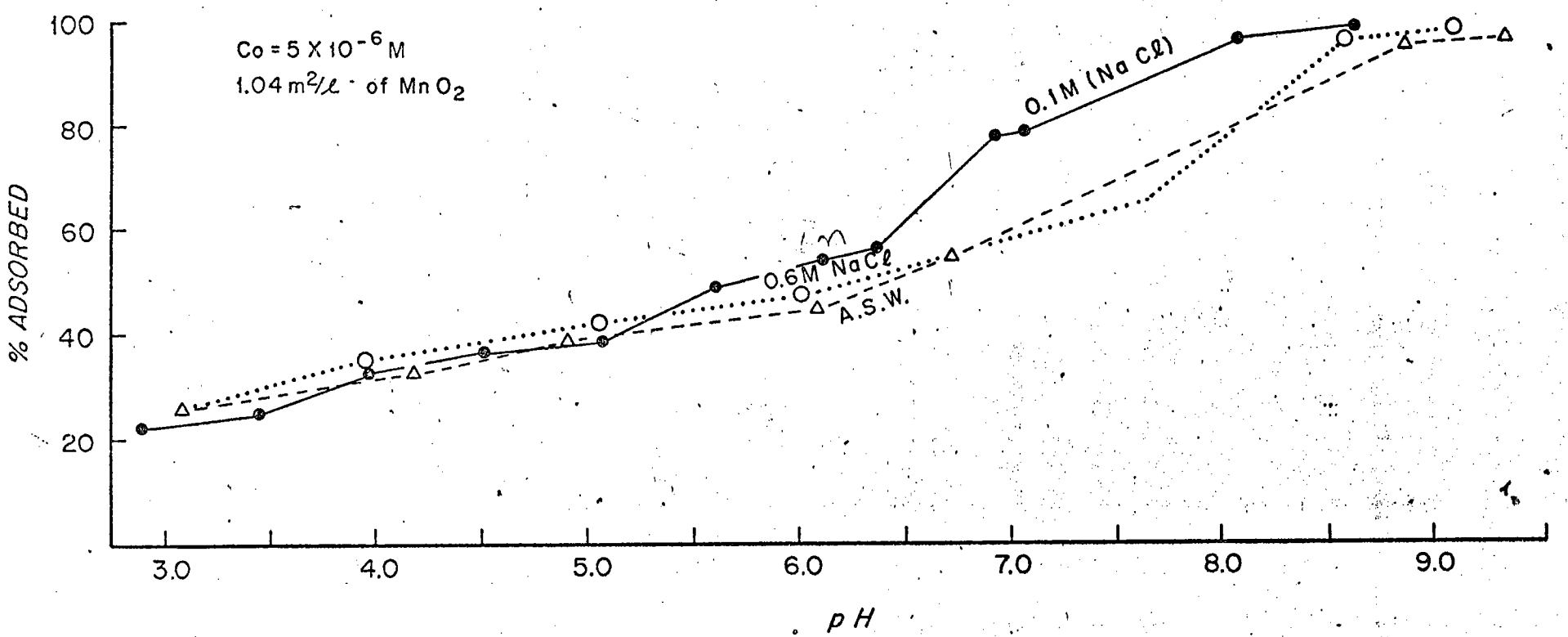
Co = 5 X 10⁻⁶ M
1.04 m²/ℓ of Mn O₂
0.1M (Na Cl)
0.6M Na Cl
A.S.W.
% ADSORBED
pH
100
80
60
40
20
3.0
4.0
5.0
6.0
7.0
8.0
9.0

Figure 10

The same conditions as the experiment in Figure 9 except cobalt = 1×10^{-7}M and the surface area = $0.52 m^2/l$ of δMnO_2.

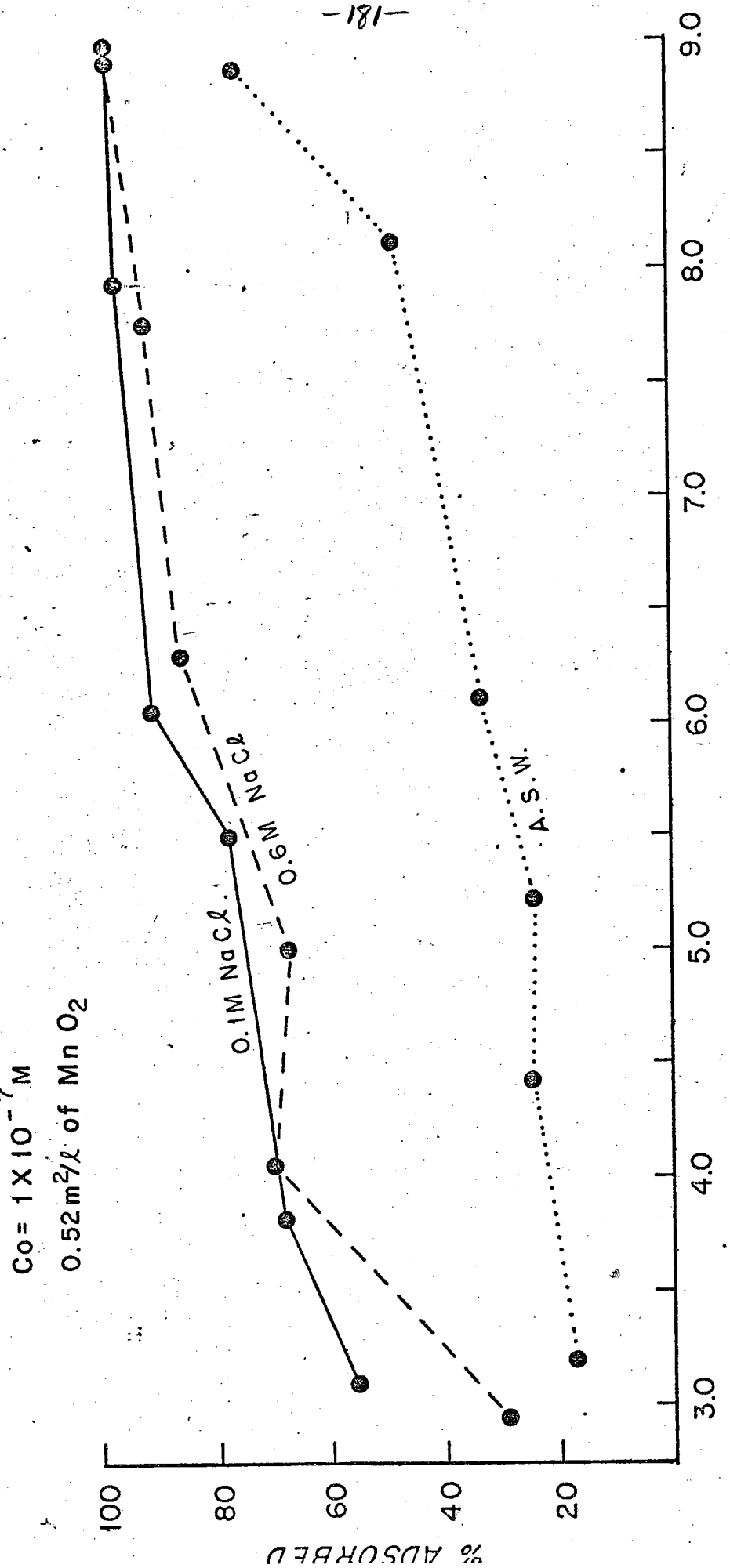
Co= 1X10⁻⁷M
0.52 m²/ℓ of Mn O₂
0.1M NaCℓ
0.6M NaCℓ
A.S.W.
% ADSORBED
100
80
60
40
20
3.0
4.0
5.0
6.0
7.0
8.0
9.0
pH

Figure 11

The same conditions as the experiment in Figure 9 except cobalt = 5×10^{-8}M and the surface area = $0.52 m^2/l$ of δMnO_2.

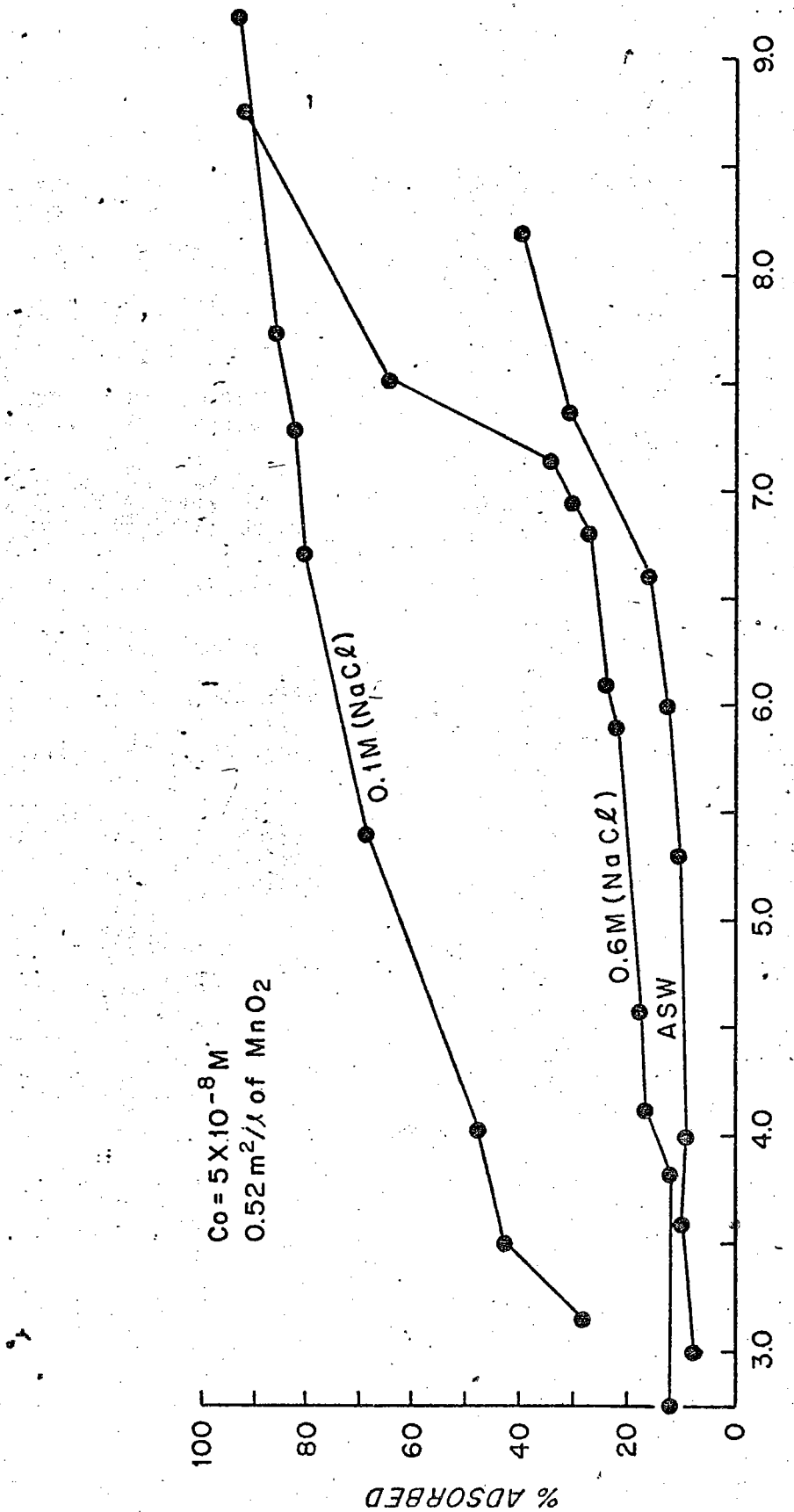
% ADSORBED
100
80
60
40
20
0
3.0
4.0
5.0
6.0
7.0
8.0
9.0
pH
0.1M (NaCl)
0.6M (NaCl)
ASW
Co = 5 X 10⁻⁸ M
0.52 m²/l of MnO₂

Figure 12

Electrophoretic mobility values for δMnO_2 in the presence of cobalt(II) (1×10^{-5}M to 1×10^{-3}M) and manganese(II) (1×10^{-4}M to 1×10^{-3}M). The surface area for all these experiments was $1.13 m^2/l$ and the ionic strength was 1×10^{-3}M (NaCl).

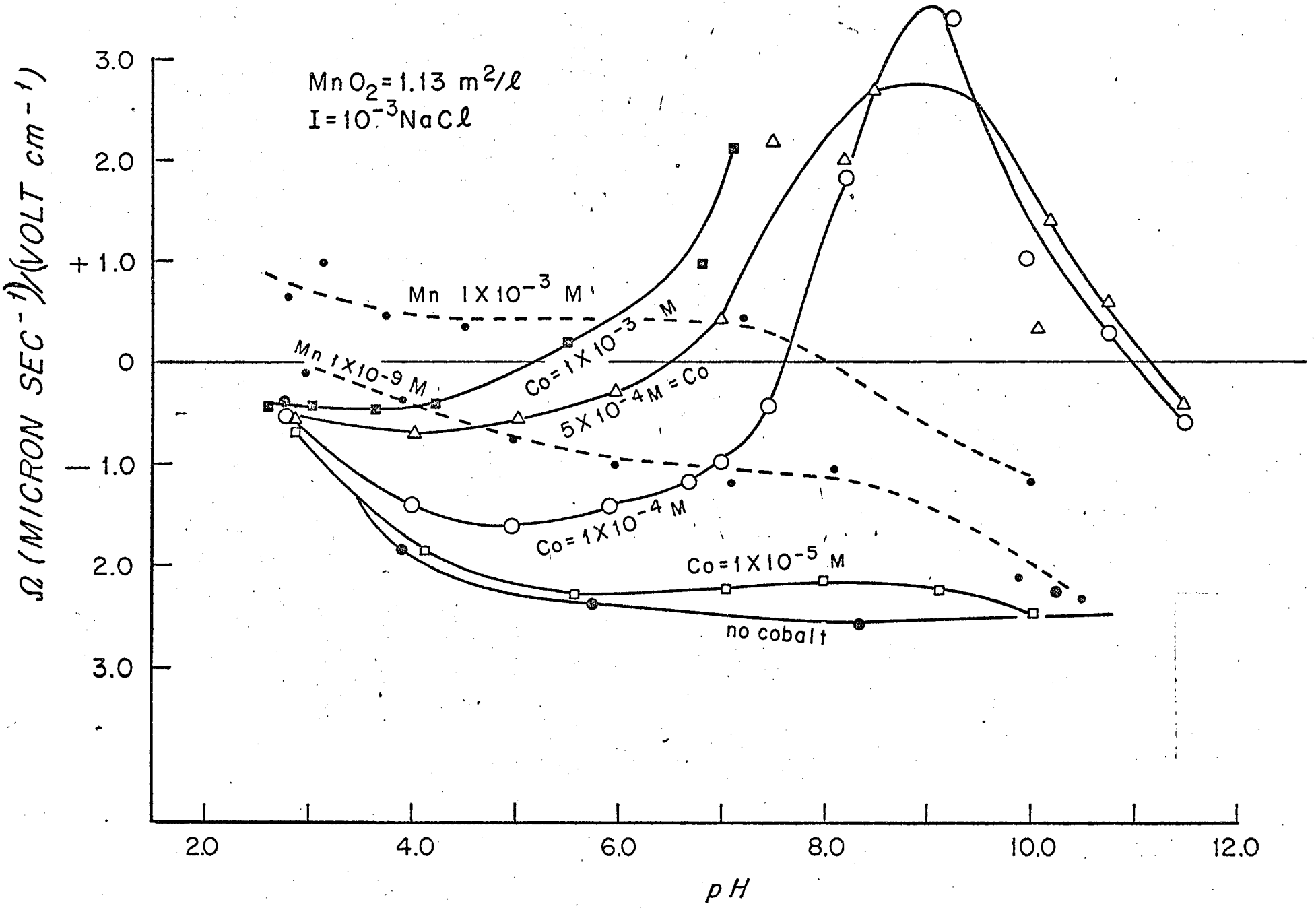
$MnO_2 = 1.13\ m^2/\ell$
$I = 10^{-3}\ NaCl$
Mn 1×10^{-3} M
Mn 1×10^{-9} M
Co = 1×10^{-3} M
5×10^{-4} M = Co
Co = 1×10^{-4} M
Co = 1×10^{-5} M
no cobalt
3.0
2.0
+ 1.0
0
− 1.0
2.0
3.0
2.0
4.0
6.0
8.0
10.0
12.0
pH
Ω (MICRON SEC^{-1})/(VOLT cm^{-1})

Figure 13

The electrophoretic mobility as a function of surface area for a constant cobalt concentration (5×10^{-4}M). The insert shows the values for the second charge reversal (C.R.2) plotted as a function of surface area. The extrapolated value for C.R.2 at zero surface area is 6.18.

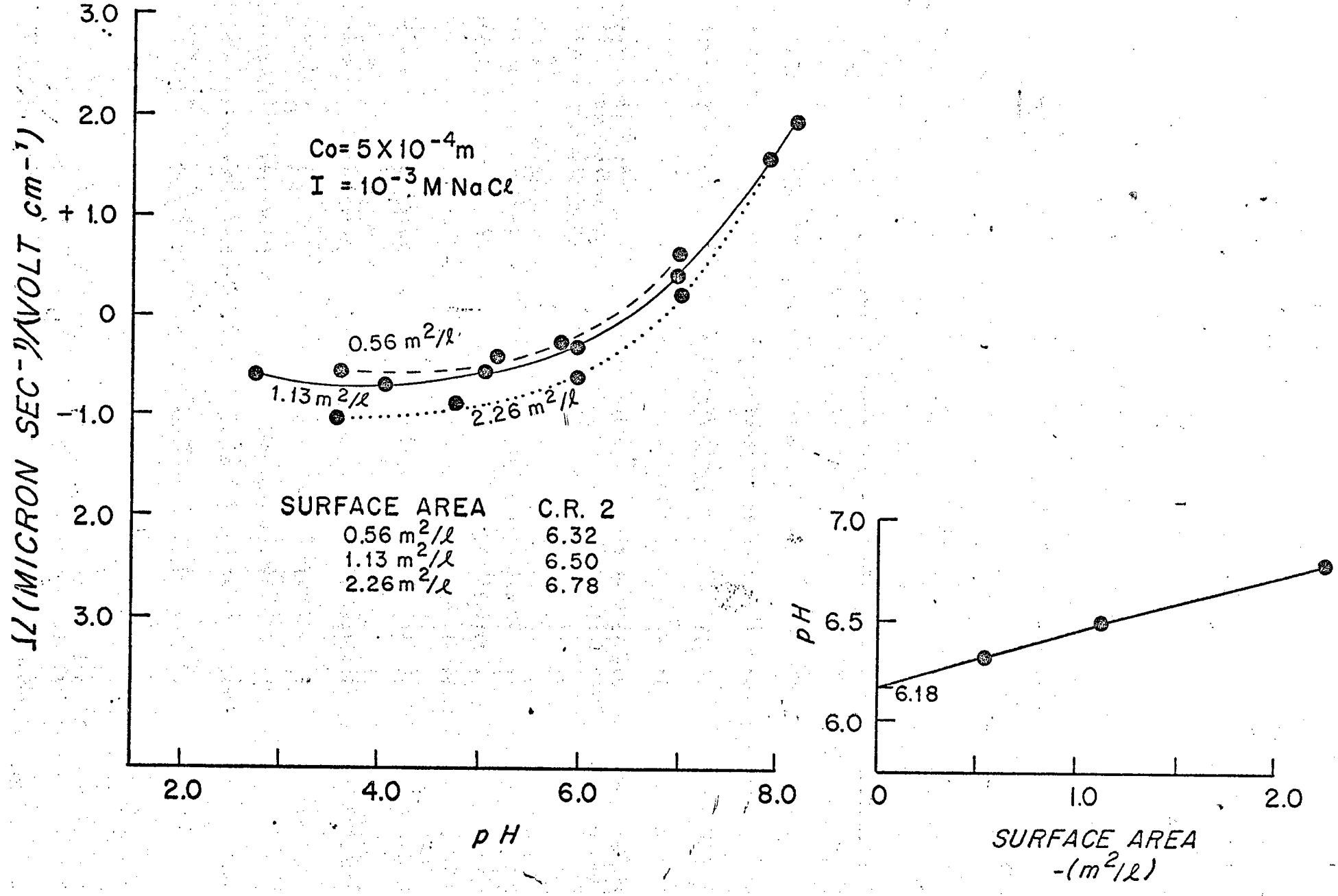
3.0
2.0
+ 1.0
0
−1.0
2.0
3.0
μ (MICRON SEC⁻¹/VOLT cm⁻¹)
Co= 5 X 10⁻⁴m
I = 10⁻³ M NaCl
0.56 m²/ℓ
1.13 m²/ℓ
2.26 m²/ℓ
SURFACE AREA C.R. 2
0.56 m²/ℓ 6.32
1.13 m²/ℓ 6.50
2.26 m²/ℓ 6.78
2.0
4.0
6.0
8.0
pH
7.0
6.5
6.0
pH
6.18
0
1.0
2.0
SURFACE AREA
-(m²/ℓ)

Figure 14

Solubility diagram for $Co(OH)_2$ (solid) at 25°C and infinite dilution. Constructed from Co(II) hydrolysis constants given in Sillen and Martell (1964). $pK_{so} = 14.9$; $p^*K_1 = 9.6$; $p^*K_2 = 9.2$; $pK_{s2} = 5.7$; $p^*K_3 = 12.7$.

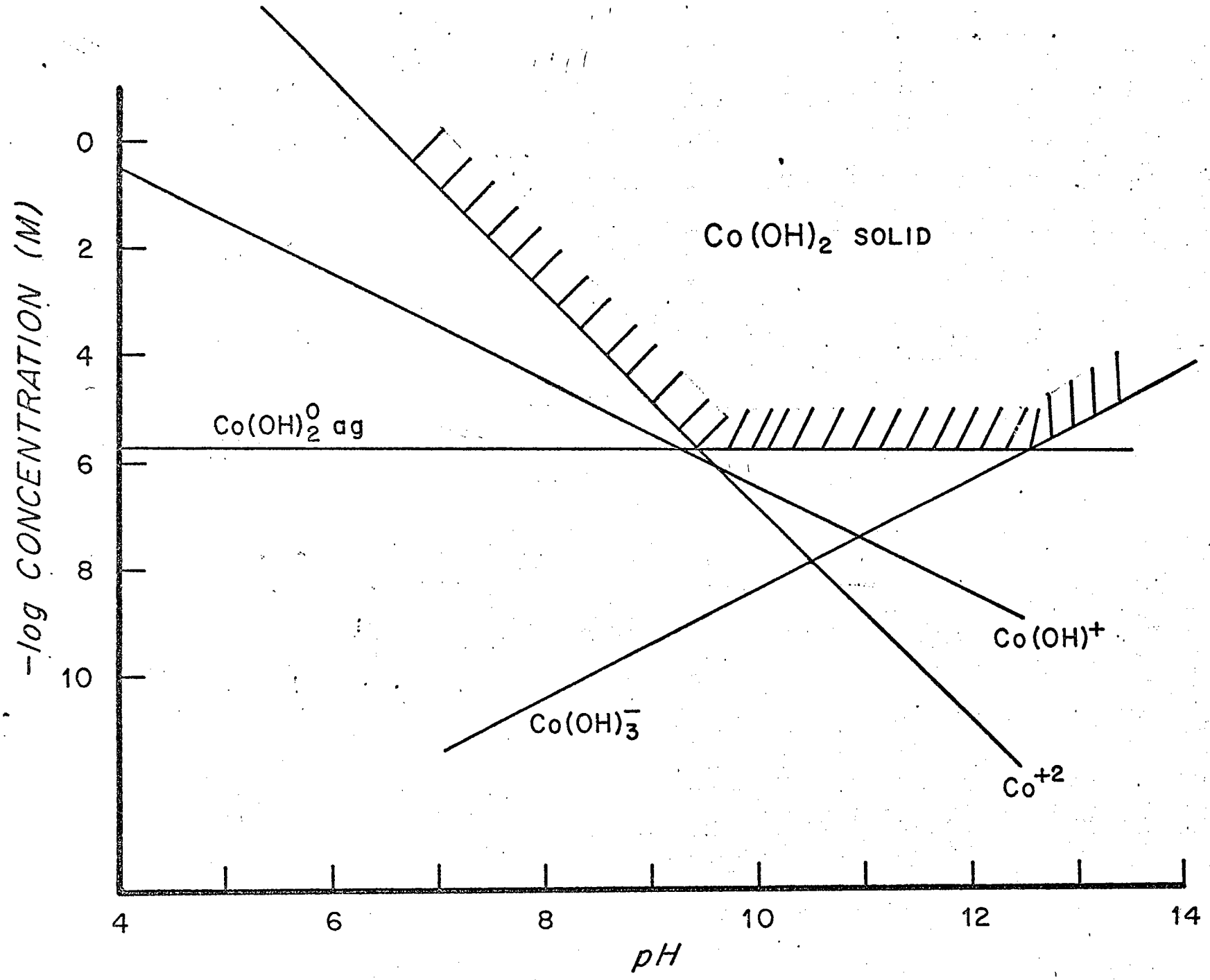
$Co(OH)_2$ SOLID
$Co(OH)_2^0$ aq
$Co(OH)^+$
$Co(OH)_3^-$
Co^{+2}
-log CONCENTRATION (M)
0
2
4
6
8
10
4
6
8
10
12
14
pH

Figure 15

A Kurbatov Plot (Kurbatov et al. 1951) constructed using the adsorption data from Figure 7 for 1 x 10^{-5} Mcobalt.

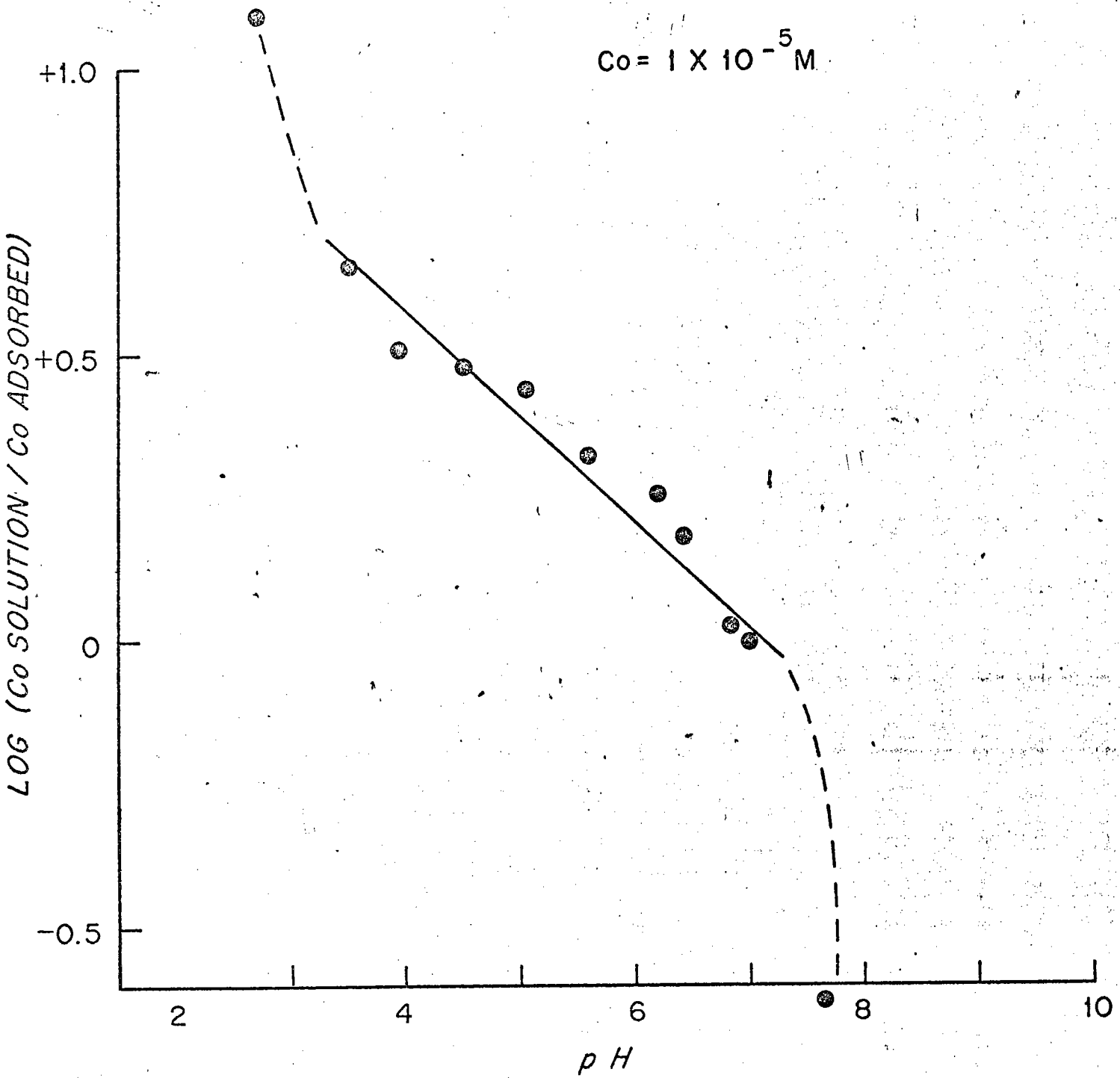
Co = 1 X 10 -5 M
+1.0
+0.5
0
-0.5
LOG (Co SOLUTION / Co ADSORBED)
2
4
6
8
10
p H

Figure 16

The standard free energy for the reaction

$2Co^{+2}aq + 4OH^{-}aq + \frac{1}{2}O_2(g) + H_2O = 2Co(OH)_3$ (solid) as a function of pH. The pH which this reaction is favorable is compared with with the pH of precipitation of $Co(OH)_2(s)$.

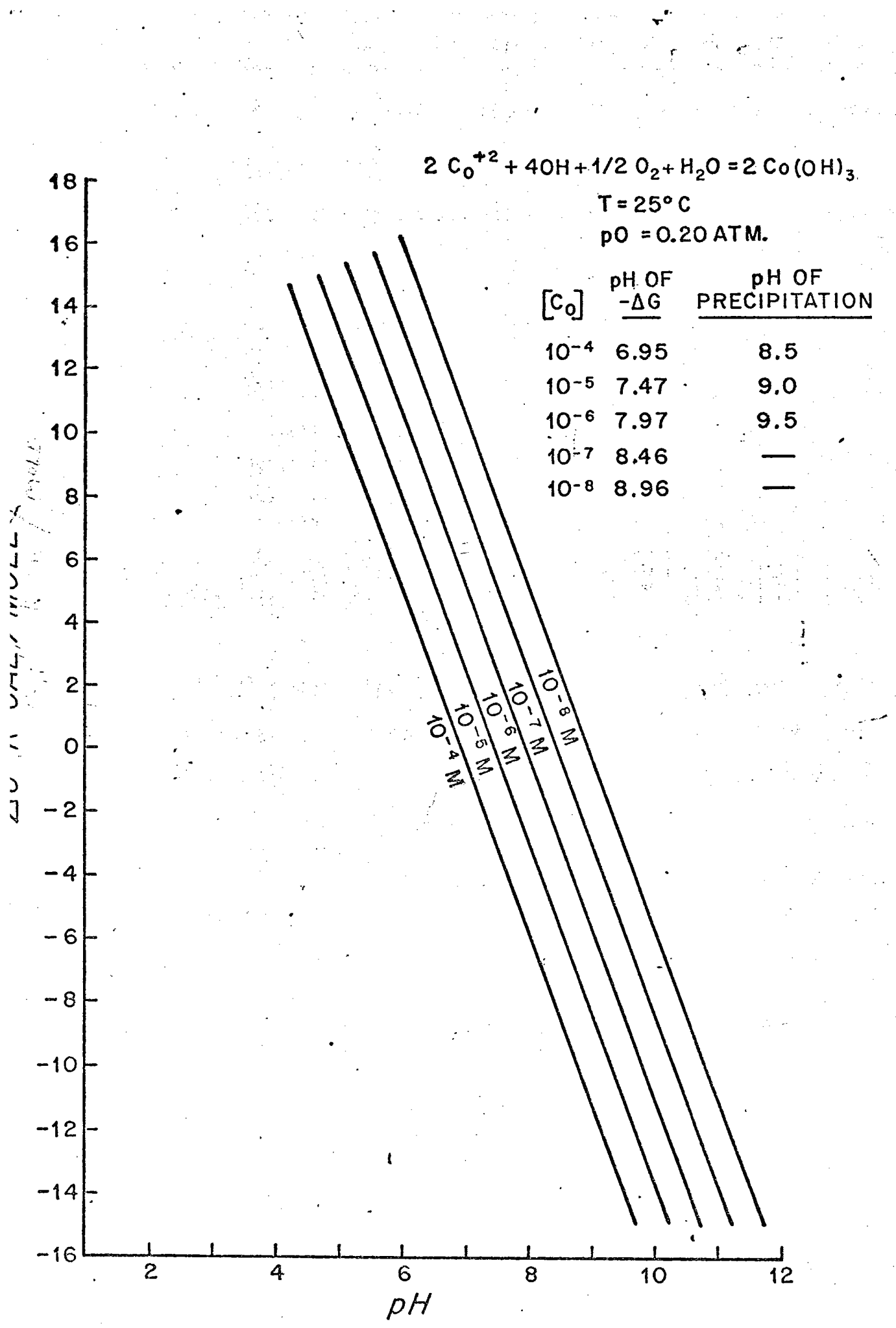
$2\ Co^{+2} + 4OH + 1/2\ O_2 + H_2O = 2\ Co(OH)_3$
T = 25° C
pO = 0.20 ATM.
[Co] | pH OF -ΔG | pH OF PRECIPITATION
10^{-4} 6.95 8.5
10^{-5} 7.47 9.0
10^{-6} 7.97 9.5
10^{-7} 8.46 —
10^{-8} 8.96 —
10^{-4} M
10^{-5} M
10^{-6} M
10^{-7} M
10^{-8} M
18
16
14
12
10
8
6
4
2
0
-2
-4
-6
-8
-10
-12
-14
-16
2
4
6
8
10
12
pH

BIBLIOGRAPHY

Burns R.G. (1965) Formation of cobalt in the amorphous $FeOOH \cdot nH_2O$ phase of manganese nodules. Nature 205, 999.

Carvajal M.C. and Landergren S. (1969) Marine sedimentation processes: the interrelationships of manganese, cobalt and nickel. Stockholm contributions in geology 18, 99-122.

Cotton F.A. and Wilkinson G. (1966) Advanced Inorganic Chemistry. 1136 pp. Wiley-Interscience.

Fukai R. (1968) A spectrophotometric method for determination of cobalt in seawater after enrichment with solid manganese dioxide. J. Oceanographic Soc. Japan 24, 1-9.

Goldberg E.D. (1954) Marine geochemistry. 1. Chemical scavengers of the sea. J. Geol. 62, 249-265.

Hahn H. and Stumm W. (1968) Coagulation by Al(III): The role of adsorption of hydrolyzed aluminum in the kinetics of coagulation. Advan. Chem. Ser. 79, 91-111.

Hodgson J.F. (1960) Cobalt reactions with montmorillonite. Soil Sci. Soc. Proc. 24, 165-168.

James R.O. and Healy T.W. (1972a) Adsorption of hydrolyzable metal ions at the oxide-water interface (I) Co(II) adsorption on SiO_2 and TiO_2 as model systems. J. Colloid Interface Sci. 40, 42-52.

James R.O. and Healy T.W. (1972b) Adsorption of hydrolyzable metal ions at the oxide-water interface (II) Charge reversal of SiO_2 and TiO_2 colloids by adsorbed Co(II), La(II) and Th(II) as model systems. J. Colloid Interface Sci. 40, 53-64.

James R.O. and Healy T.W. (1972c) Adsorption of hydrolyzable metal ions at the oxide-water interface (III) A thermodynamic model of adsorption. J. Colloid Interface Sci. 40, 65-81.

Kurbatov M.H.,Wood G.B. and Kurbatov J.D. (1951) Application of the mass law to adsorption of divalent ions on hydrous ferric oxide. J. Phys. Chem. 55, 258-259

Kurbatov M.H. and Wood G.B. (1952) Rate of adsorption of cobalt ions on hydrous ferric oxide. J. Phys. Chem. 56 , 698-701.

Loganathan P. and Burau R.G. (1973) Sorption of heavy metal ions by a hydrous manganese oxide. Geochim. Cosmochim. Acta, in press.

Matijevic E., Abramson M.B., Schulz K.F. and Kerkes M. (1960) Detection of metal ion hydrolysis by coagulation (II) Thorium. J. Phys. Chem. 64, 1157-1161.

Matijevic E., Abramson M.B., Ottewill R.H., Schulz K.F. and Kerkes M.(1961) Adsorption of thorium ions on silver iodide sols. J. Phys. Chem. 65, 1724-1729.

Matijevic E. (1967) Charge reversal of lyophobic colloids. In Principles and Applications of Water Chemistry (editors S.D. Faust and J.V. Hunter), pp. 328-369, Wiley.

Morgan J.J. and Stumm W. (1964) Colloid-chemical properties on manganese dioxide. J. Colloid Sci. 19, 347-359.

Murray D.J., Healy T.W. and Fuerstenau D.W. (1968) The adsorption of aqueous metal on colloidal hydrous manganese oxide. Advan. Chem. Ser. 79, 74-81.

Parks G.A. (1965) The isoelectric points of solid oxides, solid hydroxides and aqueous hydroxo complex systems. Chem. Rev. 65, 177-198.

Perrin D.D. (1962) The hydrolysis of manganese(II) ion. J. Chem. Soc. 2197-2200.

Posselt H.S.,Anderson F.J. and Weber W.J. (1968) Cation sorption on colloidal hydrous manganese dioxide. Environ. Sci. Technology 2, 1087-1093.

Sillen L.G. and Martell A.E. (1964) Stability constants of metal-ion complexes. Spec. Publ. No. 17, Chem. Soc. London.

Spencer D.W., Brewer P.G. and Sachs P.L. (1972) Aspects of the distribution and trace element composition of suspended matter in the Black Sea. Geochim. Cosmochim. Acta 36, 71-86.

Tewari P.H., Campbell A.B. and Lee W. (1972) Adsorption of Co^{+2} by oxides from aqueous solution. Can. J. Chem. 50, 1642-1648.

Turekian K.K. and Imbrie J. (1966) The distribution of trace elements in deep sea sediments of the Atlantic Ocean. Earth Planet. Sci. Letters 1, 161-168.

CHAPTER 5

THE INTERACTION OF METAL IONS WITH HYDROUS MANGANESE DIOXIDE IN THE MARINE ENVIRONMENT

I. INTRODUCTION

The evidence for adsorption of metal ions on manganese dioxide in the marine environment was reviewed in chapter 1. Though the evidence is abundant, the hypothesis has yet to be adequately tested. We lack both a qualitative understanding of the mechanism of adsorption (i.e. the types of reactions that take place on the surface) and a quantitative means of predicting how much adsorption can take place. Those few models proposed to explain this process (e.g. Goldberg 1954, Goldberg and Arrhenius 1958) have been based on little or no experimental evidence and do not adequately explain many of the important observations.

Research has been done on the surface chemistry of hydrous manganese dioxide (e.g Posselt et al. 1968, D.J. Murray et al. 1968, Morgan and Stumm 1964); however, little of it is useful for extrapolation to explain phenomena in the marine environment. Krauskopf (1956) was the first to attempt to quantify the adsorption mechanism. He performed some simple qualitative experiments in an attempt to evaluate Goldschmidt's (1937) suggestion that rare metal concentrations in sea water were kept less than the limiting solubility concentration because of removal by adsorption. MnO_2 was the most efficient of the various adsorbents he tested; however, quantitative interpretation of his data is difficult because he used metal concentrations two or more orders of magnitude higher than found in sea water. Evaluation of the effectiveness of the various adsorbents is also difficult because he used different concentrations and presumably different surface areas for each. He made two important observations, however, that indicate the complexity of the adsorption mechanism. He found that the anion forming elements Cr and W are as effectively adsorbed by

MnO_2 as are the cation forming elements Ni and Co, and that elements that possess similar charge densities in sea water frequently exhibit large differences in their degree of adsorption. It had previously been proposed (Goldberg 1954) that negatively charged MnO_2 adsorbs only the cation forming elements, while positively charged iron oxide attracts only anions.

Kharkar et al. (1968) did some adsorption-desorption experiments as part of their study of the supply of metals by streams to the ocean. Metals were taken up on various adsorbents in distilled water, then transferred to sea water and the release of the metals monitored. Unfortunately, the manganese phase they used was βMnO_2 (pyrolusite), which is not found in the marine environment and has very different surface properties from δMnO_2 (Healy et al. 1966, Jenkins 1970, Stumm et al. 1970).

My experiments were performed using a synthetically prepared hydrous manganese dioxide that was similar structurally (broad X-ray diffraction peaks centered at 7.4Å, 2.43Å and 1.63Å) and in oxidation grade ($MnO_{1.93}$) to manganese phases found in nature. It is referred to here as δMnO_2 rather than 7Å manganite because of controversy in the literature (Brown 1971) regarding the existance of 7Å manganite.

In this chapter, I will use the experimental data presented in chapters 2, 3 and 4 to close some of the gaps in our understanding of the adsorption mechanism and to provide quantitative estimates of the metal enrichment in natural manganese deposits.

II. ELECTROSTATIC ASPECTS

The importance of the acidic properties of the surface of δMnO_2 was suggested by Sevast'yanov and Volkov (1966). They hypothesized that because solid MnO_2 behaves like an acid, it will tend to form salts with metal ions in solution. The results presented in chapter 2 indicate that to some extent this is true.

The surface charge of δMnO_2 is pH dependent and the pH of zero point of charge, pH(ZPC), is located at pH 2.25. This means that for pH values greater than 2.25, the surface of δMnO_2 has a negative charge. Electrophoresis measurements indicate that the surface charge is a function of pH and that variation of the concentration of NaCl has little effect on the mobility of the particles. Thus H^+ and OH^- are the potential determining ions for the surface of δMnO_2, which behaves like a weak acid in solution. Surface metal hydroxide groups participate in amphoteric acid-base reactions to produce a positively or negatively charged surface.

$$-\overset{|}{\underset{|}{Mn}}-OH_2^+ \;=\; -\overset{|}{\underset{|}{Mn}}-OH^0 \;+\; H^+ \;=\; -\overset{|}{\underset{|}{Mn}}-O^- \;+\; 2H^+ \qquad (1)$$

Though eqn. 1 is written as a dissociation reaction, one cannot distinguish by conventional analytical means between dissociation of protons from the surface or the binding or sorption of OH^- ions from solution.

Using alkalimetric titration curves to obtain the amount of strong base consumed by the surface, surface charge values were calculated that approached $-100\ \mu coul/cm^2$ at pH 8.0 in 0.01M NaCl. This would be equivalent to an adsorption capacity of 1×10^{-5} eq/m^2 or 5×10^{-6} moles/m^2 of divalent cations. Using the surface area of 260 m^2/g, this electrostatic adsorption capacity can be expressed in the same units used to express the ion exchange capacity of clays (meq/100g). The ion exchange capacity of

δMnO_2 is compared with kaolinite and montmorillonite in table 1.

TABLE 1

Material	Ion exchange capacity
Kaolinite	5-15 meq/100g
Montmorillonite	50-150 meq/100g
δMnO_2	250 meq/100g at pH 8.0

This large negative charge produced by the acid-base properties of the surface only explains in part the high adsorption capacity of δMnO_2. It cannot account for all the adsorption, as much higher adsorption densities (at least 1×10^{-5} moles/m^2) were found for the transition metals (chapters 3 and 4).

III. CHARGE DENSITY

The Gouy-Chapman Theory (see Stumm and Morgan 1970 p.458) predicts that multivalent ions are concentrated in the double layer to a much larger extent than monovalent ions. On the basis of this theory, it is frequently proposed (e.g. Goldberg 1954, Goldberg and Arrhenius 1958) that the degree of adsorption is a function of the charge density of the ions. However, this is apparently not reflected in the selectivity sequence shown earlier for δMnO_2. For example, Mg^{+2} has a higher ionic potential (charge to radius ratio) than Ba^{+2} but adsorbs much less (see chapter 3). However, using the unhydrated radii to calculate charge density may be unrealistic because of the large energy of hydration of some ions. When hydrated radii are used to calculate ionic potential, Ba^{+2} has a larger value than Mg^{+2} (Table 2), and this might explain its greater adsorption. But, if charge

density were the controlling factor, it would also be difficult to explain why Co^{+2} adsorbs much more strongly than Ni^{+2} (see chapter 3). Both ions have similar radii and solution chemistry. There are obviously other controls on the adsorption of metal ions than simply coulombic attraction and charge density.

IV. SPECIFIC CHEMICAL ASPECTS

Goldberg (1954) suggested that if MnO_2 were negatively charged and iron oxide positively charged, the distribution of adsorbed ions between these two phases should indicate which elements are present in sea water as cations and which as anions. Those metals that exist in sea water as cations would adsorb on MnO_2, and those as anions would adsorb on hydrous iron oxide.

The surface of iron oxide has a pH dependent surface charge (Parks and de Bruyn 1962), however the pH(ZPC) of colloidal iron oxide in sea water is uncertain (Harvey 1937). Goldberg (1954) and Goldberg and Arrhenius (1958) have stated that iron oxides in sea water are positively charged. However, experimental determinations of the pH(ZPC) of various modifications of iron oxide indicate that it can range from pH 6 to 9 depending on the mode of formation and subsequent aging. In general, samples with more ordered structures have a more acid pH(ZPC) (Schuylenborg and Arens 1950). Most of the values for goethite, the most common form of iron oxide in sediments, fall between pH 6 and pH 7. A summary of the literature values of the pH(ZPC) of iron oxides is shown in Table 3.

In addition, such a classification is complicated by the fact that adsorption can be due to more than electrostatic forces. For example,

TABLE 2

Charge Densities

Metal ion	Crystallographic[1] radius	Hydrated[2] radius	ionic charge density	Hydrated charge density
Mg^{+2}	0.65	4.4	3.08	.454
Ca^{+2}	0.99	4.2	2.02	.476
Si^{+2}	1.13	4.2	1.77	.476
Ba^{+2}	1.35	4.1	1.48	.488
Mn^{+2}	0.80		2.50	
Co^{+2}	0.72		2.78	
Ni^{+2}	0.69		2.90	
Cu^{+2}	0.96		2.08	
Zn^{+2}	0.74	4.4	2.70	.454

(1) Crystallographic radii are from Pauling (1960) p 518.

(2) Hydrated radii are from Robinson and Stokes (1959) p 126.

TABLE 3

LITERATURE VALUES FOR THE pH(ZPC) OF SYNTHETIC IRON OXIDES

PHASE	INVESTIGATOR	pH(ZPC)
αFe_2O_3 (Hematite)	Parks and De Bruyn (1962)	8.4±0.1
	Albrethson (1963)	8.7±0.1
	Korpi (1960)	9.04±0.05
γFe_2O_3	Iwasaki et al. (1962)	6.7±0.2
αFeOOH (Goethite)	Flaningham (1960)	6.1±0.1
	Iwasaki et al. (1960)	6.7±0.2
	Lengweiler et al. (1961)	6.7
	Schuylenborg and Arens (1960)	5.9 to 7.2
γFeOOH (Lepidocrocite)	Iwasaki et al. (1960)	7.4±0.2
	Schuylenborg et al. (1950)	5.4 to 7.3
Amorphous iron Hydroxides	Schuylenborg et al. (1950)	8.5
	Hazel and Ayres (1931)	8.6
	Mattson and Pugh (1934)	7.1

$SO_4^{=}$ and HPO_4^{-} are known to adsorb on negatively charged iron oxide surfaces (James, personal communication, and Hingston et al. 1967) and $MoO_4^{=}$ on negatively charged MnO_2 surfaces (Chan and Riley 1966). Clearly, we cannot state that metals associated with MnO_2 exist as cations and that metals associated with iron oxide exist as anions in sea water.

The interaction of metal ions with metal oxides is best explained in terms of both chemical and coulombic attraction (Grahame 1947, Stumm et al. 1970, James and Healy 1972). The total standard free energy of adsorption, $\Delta\bar{G}^{o}$, is the sum of the total specific (chemical) adsorption energy, ϕ , and the electrochemical adsorption energy $ZF\psi_s$ (eqn. 2)

$$\Delta\bar{G}^{o} = - \phi + ZF\psi_s \qquad (2)$$

where ψ_s is the potential drop at the surface, F is the Faraday, and Z is the charge. Experimentally, it is very difficult to separate the energy of adsorption into its chemical and electrostatic components. Ionic species adsorbed in response to coulombic attraction alone obviously cannot adsorb in amounts greater than the number of equivalents necessary to neutralize the surface charge.

The experimental results presented in chapters 2 and 3 indicate that the alkali metal ions have no specific adsorption contribution, thus they only react electrostatically with the surface. No Na^{+} or K^{+} were found to adsorb on δMnO_2 below the pH(ZPC). As a group, the transition metal ions react more strongly with δMnO_2 than do the alkaline earths. Within each group there is a well defined selectivity sequence. Among the alkali earths, Ba interacts more strongly than Mg, and among the transition metals, Co interacts more strongly than Ni. The selectivity sequence for all of the metals studied is:

$$Na = K < Mg < Ca < Sr < Ba < Ni < Zn < Mn \leq Co$$

Those ions that are most easily adsorbed by increasing the pH are the most difficult to desorb by decreasing the pH. This is a reflection of the specific adsorption potentials that increase from the alkali earths to the transition metals (chapter 3).

Specific adsorption is thus the most likely explanation for the selectivity sequence. Unfortunately, the chemical processes controlling it are not well understood. Loganathan and Burau (1973) maintain that during the adsorption process charge is conserved. When a metal ion is adsorbed, equivalent amounts of protons and structural cations are released. In their model of the surface, a metal ion that exhibits specific adsorption must penetrate into the structure of the δMnO_2 and replace structural Mn(II) or Mn(III). The experiments reported in chapter 3 demonstrated that this mechanism is much less important than suggested by Loganathan and Burau. In the most extreme case, only 10% of the cobalt adsorbed could be accounted for by manganese released to solution. Furthermore, electrophoresis experiments using Co(II) and Mn(II) demonstrated that charge was not conserved during adsorption (chapter 4). Thus, the most consistent explanation for specific adsorption on δMnO_2 is that it is a chemical reaction of the metal ions with the surface.

Alkalimetric titrations of δMnO_2 in the presence of metal ions (chapter 3) indicated that the metal ions can penetrate in increasing amounts from Mg^{+2} to Co^{+2} into the compact part of the double layer to react with protonated sites on the δMnO_2 surface. Any ion that enters the compact layer can modify the double layer in such a way that the charge of the

diffuse layer may become reversed. This reaction involves the replacement of a proton on the surface by a divalent metal ion on a one to one molar basis as shown by reaction 3.

$$-\overset{|}{\underset{|}{Mn}}-OH^{o} + Co^{+2} = -\overset{|}{\underset{|}{Mn}}O-Co^{+} + H^{+} \qquad (3)$$

It is possible that the metal ions are associated with more than one surface group. However, using a formation curve (a plot of ligand number versus the ligand concentration), Stumm et al. (1970) demonstrated that only monodentate associations ($-\overset{|}{\underset{|}{Mn}}O-Co^{+}$) are formed. A similar reaction was found by Huang (1971) for metals interacting with γ-Al_2O_3.

This reaction is supported by the observation that monolayer adsorption is larger than would be expected if the adsorbed metal ions retained their inner hydration sheath (see chapters 3 and 4). This suggests that when adsorbed species exhibit direct chemical bonding with the surface, they are not separated from the surface by a layer of water molecules as suggested by James and Healy (1972).

Thus, my experimental evidence suggests we can explain the adsorption process as a combination of electrostatic attraction and specific adsorption. On the basis of its surface charge alone, δMnO_2 is an exceptional adsorbent. It has almost twice the electrostatic adsorption capacity of the most surface active clay minerals (Table 1). This adsorption is enhanced greatly for some metals by specific adsorption.

V. EXTENSION OF THE MODEL TO LOW CONCENTRATIONS

Cobalt adsorption was measured as a function of pH over a wide range of cobalt concentrations. These experiments verify the proposed adsorption model and justify its extension to sea water metal concentrations. Cobalt adsorption was pH dependent, and specific adsorption occurred at all cobalt

concentrations. At cobalt concentrations greater than 1×10^{-7}M, precipitation of $Co(OH)_2$ may be induced, above pH 6, by the presence of the charged surface. This possibility, which was discussed in detail in chapter 4, must be considered when evaluating adsorption data for cobalt and other metals at high concentrations.

VI. A QUANTITATIVE EVALUATION OF THE ADSORPTION MECHANISM

The proposal that the removal of metals from sea water by adsorption on δMnO_2 is an important enrichment mechanism was made in chapter 1. An important aspect of this experimental study was to provide a quantitative evaluation of how much metal enrichment can be accounted for by adsorption. Clearly, these calculations will neglect the effect of factors such as organic complexing and other phases present that may also remove metals from sea water by adsorption. However, these calculations will provide an estimate of how effective the adsorption of uncomplexed metals by δMnO_2 is as a removal mechanism.

Bearing in mind the problems of extrapolation, I will use the experimental results of chapters 3 and 4 to explain the observed metal distributions in two examples: the suspended matter of the Black Sea and manganese rich sediments on the East Pacific Rise.

A. The Black Sea

Spencer et al. (1972) observed a correlation between Co and Mn in the suspended matter of the Black Sea, and they suggested that this correlation is due to the adsorption of Co by δMnO_2 that is precipitated just above the oxygen zero boundary. The results of the tracer experiments can be used to test this explanation. Values for adsorption density as a function of pH for cobalt concentrations from 10^{-3} to 10^{-8}M have been determined

(chapter 4). A separate experiment showed that the adsorption density was independent of the amount of solid δMnO_2 for solid concentrations that approach the maximum amount of particulate Mn found in the Black Sea (chapter 4). An adsorption isotherm, adsorption density as a function of equilibrium cobalt concentration, is plotted in Figure 1 for pH 8. With increasing cobalt in solution, the amount adsorbed increases until monolayer saturation is reached at 1×10^{-5} moles/m^2. The data for this figure were obtained in 0.1M NaCl; thus, for applications to sea water, a correction factor must be applied because of the competitive effect of Na, Ca and Mg. At 1×10^{-8}M Co, this correction factor is approximately 50%, and it decreases to zero at 5×10^{6}M (chapter 4). The corrected relationship for artificial sea water is given in Figure 1. The precision of these curves as determined by triplicate analyses at 1×10^{-8}M and 1×10^{-6}M is $\pm$ 25%.

We can now use these experimental data to compare with actual observations from station 1449 from cruise 49 of the R.V. Atlantis II in the Black Sea. The dissolved cobalt values were reported in Spencer and Brewer (1971) and the particulate values in Spencer et al. (1972).

Figure 2 shows the suspended Mn concentration, the total suspended matter concentration, and the observed ratio of cobalt to manganese in the suspended matter. The expected ratio of particulate Co to Mn can be calculated using the experimental data in Figure 1. The adsorption density was converted to grams of cobalt adsorbed per gram of Mn (as δMnO_2) assuming a surface area of 260m^2/g. This was the experimentally measured surface area for the adsorption experiments reported in chapters 2, 3 and 4. The experimentally predicted ratio of particulate Co to Mn is shown in Figure 2.

The predicted ratio agrees well with the observed ratio at the point corresponding to high suspended Mn concentrations; however, it is much lower than the observed ratios at low Mn concentrations. At depths above and below the particulate Mn maximum, both Mn and Co concentrations are low. The Co/Mn ratio for average crustal material ranges from 4×10^{-1} to 1×10^{-2}. The slightly higher ratio observed suggests there may be some additional cobalt adsorbed on the detrital material or associated with another phase such as a sulfide or with biological material.

Figure 3 shows the profile of the observed values of particulate Mn and Co and predicted particulate Co calculated from the ratios in Figure 2. Except for where particulate Mn is at a maximum, the observed Co is larger than that predicted. It is conveivable that this anomaly between the experimentally predicted and the observed value is influenced by the contribution of Co and Mn in detrital phases. In order to estimate the detrital component, the average of the samples at 50m, 300m, 400m, and 500m was used. The detrital manganese was found to be 91 ng/kg and the detrital cobalt 9.1 ng/kg. The resulting detrital Co/Mn ratio is 10^{-1}. These estimated detrital components were subtracted from the observed values, and the resulting "nondetrital" Mn and Co values are given in Figure 4. The agreement between observed and predicted values isn't perfect but is now substantially improved.

It is only proper that we consider the alternate hypothesis that the particulate Mn and Co values are unrelated. Total suspended matter also increases with increased particulate Mn at 250m, and the latter only accounts for 5% of the total suspended matter. Thus, the possibility exists that the particulate Mn increases by precipitation of MnO_2, and the Co increases by some other reason such as adsorption on precipitated iron oxides. It

appears, however, that there is no large increase in "nondetrital" iron as there is for Mn. Figure 5 shows the particulate Fe, Sc, and La values for station 1449. The high correlation of Fe with Sc and La suggests that the increase in Fe is due to an increase in detrital iron as a silicate. Using an advection-diffusion model, Brewer and Spencer (1973) have calculated the upward flux of iron from the anoxic water. If the oxidation kinetics for iron and manganese are the same, they predict a standing crop of precipitated ferric hydroxide of approximately 4mg/m^3 in the water column just above oxygen zero. The maximum observed values are about 70 mg/m^3, thus the precipitate is being masked by the iron associated with the silicate detrital flux from above.

The hypothesis proposed by Spencer et al. (1972) that the correlation between particulate Co and Mn is due to adsorption of Co by MnO_2 appears substantiated by the experimental evidence in spite of some gross assumptions in comparing the experimental data with the field data. These assumptions are that the surface area of the experimental MnO_2 and the particulate Mn in the Black Sea are similar, that the mineralogy of the phases is similar, and that cobalt is incorporated only by surface adsorption and that no Co is included in growing MnO_2 particles. The coefficient of variation of the dissolved cobalt measurements is $\pm$ 15%. No estimate was given for the coefficient of variation for the particulate Co; however, for the blank nucleopore filters, the value was 50%. Thus considering the errors in extrapolation and the errors in the analytical measurements, the agreement between the observed and predicted particulate Co values is quite good.

B. East Pacific Rise Sediments

Geochemical studies of iron and manganese rich sediments from the East Pacific Rise have been reported by several authors (Revelle 1944, Boström and Peterson 1966, 1969, Dasch et al. 1971, Bender et al. 1971, Sayles and Bischoff 1973). The metal enrichments are associated primarily with the acid insoluble fraction. This fraction varies widely; the samples studied by Bostrom and Peterson were primarily carbonate oozes (up to 90% $CaCO_3$), while those studied by Sayles and Bischoff often contained little or no carbonate. The $CaCO_3$ content appears to be controlled primarily by the water depth as $CaCO_3$-free metalliferous sediments occur only at depths greater than 4200m. This observation along with the fact that these sediments are also Al poor (Boström 1966, 1969) suggests that the metal enrichments are not due to normal detrital or biogenic inputs.

Boström and Peterson (1969) suggested that the source of the metals was volcanic emanations that debouch from the crest of the ridge and react with sea water to precipitate oxides of iron and manganese. The deposition rates of iron and manganese in these deposits are several times higher than in average pelagic sediments suggesting a local source and supporting Bostrom et al.'s proposal (Bender et al. 1971, Bostrom 1970). Further diagenetic reactions in the sediments may be possible as Sayles and Bischoff (in press) found that most of the iron occurs as a poorly crystalline silicate (smectite), and the manganese is primarily in micro-manganese nodules.

The origin of the minor elements in these sediments is problematical. The isotopic data of Dasch et al.(1971) suggests that while volcanogenic Sr apparently contributes less than 3% of the total Sr, most of the Pb is

of magmatic origin. The $^{234}U/^{238}U$ ratio of 1.16 indicates that the uranium in these cores comes from sea water (Bender et al. 1971, Veeh and Bostrom 1971), and the rare earth distribution occurs in the same proportions as in sea water with the depletion of Ce being a diagnostic feature (Bender et al. 1971). Whether the ultimate origin of the metals in these sediments is from hydrothermal solutions or from sea water is not important to this study. The critical point is that the likely transport mechanism to the sediments is by adsorption onto manganese and iron oxides.

The fact that the Co/Mn ratio falls within the range of ratios reported for manganese nodules (Cronan and Tooms 1969) suggests that the same removal mechanism is operating in these sediments as in manganese nodules.

Further leaching experiments done by Sayles (personal communication) support the hypothesis that the minor elements are associated with manganese. The results of some of these leaching experiments (using the acid-reducing solution suggested by Chester and Hughes 1967) are shown in Table 4. For each sample, the total amount of Mn, Fe, Co, Cu and Ni leached is shown. In Figure 6, the amount of cobalt leached is plotted against the amounts of manganese leached. Clearly, there is a significant correlation of cobalt with manganese. The linear correlation of cobalt with manganese suggests that there is indeed a genetic relationship between these two metals that could be due to the adsorption of cobalt by solid MnO_2.

The average cobalt concentration in sea water is 30 ng/kg (Robertson 1970) or approximately 1×10^{-9}M. Using this concentration and the adsorption density data calculated from my experimental data as shown in Figure 1,

TABLE 4

EAST PACIFIC RISE SEDIMENTS (1)

SAMPLE	Mn (2) LEACHED	Fe LEACHED	Ni LEACHED	Co LEACHED	Cu LEACHED
11/6-23	2.06%	2.94	540 ppm	241 ppm	577 ppm
11/3-137	6.67	5.62	1650	245	912
11/1-140	3.93	2.81	982	229	774
14/4-12	5.33	5.49	832	118	641
14/3-44	1.75	2.58	259	106	249
14/2-70	2.75	3.61	272	77	359
14/1-110	4.14	4.79	554	102	544

(1) Analyses by F. Sayles, Mn, Fe, and Cu by X-ray fluorescence; Ni and Co by emission spectroscopy.

(2) Samples were leached with a combined acetic acid (25%v/v) and hydroxylamine hydrochloride (1M) solution at 25°C.

we can predict an expected Co/Mn ratio assuming adsorption is the sole control on the Co concentration. Unfortunately, this ratio (2.5×10^{-4}) is about one to two orders of magnitude smaller than the ratio observed in the East Pacific Rise. Thus, this ratio only predicts 10% of the Co observed in these sediments. This implies that Co is being removed from sea water by other mechanisms.

The difficulty in making such estimates for these natural samples is in the validity of the comparison of the experimental results with the field observations. The adsorption experiments were performed on discrete particles of a finite size. On the other hand, the manganese micronodules in the East Pacific Rise sediments may grow continuously (perhaps one unit cell at a time) and depending on the growth rate, they have the opportunity to equilibrate continuously with sea water. Thus, from comparison with the laboratory experiments, we would predict less Co because a major part of the Mn in the colloidal particles in the experiments would be tied up in the interior and never have a chance to adsorb cobalt. That is to say, the δMnO_2 used in these experiments would have to have a surface area of 2400 m^2/g in order to predict the Co found in manganese nodules. This is 9 times greater than the surface area actually used in the computations.

If we assume that the experimental results reflect non-availability of surface, then we can correct by calculating the relative volume of the surface layer 7 $\mathring{A}$ wide (the basal spacing of the experimental MnO_2) and comparing it with the total volume sufficient to give a surface area of 260 m^2/g. Then only 25% of the experimental MnO_2 is in contact with the solution and the estimates can be increased by a factor of 4.

Another problem is that the Co/Mn ratio is a strong function of the Co concentration in sea water. If the Co concentration at the site of formation was 1.4 μg/kg (a factor of 50 greater than Robertson's average value), it would be possible to explain all of the cobalt in the East Pacific Rise. Cobalt concentrations in pore waters from oxidizing sediments on the East Pacific Rise have been reported up to 20 μg/kg (Presley et al. 1967).

Finally, there is no a priori reason why all of the cobalt should be explained by the manganese concentration. Iron oxide may also adsorb significant amounts of cobalt, and cobalt may also be leached from other phases. Unfortunately, correction factors cannot be calculated as they could for the Black Sea particulate matter.

Using the correction for surface availability, then 40% of the cobalt in the East Pacific Rise sediments can be accounted for by the adsorption process as determined experimentally. Allowing for the uncertainties in the Co concentration at the adsorption sites and the availability of other cobalt containing phases, then this is a reasonable estimate. It certainly supports the hypothesis that adsorption of cobalt onto manganese oxide is a major process in the East Pacific Rise sediments.

Figure 1

Adsorption density as a function of equilibrium cobalt concentration at pH 8.0. The curves for δMnO_2 were calculated from experimental data presented in chapter 4. The cobalt concentration scale is in molarity.

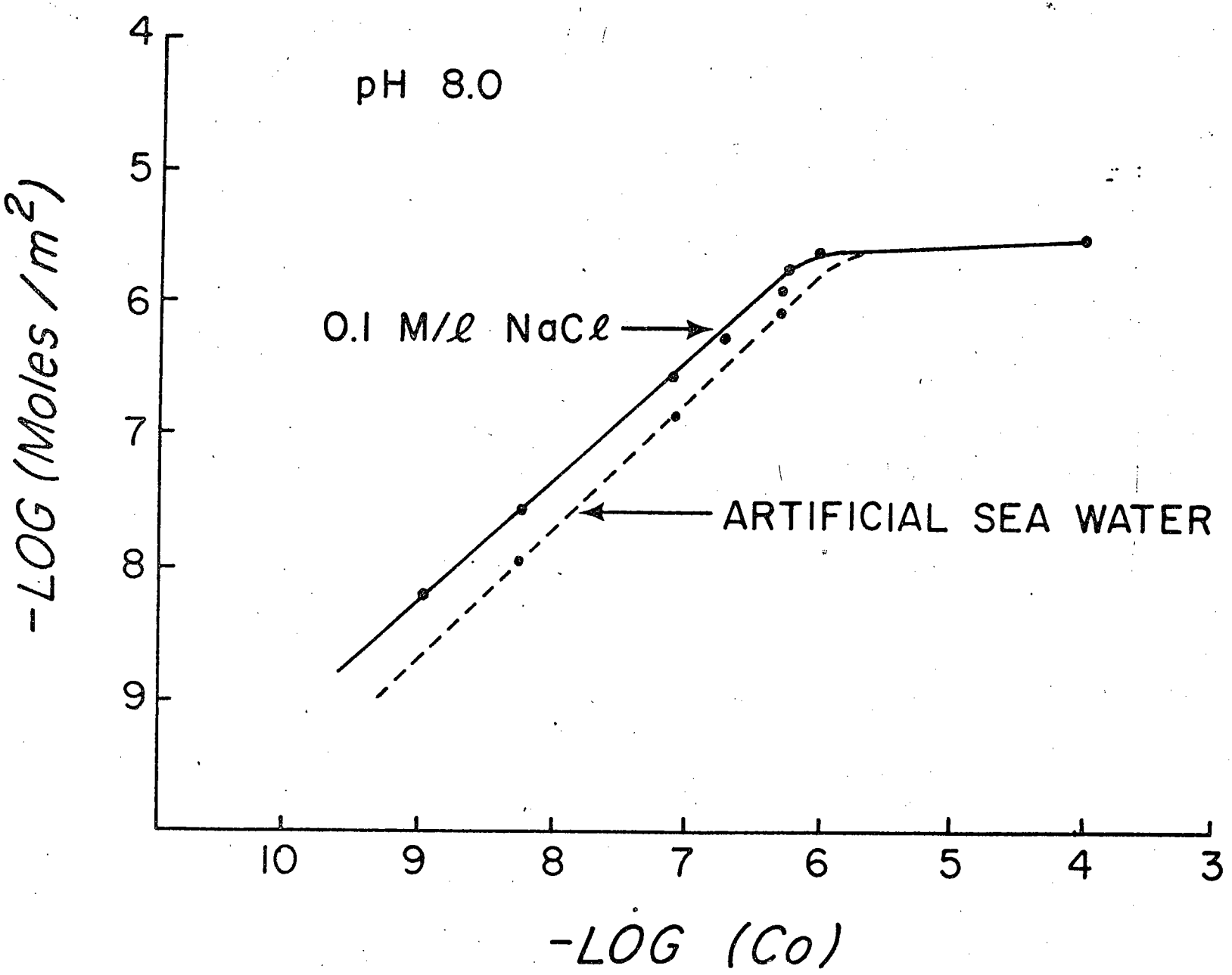
pH 8.0
0.1 M/ℓ NaCℓ
ARTIFICIAL SEA WATER
-LOG (Moles / m²)
-LOG (Co)
4
5
6
7
8
9
10
9
8
7
6
5
4
3

FIGURE 2

Profiles for suspended Mn and total suspended matter for station 1449 in the Black Sea. Also shown are the observed and predicted Co/Mn ratios. The predicted Co/Mn ratios were calculated using the dissolved Co concentrations for this station (Spencer and Brewer 1971) and the experimental data in Figure 1.

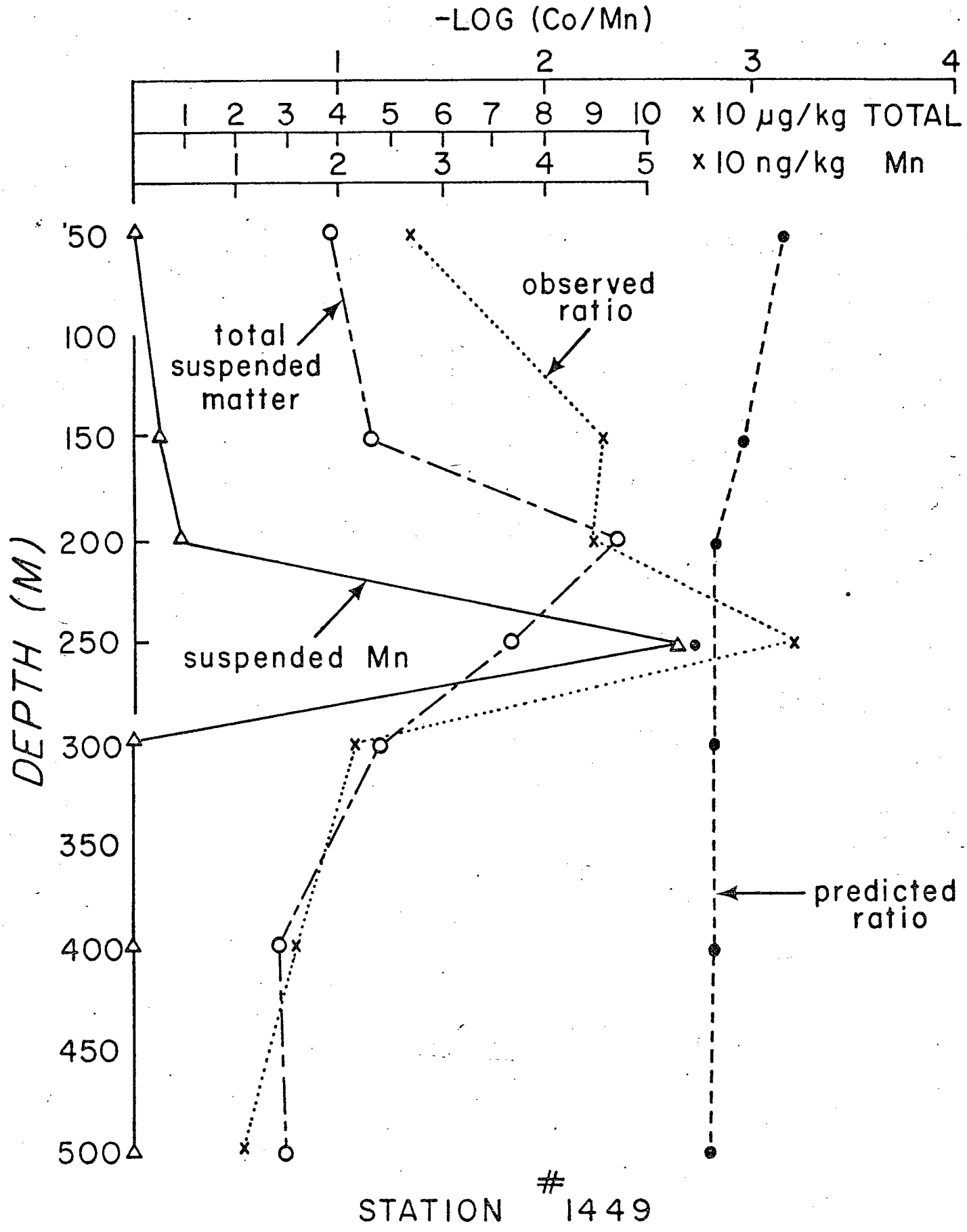
-LOG (Co/Mn)
1
2
3
4
1 2 3 4 5 6 7 8 9 10 x 10 µg/kg TOTAL
1 2 3 4 5 x 10 ng/kg Mn
'50
100
150
200
250
300
350
400
450
500
DEPTH (M)
total suspended matter
observed ratio
suspended Mn
predicted ratio
STATION # 1449

FIGURE 3

This figure gives the observed particulate Mn and Co profiles for station 1449. The predicted particulate Co values were obtained by multiplying the particulate Mn concentration by the predicted Co/Mn ratio.

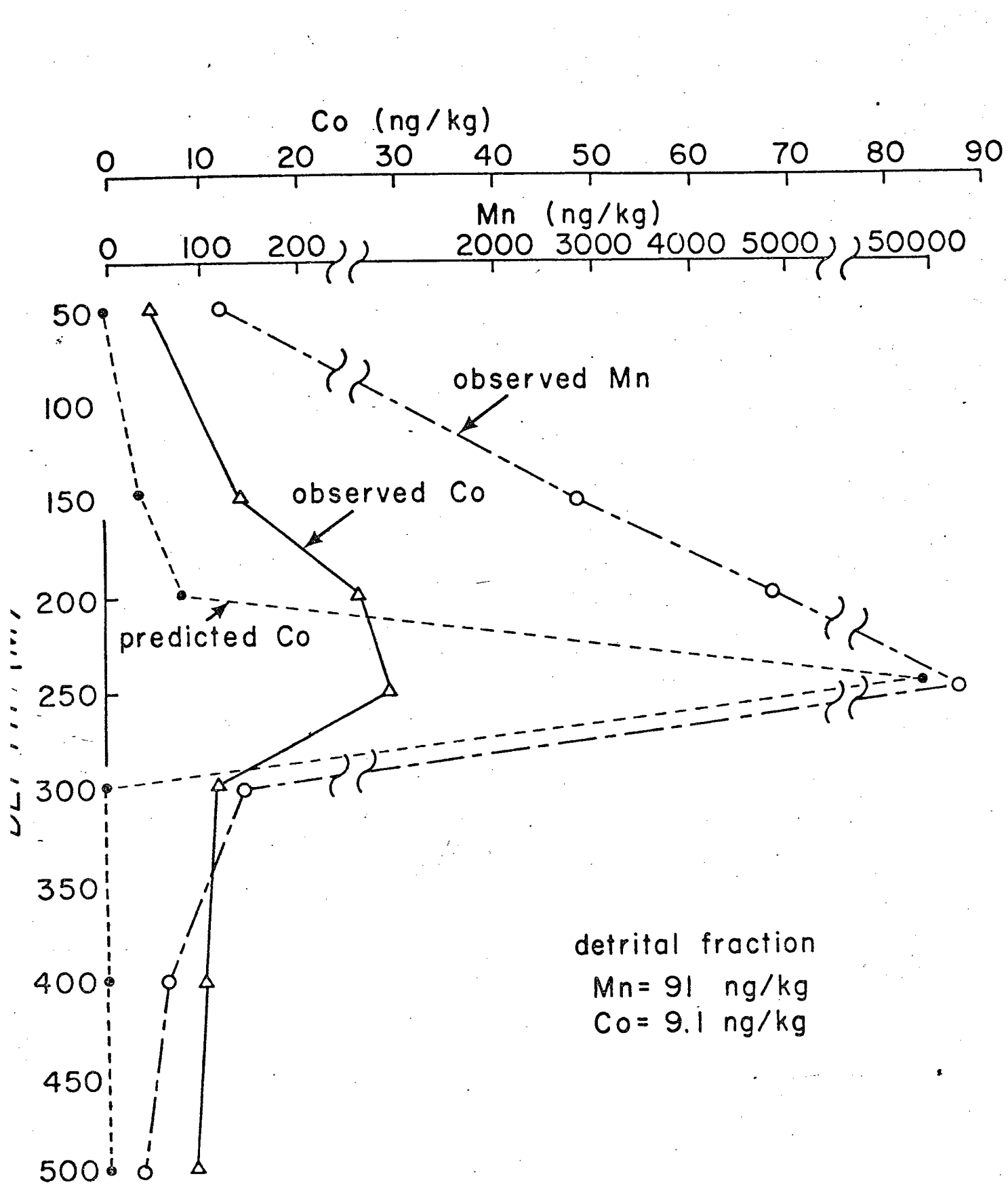
Co (ng/kg)
0 10 20 30 40 50 60 70 80 90
Mn (ng/kg)
0 100 200 2000 3000 4000 5000 50000
50
100
150
200
250
300
350
400
450
500
observed Mn
observed Co
predicted Co
detrital fraction
Mn= 91 ng/kg
Co= 9.1 ng/kg

FIGURE 4

The nondetrital Mn and Co values were calculated by subtracting the estimated detrital concentrations from the total concentrations. The predicted nondetrital Co was calculated by multiplying the nondetrital Mn times the predicted Co/Mn ratio.

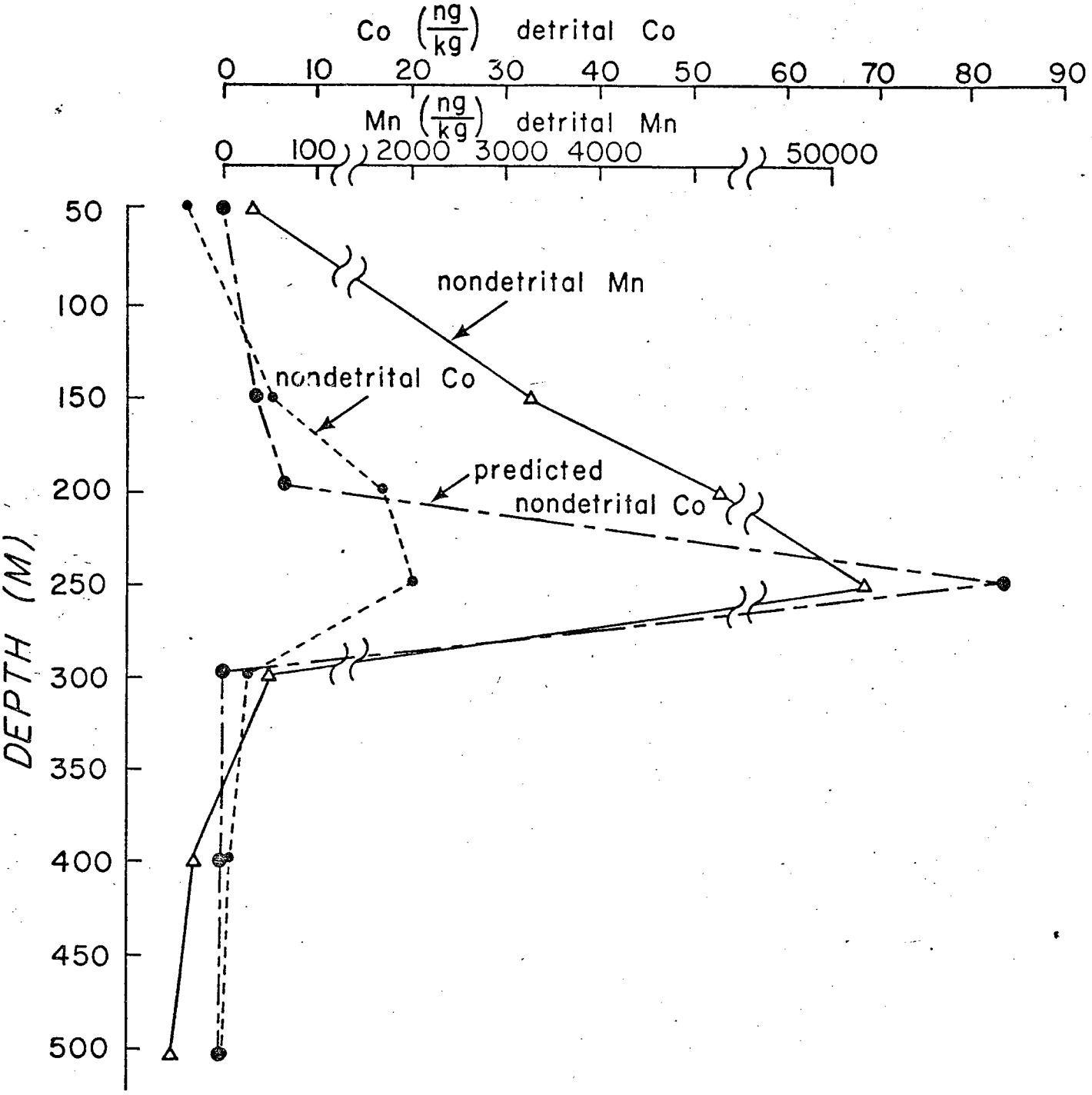
Co (ng/kg) detrital Co
0 10 20 30 40 50 60 70 80 90
Mn (ng/kg) detrital Mn
0 100 2000 3000 4000 50000
DEPTH (M)
50
100
150
200
250
300
350
400
450
500
nondetrital Mn
nondetrital Co
predicted
nondetrital Co

FIGURE 5

The La, Sc, Fe profiles for station 1449.

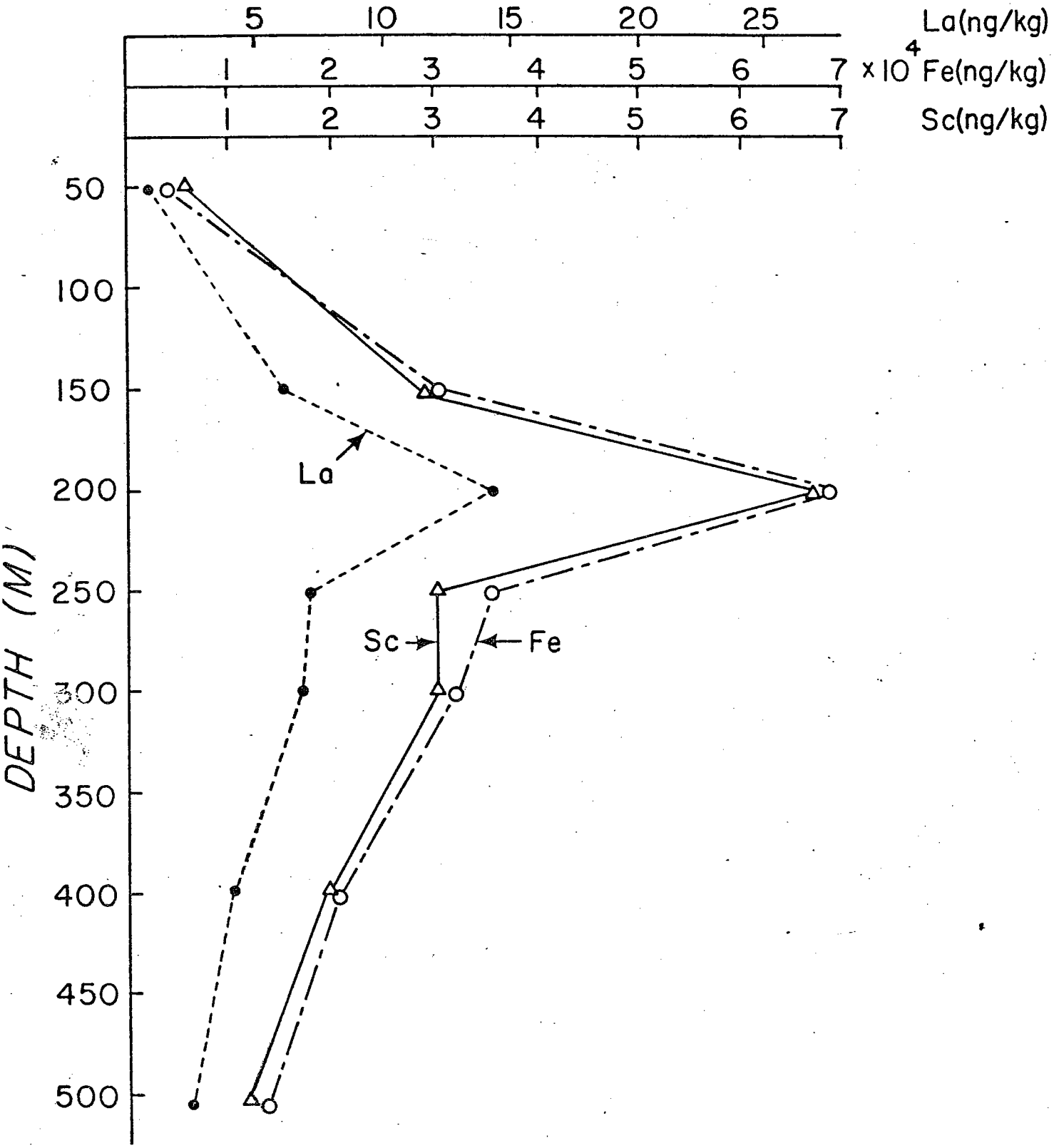
5
10
15
20
25
La(ng/kg)
1
2
3
4
5
6
7
x 10^4 Fe(ng/kg)
1
2
3
4
5
6
7
Sc(ng/kg)
50
100
150
200
250
300
350
400
450
500
DEPTH (M)
La
Sc
Fe

FIGURE 6

A plot of the amount of Co leached versus the amount of Mn leached. Data from F. Sayles (1973 personal communication).

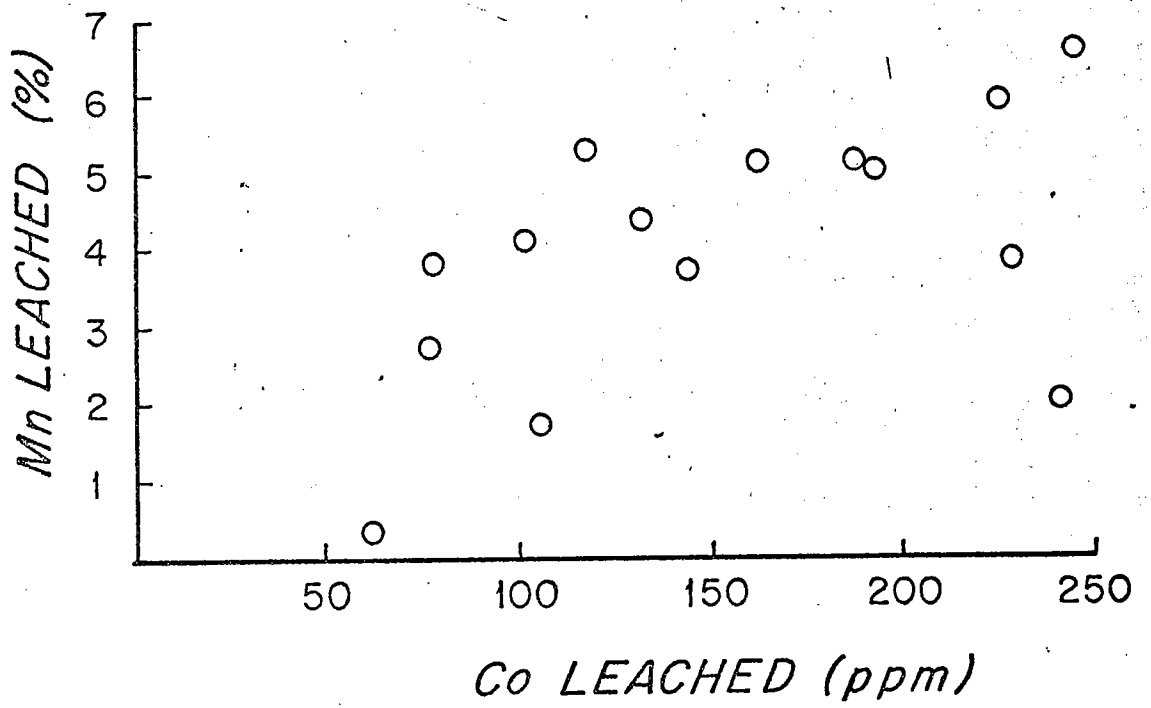
Mn LEACHED (%)
7
6
5
4
3
2
1
50
100
150
200
250
Co LEACHED (ppm)

BIBLIOGRAPHY

Albrethson A.E. (1963) An electrochemical study of the ferric oxide-solution interface. PhD. Thesis, M.I.T.

Bender M.L., Broecker W., Gornitz V., Middel U., Kay R., Sun S. and Biscaye P. (1971) Geochemistry of three cores from the East Pacific Rise. Earth Planet. Sci. Lett. 12, 425-433.

Boström K. and Peterson M.N.A. (1966) Precipitates from hydrothermal exhalations on the East Pacific Rise. Econ. Geology 61, 1258-1265.

Boström K. and Peterson M.N.A. (1969) The origin of aluminum poor ferromanganoan sediments in areas of high heat flow on the East Pacific Rise. Marine Geol. 7, 427-447.

Boström K. (1970) Submarine volcanism as a source for iron. Earth Planet. Sci. Lett. 9, 348-354.

Brewer P.G. and Spencer D.W. (1973) The distribution and flux of some trace elements between dissolved and particulate phases in the Black Sea. In: The Black Sea: Its Geology, Chemistry and Biology. E.T. Degens and D.A.Ross, editors. Mem. Am. Ass. Pet. Geol. (in press)

Brown B.A. (1971) A geochemical investigation of inter-element relationships in deep sea ferromanganoan nodules. PhD. Thesis, Oxford University.

Chan K.M. and Riley J.P. (1966) The determination of molybdenum in natural waters, silicates and biological materials. Anal. Chim. Acta 36,220-229.

Chester R. and Hughes M.J. (1967) A chemical technique for the separation of ferro-manganese minerals, carbonate minerals and adsorbed trace elements from pelagic sediments. Chem. Geol. 2, 249-262.

Cronan D.S. and Tooms J.S. (1969) The geochemistry of manganese nodules and associated pelagic deposits from the Pacific and Indian Oceans Deep-Sea Res. 16, 335-359.

Dasch E.J., Dymond J.R. and Heath G.R. (1971) Isotopic analysis of metalliferous sediment from the East Pacific Rise. Earth Planet. Sci. Lett. 13, 175-180.

Flaningham O.L. (1960) The electrokinetic properties of goethite. M.S. Thesis, Michigan College of Mining and Technology.

Goldberg E.D. (1954) Marine geochemistry 1. Chemical scavengers of the sea. J. Geol. 62, 249-265.

Goldberg E.D. and Arrhenius G.O.S. (1958) Chemistry of Pacific Pelagic sediments. Geochim. Cosmochim. Acta 13, 153-212.

Goldschmidt V.M. (1937) The principles of distribution of chemical elements in minerals and rocks. J. Chem. Soc. p. 655.-674

Grahame D.C. (1947) The electrical double layer and the theory of electrocapillarity. Chem. Rev. 41, 441-501.

Harvey H.W. (1937) Note on colloidal ferric hydroxide in sea water. Journ. Mar. Biol. Assoc. 22, 221-225.

Hazel F. and Ayres G.H. (1931) Migration studies with ferric oxide sols. J. Phys. Chem. 35, 2930-2942

Healy T.W., Hearing A.P., and Fuerstenau D.W. (1966) The effect of crystal structure on the surface properties of a series of manganese dioxides. J. Colloid Interface Sci. 21, 435-444.

Hingston F.J., Atkinson R.J., Posner A.M. and Quirk J.P. (1967) Specific adsorption of anions. Nature 215, 1459-1461.

Huang C.P. (1971) The chemistry of the aluminum oxide-electrolyte interface. PhD. Thesis, Harvard University.

Iwasaki I., Cooke S.R.B. and Choi H.S. (1960) U.S. Bur. Mines Rept. 5593 (cited in Parks 1965)

Iwasaki I., Cooke S.R.B. and Yim Y.S. (1962) Trans. A.I.M.E. 223, 113 (cited in Parks 1965)

James R.O. and Healy T.W. (1972) Adsorption of hydrolyzable metal ions at the oxide-water interface 1. Co(II) adsorption on SiO_2 and TiO_2 as model systems. J. Colloid Interface Sci. 40, 42-52.

Jenkins S.R. (1970) The colloid chemistry of hydrous MnO_2 as related to manganese removal. PhD. Thesis, Harvard University.

Korpi G.K. (1960) Measurement of streaming potentials. M.S. Thesis, M.I.T.

Kharkar D.P., Turekian K.K. and Bertine K.K. (1968) Stream supply of dissolved silver, molybdenum, antimony, selenium, chromium, cobalt and cesium to the oceans. Geochim. Cosmochim. Acta 32, 285-298.

Krauskopf K.B. (1956) Factors controlling the concentrations of thirteen rare elements in sea water. Geochim. Cosmochim. Acta 9, 1-32B.

Lengweiler H., Buser W. and Feitknecht W. (1961) Die Ermittlung der Löslichkeit von Eisen (III)-hydroxiden mit $^{59}Fe(II)$. Helv. Chim. Acta 44, 796-811.

Loganathan P. and Burau R.G. (1973) Sorption of heavy metal ions by a hydrous manganese oxide. Geochim. Cosmochim. Acta, in press.

Mattson S. and Pugh A.J. (1934) The laws of soil colloidal behavior XIV. The electrokinetics of hydrous oxides and their ionic exchange. Soil Sci. 38, 299

Morgan J.J. and Stumm W. (1964) Colloid-chemical properties of manganese dioxide. J. Colloid Sci. 19, 347-359.

Murray D.J., Healy T.W. and Fuerstenau D.W. (1968) The adsorption of aqueous metal on colloidal hydrous manganese oxide. Adv. in Chemistry 79, 74-81

Parks G.A. (1965) The isoelectric points of solid oxides, solid hydroxides and aqueous hydroxo complex systems. Chem. Rev. 65, 177-198

Parks G.A. and deBruyn P.L. (1962) The zero point of charge of oxides. J. Phys. Chem. 66, 967-973.

Pauling L. (1960) The Nature of the Chemical Bond, Cornell University Press, Ithaca, N.Y., 644 pp.

Posselt H.S., Anderson F.J. and Weber W.J. (1968) Cation sorption on colloidal hydrous manganese dioxide. Environ. Sci. Tech. 2, 1087-1093.

Presley B.J., Brooks R.R. and Kaplan I.R. (1967) Manganese and related metals in the interstitial water of marine sediments. Science 158, 906-910.

Revelle R.R. (1944) Marine bottom samples collected in the Pacific by the Carnegie on its seventh cruise. Carnegie Institute, Washington, Publ. 556.

Robertson D.E. (1970) The distribution of cobalt in oceanic waters. Geochim. Cosmochim. Acta 34, 553-567.

Robinson R.A. and Stokes R.H. (1959) Electrolyte Solutions, Butterworths Scientific Publ., London. 571 pp.

Sayles F.L. and Bischoff J.L. (1973) Ferromanganoan sediments in the equitorial East Pacific. Earth Planet. Sci. Lett., in press.

Schuylenborg J. and Arens P.L. (1950) The electrochemical behavior of freshly prepared α- and γ- FeOOH. Rec. Trav. Chim. 69, 1557-1565.

Sevast'yanov V.F. and Volkov I.I. (1966) Chemical composition of iron-manganese concretions of the Black Sea. Dokl. Akad. Nauk. S.S.S.R. 166, 701-704.

Spencer D.W., Brewer P.G. and Sachs P.L. (1972) Aspects of the distribution and trace element composition of suspended matter in the Black Sea. Geochim. Cosmochim. Acta 36, 71-86.

Spencer D.W. and Brewer P.G. (1971) Vertical advection diffusion and redox potentials as controls on the distribution of manganese and other trace metals dissolved in waters of the Black Sea. J.G.R. 76, 5877-5892.

Stumm W., Huang C.P. and Jenkins S.R.(1970) Specific chemical interaction affecting the stability of dispersed systems. Croatica Chemica Acta 42, 223-245.

Stumm W. and Morgan J.J. (1970) Aquatic Chemistry, Wiley-Interscience, N.Y. 583 pp.

Veeh H.H. and Bostrom K. (1971) Anomalous $^{234}U/^{238}U$ on the East Pacific Rise. Earth Planet. Sci. Lett. 10, 372-374.

Appendix (I-A)

MASS BALANCE CALCULATIONS

I) INPUT FLUXES

A) DISSOLVED RIVER INPUT

River volume = 2.9×10^{16} l/yr
(Garrels and Mackenzie 1971, p.119)

Dissolved river concentrations (including desorbable fraction) (Riley and Chester 1971 p. 64-67)

METAL	CONCENTRATION
Mn	5 µg/l
Co	0.2 µg/l
Ni	0.3 µg/l
Cu	5 µg/l

B) SUSPENDED RIVER INPUT

Suspended load of rivers = 1.83×10^{16} g/yr

(Garrels and MacKenzie 1971 p.105)

Assume composition is the same as the average crustal composition (Parker 1967)

METAL	AVERAGE CRUSTAL COMPOSITION
Mn	950 ppm
Co	25 ppm
Ni	75 ppm
Cu	55 ppm

C) ATMOSPHERIC DUST INPUT

Total amount of dust = 6.0×10^{13} g/yr
(Garrels and Mackenzie 1971, p.111)

Assume composition of dust is same as continental crust

D) HYDROTHERMAL EMANATIONS ASSOCIATED WITH SPREADING RIDGES

Assume the rate of heat loss of the cooling lithosphere is = 4.2×10^{12} cal/sec (D. Williams, personal communication) and that all of this heat is removed by sea water circulating through this lithosphere. If the sea water is warmed from $0^{o}C$ to $100^{o}C$ and the heat capacity of water is 1.0 cal/g ^{o}C, then the amount of water required is:

$$\frac{4.2 \times 10^{12} \text{ cal/sec}}{(100^{o})\ (1.0 \text{ cal/g } ^{o}C)} = 4.2 \times 10^{10} \text{ g } H_2O/\text{yr}$$
$$= 1.2 \times 10^{18} \text{ g } H_2O/\text{yr}$$
$$= 1.2 \times 10^{15} \text{ l/yr}$$

The average concentration of Mn in thermal springs from basalts is 1.0 ppm.(White et al. 1963). Thus the input flux of hydrothermal Mn would be

$$(1.2 \times 10^{15} \text{ l/yr})\ (1.0 \times 10^{-3} \text{ g/l}) = 1.2 \times 10^{12} \text{ g/yr}$$

II) REMOVAL FLUXES

A) ADJACENT SEA SEDIMENTS

Area of adjacent seas = 40×10^{16} cm^2 (Sverdrup, Johnson and Fleming 1942, p. 15)

Sedimentation rate = 42 $g/cm^2/1000yr$

This rate was estimated by subtracting the amount of sediment deposited in the deep sea from the total suspended river load. The remaining sediment is deposited in adjacent seas.

Sedimentation rate = $(1.83 \times 10^{16}$ g/yr$) - (321 \times 10^{16}$ $cm^2)(0.5$ $g/cm^2/1000yr)$

$= 1.67 \times 10^{16}$ g/yr

and then dividing this by the area of the adjacent seas

$$\frac{1.67 \times 10^{16} \text{ g/yr}}{40 \times 10^{16} \text{ cm}^2} = 42 \text{ g/cm}^2/1000\text{yr}$$

The metal content of adjacent seas was taken from Riley and Chester (1971). p. 391.

METAL	CONCENTRATION
Co	13 ppm
Cu	48 ppm
Ni	55 ppm
Mn	850 ppm

B) DEEP SEA SEDIMENTS

Area of deep sea sediments = 320×10^6 km^2 (Sverdrup et al. 1942 p.15)

If 1/4 is covered by manganese nodules

then the remaining area = 243×10^6 km^2.

Assume an average rate sedimentation of 0.5 g/cm^2/1000yr

(Riley and Chester 1971, p. 289)

Assume 50% of the sediments are $CaCO_3$ and 50% are red clay.

Use $CaCO_3$ and red clay metal compositions from Riley and Chester (1971, p.390), then the average of these two represents the composition of deep sea sediments.

METAL	DEEP SEA CARBONATE	DEEP SEA CLAY	AVERAGE
Co	7 ppm	74 ppm	40 ppm
Cu	30 ppm	250 ppm	140 ppm
Ni	30 ppm	225 ppm	127 ppm
Mn	1000 ppm	6700 ppm	4350 ppm

C) MANGANESE NODULES

Assume total area of manganese equals the area of deep sea sediments = 243×10^6km^2

Assume an average nodule growth rate of 0.5 mg/cm^2/1000yr (Bender et al. 1970)

The average composition of manganese nodules is (Riley and Chester 1971, p. 362)

METAL	CONCENTRATION
Co	0.34%
Ni	0.57%
Zn	0.35%
Mn	22.06%

REFERENCES

Bender M.L., Ku T-L, and Broecker W.S. (1970) Accumulation rates of manganese in pelagic sediments and nodules. Earth Planet. Sci. Let., 8 143-148

Garrels R.M. and Mackenzie F.T. (1971) Evolution of Sedimentary Rocks Norton, 397 pp.

Parker P.L. (1967) Composition of the Earth's crust in Data of Geochemistry (editor M. Fleischer) , U.S.Geol. Prof. Pap. 440-D.

Riley J.P. and Chester R. (1971) Introduction to Marine Chemistry Academic Press, 465 pp.

Sverdrup H.U., Johnson M.W. and Fleming R.H. (1942) The Oceans Prentice-Hall , 1087 pp.

White D.E., Hem J.D. and Waring G.A. (1963) Chemical composition of subsurface waters, in Data of Geochemistry (editor M. Fleischer) U.S.Geol.. Surv. Prof. Pap. 440-F.

APPENDIX (II - A) STOICHIOMETRY OF MnO_x

Introduction

It was necessary to determine the oxidation grade of the MnO_x used in the experiments in this thesis in order to verify that the experimental solid resembled phases found in nature. Unfortunately, few analyses of oceanic manganese nodules include the oxidation grade, and none has been related to the mineral phases of the nodules. The values that have been reported have been summarized by Manheim (1965). Figure 1 (taken from Manheim's paper) is a plot of available literature values of the O/Mn ratio plotted as a function of depth. The O/Mn ratio for deep ocean nodules appears to average approximately 1.90, while near-shore concretions show appreciably lower oxidation grades.

Method

The method used to determine the oxidation grade was suggested by Morgan (1964). It consists of measuring the equivalent concentration of oxidized manganese by the O-Tolidine method (Morgan and Stumm 1965) and the total manganese by atomic absorption spectrophotometry.

The oxidized equivalents of manganese ((OX.) = 2(Mn(IV)) + (Mn(III)) were determined as follows. A small amount of solid MnO_x (the exact weight is not necessary) was placed in a 100 ml volumetric flask. Then 25 ml of 3M perchloric acid plus 10 ml of 0.1% O-Tolidine perchlorate were added, and the solution was brought to the mark using distilled-deionized water. After 15 minutes, the solution was read at 440 mμ on a Beckman DU Spectrophotometer using 1 cm cells. A standard curve was prepared using $NaMnO_4$ solutions previously standardized using sodium oxalate (Skoog and West 1963, p. 436.)

Figure 1

The oxidation grade of manganese concretions plotted as a function of depth. The O/Mn ratio may be regarded as denoting the exponent in MnO_x.

Explanation of symbols: (references cited in Manheim 1965)

1. Baltic Sea (Gulf of Finland); Samoilov and Titov, 1922.
2. Barents Sea; Samoilov and Titov, 1922.
3. White Sea; Gorshkova, 1931.
4. Black Sea; Samoilov and Titov, 1922.
5. Lochs Striven and Goil (Clyde Estuary); Murray and Irvine, 1894.
6. South Pacific and Loch Fyne (Clyde Estuary); Buchana, 1891.
7. Ceram and Timor Seas; Böggild, 1916 (Analyst: Niels Bjerrum).
8. Pacific Ocean; Skornyakova and others, 1962.
9. Pacific Ocean; Skornyakova and others, 1962.
10. Pacific Ocean; Riley and Sinhaseni, 1958.
11. Atlantic Ocean; Murray and Philippi, 1908.

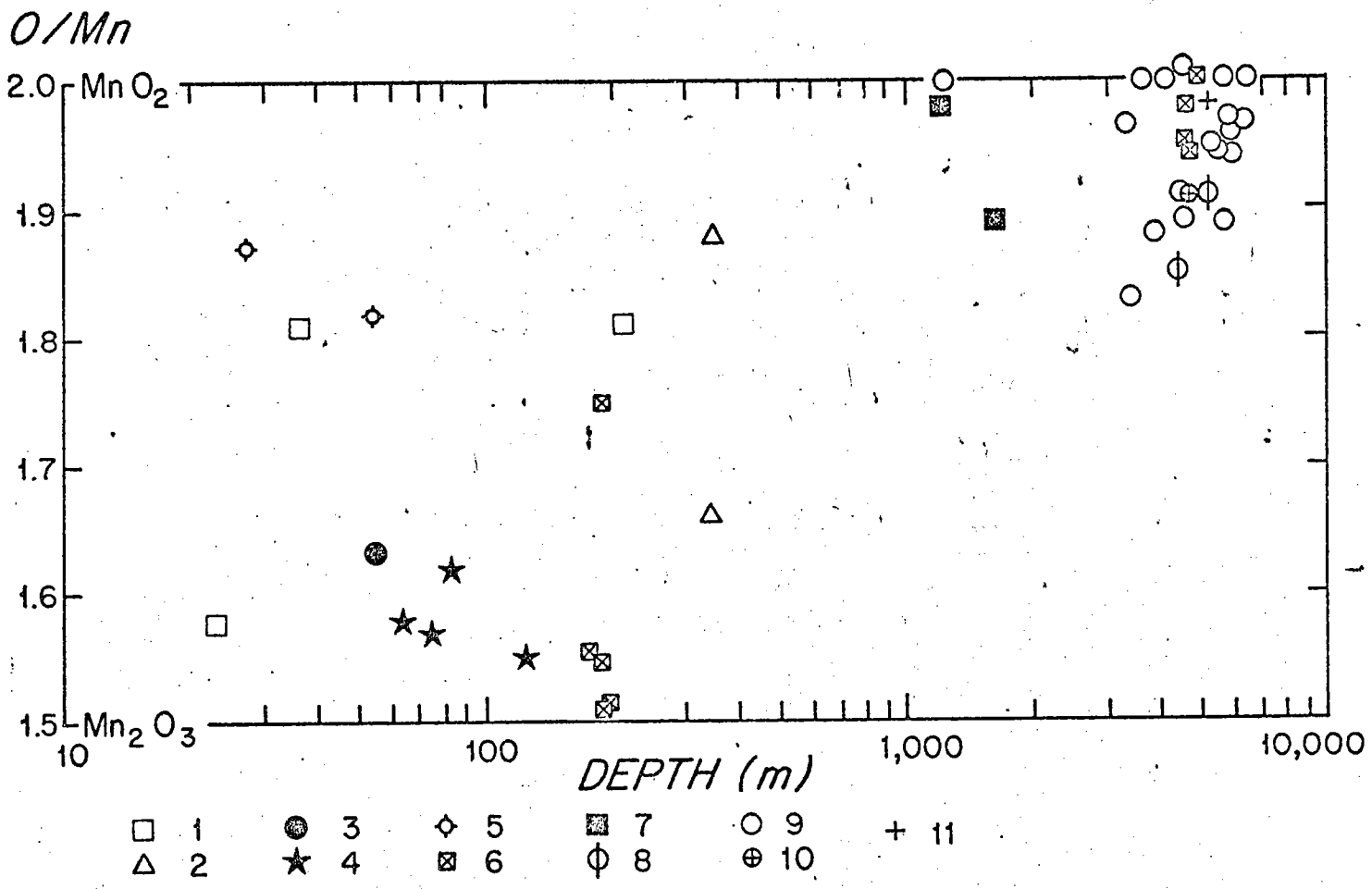
O/Mn
2.0
Mn O2
1.9
1.8
1.7
1.6
1.5
Mn2 O3
10
100
1,000
10,000
DEPTH (m)
1
2
3
4
5
6
7
8
9
10
11

The total manganese was determined on the same samples used for the O-Tolidine measurements by Atomic Absorption Spectrophotometry. The solutions were aspirated directly and compared with a standard curve prepared using $MnCl_2$ standard solutions.

The coefficient X for MnO_x was calculated as:

$$X = 1 + \frac{1}{2}\frac{Mn(oxid.eq.)}{Mn(total)}$$

where it is assumed that all the oxidized manganese is present as Mn(IV), i.e. Mn(oxid.) = Mn(IV). There is no evidence for the existence of Mn(III) in manganese nodules or in solution in the absence of strong chelators, and thermodynamic data suggest that Mn(III) should disproportionate into Mn(II) and Mn(IV) according to reaction 1 (Stumm and Morgan 1970, p. 525).

$$2\,Mn^{+3} + 2H_2O = Mn^{+2} + MnO_2\,(s) + 4H^+;\ \log K = 9 \qquad (1)$$

Results

The results of these determinations are shown in Table 1. The average stoichiometry of four MnO_x samples was 1.93. This value falls within the range observed for deep sea nodules (Figure 1).

References

Manheim F.T. (1965) Manganese-iron accumulations in the shallow marine environment. Univ. Rhode Island, Occ. Publ. No. 3, 217-275.

Morgan J.J. and Stumm W. (1965) Analytical chemistry of aqueous manganese. J. Amer. Water Wks. Assn. 57, 107-199.

Morgan J.J. (1964) The chemistry of aqueous manganese(II) and (IV) Ph.D. Thesis. Harvard Univ.

Stumm W. and Morgan J.J. (1970) Aquatic Chemistry. Wiley-Interscience, 583 pp.

Skoog D.A. and West D.M. (1963) Fundamentals of analytical chemistry. Holt, Rinehart and Winston, 786 pp.

Table 1

Sample	Mn(oxid.eq.)	Mn(total)	X
1	14.6 eq/l	7.4 m/l	1.95
2	8.0 eq/l	4.25 m/l	1.89
3	7.5 eq/l	4.0 m/l	1.88
4	12.4 eq/l	6.25 m/l	1.98
		average	1.93

APPENDIX (II-B) X-RAY DIFFRACTION

Introduction

Although the oxides of manganese have been studied extensively (Buser et al. 1954, Buser and Graf 1955, Buser and Grutter 1956, Buser 1959, Manheim 1965, Bricker 1965, Giovanoli et al. 1969, Giovanoli and Stahli 1970) , many ambiguities concerning their structural properties still exist. This is due to the fact that many of these oxides are poorly crystalline. The basic structure of these minerals appears to consist of sheets of MnO_2 interlayered with Mn^{+2}, H_2O, OH^- and other metal ions. A review of synthetic and naturally occurring manganese oxides is given by Manheim (1965).

The x-ray diffraction spacings for phases reported to occur in nature and for synthetic ferromanganese material have been summarized by Hathaway (personal communication) and are shown in Table 1. The synthetic δMnO_2 used in the experiments of this thesis was analyzed by x-ray diffraction to verify that it was structurally similar to the naturally occurring phases.

Methods and Results

A slurry of δMnO_2 was air dried at room temperature and then ground with a mortor and pestle until the sample could pass through a Tyler 400 mesh sieve. The sample was then x-rayed using Cu radiation (Ni-filter) at 45kv and 30 ma. A curved crystal monochrometer was used to minimize background fluorescence.

The 2-θ peak locations and corresponding spacings in angstroms are shown in Table 2. For comparison, the peak locations of the naturally occurring minerals todorokite and birnessite are also shown.

TABLE 1

Phases reported to occur in natural and synthetic ferro-manganese material (from Hathaway)

PHASE	COMPOSITION	CRYSTAL SYSTEM	CELL PARAMETERS a	b	c	β	CHARACTERISTIC X-RAY LINES (in Å)
Pyrolusite	β- MnO_2	Tetragonal	4.4		2.8		3.14(10), 2.41(5), 1.63(5)
Nsutite	γ- MnO_2	Orthorhombic	4.4	9.4	2.8		3.96(10), 2.42(10), 2.32(8)
Birnessite	δ- MnO_2	Hexagonal	2.4				7.4, 3.7, 2.44(10)
Hausmannite	$MnMn_2O_4$	Tetragonal	5.7		9.4		2.49(10), 2.77(9), 1.54(8)
Manganese oxide	Mn_3O_4	Cubic	8.4				2.54(s), 1.49(m), 4.86(m)
Partridgeite	Mn_2O_3	Cubic	9.4				2.72(10), 1.66(3), 3.84(2,5)
Groutite	MnO(OH)	Orthorhombic	4.6	10.7	2.8		4.20(10), 2.81(7), 2.67(7)
Pyrochroite	$Mn(OH)_2$	Hexagonal	3.4		4.7		4.73(10), 2.45(4), 1.83(3)
Manganous Manganites	$MnO.H_2O$	Tetragonal	5.8		9.5		
	$Mn_2O_3.H_2O$	Monoclinic	8.9	5.2	5.7	90°	3.40(s), 2.64(m), 2.28(m)
	$4MnO_2.Mn(OH)_2.2H_2O$	Hexagonal	5.8		14.6		
	$Mn_3O_4.H_2O$	Tetragonal	5.8		1.6 or 9.5		
10 Å Ferrous Manganites	Layered alternations of MnO_2, $Mn(OH)_2$, H_2O	Hexagonal	8.4		9.8		9.8(s), 4.8(m), 2.44(m)
Todorokite	(Mn^{2+}, Mg,Ca,Ba,Na,K) $Mn^{4+}_5O_{12}.3H_2O$	Monoclinic	9.7	2.8	9.6	90°	

Table 2

X-ray diffraction spacings for the synthetic manganese dioxide used in this thesis compared with naturally occurring manganese oxide minerals. The spacings are in angstroms.

Synthetic manganese dioxide	birnessite (1)	todorokite (2)
7.44	7.27	9.6
		7.17
		4.76
		4.42
4.04		
	3.60	
2.423	2.44	2.45
		2.39
		2.34
2.122		2.22
1.626		
		1.42
	1.412	1.39
1.389		

(1) birnessite from Jones and Milne (1956)

(2) todorokite from Manheim (1965)

Conclusions

Though the comparison is not exact, the synthetic MnO_2 used in these experiments resembles closely the naturally occurring mineral birnessite. This result agrees with the stoichiometry results as birnessite is considered to have a higher ratio of oxidized to reduced manganese than todorokite.

References

Bricker O. (1965) Some stability relations in the system $Mn-O_2-H_2O$ at 25^o and one atmosphere total pressure. Amer. Mineral 50, 1296-1354.

Buser W. (1959) The nature of the iron and manganese compounds in manganese nodules. Inter. Oceanogr. Congr. Preprints, 962-963.

Buser W. and Grutter A. (1956) Über die Natur der Manganknollen. Schweiz. Min. Petrogr. Mitt. 36, 49-62.

Buser W. and Graf P. (1955) Differenzierung von Mangan(II)-Manganit und δMnO_2 durch Oberflachenmessung nach Brunauer-Emmet-Teller. Helv. Chim. Acta 38, 830-834.

Buser W., Graf P. and Feitknecht W. (1954) Beitrag zur Kenntnis der Mangan(II)-Manganite und des δMnO_2. Helv. Chim. Acta 37, 129-148.

Giovanoli R., Stahli E. and Feitknecht W. (1969) Über Struktur und Reaktivitat von Mangan(IV) Oxiden. Chimia 23, 264-266.

Giovanoli R. and Stahli E. (1970) Oxide und Oxidhydroxide des drei - und vierwertigen Mangans. Chimia 24, 49-61.

Jones L.H.P. and Milne A.A. (1956) Birnessite, a new manganese oxide mineral from Aberdeenshire, Scotland. Mineralog. Mag. 31, 283-288.

Manheim F.T. (1965) Manganese-iron accumulations in the shallow marine environment. Occasional Publ. 3, 217-276. Narragansett Marine Laboratory, Univ. of Rhode Island.

APPENDIX (II-C) SPECIFIC SURFACE AREA DETERMINATIONS

Introduction

In order to express the results of chapters 2, 3 and 4 in terms of quantities per unit area, it was necessary to determine the specific surface area (m^2/g) of the δMnO_2 used in the experiments. One of the most widely used methods, and the method used here, is the gas adsorption technique of Brunauer, Emmett, and Teller (1938). This method is based on the adsorption of nitrogen gas on the solid surface at several different gas pressures. A variation of the N_2-adsorption method, the t-plot, was also used (de Boer et al. 1966).

Sample Preparation

A major difficulty with using the N_2-adsorption method is that the solid δMnO_2 must be dried. Two drying methods were used.

1) A slurry of δMnO_2 was allowed to dry in a covered evaporating dish at room temperature. It took the sample several months to reach complete dryness. The sample dried into a hard brittle mass that had to be ground in a mortar and pestle and then brushed through a Tyler 400 mesh sieve (37 micron).

2) A slurry of δMnO_2 was freeze dried under vacuum. The dry solid was a granular power that disintegrated into finer particles when brushed with a stiff brush. A portion of this solid was used for surface area determinations. The rest of this dry δMnO_2 was resuspended in acetone, agitated using an ultrasonic vibrator and again freeze dried. The resulting solid was fluffy and extremely finely divided, and the entire sample passed easily through a 400 mesh sieve with no additional treatment.

It is possible that drying the samples reduces the available surface area through particle agglomeration. However, confirmation of the B.E.T. results on dried solids has been obtained using negative adsorption, (Schofield, 1947), a technique in which the solids remain in solution (van den Hul and Lyklema, 1967 and Huang, 1971). The negative adsorption technique is based on the condition that ions with the same charge as the surface are repelled from the surface, leading to an increase in their concentration in the bulk solution. An attempt was made to determine the surface area of the δMnO_2 by negative adsorption, however it was unsuccessful because the anion used, $SO_4^{=}$, exhibited specific adsorption on the negative δMnO_2 surface.

The B.E.T. Plot

The interpretation of the B.E.T. method involves essentially two steps. (1) From the amount of material adsorbed under various conditions (adsorption isotherm), the number of molecules adsorbed in a monolayer is established. (2) After assigning the approximate value to the molecular cross section, a_o, the surface area is calculated. The assumptions of the B.E.T. Theory have been critically reviewed by McMillan and Teller (1951).

The B.E.T. equation (Brunauer et al, 1938) can be expressed as:

$$\frac{P}{V_a(P_o-P)} = \frac{(C-1)\,P}{V_m\,C\,P_o} + \frac{1}{V_m\,C} \qquad (1)$$

where P = partial pressure of the adsorption gas

P_o = saturation pressure of the adsorption gas at the temperature of the coolant, liquid nitrogen.

V_a = Total volume (ml at S.T.P.) of adsorbed gas on the surface of the adsorbent.

V_m = volume (S.T.P.) of adsorbed gas when the entire adsorbent surface is covered with a monomolecular layer. The cross sectional area of the adsorbed nitrogen molecule is assumed to equal 16.3 Å^2.

C = A constant expressing the net adsorption energy.

The N_2 - adsorption measurements were made a method similar to the one described in Nelsen and Eggertsen (1958). Three samples of the freeze dried and acetone freeze dried, one freeze dried sample, and one air dried sample were weighed into glass sample tubes. The samples were degassed for 12 hours with helium gas at 20" pressure before the N_2 - adsorption measurement. To measure the amount of N_2 gas adsorbed a known mixture of nitrogen and helium was passed through the sample, the effluent being monitored by a thermal conductivity probe. The output signal was monitored by a Perkin Elmer Sorptometer (model 212D) and was recorded with time on a recorder chart (Sargent).

When the sample is cooled in liquid nitrogen, the adsorption of nitrogen is indicated by a peak on the recorder chart. After adsorption equilibrium is reached the recorder pen returns to its original position. The sample tube is allowed to warm by removing the liquid nitrogen, causing desorption of nitrogen and producing a peak on the chart which is in the reverse direction of the adsorption peak. The adsorption and desorption peaks should be of equal area and thus provide a check on the measurement. The absolute volume of N_2 gas adsorbed is calibrated by two loops with a given volume built into the sorptometer.

The average specific surface area for the three freeze dried and acetone freeze dried samples was 263 m^2/g. The sample that was only freeze dried had a surface area of 160 m^2/g and the air dried sample had a value of 43.9 m^2/g.

The t-plot

The universal multimolecular adsorption curve has shown to be a useful means of looking at the size distribution of porous capillaries of solid particles (de Boer et al. 1966). This method expresses the quantities of adsorbed gas as a function of t, which is the average thickness of the adsorbed layer in Angstroms. Hence $V = f(t)$ instead of $V = f(P/P_o)$ as in the B.E.T. method. In any normal case of multimolecular adsorption, the experimental points should fall on a straight line through the origin. The slope of this line gives the specific surface area (m^2/g) by means of equation (2):

$$S = 15.47\ V_a/t \qquad (2)$$

S = specific surface area (m^2/g)

where V_a = adsorbed volume of gas (S.T.P.)

t = the average thickness of the adsorbed layer. The statistical value for one layer of adsorbed N_2 gas is 3.54 Å; therefore $t = n \times 3.54$ where $n = V_a/V_m$ layers. V_m is the monolayer volume.

Values for t were obtained from the nitrogen adsorption data as described in de Boer et al. (1966) and Huang (1971), and the t-curve for δMnO_2 is shown in Figure 1. The linearity of the t-plot suggests that there was no

Figure 1

The nitrogen gas adsorption data for two samples of δMnO_2 plotted as a t-plot.

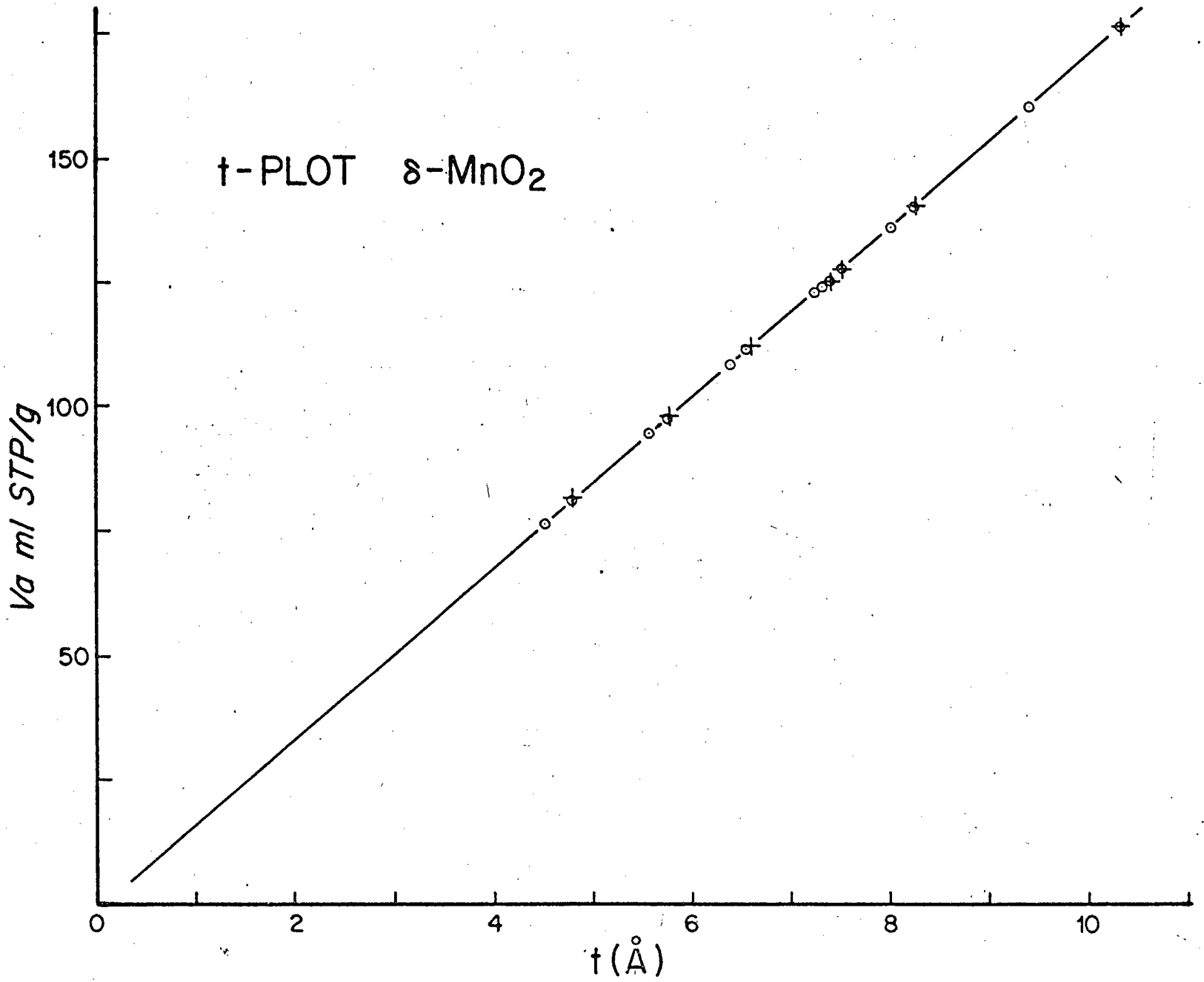
t-PLOT δ-MnO2
Va ml STP/g
150
100
50
0
2
4
6
8
10
t (Å)

capillary condensation or closing of micropores during the adsorption process, and there were no porous capillaries with openings larger than the diameter of the nitrogen gas molecules (3.54 Å). In other words, the colloidal particles of δMnO_2 are flat and don't have large pores. An additional value for the surface area can be calculated from the slope of the t-plot using eqn. 2. The value obtained was 270 m^2/g .

Conclusions

As a result of these determinations, a value of 260 m^2/g was used for the surface area of the δMnO_2 used in this thesis.

BIBLIOGRAPHY

de Boer J.H., Lippens B.C., Linsen B.G., Broekhoff J.C.P., van den Heuvel A. and Osinga Th.J. (1966) The t-curve of multimolecular N_2-adsorption. J. Colloid Interface Sci. 21, 405-414.

Brunauer S., Emmett P.H. and Teller E. (1938) Adsorption of Gases in Multimolecular layers. J. Am. Chem. Soc. 60, 309-319.

Huang C.P. (1971) The chemistry of the aluminum oxide-electrolyte interface. Ph.D. Thesis, Harvard University.

McMillan W.G. and Teller E. (1951) The assumptions of the B.E.T. Theory. J. Phys. and Colloid Chem. 55, 17-20.

Nelson F.M. and Eggertsen F.T. (1958) Determination of surface area. Anal. Chem. 30, 1387-1390.

Schofield R.K. (1947) Calculation of surface areas from measurements of negative adsorption. Nature 160, 408-410.

Van den Hul H.J. and Lyklema J. (1967) Determination of specific surface areas of dispersed materials by negative adsorption. J. Colloid Interface Sci. 23, 500-508.

APPENDIX (III-A) ATOMIC ABSORPTION ANALYSES

Experimental Set Up and Sample Collection

The adsorption experiments were set up by adding the appropriate amounts of Reagent Grade $Co(NO_3)_2$, $Cu(NO_3)_2$, $MnCl_2$, $ZnSO_4$, $CaCl_2$, $MgSO_4$, $SrCl_2$ or $BaCl_2$ stock solutions and 0.10 g of δMnO_2 to an acid washed polyethylene beaker. The ionic strength was adjusted by adding NaCl, and the total volume was brought to 200 ml using distilled-deionized water. The pH was adjusted to approximately 2.25 before the addition of the metals. After equilibration, three ml aliquots were withdrawn from the suspension, the δMnO_2 was removed by centrifugation (30 min at 15000 rpm), and the supernatant was analyzed by atomic absorption spectrophotometry. After each sample was drawn, the pH of the experiment was adjusted using 0.1N NaOH or 0.1N HCl. Equilibration took less than 10 minutes when the pH was increased by less than 1.0 pH units.

Atomic Absorption Analyses

The concentrations of Co, Cu, Ni, Mn, Zn, Ca, Mg, Sr, and Ba were determined by atomic absorption spectrophotometry. Two to three ml aliquots of the separated supernatent solution were aspirated directly into a Perkin Elmer model 403 Atomic Absorption Spectrophotometer equipped with a digital concentration readout. An air-acetylene flame was used for all the metals except Ba, which required nitrous oxide-acetylene. Wavelength settings and the other operating adjustments were made as described in the Perkin Elmer operators manual.

The sample absorbances were compared with standards prepared from the same reagent grade salts used in the experiments. The standards were prepared to have the same ionic strength as the experiments. The samples and standards for the alkaline earths were prepared containing 1% lanthanum in 5% v/v HCl to act as interference-suppressing electrolytes.

APPENDIX (III-B) DIELECTRIC CONSTANT MEASUREMENT

Introduction

The dielectric constant, ε, of solids can be measured by comparing the capacitance of a capacitor filled with a vacuum (C).

$$\varepsilon = \frac{C'}{C} \qquad (1)$$

James and Healy (1972) have proposed a model for the surface chemistry of metal oxides in which the dielectric constant of the solid is one of the most important parameters that can be used to predict the types of reactions that might occur on the surface. No value could be found in the literature for the dielectric constant of MnO_2. Thus in order to compare the results of this thesis with the model of James and Healy, a value for the dielectric constant had to be measured.

Method

A capacitor was made of two 3" x 3" copper plates with a fiberglass cell designed to hold the powdered MnO_2.

The capacitance of the cell was measured with only air in the cell and then with the cell packed with the solid sample. The volume of the sample was calculated from its weight and density. The measurements were made using a General Radio Company Capacitance Bridge (Type 1615-A) at $10KH_z$.

Results

The dielectric for both βMnO_2 (Baker Chemical Co.) and δMnO_2 (made using the method described in Chapter 2) were measured, and the results are shown in Table 1. For an estimate of accuracy, the dielectric

Table 1

βMnO_2	32.1
δMnO_2	28.5
NaCl	7.5

of NaCl was measured, and it agreed to within 20% its known dielectric (6,12).

BIBLIOGRAPHY

James, R.O. and Healy, T.W. (1972) Adsorption of hydrolyzable metal ions at the oxide-water interface, III. A thermodynamic model of adsorption. J.Colloid. Interface Sci. 40, 65-81.

APPENDIX (IV-A) TRACER EXPERIMENTS

Materials

The δMnO_2 used in these experiments was prepared in the same manner as described in chapter 1. The resulting solid has a B.E.T. surface area of 260 m^2/gm (Appendix II-A) and a stoichiometry of $MnO_{1.93}$ (Appendix II-B). A stock suspension was prepared with a δMnO_2 concentration of $1 \times 10^{-3}M$ and diluted when necessary for the subsequent experiments. The δMnO_2 was kept in suspension at all times and was not allowed to dry, as this would cause the surface to dehydrate, thus changing its adsorptive properties (Parks 1965). Na^+ adsorption, electrophoresis and alkalimetric titration experiments on this preparation of δMnO_2 gave results similar to those reported in chapter 2, thus indicating that both precipitates are equivalent. The cobalt solutions were prepared from analytical grade $Co(NO_3)_2$ salts. Distilled-deionized water was used in all the experiments. When necessary, the pH was adjusted using A.R. HCl or NaOH, and A.R. NaCl was used to adjust the ionic strength. For the sea water experiments, the appropriate amounts of NaCl, $CaCl_2$ and $MgSO_4$ stock solutions were added to bring the concentrations of Na^{+2}, Ca^{+2}, and Mg^{+2} up to sea water concentrations.

All tracer and electrophoresis experiments were done at room temperature (25 ± 2^oC).

Tracer Experiments

Cobalt-58 (Amersham Searle Corp.) was used for the tracer experiments because of its suitable half life (71d), its decay mode (γ, 0.810 MEV (99%)), and its availability as a carrier free isotope (> 2mCi/μg Co). The ^{58}Co was purchased in the form of cobaltous chloride in 0.1N HCL. The decay rate of the purchased isotope was checked, and the resulting half life was found to agree well with the expected 71 day half life.

The ^{58}Co was quantitatively (84%) transferred from the delivery vial to a polypropylene erlenmeyer flask containing 5 gm of HCl (conc.) and 95 gm of H_2O. A stock solution of 1×10^{-2}M $CoCl_2$ was prepared and diluted when necessary for the experiments. The ^{58}Co was added to the diluted stock solution by adding approximately 0.2 ml of the tracer solution. The volume of tracer solution added was increased slightly during the course of the experiments because of decay. The total count rate of individual experiments (total volume - 200 ml) was kept between 10000 to 20000 counts per minute (c.p.m.) above background (5-10 c.p.m.). Each experiment contained approximately 2×10^{-3} mCi of ^{58}Co.

The samples were counted in a NMC-Well Scintillation Counter (NaI(Tl), yield 50%) combined with a RIDL-single channel analyzer. By proper adjustment of the upper and lower energy discriminators, the 0.808 MEV peak of cobalt-58 could be counted with the background decreased by a factor of 33 (270 to 8 c.p.m.) (Figure 1). The efficiency of the NaI(Tl) crystal is a function of sample volume, so this effect was checked in order to obtain the optimum counting volume. The results illustrated in Figure 2 show that the count rate is independent of volume up to greater than 5 ml.

Figure 1

Determination of the upper and lower energy discriminators for optimum counting conditions of the 0.808 MEV peak of ^{58}Co with the differential mode (the width of the energy window) set at 50, the threshold (lower edge of energy window) was varied from 200 to 700 to define the peak location. Then with the threshold set at 450 (the lower energy side of the 0.808 MEV peak), the differential mode was increased from 50 to 200 to open the energy window so that it included all of the 0.808 MEV peak. The inflection in the curve at differential mode = 150 indicates that the 0.808 MEV peak is included on the window. The differential mode and threshold settings are in arbitrary instrument units.

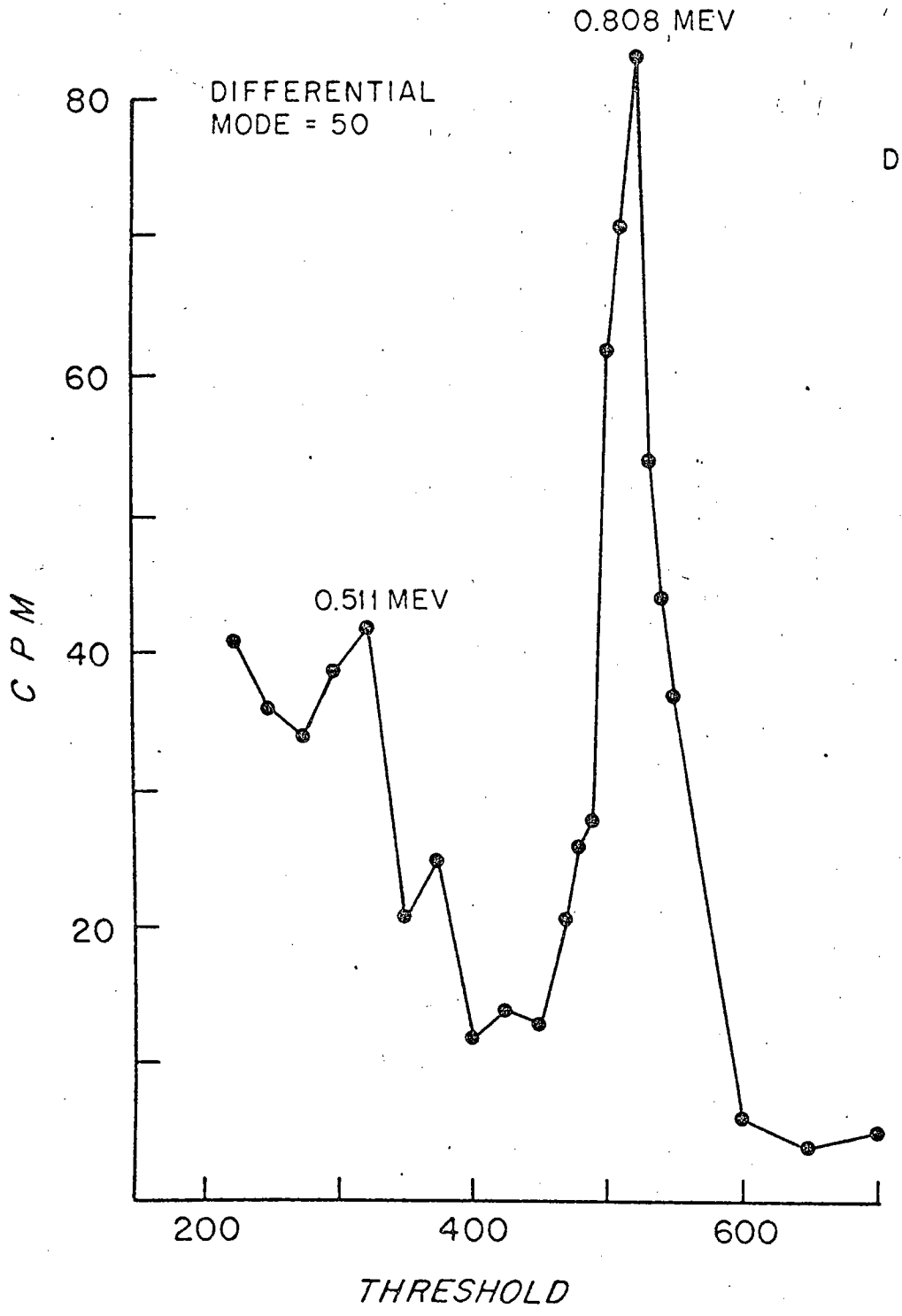

DETERMINED OPTIMUM SETTINGS

THRESHOLD 450 (LOWER VOLTAGE LEVEL)
WINDOW 150 (VOLTAGE WINDOW WIDTH)

DIFFERENTIAL MODE DETERMINATION
THRESHOLD = 450

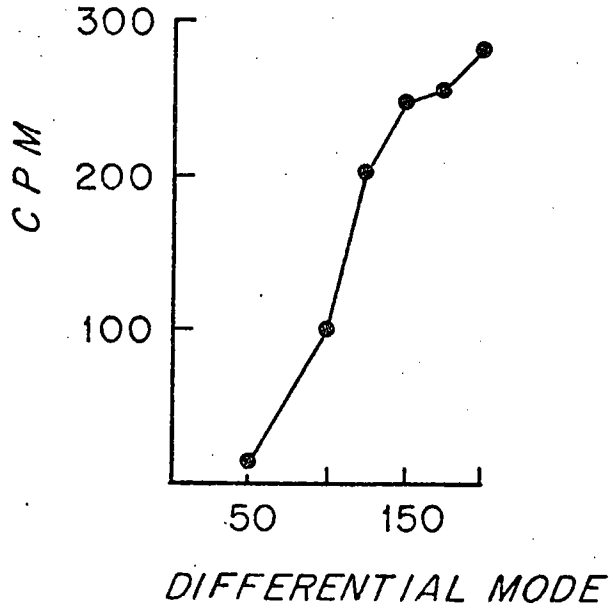

Figure 2

The count rate as a function of sample volume.

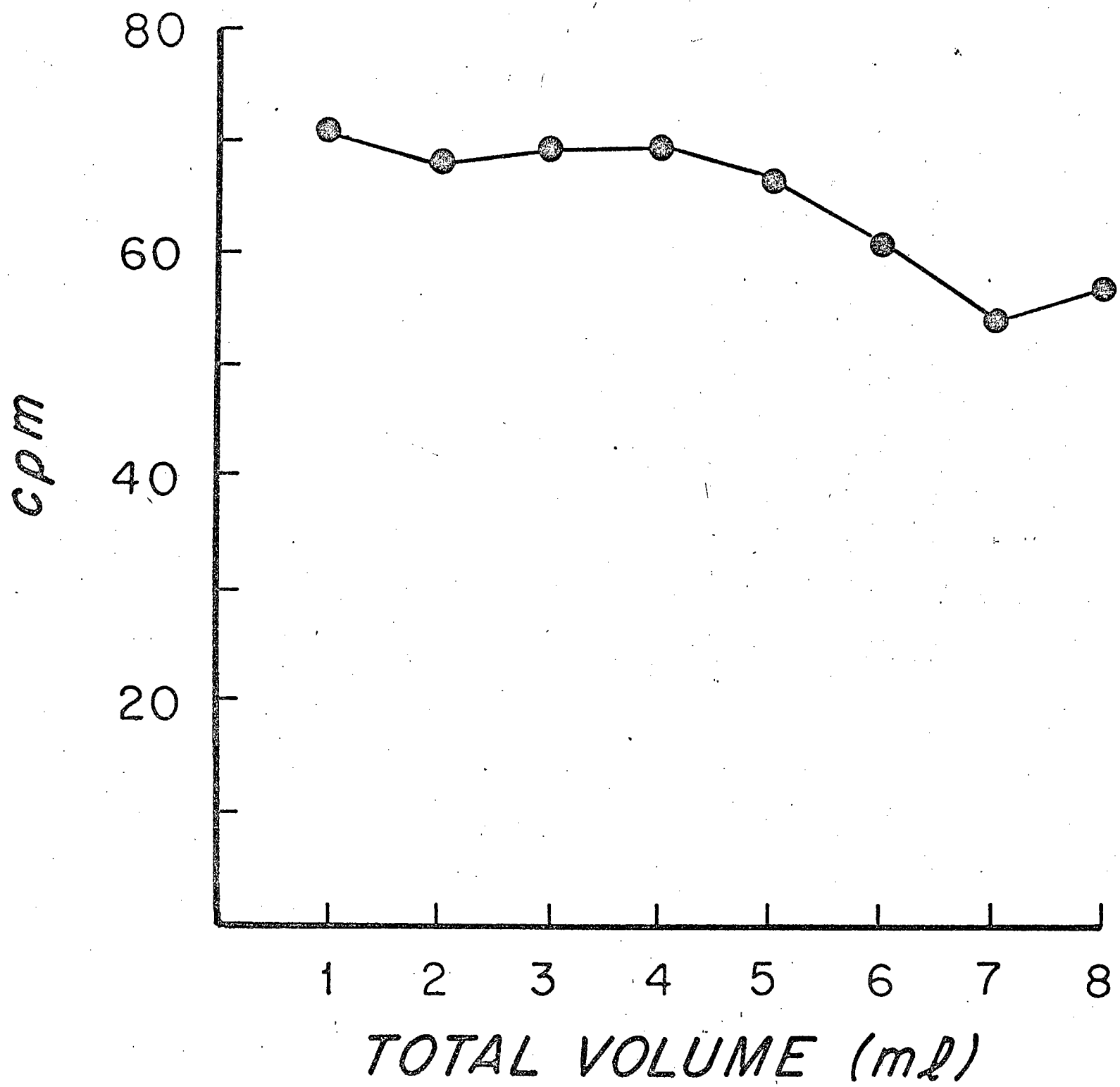
80
60
40
20
cpm
1
2
3
4
5
6
7
8
TOTAL VOLUME (mℓ)

Some of the samples counted contained solid δMnO_2, and a comparison of the count rate of the sample with and without the reduction of the δMnO_2 revealed a slight difference due to the difference in geometry. Thus, before counting samples with solid δMnO_2, the solid was reduced by the addition of hydroxylamine hydrochloride.

The experiments were carried out in 500 ml polypropylene beakers. The ionic strength was adjusted using 1.0M NaCl, the pH was adjusted to approximately 2.5 by 0.1 HCl, the proper amount of δMnO_2 was added from the stock suspension, and finally the labeled cobalt solution was added. The pH was adjusted before the cobalt was added, because the results of chapter 3 showed that adsorption was partially irreversible as a function of pH. Thus, all experiments were begun at low pH, and the pH was adjusted upward for each successive sample by the addition of 0.1N NaOH. The samples were prepared for counting in the following manner. After equilibration at a given pH, a 5 ml sample of the supernatant was withdrawn, using a calibrated 5 ml polypropylene pipette and placed in a polypropylene centrifuge tube. The sample was then centrifuged (2000 rpm, 5-10 min) to remove the solid. A 2 ml sample of the supernatant was withdrawn using a calibrated plastic pipette, and transferred to a second centrifuge tube. Three ml of H_2O was added to bring the total volume up to 5 ml. Two ml of a 10% hydroxylamine hydrochloride solution was added to the original centrifuge tube to bring the total volume to 5 ml and to reduce the solid δMnO_2. By counting both centrifuge tubes, it was possible to determine the amount of cobalt adsorbed on the δMnO_2 and to monitor the total counts to ensure that cobalt was not being lost by adsorption onto the walls of the experimental beaker. One rinse of the plastic pipettes with a 1M HNO_3 + 10% hydroxylamine

hydrochloride solution after the transfer of cobalt-58 solution was sufficient to bring the count rate of the rinsing solution to background.

It was found that during the course of the experiments using low cobalt concentrations there was some loss of activity that could not be accounted for by decay (the average experiment lasted approximately 16 - 18 hours). After the experiments were completed, the solutions were removed, and the empty beakers were rinsed with 3 ml of a 10% hydroxylamine hydrochloride solution. This rinse process recovered the lost activity. Blank experiments with no δMnO_2 present showed no loss of activity. Thus, it was assumed that the loss was due to the adsorption of some of the δMnO_2 with its adsorbed cobalt onto the beaker walls. As would be expected if this were the case, the loss was greatest at the lowest concentrations of δMnO_2 used. This loss amounted to 5% at 5×10^{-6}m Co and 7% at 1×10^{-8}m and thus was not enough to seriously affect the interpretation of the experiments.

To ensure that the cobalt removed by the centrifuging was adsorbed by the δMnO_2 and not removed by the formation of radiocolloids (Schweitzer and Jackson 1952), experiments were designed to test this possibility. Cobalt solutions of 5×10^{-6}m and 5×10^{-8}m were set up, buffered at pH 3.7 (acetic acid-sodium acetate) and 8.1 (bicarbonate), with no δMnO_2 present. Samples were withdrawn and centrifuged at high speed (15000 rpm) for one hour. After centrifuging, the sample was split as mentioned in the previous paragraph and counted. No evidence was found for the existence of radiocolloids.

REFERENCE

Parks G.A. (1965) The isoelectric points of solid oxides, solid hydroxides and aqueous hydroxo complex systems. Chem. Rev. 65, 177-198.

Schweitzer G.K. and Jackson M. (1952) Radiocolloids. J. Chem. Ed. 29, 513.

APPENDIX (IV-B) ELECTROPHORESIS EXPERIMENTS

The measurements of electrophoretic mobility were obtained using a Briggs microelectrophoresis flat cell (Figure 1). The potential difference was applied by a Beckman Duostat power supply, and the current was measured with a Kiethley 610B electrometer. The resistivity was measured using a Schlumberger Type EMT-C resistivity cell. The electrochemical cell can be represented by:

(Pt), Hg, $Hg(NO_3)_2$, KNO_3/ suspension / KNO_3, Hg, (Pt)

The mobility is calculated from the equation:

$$\mu = \frac{d\ x}{t\ I\ R_s} \qquad (1)$$

where d is the width of the grid, x is the cross sectional area of the cell, t is the time for the particle to traverse the distance d, I is the current, and R_s is the specific resistance of the suspension.

Scrupulous cleaning of the cell and the electrodes is an essential part of the electrophoretic technique. The electrode cavities were closed with ground glass stoppers and the cell filled with a 10% solution of hydroxylamine hydrochloride, rinsed thoroughly with distilled-deionized water, and filled with concentrated HNO_3. After allowing the acid to stand in the cell for fifteen minutes, the cell was thoroughly rinsed again with distilled water. The electrodes were cleaned by washing with 3NHCl and distilled water. After washing, the electrodes were allowed to dry before use.

In most of the experiments, the surface area of δMnO_2 used was $1.15 m^2/l$. For comparison of the experiments done at different metal ion concentrations, it was necessary to use a constant surface area since the

Figure 1

(Upper) A side view of a Briggs microelectrophoresis flat cell.

(Lower) Electrical schematics for the electrophoresis measurements.

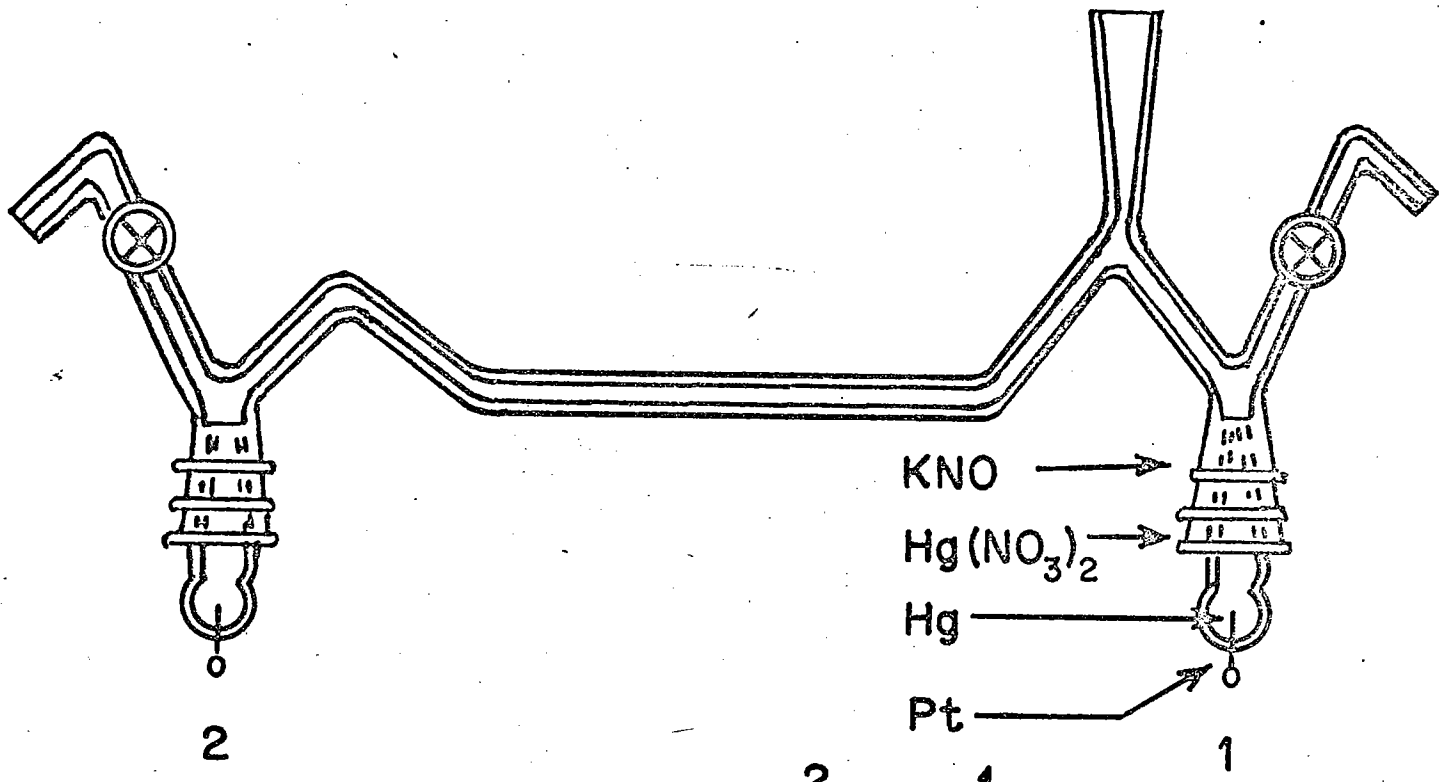
KNO
$Hg(NO_3)_2$
Hg
Pt
2
1

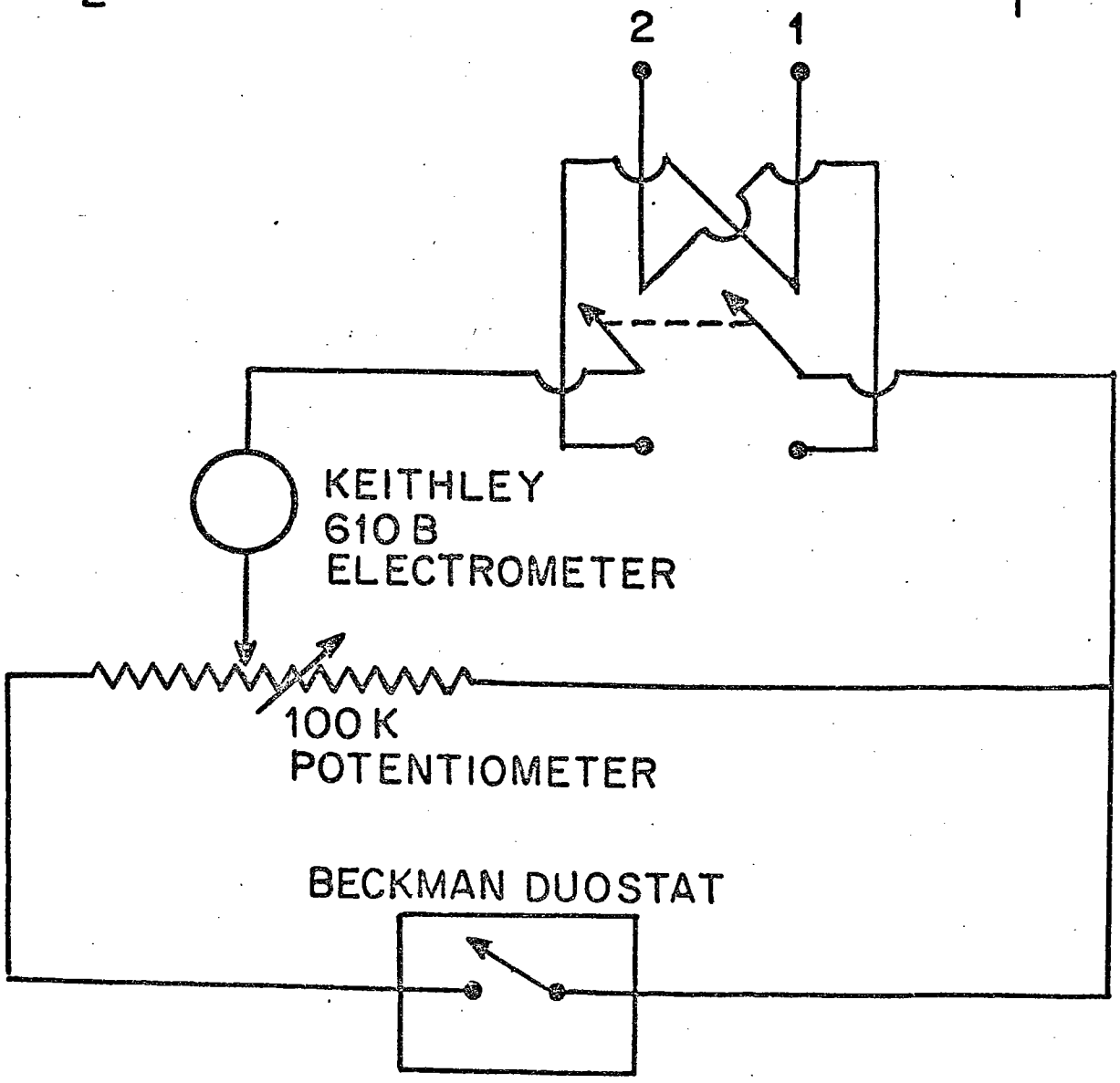
2
1
KEITHLEY
610 B
ELECTROMETER
100 K
POTENTIOMETER
BECKMAN DUOSTAT

characteristic charge reversals of the electrophoretic mobility curves are a function of surface coverage. The effect of surface area was studied in a separate experiment. The experiments were set up by adding 20 ml of 0.1M HCl, the required amount of 10^{-1}M or 10^{-2}M stock $Co(NO_3)_2$ or $MnCl_2$ solutions, and 50 ml of a stock 1 x 10^{-3}M δMnO_2 suspension to a 1 liter beaker. The total volume was then brought to 1 liter by distilled-deionized H_2O. After equilibration of the cobalt with the δMnO_2, approximately 100 ml were withdrawn and placed in the electrophoresis cell for measurement. The pH of the experiment was then adjusted upward using 0.1M NaOH. In making the mobility measurements, ten particles were timed going in one direction, and then with the polarity reversed, ten readings were taken in the opposite direction. With the electrodes and the cell set up properly, there was good agreement between these readings. In the mobility calculations, the average of the 20 velocity determinations was used.

APPENDIX (IV-C) THE EFFECT OF SURFACE CHARGE ON THE SOLUBILITY PRODUCT OF $Co(OH)_2$

Consider the system of solid, interface and bulk aqueous solution. At equilibrium in free solution, we can write:

$$Co(OH)_2 \text{ (solid)} = Co^{+2} + 2\ OH^- \qquad (1)$$

with $K_{so} = a_{Co} + 2 \cdot a_{OH^-}^2$ (2)

and $\Delta G^o = -RT \ln K_{so}$

since $\Delta G = 0$ at equilibrium

The activity of the solution species is represented by a and the solubility product by K_{so}. The change in free energy and the change in standard free energy for the dissolution of the hydroxide at constant temperature, pressure, gravitational potential and electrical potential are represented by ΔG and ΔG^o. The same conditions are not satisfied at the solid-solution interface because of the effect of the large electric fields present. At sea water, ionic strength with a double layer thickness of 3.5 Å (Stumm and Morgan 1970, p. 459) and a hypothetical surface potential of 100mV, the electric field is 2.9×10^8 volt/cm. The primary consequence of this field is to lower the dielectric constant of the interfacial medium to a value well below that of the bulk aqueous solution.

If the interface can be regarded as a separate phase, then in the presence of an electric field at constant temperature and pressure

$$-\Delta G^{o'} = (G^{\circ}_{Co^{+2}} + G'_{Co^{+2}} + G_{OH^-}^{o} + G_{OH}^{o'} - G_{Co^{o}_{(OH)_2(s)}} - G_{Co'_{(OH)_{2(s)}}}) \qquad (4)$$

where the primed quantities are the excess contributions due to the electric field. In free solution, in the absence of the electric field, the G' quantities are zero, thus

$$-\Delta G^{o'} \simeq \Delta G^{o} - (G'_{Co^{+2}} + G'_{OH^-}) \qquad (5)$$

The effect of the field on the solid $Co(OH)_2$ has been neglected. The G' terms represent the excess free energy of the ions in a medium where the electric field is not zero. Thus, the solubility product of the hydroxide in the presence of an electric field is:

$$RT \ln K_{so}' = RT \ln K_{so} - (G'_{Co^{+2}} + G'_{OH^-}) \qquad (6)$$

The G' terms can be expressed in the form of the Born charging equation where the free energy is:

$$G' = \frac{(ze)^2 N}{8\pi r_{ion} \varepsilon_o} \cdot \left(\frac{1}{\varepsilon_i} - \frac{1}{\varepsilon_b}\right) \cdot g(\theta)$$

where z is the charge on the ion, e is the electronic charge, N is Avogadros number, r_{ion} is the ionic radius, ε_o is the permittivity of free space (8.85×10^{-12} coulomb/volt/mole, ε_i and ε_b are the dielectric constants of the solvent at the interface and in bulk solution and $g(\theta)$ is a geometrical function. The dielectric constant, ε_i, is a function of the square of the electric field; thus ε_i is less than ε_b for a charged surface.

Since ε_i is less than ε_b and the valence is squared, both terms are positive. Thus from equation 6:

$$K_{so} > K_{so}'$$

Thus $Co(OH)_2$ is more insoluble and will precipitate at a lower pH in the presence of the electric field at the interface.

REFERENCE

James R.O. and Healy T.W. (1972) Adsorption of hydrolyzable metal ions at the oxide-water interface (II) Charge reversal of SiO_2 and TiO_2 colloids by adsorbed Co(II), La(III) and Th(IV) as model systems. J. Colloid Interface Sci. 40, 53-64.